ON THE DEVELOPMENT OF A GroEL BASED PLATFORM FOR IDENTIFYING PHARMACOLOGICAL CHAPERONES

BY

SUBHASHCHANDRA NAIK

Submitted to the graduate degree program in Biochemistry and Molecular Biology and the Graduate Faculty of the University of Kansas Medical Center in partial fulfillment of the requirements for the degree of Doctor of Philosophy

.

Dr. Mark T. Fisher

Chairperson

Committee members*

Dr. Aron W. Fenton

Dr. Kenneth Peterson

Dr. James P. Calvet

Dr. Wolfram R. Züeckert

Date defended: November 29th 2012

The Dissertation Committee for Subhashchandra Naik certifies that this is the approved version of the following dissertation:

ON THE DEVELOPMENT OF A GroEL BASED PLATFORM FOR IDENTIFYING PHARMACOLOGICAL CHAPERONES

Dr. Mark T. Fisher

Chairperson

Committee*

Dr. Aron W. Fenton

Dr. Kenneth Peterson

Dr. James P. Calvet

Dr. Wolfram R. Züeckert

Date approved : January 30th 2013

ABSTRACT

Many protein misfolding diseases are due to changes in protein homeostasis. This might lead to protein misfolding and possibly intra- or extracellular aggregation, causing loss of protein function or gain of toxic function. In several cases, the cellular clearance mechanism is sometimes inhibited and unable to degrade the aggregated forms leading to cell injury and death. This is frequently observed in misfolding diseases like Parkinson's disease, Cystic fibrosis, Alzheimer's, etc. These diseases account for nearly 30-50 % of all known human diseases afflicting millions and have a significant economic impact. However, there are currently few treatments to counteract these diseases. Thus, there is a pressing need to develop strategies to treat these diseases. One strategy is to develop small molecule ligand drugs that prevent the initial protein misfolding reaction. Proteins are somewhat metastable and naturally exist in dynamic equilibria between native fold and an ensemble of partially unfolded forms. This makes the misfolded forms moving targets and thus difficult to stabilize. This difficulty is compounded while developing high throughput assays to screen for stabilizing ligands for these moving protein targets. Consequently, these assays depend on detecting secondary misfolding events such as aggregation or removal of misfolded species, thus increasing the duration of the assays (hours-days). Additionally, in most instances specific cell-based assay systems have to be developed for each misfolding protein. This inhibits the development of broad based assays and complicates rapid screening of the huge compound libraries developed by rational drug design and combinatorial chemistry. In this dissertation, the development of a broad based high throughput assay for identifying novel stabilizers for protein misfolding diseases has been

presented. The bacterial chaperonin GroEL binds to proteins that are partially unfolded or exist in a folded to partially folded dynamic equilibrium. Based on this property, the development of a generic broad based assay to probe a multitude of protein substrates based on changes in hydrophobic character was hypothesized and carried out. Using the chaperonin as a detection platform will enable the extension of this detection platform to identify potential stabilizers of the native fold that prevent or inhibit protein misfolding.

ACKNOWLEDGEMENTS

I am deeply indebted to my mentor Dr. Mark T. Fisher, a resercher and a teacher par excellence. I would like to thank Mark taking me on as his student, for instilling in me a commitment towards science, for challenging me to move beyond my comfort zone and helping me become a better researcher. His boundless, infective enthusiasm, patient advice and unwavering support made working on this dissertation a real pleasure.

In addition, I am also grateful to my doctoral committee (Dr. Aron Fenton, Dr. James Calvet, Dr. Wolfram Züeckert and Dr. Kenneth Peterson) for being so generous with their time and expertise. Their patience, suggestions, constructive criticisms and willingness to help me in solving various challenges is deeply appreciated.

I am also thankful to the past and present of the Fisher lab for their support, ideas, and criticisms and for making the work in the lab pleasant and motivating.

I am grateful to Dr. Philip Gao and Dr. Na Zhang as well as Dr. Wesley McGinn-Straub and others at ForteBio Inc. for allowing me to use their facilities and training me in surface plasmon resonance and bio-layer interferometry respectively.

I am thankful to the graduate studies director Dr. Liskin Swint-Kruse as well as the administrative personnel in the department, for their help in making sure that I stuck to all deadlines and for helping me out with all the administrative paperwork through these years.

I am also thankful to KU IAMI for financial assistance.

Special thanks are due to all my friends who have supported me through these years and made this time enjoyable and memorable. I am deeply grateful to Sarika Kshirsagar for being a

strong supporter and an exceptional friend. It would have been a different and difficult experience without her.

To wrap this up, the biggest thanks goes out my parents for being my bedrock with their unconditional love and support. Their unwavering faith in me and confidence in my abilities has helped to shape me in the person I am today. Words fail me to thank them for their countless sacrifices, steady guidance and constant encouragement. This dissertation is dedicated to them.

- Subhashchandra Naik

TABLE OF ABBREVIATIONS

ANS	8-anilino-1-naphthalenesulfonic acid
ATP	Adenosine-5'-triphosphate
ADP	Adenosine diphosphate
BLI	Bio-layer interferometry
CF	Cystic fibrosis
CFTR	Cystic fibrous transmembrane conductance regulator
CHOP	C/EBP homologous protein
DHFR	Dihydrofolate reducatse
DMSO	Dimethyl sulfoxide
DTT	Dithiothreitol
EDC	1-Ethyl-3-(3-dimethylaminopropyl)carbodiimide hydrochloride
EF	Edema factor
ER	Endoplasmic reticulum
ERAD	Endoplasmic reticulum associated degradation
FRDA	Friedreich ataxia
FRET	Förster (Fluorescence) resonance energy transfer
HEPES	(4-(2-hydroxyethyl)-1-piperazineethanesulfonic acid)
HPLC	High pressure liquid chromatograph
HSF	Heat shock transcription factors
HSR	Heat shock response
HTS	High throughput screening

ICH	International Conference on Harmonization
ISC	Iron-sulfur clusters
LF	Lethal factor
LF_N	N-terminal fragment of LF
NADPH	Nicotinamide adenine dinucleotide phosphate
NBD	Nucleotide binding domains
NHS	N-hydroxysuccinimide
PA	Protective antigen
PDEA	2-(2-pyridinyldithio) ethaneamine hydrochloride
PDI	Protein disulfide isomerase
RI	Refractive index
RU	Resonance unit
SPR	Surface plasmon resonance
TRIS	Tris(hydroxymethyl)aminomethane
TMAO	Trimethylamine N-oxide
UPR	Unfolded protein response

TABLE OF CONTENTS

CHAPTER 1: ON THE NEED FOR A PLATFORM FOR IDENTIFYING PHARMACOLOGICAL CHAPERONES

1.1 Protein misfolding and proteostasis.

1.1.1 Protein folding and misfolding.

a Protein folding and function.

Proteins are crucial for all essential life functions as they act as catalysts, molecular machines, signaling molecules and structural scaffolds. In order to be active and carry out these functions, they adopt specific three-dimensional (3D) shapes. Proteins consist of several such 3D conformational shapes giving rise to an ensemble of conformations. The conformational shape is generally determined by the primary sequences of the amino acid residues. This relationship between the protein sequence and its structure has been studied for more than 70 years. Some of the initial studies in the field of protein folding were performed by Linus Pauling and E.J. Corey, who first discovered that polypeptides form secondary structure elements such as alpha helices and beta sheets (*1*). Later, Christian Anfinsen used the protein ribonuclease to demonstrate that the thermodynamically stable native structure dictates protein function and that structure depends on the protein sequence (*2*).

The protein sequence is essentially a long polypeptide chain. In a denaturing solution *in vitro*, this polypeptide chain behaves like a random coil, whose average radius of gyration can be calculated (*3, 4*). Under folding conditions, the polypeptide is driven towards a conformational state that optimizes its interaction with the surrounding solution as well as with itself to attain its lowest free energy state. While attaining the lowest free energy state, the polypeptide chain residues interact locally to form a variety of folding states with varying degrees of thermodynamic stabilities. Collectively these transitional states lead towards a conformational

ensemble with the lowest stability and is commonly referred to as the native state of the protein. This folding reaction typically occurs in microseconds-milliseconds range *in vitro*. CspB, a 67-residue protein has been measured to fold in 1 millisecond, while the reduced form of the 104-residue Cytochrome c protein folds in 130 microseconds (*5*). *In vivo*, the folding is also dictated by the translational rate as well as its interaction with other macromolecules. Given the conformational flexibility that a polypeptide can achieve, the act of folding was postulated to theoretically sample incredibly large numbers (approximately 10^{95} different conformations for a 100 residue polypeptide) of different folded conformational states (and thus a large number of folding options) available to the unfolded polypeptide chain. However, the protein frequently achieves its native state in a relatively short time. This conundrum is commonly known as Levinthal's paradox and it was concluded that there has to be specific folding pathways (folding intermediates) that decreases the folding speed to biologically relevant times (*6, 7*). This concept of folding pathways gave rise to many theoretical models that attempted to describe the folding process where the protein is driven towards the native state with increasing speed as the folding progresses. In one of the earliest models known as nucleation theory, there are potential folding nuclei in the structure around which folding occurs in a stepwise manner (*8*). An alternative model was the hydrophobic collapse theory than envisions the hydrophobic residues collapsing to form an intermediate that then rearrange to give the native structure (*9*).

A new model of protein folding that gained popularity in the late 90s replaces the idea of specific folding pathways with multiple folding routes and the energy landscape. This energy landscape, which is the free energy of each conformation as a function of the degrees of freedom, is frequently described in terms of a folding funnel energy landscape (Figure 1.1) (*10*). In the Figure, the vertical axes represent the internal free energy of the protein while the horizontal axes

represent the conformational entropy. Thus a protein that undergoes folding goes from the large conformational freedom and entropy available to the unfolded protein at the top to the native state ensemble at the bottom (*11*). Each protein molecule may follow a different route from the top to the bottom and each conformational state is a point on the energy surface of the funnel. As an unfolded protein starts folding, the protein changes its conformation by making new interactions that lower its energy. This frequently leads to compaction of the chain thus reducing the number of available conformational states to sample and, thus, narrowing of the funnel. This compaction might be due to the formation of secondary structural elements or collision of preformed secondary structures.

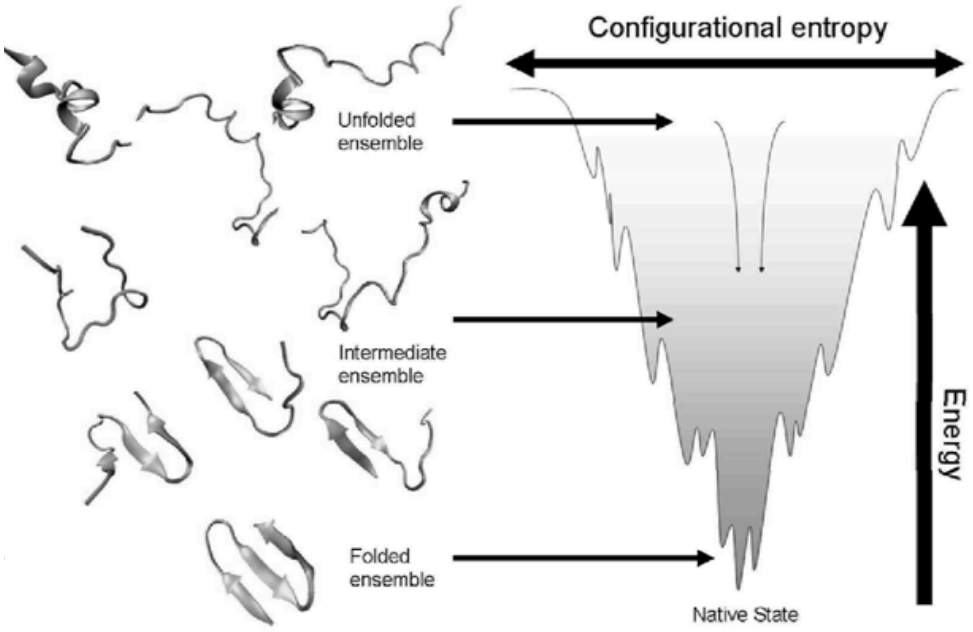

Figure 1.1: The energy landscape of protein folding can be projected as a folding funnel with the native state at the bottom. Each conformational state of the protein represents a point on the funnel surface indicating the many routes available to an unfolded protein to achieve its native state. As the protein folds the available conformation space decreases narrowing the funnel. Figure adapted from [12]

A smooth surface of the folding funnels denotes that the unfolded polypeptide has equal chances of reaching the native state no matter what route down the funnel it takes. However, this is only true in the case of small, single domain proteins that demonstrate two-state folding, at low concentrations *in vitro*. Multi-state folding might lead to the formation of folding intermediates that have low free energy of folding and such folding funnels are characterized by the presence of a rough surface with kinetic traps and energy barriers (*12*). During such a folding process, certain intermediate conformations can get stuck in a kinetic trap, where the non-native conformation has a favorable energy state. These kinetic trapped non-native intermediates often have to partially or completely unfold to overcome the activation barrier to get back "on path" to the native state. This step is what usually slows down protein folding, and might cause the partially folded intermediates to interact with themselves, leading to protein misfolding and aggregation. Such aggregates and misfolded proteins are energetically favored when the cell is being constantly challenged by changes in metabolite concentrations, ion balance, and physical insults including temperature stress and pathogens leading to the generation non-functional entities. To prevent this and in order to maintain a viable concentration of folded functional proteins, the cell utilizes other protein systems to achieve or maintain their folded states at appropriate concentrations using a process termed as protein homeostasis or proteostasis.

b Proteostasis and Proteostatic networks.

Proteostasis is defined as a state of dynamic equilibrium in which protein synthesis and folding is balanced against degradation to maintain protein conformational flexibility, leading to a healthy proteome (*13, 14*). The cell maintains proteostasis within the proteome by controlling the concentration, conformation, location and the binding interactions of a protein to maintain its fold and function.

The steady state protein concentrations within the proteome is hence defined by biosynthetic processes such as protein synthesis and folding, post translational modifications, trafficking and degradation. These biosynthetic processes are kinetic processes in themselves and are regulated through a network of different proteins that are commonly called as proteostasis networks (Figure 1.2) (*15*) The proteostatic networks include about seventeen different pathways including in total about 1000 different assistant proteins such as folding enzymes, chaperones and trafficking components. These assistant proteins act through transcriptional and post translational mechanisms to balance protein folding and functional capacity by reducing protein synthesis, by enhancing folding and repair processes, and/or by mediating degradation. (*15*). Some of the more commonly known proteostatic network component includes the heat shock response pathway, the unfolded protein response pathway and the oxidative stress response. Figure 1. 2 shows five of the more common proteostatic networks and some of the biosynthetic processes that define protein concentration.

Proteostasis helps proteins remain in a metastable active state that is required for their function. Being metastable is important for protein function because this marginal stability (The free energy difference between the folded and unfolded protein is in the range of 5-10 kcal.) allows the proteins to interact with other biomolecules, maintaining active conformers. In addition, a large number of proteins in the cell (>30%) are unfolded and refold during trafficking between the endoplasmic reticulum and cytosol. This dynamic equilibrium (*16*) between folded and partially unfolded or inactive forms (*17*) of a protein is also affected by several factors like temperature, mutations, etc. Other external stress elements also strongly influence the kinetic competition between folding, misfolding and concentration dependent aggregation. Proteostasis is thus a dynamic process as the proteome itself undergoes constant changes over the course of

development of the cell (*13*). The proteostasis network is highly adaptive (*18*) and helps to preserve the synergy between productive folding and degradation in the proteome of an organism during stress, developmental changes, mutations, environmental stress, infectious disease and aging.

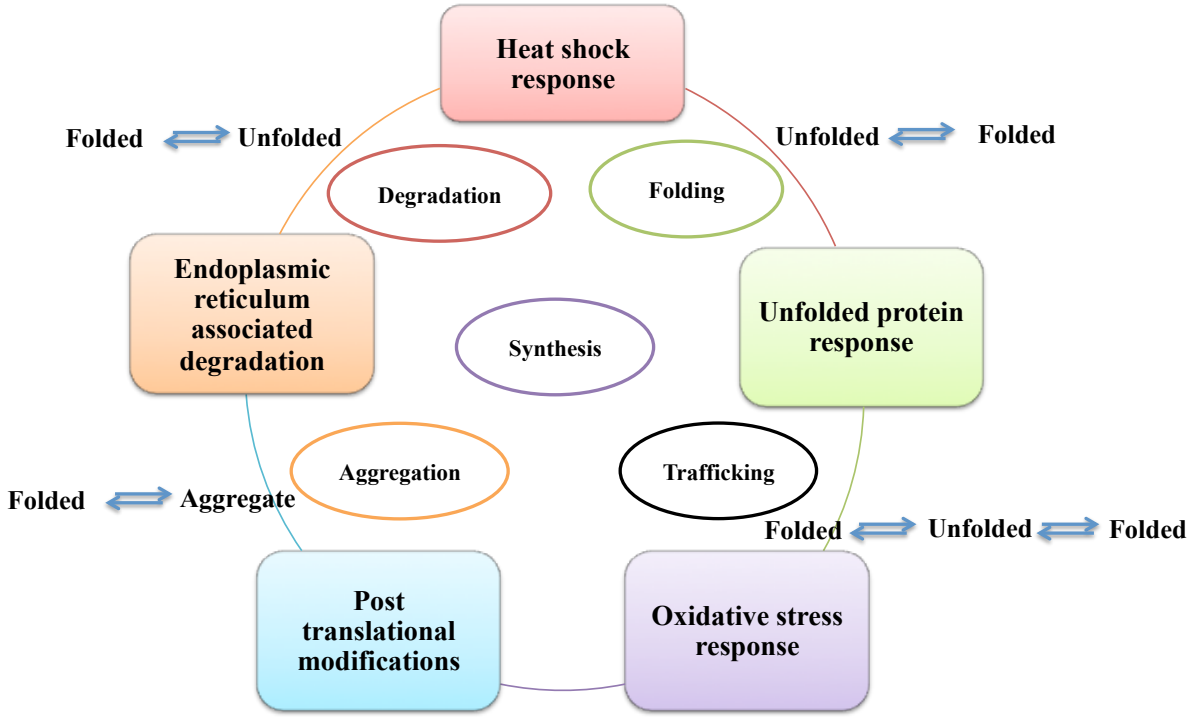

Figure 1.2: Proteostasis network as a complex network of integrated pathways. These pathways are in a constant crosstalk with each other to balance the protein folding with its functional capacity. Here five common networks that influence a protein during its life cycle are shown. Each of these networks is involved in the protein lifecycle from its synthesis to folding to trafficking and finally degradation. These networks are also involved in case the protein undergoes aggregation due to stress.

c Chaperones and heat shock proteins.

Several extraneous factors like chaperones, metabolic enzymes, osmolytes as well as small inorganic molecules affect the kinetics of protein folding (*19-21*). To monitor these constant changes, the cell utilizes stress sensors such as the heat shock response and the unfolded protein response pathways. The heat shock response (HSR) pathway is a key element of the proteostasis networks. This response is conserved in all organisms. The primary role of the HSR pathway is maintaining the proteome integrity and allowing cells to survive environmental changes such as heat, oxidative, and/or chemical stresses. Under such stress conditions, the initial response of the cell is to upregulate the expression of highly conserved cytoprotective gene products. These cytoprotective stress response proteins are known as heat shock proteins (Hsps).

Genome wide studies in different model organisms have shown that the HSR significantly induces the expression of a total of about 50–200 genes, including the heat shock proteins (*22*). Although overexpressed under stress conditions, many of these proteins are also essential housekeeping proteins and are thus constitutively expressed under non-stress conditions. Before their function was known, these proteins were initially named according to their molecular masses that were resolved on SDS-PAGE. Many Hsp proteins function as molecular chaperones that bind to exposed hydrophobic surfaces or sequences and prevent general stress induced aggregation. Even under non-stress conditions, chaperones bind to nascent polypeptides thus inhibiting misfolding and protein aggregation. They thus help to protect the cells from toxic effects of protein misfolding.

The term molecular chaperone was coined by John Ellis in 1987 (*23*). He defined these proteins as a “Class of proteins whose function is to ensure that the folding of certain other

polypeptide chains and their assembly into oligomeric structures occur correctly" without becoming part of the final structure (*24*). Molecular chaperones are nature's protectors against aggregation and actively or passively assist in the process of protein folding. There are instances where specific folding chaperones like PapD chaperone (*25*) are directly involved in assisting in the final fold for bacterial pili elongation. However contrary to popular interpretations, a substantial number of general heat shock chaperone proteins passively or actively unfold (rather than fold) non-native proteins. In fact, most chaperones bind to misfolded proteins and facilitate active (Adenosine-5'-triphosphate [ATP] driven) or passive unfolding reactions (*26, 27*) increasing the free energy and entropy to a higher level, from which proper folding can resume. This unfolding reaction prevents proteins from populating the kinetic traps associated with misfolded proteins (Figure 1.1). The unfolding is carried out by means of applying a force (active unfolding through ATP binding energies) or passively (followed by hydrogen exchange measurements), forming interactions and sequestering exposed hydrophobic regions (*28, 29*). Some chaperones, such as the Hsp100 classes, act by active unfolding to completely unfold proteins and rescue aggregates (*30*). Thus by inhibiting the accumulation of partially folded proteins sequestered in kinetic traps, chaperones are the key elements of the proteostasis networks.

In addition to their roles in shepherding nascent polypeptide folding and trafficking, chaperones also act as buffering systems to maintain the protein population in their active states. This is an exquisite balance since chaperones are often not in vast excess within the cell (*31*). A particular protein may encounter numerous chaperones during its life cycle of synthesis, folding and degradation. With the help of chaperones, proteostasis monitors several networks that regulate proteins to maintain the cellular proteome. Most of the chaperone proteins (functioning

as both buffers and folding assistants) that bind transiently to partially folded proteins, cycle between high and low affinity states using the nucleotide binding free energies (e.g. ATP hydrolysis to adenosine diphosphate (ADP)) to drive conformational changes. The distribution of these two affinity states is governed by the intrinsic ATP hydrolysis rate of the chaperone. Other co-factors such as nucleotide exchange factors or nucleotide hydrolysis factors also act in concert with the chaperone to fine tune the ATP hydrolysis, which in turn regulates substrate binding.

d Control of the heat shock response pathway.

The HSR pathway is one such eukaryotic signaling pathway that leads to activation of the proteostatic network. The pathway is initiated by the heat shock transcription factors (HSFs). These are specific transcriptional regulators that bind to Hsp genes and act as master regulators for Hsp expression (*32*). HSF proteins are essential for maintaining cellular integrity and thermostability via Hsp. HSF proteins are constitutively expressed but negatively regulated in an inert, stress-sensing state (a monomeric state) by interactions with the chaperones, Hsp90 and Hsp70. These chaperones bind to the monomers and prevent oligomerization of the HSF proteins. However, as stress conditions lead to general protein unfolding, the chaperone proteins kinetically partition onto unfolded proteins, allowing the now free HSF monomers to assemble into transcriptionally active trimers. This trimerization occurs via hydrophobic heptad repeats (HR-A and HR-B) that form a characteristic coiled coil Leu zipper (*33*). Additionally disulphide bonds between the HSF1 monomers stabilize the trimer. These newly formed HSF oligomers have a high affinity towards DNA HSR elements (*34*). Before binding to the response elements, they first traverse across the nuclear membrane. Once bound to the gene promoter regions, they turn on the expression of the heat shock proteins (Hsps), resulting in a transient overexpression of these Hsp/chaperone proteins, which then prevent the partially folded or nascent polypeptides

from aggregating. This overexpression allows cells to survive and recover from stress induced protein denaturation damage. Once enough Hsp proteins are produced, the HSF1-dependent transactivation is repressed via a negative feedback loop, whereby Hsp70 and Hsp40 re-associate with the HSF1 transactivation domain, and HSF1 becomes dissociated from DNA following acetylation of Lys80 in its DNA binding domain. The activation of the HSR thus prevents the overload of unfolded/misfolded proteins within the cell through an up-regulation of chaperones that is proportional to the stress induced (*35, 36*). The chaperones thus assist in balancing proteostasis through protein refolding or degradation.

e Chaperones influence proteostasis during protein folding.

The proteome is in a constant state of flux. Many cellular processes are involved in maintaining normal biological function and the proteostatic network functions as a surveillance operation that constantly inhibits misfolding due to stress or missense mutants that normally occur within the proteome. As discussed, large shifts in the dynamic equilibrium of the protein towards misfolded or aggregation prone state causes the proteostasis system to intervene, usually through chaperones. One such example where the proteostasis network chaperones can play an essential role is in the maintenance of the intrinsic dynamic equilibria involved in protein folding. Although the protein folding is dependent on its sequence, efficient folding for various oligomers, transport competent or hard to fold proteins *in vivo* are usually dependent on the chaperone proteins to facilitate the acquisition of the correct or active fold. In this buffering capacity of folding function, the binding of the chaperones depends on the forward and backward folding rate constants of the protein targets (*37*). Proteins that fold rapidly to their native states sequester any putative hydrophobic binding sites that are recognition sites for interaction with chaperone proteins. Proteins that fold slowly need to avoid kinetic traps. These proteins benefit from

chaperone interactions to facilitate the early stages of folding and assembly reactions thus helping it attain the proper fold (*38*).

The chaperones are involved in nascent protein folding events that follows ribosomal polypeptide synthesis by facilitating folding in the cytosol, as proteins emerge into the endoplasmic reticulum (ER) or after transport into the mitochondria. As discussed earlier, some folding seems to occur as the protein emerges from the ribosome (as soon as the N-terminal domain exits the ribosome pore). In certain instances, folding might occur within the ribosomal tunnel itself leading to formation of secondary structural elements (alpha helices) (*39*). In prokaryotes, the translated nascent polypeptide chain exiting the ribosome interacts with trigger factor (a cis-trans peptidyl prolyl isomerase), while in eukaryotes the peptide binds co-translationally to the nascent associated complex (NAC) (*40*) / Ssb complex (*41*), both of which shields exposed hydrophobic residues to prevent aggregation (*42*) and to catalyze proline isomerization. Folding is then initiated in the presence of ATP dependent chaperones such as DnaK. In eukaryotes, approximately 1/3rd of all proteins are translocated to the ER for folding, processing and secretion (*43*). This translocation occurs via short tags known as signal sequences (*44*) that bind to a ribonucleoprotein called signal recognition particle (SRP) (*45*), which then helps to target the bound signal peptide towards the Sec translocon (*46*). One of the first chaperone proteins encountered by the nascent polypeptide is the Hsp70 protein class. As the nascent peptides emerge from the ribosome, they bind to Hsp70 (DnaK in prokaryotes) and its co-chaperones such as Hsp40 (DnaJ in prokaryotes). Hsp40 is a nucleotide hydrolysis factor and can also bind partially folded proteins. Together, the nascent polypeptide along with the Hsp70 and Hsp40 classes forms a transient ternary complex. Hsp70 binds to the polypeptides in an extended conformation. Hsp40 stimulates the ATP hydrolysis rate of Hsp70, resulting in an

ADP-Hsp70 complex that has a higher affinity for the extended substrate. Finally, a nucleotide exchange factor such as BAG (GrpE in prokaryotes) facilitates ATP dissociation and ATP exchange completing the cycle. The released protein can then undergo additional folding, transport, and degradation or might interact with other chaperones. In such instances the nascent polypeptide chain in a partially folded form is transferred to the Hsp90 complex or Hsp60/Hsp10. The Hsp60/Hsp10 help the partially folded polypeptide to fold by sequestering the proteins in a folding cavity (Hsp60 proteins class of molecular chaperones are also called as chaperonins and will be discussed later in this chapter). The Hsp90 chaperones act in combination with a very large subset of specific co-chaperones to aid protein folding and activation. Hsp90 chaperones show a binding preference towards positively charged or hydrophobic proteins (*47*). In concert, these different chaperones help the substrate achieve its functional native state.

However, if the protein still remains unfolded, which might occur in case of missense mutant proteins, the protein is either degraded by the proteasome (also with the help of accessory chaperones) or can be captured by dynamic oligomers comprised of the smaller Hsps (the Hsp20s). In the latter case, these small Hsps assemble into large multiple subunit oligomers where they act as holding chaperones until the proteins fold via the Hsp70 class or are shuttled to the proteosome for degradation. Despite all of these checkpoints against protein aggregation, some proteins still are unable to fold, overwhelm the chaperone systems and consequently undergo intracellular aggregation. Even in these instances, there are classes of chaperones called the Hsp100 chaperones (*48*) that actively (i.e. require ATP binding and hydrolysis) disaggregate the problem proteins and either folds these with the above mentioned chaperone classes or in cases where protein folding is no longer kinetically viable, shuttles the disaggregated protein towards proteosomal degradation.

As discussed earlier, a significant portion of eukaryotic proteins is translocated into the ER lumen co-translationally via the sec translocon. This ER translocation occurs with soluble proteins or in cases of membrane proteins, the membrane protein is incorporated into the ER membrane. As with most proteins that undergo efficient translocation inside the cellular environment, it is paramount that these proteins remain in their unfolded/partially folded states (the diameter of the translocation pore is too small for the passage of folded proteins) (*38*). The presence of the signal sequence usually introduces a measure of instability in the polypeptide and prevents it from rapidly achieving a compact thermodynamically stable native state even within the cytoplasm. Once translocation occurs, the unfolded peptide binds to chaperones such as Binding immunoglobulin protein (BiP) (*49*) (belonging to Hsp70 family) and other ER associated co-chaperones that delay folding and prevents the polypeptide from being trapped into a non-native state. The chaperone BiP has been termed as the master regulator of the ER and is instrumental in maintaining ER translocation, protein folding, calcium homeostasis, as well as the regulation of protein degradation (discussed in the next section). The peptide binding site of BiP is composed of seven residues and it recognizes sequences that are usually in the interior of a folded protein (*50, 51*). This sequence is usually a heptameric motif with the sequence Ar(WX)ArXArXAr, where Ar is a bulky aromatic or hydrophobic residue (frequently tryptophan, phenylalanine or leucine, but also methionine and isoleucine), W is tryptophan, and X is any amino acid (*52, 53*). BiP is also involved in protein translocation through the membrane and is involved in occluding the translocational pore when translocation is not occurring (*54*). The level of BiP in the ER is critical and tightly regulated at the post-transcriptional level. Under environmental stress conditions, the levels of BiP are increased leading to increased protein levels (*55*). The oxidizing environments of the ER, as well as specialized chaperones such as

protein disulfide isomerases, help in folding of the nascent polypeptide chain, especially in the formation of disulfide bonds. These protein disulfide isomerases are actually oxidoreductases that catalyze disulfide bond shuffling and ultimately the correct disulfide bond locks into place and the protein disulfide isomerase (PDI) no longer interacts with the properly folded protein (*56*). The properly folded proteins are then exported to various cellular organelles through COP II coated vesicles. The repeated binding and release of the substrates with various chaperones ensures that the improperly folded proteins do not exit the ER. These improperly folded proteins however, are subject to quality control courtesy of the chaperone proteins and are in some cases ultimately degraded.

f Chaperones influence protein folding quality control.

The ER is involved in protein quality control and degradation of proteins that are improperly folded or improperly processed and do not achieve their native conformation. This proteostatic process is called endoplasmic reticulum associated degradation (ERAD). The quality control within the ER helps to recognize and sequester proteins that have exposed hydrophobic regions or have incorrect or missing disulfide bonds, both properties that can result in inappropriate aggregation (*57*). Such proteins are initially recognized by the specific Hsp70 chaperones (BiP) in the ER lumen. If the substrate protein fails to fold rapidly, this prolongs the interaction between BiP and the substrate protein leads to that protein being transferred to the ubiquitin ligase E3 (*58*) where it can be ubiquitinated and ultimately cleared. There are also instances where the misfolded ER protein is retrotranslocated from the ER via the sec translocon back out into the cytosol, where it is polyubiquitinated and then degraded by the proteasome (*59*).

If high levels of unfolded proteins or aggregated proteins accumulate within the ER, this event leads to a general ER stress. If this stress event occurs, this results in the initiation of a

conserved proteostatic pathway called the unfolded protein response (UPR) (*60*). UPR can be initiated by several other stress conditions such as calcium homeostasis changes, energy deprivation, redox changes, infections and mutations (*61*). During UPR, the chaperone BiP acts as a stress sensor. The stress condition leads to general protein unfolding, wherein BiP binding to the accumulating unfolded protein(s) decreases the BiP/Grp78 concentration levels within the ER. As BiP levels fall, a normally BiP bound protein called the ER Transmembrane RNase Inositol Regulating Element 1 (IRE1), loses BiP binding because BiP is titrated away by unfolded proteins. This loss of BiP binding allows the IRE1 protein to undergo dimerization and activation (*62*). The activated IRE1 dimer catalyzes alternative splicing of a UPR specific transcription factor called XBP1 (X-box binding protein 1) messenger RNA. The cleaved mRNA now encodes the XBP1 transcriptional activator that binds to the unfolded protein response element responsible for inducing the UPR.

UPR induction leads to three different protein protective functions: (i). Up-regulation of BiP translation, (ii). Decreased protein synthesis (*63*) and (iii). Increased degradation by the network of proteins associated with ERAD. These three functions act to counter the accumulation of unfolded proteins leading to ER stress, thus maintaining the viability of the cell. If these steps fail to initiate UPR, pro-apoptotic factors are activated leading to inflammation and eventually leading to apoptosis (*64*). An example of this is the relation between insulin misfolding and ER stress, which is found in some instances of type II diabetes. ER stress in the pancreatic beta cells is caused by a variety of factors such as insulin overproduction and can lead to insulin misfolding, insulin resistance, calcium depletion and mutations. This stress leads to the activation of the UPR to restore function within the pancreatic beta cells by upregulating its folding capacity. However, any prolonged ER stress leads to apoptosis because an apoptosis

factor C/EBP homologous protein (CHOP) is activated (*65*), which then leads to beta cell death and subsequent induction of type II diabetes.

1.1.2 Proteostasis diseases.

a Protein folding diseases are kinetic events.

As folding progresses through numerous possible routes dictated by a rough energy landscape, the energy landscape hypothesis predicts that there are many different folding intermediates all leading to more stable collapsed and compact natively folded states. These represent both intermediates at different stages on a linear pathway to proper folding and intermediates on parallel pathways to proper folding. Therefore, this energy landscape hypothesis also predicts that multiple folding intermediates should exist simultaneously. In support of this notion, moderate resolution cryoEM single particle analysis by Helen Saibil and colleagues resolved a minimum of five multiple GroEL–substrate complexes (*66*), in which the substrate itself was clearly observed to be folded in numerous unique compact forms. If chaperone proteins concentrations become limiting, it is apparent that these metastable intermediate populations (e.g. monomeric subunits of oligomers) have a tendency to misfold and aggregate inappropriately. This is because the aggregation leads to an overall lower free energy state and increased stability. Under normal growth conditions, a majority of folded proteins is generally only about –5 kCal/mol to –10 kCal/mol more stable than their unfolded states (*67*). Protein conformations with lower energy stabilization parameters are more susceptible to transiently explore less stable states dynamically within narrow temperature ranges. When populations of these transients becomes large (in concentrated solutions), they have a tendency to self aggregate forming either amorphous aggregates or in ordered fibrils both of which possess dramatically stable energy states (*68*) (see Figure 1.3). The tradeoff of this dynamic behavior is

that it is an important property for protein function, from maintenance of active enzymatic conformations to allowing proteins to be able to be transported across multiple cellular compartment boundaries. Most dramatically, proteins that must be degraded by the proteasome are, in most cases, unfolded. Thus proteins are dynamic moving entities, in constant kinetic flux between folded and partially folded forms. The longer an intermediate metastable population exists in a transient state, the more the chances for it to interact with each other and possibly a kinetic selection toward degradation or aggregation. As stated earlier, the concentration shift of this dynamic population depends on environmental as well as mutational stress.

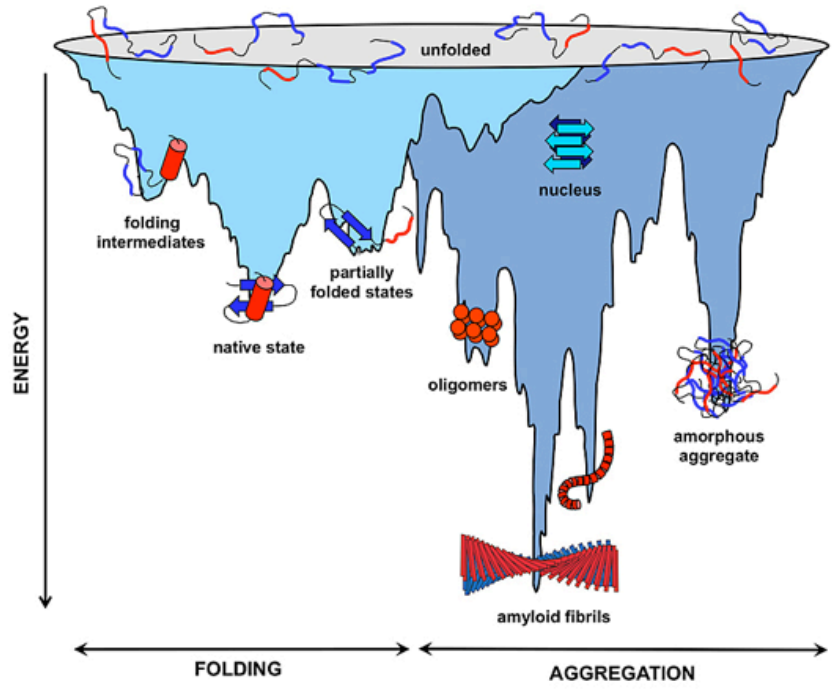

Figure 1.3: Proteins are metastable entities that are in a constant equilibrium between their native and partially unfolded forms. At higher concentrations, the transient partially unfolded species have a tendency to interact with each other leading them to aggregate or form ordered fibrils. Such structures have comparatively lower energy and more stability. Figure sourced from (*69*)

b Implications of misfolding – protein misfolding diseases.

As discussed previously, the balance between stress and HSR/UPR for proteostasis and cell survival is important. This delicate balance shifts toward more destabilized populations during chronic stress conditions due to unfolding. This increase in the destabilized protein populations overwhelms the intrinsic buffering capacity of the proteostatic machinery. In such instances, the existing cell infrastructure becomes unable to deal with changes in proteostasis leading to both loss and gain of function diseases (*70*). Such disorders often result in protein misfolding diseases. These include loss of function diseases such as cystic fibrosis and Gaucher's disease where inefficient folding and excessive degradation leads to a decreased or complete elimination of functional protein levels within a cell. If proteins accumulate as aggregates that manifest disease states, this leads to instances where a new function (called gain of toxic function) arises. This aspect of reduced clearance of a misfolded protein can lead to cell death. Curiously in most instances, it is now realized that large aggregates of proteins that are not easily degraded appear to play a protective role (*71*). It is becoming apparent that the actual toxic forms of a number of folding diseases such as Alzheimer's disease, Huntington's disease and Parkinson's disease may be dictated by smaller oligomers. The mechanism by which these small toxic oligomers lead to cell lethality is still under investigation. Regardless of the mechanism, a viable treatment strategy for these diseases is the control of the cells own proteostatic network as a means of controlling the levels of these misfolded proteins. Some of the strategies currently being pursued to induce or upregulate the proteostasis networks are discussed in the next section. Current strategies that will be discussed include i) replacing proteins, ii) utilizing protein stabilizers and iii) chemically controlling levels of proteostasis regulators (*13*).

1.1.3 Therapeutic approaches for misfolding diseases.

a Protein replacement.

The protein replacement approach is the earliest approach that was utilized for loss of function diseases resulting from decreased protein concentrations within the cell. In some instances, the main mode of therapeutic intervention literally involves injecting wild type protein into the body where appropriate trafficking hopefully exists to insure that the replacement protein/enzyme targets the deficient cells and compartments. Once transported, the next hurdle is to determine if this procedure restores functional levels of enough protein to enhance the quality of life. Protein replacement has been found to be beneficial in individuals with lysosomal diseases such as Gaucher's disease. Protein replacement therapies have several drawbacks that limit its general use. One of the primary reasons for the failure of therapy involves premature removal and/or metabolism of the protein prior to it reaching its desired location. A second reason for therapy failure is due to ineffective transport to the affected organelle within the cell. The administration of an external protein also carries the risk of inducing an immune response. Additionally, the loss of protein function that causes the disease is often a secondary effect, usually due to factors such as genetic mutations. Hence, the large-scale protein replacement does not affect the underlying cause of the disease thus failing to completely ameliorate the pathogenesis of the disease.

b Gene therapy.

The promise of gene-based therapy hinges on proper delivery of a therapeutic protein through direct production (transcription/translation) inside specific targeted areas, usually those that are refractory toward protein replacement therapies. The best candidates for gene therapy are single gene disorders that are not subjected to complex regulation. Additionally, those diseases in

which raising the protein level by just a small fraction leads to clinical efficacy are often times suitable for gene delivery (*72*). The liver has frequently been used as a depot organ to establish a sustained source of therapeutic protein using engineered adenoviral, retroviral and lentiviral gene transport vectors in animal studies (*73*). Gene transfer using viral vectors, may also lead to immune response leading to the loss of transduced cells and loss of therapeutic protein expression (*74*). Retroviral and lentiviral vectors are prone to integrate close to expressed genes, thus increasing the likelihood of transcriptional interference between the vector and flanking endogenous genes (*75*). Gene therapy studies carried out in animal models show promise but further studies are required to address important issues regarding health safety, efficacy and ethics before initiating larger scale clinical trials.

c Proteostasis regulators.

A newer approach involves strategies aimed at actually controlling the proteostatic networks themselves. Proteostasis regulator examples include both small molecule and/or biological components designed to directly control the signaling pathways that lead to the proteostatic response. This control is often accomplished by upregulating the synthesis of components of the proteostasis network. For example, the small molecule drugs diltiazem and verapamil inhibit calcium channels. This facilitates a decrease in cytoplasmic Ca^{2+} levels, which in turn upregulates the synthesis of numerous chaperones, including BiP and Hsp40. This up-regulation leads to enhanced folding and trafficking. An example where such a targeted proteostatic therapy works is in the measured increase in enzyme transport and activity of defective lysosomal enzyme levels that results in some instances of Gaucher's disease (*76*). In another application example, the administration of the natural product celastrol activates the heat shock factor transcriptional pathway, leading to an up-regulation of the several cytoplasmic

chaperones (*77*). Proteostasis regulators can affect several proteostasis network components during the protein life cycle. This has been demonstrated in Figure 1.4, where a proteostasis regulator can act on different biological pathways to enhance proteostasis

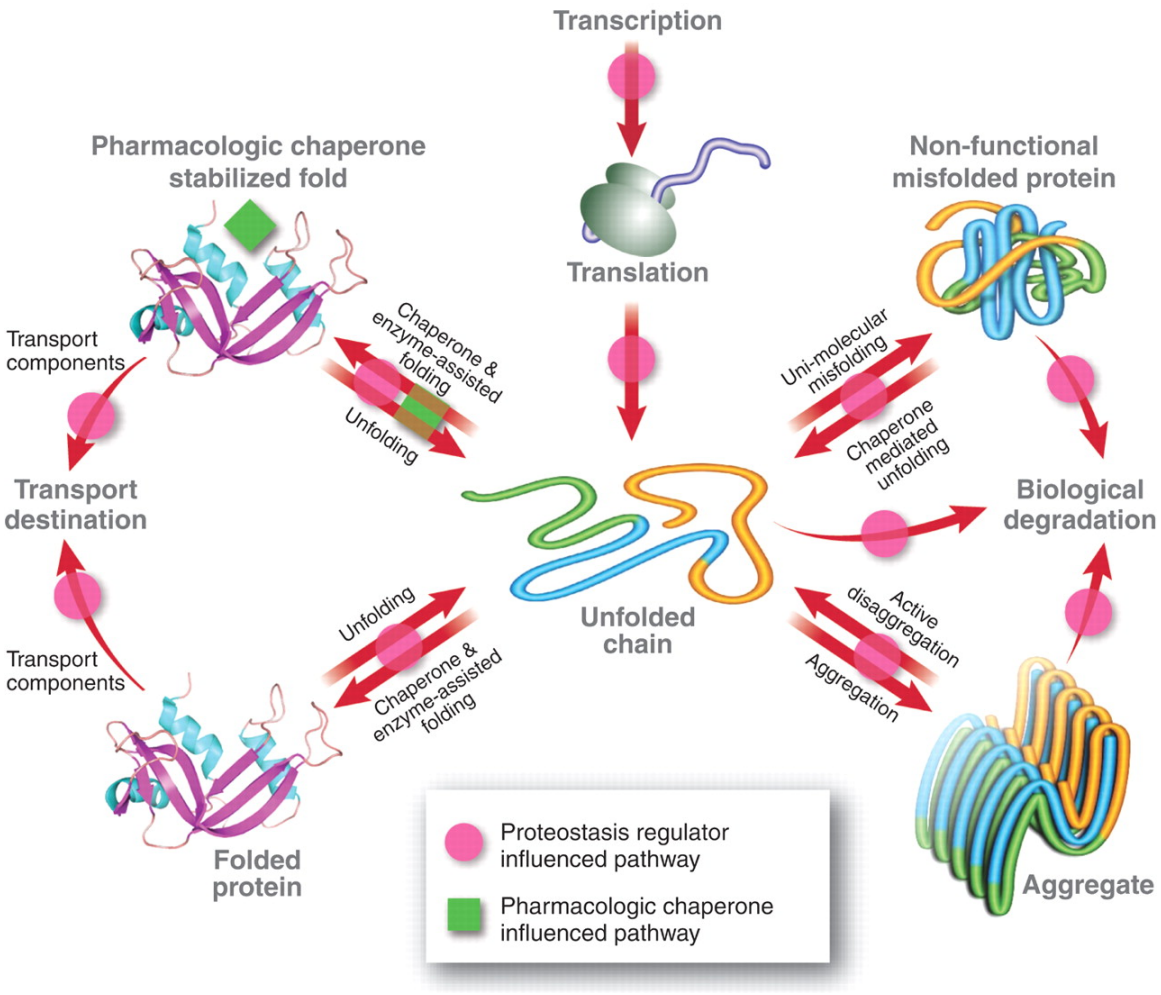

Figure 1.4: Proteostasis regulators work by acting on several proteostasis components during the protein life cycle. These include the protesostasis networks that are active in the folding, unfolding, transport, aggregation and degradation of proteins (as shown by pink dots in the Figure). On the other hand, pharmacological chaperones (green squares) act on the protein folding pathway alone. However, pharmacological chaperones

and proteostasis regulators can be used synergistically to increase the concentration of a stably folded protein. Figure sourced from (*13*)

d Osmolytes (chemical chaperones).

A common small molecule endogenous response to stress conditions, particularly water or osmotic stress involves the intracellular increase of naturally occurring protective osmolytes. Osmolytes are small organic compounds that affect protein folding. Naturally occurring osmolytes can be classified as protecting and non-protecting. Protective osmolytes shift the equilibrium towards the folded state while denaturing osmolytes shift the equilibrium towards the unfolded state. Curiously, protective osmolytes are also known as protein stabilizers and are routinely used by the biotechnology industry to stabilize protein products.

Cells routinely encounter various stress conditions due to physiological functions, surrounding habitat, or osmotic stresses, resulting in changes in the cytoplasmic volume and water content. These stress effects can lead to perturbations in the secondary and tertiary structures of proteins within the cell. This occurs as proteins have evolved to be active in only a certain range of water activities (*78, 79*). To maintain the activity of the protein, the cells frequently utilize osmolytes. The type of osmolyte used by the cell depends on the duration of the stress encountered as well as availability of the osmolyte. Cells deal with short-term osmotic stress by utilizing inorganic ions (*80*). However, the inorganic ions increase the intracellular ionic strength, which affect protein-protein interactions as well as enzyme catalysis (*81*). Under long-term stress, cells accumulate protective osmolytes. Unlike inorganic ion accumulation, protective osmolytes can accumulate at high concentrations to thermodynamically stabilize proteins without affecting normal cellular processes. For example, increased concentrations of small molecule osmolytes such as betaine, sorbitol and inositol counteract the denaturing effects

of high urea concentrations within the renal medullary cells (*82*). Sharks, rays and coelacanths accumulate high concentrations of urea, which is advantageous for water absorption from seawater. In these organisms, the urea enriched cells are still able to maintain general protein homeostasis and folding integrity because these cells produce high levels of counteracting protecting osmolytes such as trimethylamine N-oxide (TMAO) (*81, 83*). Thermodynamically, different osmolytes exert an additive effect on the protein fold (*84*). Thus, the higher concentrations of various protecting osmolytes effectively cancel out the deleterious effect of denaturing osmolytes like urea.

The protecting osmolytes can be classified into three categories based on their chemical properties (*81*):

i. The polyols typically includes sugars such as glycerol, sorbitol, trehelose and mannoses.

ii. Amino acids such as proline and arginine.

iii. Methylamines such as TMAO, betaine and sarcosine.

Though chemically diverse, these sets of protecting osmolytes show a similarity in the mechanism by which they exert their protecting effects on proteins. Timasheff and colleagues used equilibrium dialysis measurements to observe that the protecting osmolytes do not bind to the proteins and are excluded from the protein vicinity (*85*). In contrast, urea binds (*86*) to proteins. This was termed preferential exclusion phenomenon and implies that proteins are preferentially hydrated in their natively folded state. Preferential exclusion leads to an increase in the ΔG of a system between the folded and the unfolded states in the presence of an osmolyte as has been demonstrated by Timasheff and Bolen as shown in Figure 1.5 (*85, 87*). Figure 1.5 shows that transferring either a native/unfolded protein from water to osmolyte solution increases

the chemical potential of the unfolded species (ΔG2) much more than it does that of the native state (ΔG4). This means that the unfolded state of the protein is less favored than the folded state in an osmolyte solution thus resulting in its higher stability in an osmolyte solution than in aqueous solution.

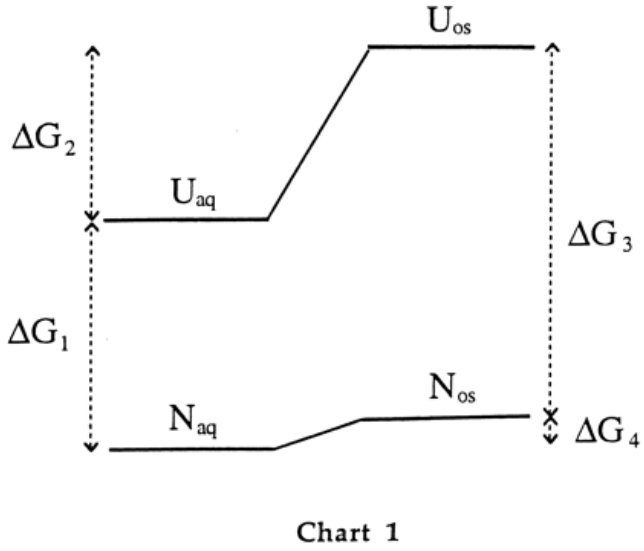

Figure 1.5: The effect of osmolytes on the native and unfolded state of a protein. Transfer from buffer to osmolyte solution increases the free energy of the unfolded protein thus forcing it to collapse to its native state. Here ΔG1 is the free energy of unfolding in aqueous solution, ΔG2 is the free energy of transfer of unfolded protein from aqueous to osmolyte solution, ΔG3 is the free energy of unfolding in osmolyte solution and ΔG4 is the free energy of transfer of unfolded protein from osmolyte to osmolyte solution. Transferring the unfolded protein from water to osmolyte solution increases the chemical potential of the unfolded species (ΔG2) much more than it does that of the native state (ΔG4) thus indicating that the unfolded protein is unfavorable in an osmolyte solution and driving it to a folded state. Image sourced from (*88*)

In a series of landmark experiments, Bolen and colleagues found that the reason for this higher instability of the unfolded protein in osmolyte is due to the decreased solubility of the peptide backbone in a protecting osmolyte solution (*88*). Thermodynamically, the transfer of a peptide backbone from an aqueous to a water-osmolyte solution is unfavorable (Figure 1.5 above). The total interaction energy between protein and the solvent depends on the interaction between the solvent with the protein backbone and with the side chains. Since the peptide backbone represents the most abundant bonds in any protein, the solution thermodynamics of backbone interaction with osmolytes far exceeds the solubility preferences of osmolyte-variable side chain interactions. These unfavorable stabilizing osmolyte interactions with the peptide leads to both thermodynamic and kinetic preferences for burying the backbone of an initially unfolded protein, facilitating rapid and stable collapse to a stable structure.

The tendency of osmolytes to drive an unfolded protein towards a folded state has been utilized as a possible treatment strategy for partially unfolded proteins. For misfolded proteins, a protecting osmolyte can facilitate proper folding and prevent inappropriate aggregation from occurring. Additionally, since these osmolytes are physiological and naturally occurring molecules, it is possible that in some instances they could rescue proteins from misfolding without worrying about deleterious side effects. For example, trehalose administration was observed to diminish the formation of polyglutamine aggregates within transgenic mouse models of Huntington's disease (*89*). Proline has been utilized to prevent the aggregation and increase the activity of chicken liver fatty acid synthase, chicken egg lysozyme, and rabbit skeletal muscle creatine phosphokinase *in vitro* (*90*). *In vitro* studies using cellular systems has shown that glycerol administration leads to an increase in folding, proper trafficking and restoration of proper ion conductance of cystic fibrous transmembrane conductance regulator (CFTR) mutants

(*91*). These observations gave credible support to the idea that one can utilize small molecules to stabilize the fold of proteins, which, in turn, can act as a therapeutic agent for protein misfolding diseases. Unfortunately, osmolyte therapies are hampered by the realization that large concentrations (molar) are needed to obtain efficacy.

e Pharmacological chaperones.

Given that the process of favorable protein folding depends on its final free energy minimum, it has long been know that small molecules or biologicals can bind to the natively folded states of proteins to stabilize this low energy state. The free energy of simple ligand binding can actually shift the folding equilibrium towards a more stable, folded form. Similarly, "pharmacological chaperones" (this nomenclature has been adopted despite the fact that these are not proteins) are small molecules that can bind to a protein to stabilize it against unfolding and aggregation. This thermodynamic stabilization is illustrated in Figure 1.6. In this example, binding of small molecules to a dimer can stabilize the dimeric state relative to its monomeric, unfolded state. As discussed earlier, a native protein has lower free energy as compared to the unfolded protein. However, a mutant might have comparatively higher energy (less stable) thus increasing the likelihood of aggregation. Therefore, the binding of the small molecule to the transient but stable native form shifts the kinetic and thermodynamic stabilized forms toward a lower more stable free energy. In the case of a destabilized mutant (Figure 1.6), this binding restores the protein stability to its normal wild type free energy state. This binding results in depopulation of the aggregation prone monomer, decreasing the rate of aggregation.

Again, the realization that small molecules can restore the properly folded state originally came from studies involving CFTR with osmolytes (*91*). In this instance, the osmolytes could stabilize properly folded conformations, which in turn allowed the originally misfolded variants

to escape the quality control system. Increased stability of the properly folded protein leads to increased levels of functional protein.

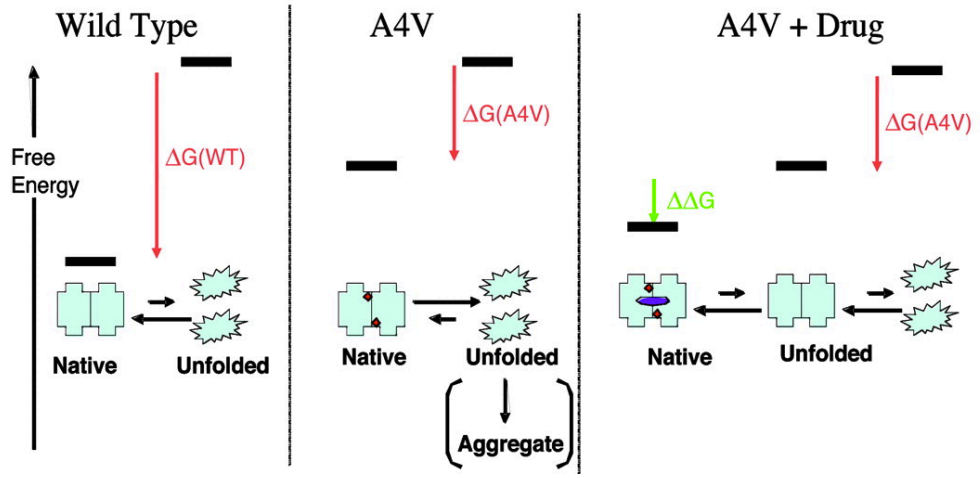

Figure 1.6: Binding of small molecules to the native state of a protein prone to misfolding decreases its relative free energy thus decreasing the rate of aggregation. Image sourced from (*92*)

Since osmolytes are not viable treatments, a very tractable therapeutic strategy that has been gaining recognition is the potential utilization of other small molecules. These small molecules can selectively bind to the mutant proteins that transiently populate native states, thereby stabilizing the fold and kinetically preventing these conformational mutants from populating their disease or aberrant non-native forms (Figure 1.7). An example of the successful utility of this small molecule pharmacological chaperones approach involves the stabilization of the multidrug resistant protein-1 (MDR-1) by capsaicin and vinblastine (*93*). In this instance as well as others, the ability of pharmacological chaperones to exert their effects on targeted protein substrates at physiologically acceptable concentrations makes them extremely attractive therapeutic candidates to treat various misfolding diseases. One of the most recent clinically

approved pharmacological chaperone is Tafamidis, which is involved in the folding rescue of mutant transthyretins involved in Type Familial Amyloid Polyneuropathy (TTR-FAP). Specifically, Tafamidis binds and stabilizes serum transthyretin tetrameric mutants, in turn preventing large-scale dissociation, aberrant amyloid formation and aggregation. (*94*). Tafamidis was discovered by *in silico* structure based drug design strategy. Unfortunately, this successful approach cannot be utilized for all diseases because the structures of the responsible proteins are often not known either in the non-mutated or the mutated variants (*92*). Fortunately, there are other generalized techniques that do not depend on the structural information to identify lead compounds that enhance specific protein stability. Some of the general screening approaches that are used to identify potential therapeutic stabilizers are discussed in the next section.

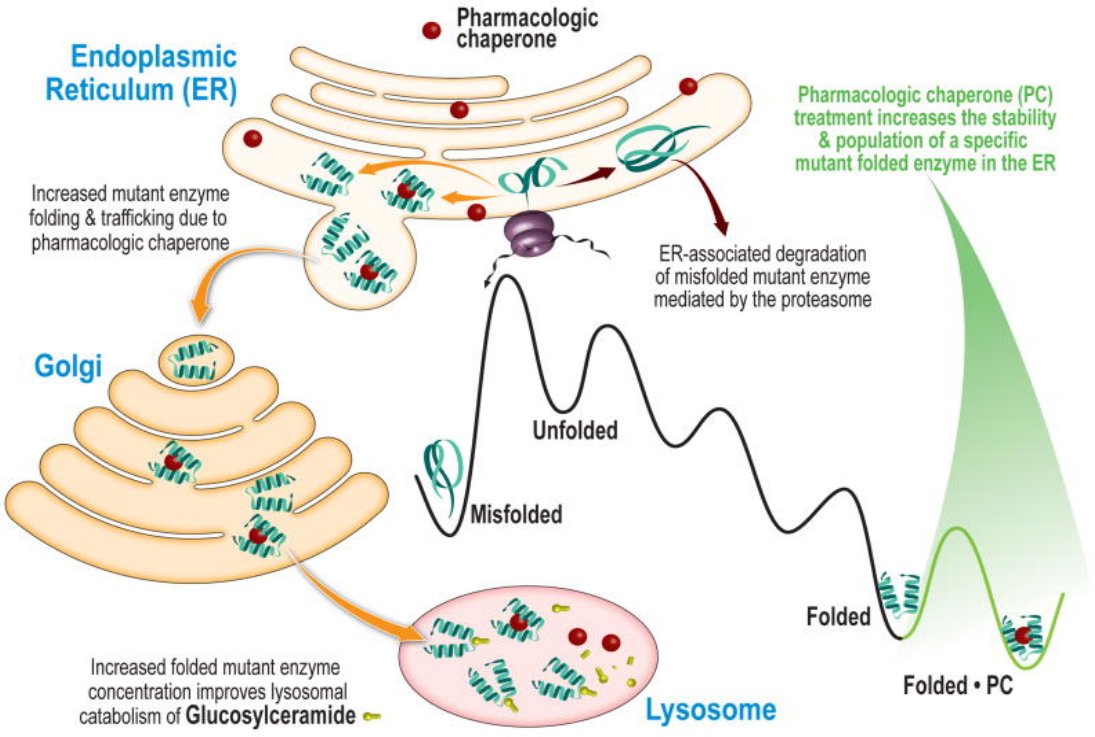

Figure 1.7: Pharmacological chaperones decreases the free energy of the ligand bound native state (Folded + PC) and thus shifts the dynamic equilibrium towards the folded state to increase the stability of the native folded state. Here the ligand stabilized native state of a

mutant protein such as the enzyme glucosylceramide can escape ER mediated degradation and undergoes increased folding and trafficking, leading to overall increase in the enzyme concentration. Image sourced from (*95*)

1.1.4 General (non-structural) approaches to search for potential pharmacological chaperones.

Using pharmacological chaperones to directly stabilize the native state of proteins and rescue misfolded proteins from degradation is an attractive proposition to treat protein misfolding diseases. The development of general *in vitro* screens for pharmacological chaperones can take advantage of large combinatorial chemistry platforms. Screening for misfolding diseases is, however, a problematic proposition because the assay (e.g. activity assays) has to be specifically designed for each misfolding disease protein. In addition, it is highly conceivable that in cases where multiple missense mutants can lead to the same folding disease, each missense mutation may require very specific individual pharmacological chaperones as opposed to the more favorable outcome where one global small pharmacological molecule can rescue all mutants. As mentioned previously, another problem of general assay design is encountered with protein folding diseases because the potential binding targets (misfolding proteins) for various misfolding diseases are in constant states of flux. The misfolding disease proteins exist in various conformational states that lead to the formation of aggregates are therefore moving targets rather than stable entities. The challenge for developing a broad based screen for folding diseases is that any test platform must be able to detect stabilizers that influence the kinetic behavior of the mutants in question. This section describes the most popular screening systems and detection methods that are available.

a ThermoFluor.

The ThermoFluor method utilizes a dye binding reaction to measure heat based perturbances in protein stability (*96*). The process involves the use of environmentally sensitive fluorescent dyes to follow the heat based unfolding of protein and determine the proteins melting point (Tm). Tm is defined as the apparent midpoint of a kinetically derived thermal melting curve and represents a temperature where the transient population of the native and non-native forms is equivalent. In this instance, the Tm is actually a kinetic parameter that depends on the heating rate. The best protein candidates that can be used for screening of stabilizers are those that show well behaved thermal transitions.

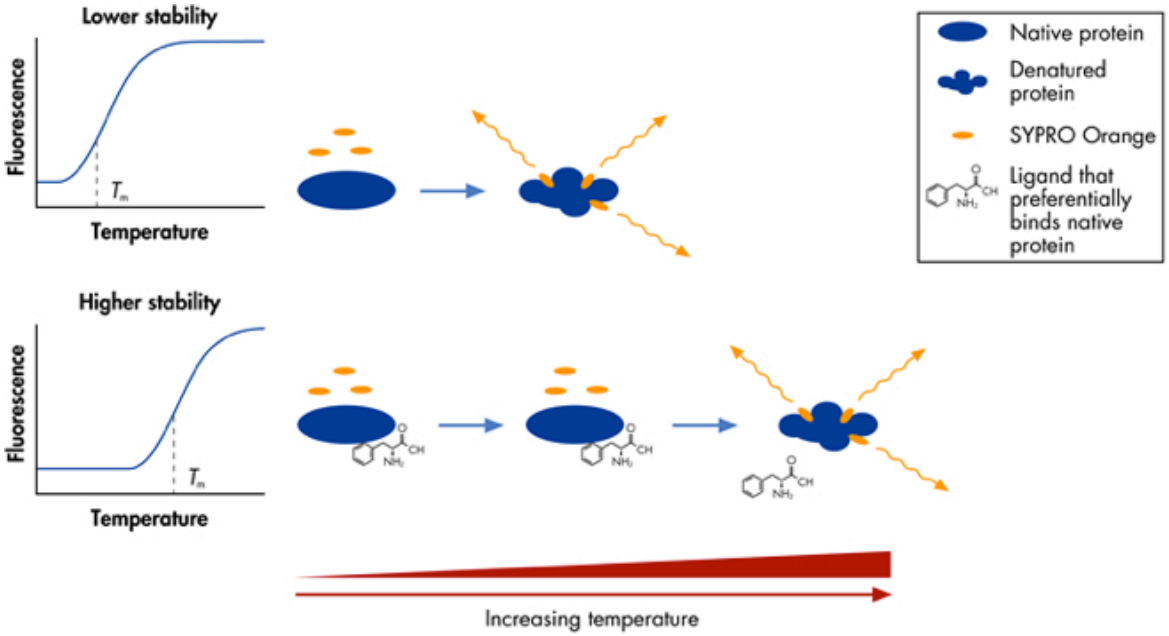

Figure 1.8: ThermoFluor utilizes hydrophobic dyes such as Sypro orange to follow the heat based unfolding of a protein alone (top panel A). In the presence of a stabilizer, the protein-ligand complex melts at a slightly higher temperature resulting in and apparent increase in the observed Tm. Adapted from (*97*).

ThermoFluor utilizes dyes such as 1-anilinonaphthalene-8-sulfonic acid (ANS) and Sypro Orange that are usually non-fluorescent in solution due to solvent quenching. After a portion of the protein unfolds during heating, the transiently exposed hydrophobic regions of the unfolding protein binds to these fluorescent dyes resulting in an increase in fluorescent signal due to an increase in the fluorescence quantum yield. In a high throughput screen set-up, the ThermoFluor instrument uses a high-resolution charge coupled device (CCD) camera to monitor transitions in a multiwell plate where each well contains the target protein, different test ligands and the reporter dye. As shown in Figure 1.8, as the entire plate is heated at a defined rate, the protein starts to unfold and the fluorescent signal gradually increases within each well. Within each well, one obtains a temperature dependent fluorescence intensity curve and the effects (or lack there-of) of the test ligand on the placement of the kinetic Tm position for each potential protein-ligand complex is determined. In wells in which a stabilizing ligand binds to the natively folded protein, the Tm shifts to a higher temperature. Typical ThermoFluor screening assays use approximately 0.5 mg of test protein in a 5 ml sample volume and a 384- well plate that can be thermally scanned in 90 min. The method is one of the commonly used high throughput methods to determine protein stabilizers and for the analysis of the thermal stability of mutant proteins. The advantages of ThermoFluor over classical thermal denaturation studies is the utilization of a common fluor (such as Sypro Orange), a large reduction in volume (each well utilizes less than 4 μl), and the ability to carry out measurements in high-density format. ThermoFluor can be also be used to identify potential stabilizing ligands for proteins whose functions are unknown or for which a functional assay is unavailable (*98*).

However, ThermoFluor has significant drawbacks that severely limit its use as a broad all-inclusive method to identify potential protein stabilizers. Unfortunately, this method works

best for protein systems that show thermodynamically reversible linear unfolding characteristics, i.e. the transition is smooth and the protein is well behaved. This method fails for proteins that aggregate at higher temperatures since the aggregation reaction itself typically leads to the burial of hydrophobic sites and thus prevents fluorescent dye binding, leading to a false positive result or an aberrant transition.

b Aggregation assays.

Proteins that misfold typically do so by transiently exposing their hydrophobic regions to solvent during the unfolding event. These transiently exposed hydrophobic regions drive aggregation and lead to an overall lower free energy state (Figure 1.3). This aggregation reaction is a function of the initial stability of the protein and kinetically depends on the collisional frequency, which in turn depends on the amount of unfolded protein that accumulates. As the protein concentration increases, aggregation increases proportionally. Given the large size of protein aggregates, this reaction can be easily measured utilizing various techniques such as light scattering, fluorescent dye binding or ultracentrifugation. Aggregation can thus be used as an indirect downstream measurement of protein stability. In the presence of a stabilizing ligand, one may observe that the aggregation reaction is delayed. Consequently, aggregation assays measure the aggregation propensity of proteins over time.

Unfortunately, some of these aggregation assays are slow in situations where the transition from folded form to partially folded form is rate limiting. It is not uncommon for some aggregation reactions to proceed at slow rates where completion can range from hours to days. Such extended time assays are naturally unsuitable for High throughput screening (HTS) studies. These types of slow transitions are typically encountered where stabilities of oligomers are tested. Alternatively, the proteins can bind to each other to bury the hydrophobic patches and lead to the

formation of small aggregates (dimers, tetramers, etc.). In this case, there still exists a misfolding and aggregation event that cannot be easily detected. In addition, the assay readout sometimes utilizes fluorescent dye binding assays or intrinsic fluorescence measurements. However, these measurements can be difficult to interpret since aggregation leads to increased light scattering, which interferes with fluorescence measurements. In addition to the time elements and the difficulties in obtaining reliable fluorescent signals, the test compounds themselves can interfere with the fluorescence analysis (both ThermoFluor and aggregation assays) (*99*). Given these various problems in assay development, one clearly needs a better system to evaluate and identify protein stabilizers for metastable misfolding disease proteins.

1.2 Introduction to using the GroEL Chaperonin as a detection platform.

1.2.1 Need for a platform that detects stabilizers for dynamic misfolding proteins.

To overcome the previously listed challenges, there is a need for a broad based assay platform that can rapidly screen for stabilizers of misfolding proteins. An optimal assay platform would be able to screen for stabilizers of metastable proteins at near physiological conditions and could also include oligomeric and membrane proteins. As with most high throughput protein stabilization assays, it would also be highly desirable if the efficacy of protein stabilizer candidates could be evaluated using small quantities of the protein. As an additional bonus, it would be valuable to be able to salvage the protein of interest after the assay is complete. This would be useful especially while screening hard-to-purify misfolding disease proteins. Most importantly, the best type of assay would evaluate the stability of the protein states that naturally exist in a dynamic equilibrium prior to larger scale unfolding and aggregation.

An assay platform that monitored the initial unfolding reaction was hypothesized to be a better strategy to search for pharmacological chaperones. We decided to utilize the broad binding property of the chaperonin to sequester partially unfolded proteins to develop a chaperone based screening platform. In the first series of proof-of-concept experiments, we will demonstrate that GroEL can capture transient folds and serve as an effective kinetic trap of the initially transient states as they appear under near physiological conditions.

1.2.2 Chaperonins and protein folding.

There are different chaperone systems such as the Hsp70 system, the Hsp60 chaperonins, Hsp90 system and Hsp100 systems that could be potentially utilized for the assay platform. However, the wide variation in binding affinities, the specificity requirements of co-chaperones with particular protein substrates and the smaller protein binding sites diminishes the

effectiveness for using the Hsp90, 100 and 70 classes of chaperones to capture dynamic protein folding states. This is not to say that these particular chaperone proteins will not be useful in capturing some specific proteins. However, the small size of the binding sites, and the reality that higher binding affinities may coincide with multi-protein functional states driven by ATP binding and hydrolysis complicates their use as a broad based screening system. In contrast, the binding site of the nucleotide free high affinity Hsp60 chaperones is large (~ 45 Å) making them attractive protein substrate capture states.

The Hsp60 chaperones (chaperonins) are comprised of two oligomeric rings that associate to form a large barrel like structure. Each ring contains homologous subunits with the inner ring surface of the rings forming a continuous binding surface. These chaperonins bind and momentarily sequester partially folded proteins and use ATP/ADP binding energies driven by hydrolysis to switch between strong and weak binding states, respectively. This produces a cycling system that can bind and release partially folded proteins. The primary role of the chaperonins is to prevent general protein aggregation. Chaperonin proteins are are found in virtually all organisms on earth. They are defined in two different classes.

a Group I chaperonins.

The most common chaperonin, the Group I class (alternatively known as Cpn60 or Hsp60), is predominantly found in prokaryotes, mitochondria and plastids. Structurally, they exist as homotetradecamers in two heptameric rings. They bind to a large variety of proteins via hydrophobic interactions. In eubacteria, these chaperonins are called the GroE chaperonin class. The GroE class consists of two proteins. The large tetradecamer is called GroEL. A smaller heptamer co-chaperone called Cpn10 (GroES in bacteria) is also required to modulate binding affinities of GroEL with partially folded proteins.

b Group II chaperonins.

The Group II chaperonins are found in the archaebacteria and in the eukaryotic cytosol. An example of this class is the eukaryotic chaperonin TCP-1 ring complex (TRiC). They contain 14-18 homo or heteromeric subunits per molecule. These subunits differ primarily in their amino acid sequence that defines the apical domain structure. They have a built-in lid segment protruding from each apical domain and hence do not require a separate co-chaperonin. TRiC is present in a lower concentration as compared to other heat shock proteins and requires the aid of an auxiliary cofactor (prefoldin or GimC) to form a complex with the substrate protein. This chaperonin protein lacks the promiscuous nature of binding to general hydrophobic proteins. This chaperonin preferentially binds more folded specific substrates like actin and tubulin through hydrophilic or charged residues. It has also been proposed that TRiC facilitates folding by a direct interaction with specific residues on the more folded substrate surface (*100, 101*).

1.2.3 GroEL is a molecular folding machine regulated by ATP hydrolysis.

The GroEL chaperonin was discovered by Costa Georgopoulos in the 1970s while studying temperature sensitive mutants of the bacteriophage tail spike protein. These proteins were observed to fold properly at lower temperatures, but aggregated at higher temperatures. The gene responsible for this phenotype was named *groE*. The gene products of this gene operon consists of two proteins, one called GroEL (L stands for large ~ 60 kDa/per subunit) and one is called GroES (S stands for small ~ 10 kDa/per subunit) (*102*). Later on, John Ellis found that ribulose-1,5-bisphosphate carboxylase oxygenase (rubisco), a chloroplast enzyme involved in carbon fixation via the Calvin cycle, copurified with a protein whose subunit molecular mass was also 60 kDa protein and called this the rubisco binding protein (*103*). The connection between GroEL and the rubisco binding protein was finally established via the cloning and

sequencing of RsuBP and of the GroE operon. The seminal experiment demonstrating GroEL function *in vitro* was done by Lorimer and colleagues, who found that purified *E. coli* GroEL and GroES binds and refolds a hard to fold bacterial dimeric rubisco with 80% efficacy (*104, 105*). Following this, it was demonstrated that GroEL alone binds protein folding intermediates, suppressing non-productive aggregation while improving the efficiency of protein folding. GroEL is absolutely essential for cell survival and GroEL deletion mutants or even lower expression of GroEL are lethal conditions (*106*). GroEL is essential for protein folding in *E coli* and the highly related mitochondrial Cpn60 class is absolutely essential for folding proteins that are imported into the mitochondria. A proteome wide analysis of folding in *E. coli* using immunoprepitation methods has demonstrated that the nucleotide free GroEL tightly binds (Kd < μM) to a wide variety of (250) intracellular proteins (*107*). Even with this large number of proteins, it appears that this immunopreciptation/mass spectroscopic analysis method may miss a larger portion of potential protein substrates.

a Structure.

The first high-resolution structure of GroEL was determined by Horwich and colleagues (*108*) (see Figure 1.7). The GroEL oligomer is a cylindrical structure with a diameter of 135 Å and length of 145 Å. Each molecule has two heptameric rings, with each 57 kDa subunit comprising of three different domains. The interior of the ring, composed of the apical domains is involved in substrate and GroES binding and the binding site is 45 Å in diameter. Each individual heptamer interacts with another heptamer in a tail-tail orientation through the equatorial domains and forms a tetradecameric cylindrical body. The ATP binding site is located in the equatorial domain facing towards the inside of the channel. The intermediate domain

forms a hinge between the other apical and equatorial domains and is important for allosteric communication (both positive and negative, details below) between the rings (*109*) (Figure 1.9).

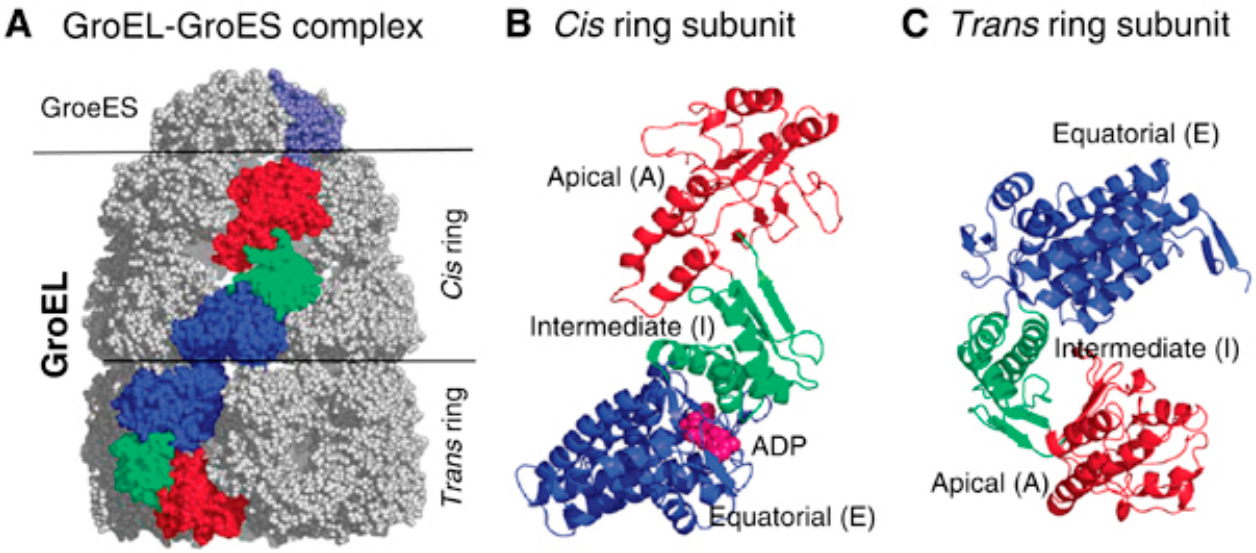

Figure 1.9: (A) GroEL tetradecameric cylindrical double barreled ring structure capped by the co-chaperonin GroES. (B & C) Each monomeric subunit consists of three different domains, apical (red), intermediate (green) and equatorial (blue). These domains differ in their conformation in the cis and trans ring due to substrate and ATP interactions. Figure sourced from (*110*).

b GroEL reaction cycle: Interaction and folding of protein substrates with the complete GroE chaperonin system (GroEL and GroES).

GroEL exerts its effect on non-native (misfolded) proteins that are released from ribosomes, Hsp70 chaperones, or those subjected to unfolding under stress conditions. In the presence of ATP, one of the heptameric rings of GroEL binds to the smaller partner protein, GroES. GroES is a 70 kDa heptameric (10 kDa monomers) structure that forms a GroEL-GroES capped nanostructured chamber (see Figure 1.10). GroES can bind to either end of GroEL but

the primary stoichiometry is one GroEL bound to one GroES (*111*). Thus, the primary working structure of the GroEL-GroES complex is an asymmetric complex, with one GroEL chamber capped with GroES, while the other binding site remains unoccupied due to negative cooperativity between binding sites (*112, 113*). GroES binding to GroEL leads to conformational change in the apical domain of the GroEL and an increase in the size of the central cavity that can accommodate non-native proteins of up to 60 kDa (*114*). In the absence of bound GroES, the GroEL heptamer binds to the hydrophobic regions on protein folding intermediates via its hydrophobic loop elements within the interior ring portion of the apical domains (*108*). This binding region was mapped using site directed mutagenesis. The location of mutations that modified substrate binding was mapped onto the structure of GroEL, defining the promiscuous hydrophobic binding site within the internal surface of the heptameric rings (*115*). Using isothermal calorimetry titration, heat capacity measurements of the protein-protein interactions between a protein substrate and GroEL determined that GroEL interacts with its substrates via hydrophobic interactions (*116*). This protein substrate can be partially folded intermediate or intermediates with secondary and tertiary structure elements (*117*).

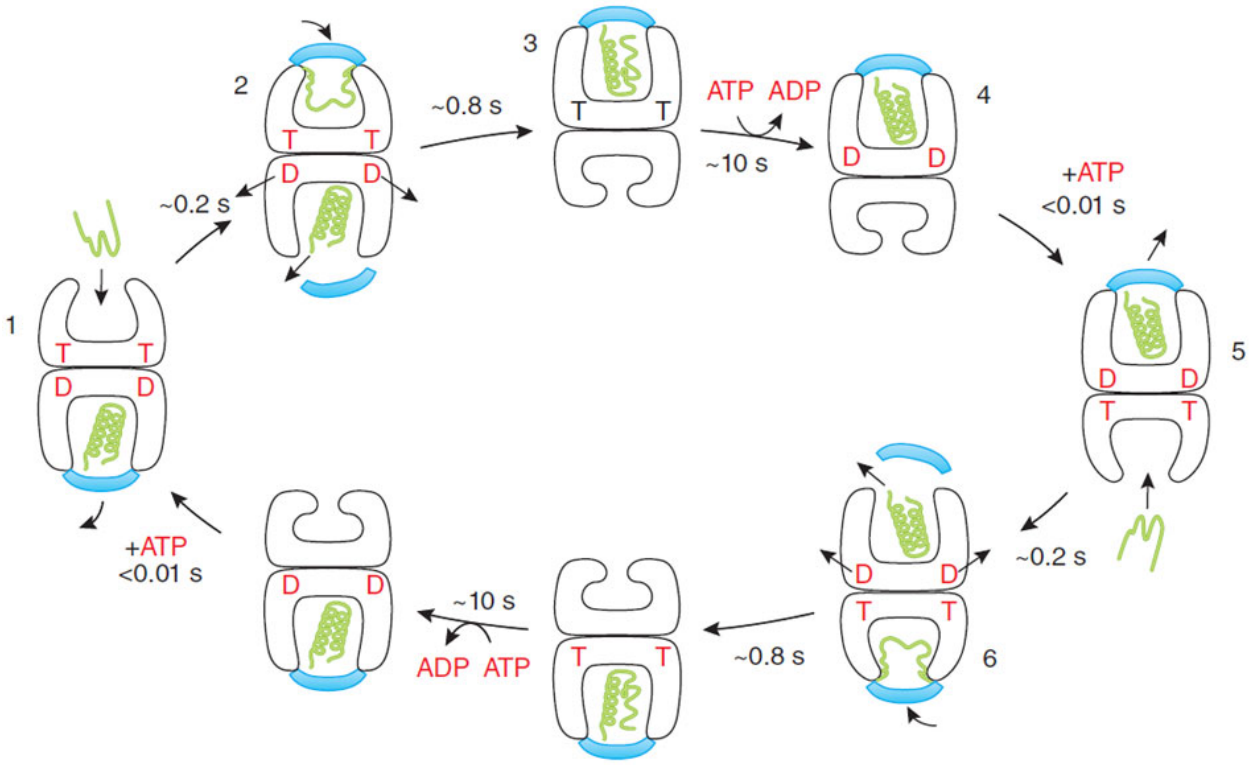

Figure 1.10: The GroEL reaction cycle with substrate in presence of GroES co-chaperone is regulated by ATP binding and hydrolysis. The red T and D symbols refer to bound ATP and ADP. Binding of the unfolded polypeptide (green squiggle) in step 1 is followed by GroES binding (step 2) and folding of the encapsulated folding. ATP hydrolysis (step 3-4) allows binding of ATP to the trans ring and the ejection of the polypeptide from the cis ring. A new folding cycle then starts on the trans ring. The numbers between the steps refers to the approximate time required for each step. Figure sourced from (*118*).

Substrate binding is regulated by ATP binding and hydrolysis at the equatorial domains. Seven ATP molecules are needed to bind to the equatorial domains per binding cycle. This ATP bound state has a lower affinity for partially folded proteins while the ADP and nucleotide free

states have substantially higher affinities for partially folded proteins (*119*). The binding of ATP to one ring inhibits simultaneous and equal ATP binding to the other ring via negative co-operativity effects as shown in Figure 1.10. This is the main reason why the dominant GroEL chaperonin states are asymmetric in character (*109*). Figure 1.10 demonstrates the various steps involved in the binding and release of substrate from GroEL. GroEL apical domain initially binds to the partially unfolded protein through hydrophobic as well as electrostatic interactions. Seven ATP molecules then bind to the equatorial domain ATP binding sites. The ATP binding causes a clockwise twisting of the intermediate domain by 25° towards the equatorial domain, closing the ATP binding site and positioning residues to facilitate easier hydrolysis. Simultaneously, the apical domain rotates 30° counterclockwise causing the exposure of the hydrophobic residues essential for GroES binding (*120, 121*). Further interaction with GroES also leads to a 50° upward and 120° degree clockwise rotation of the apical domain. As GroES caps the folding cavity, the substrate protein dissociates from the GroEL binding site and is encapsulated. This encapsulation expands the volume of the cavity from 85,000 $Å^3$ to 170,000 $Å^3$. It also changes the polarity of the central chamber from hydrophobic to highly hydrophilic with a net negative charge (*122*). Encapsulating the unfolded protein in the cavity leads to steric confinement thus preventing aggregation and helping the intermediates achieve native conformations (*123*). This model of folding is known as the Anfinsen cage model (*124*). The encapsulated protein is allowed to fold in this environment until ATP hydrolysis occurs in the cis-ring (approximately 10 seconds). Once released (detailed mechanism in next paragraph), the protein either proceeds towards the native fold or rebinds to GroEL if folding is incomplete and another round of chaperonin cycle ensues (*125*).

ATP hydrolysis within the protein occupied cis-ring causes several conformational changes in all three domains of the empty trans-ring. The equatorial domain rotates leading to upward movement of the apical domain (*126*). This rotation also leaves the nucleotide binding site open for the next cycle of ATP binding. The cis-ring, however, still has the substrate GroES and the ADP bound to it. ATP binding on the trans-ring leads to release of the substrates from the chamber of the cis-ring, along with the release of GroES and ADP. The steps during the release of the substrate are the reverse of what is observed during the encapsulation process i.e., the reduction of the volume and change in cavity surface to a hydrophobic nature. Thus, ATP hydrolysis regulates a dynamic cycle of substrate binding and release until folding occurs.

1.2.4 The nucleotide free GroEL tetradecamer as a protein capture platform for the chaperonin sink assay.

Although ATP hydrolysis is important in the release of the substrate, it does not play an important role in the binding to substrates. The ATP-free form of the chaperonin (which is generated during purification and is not widely existent in the cell), in fact binds to partially unfolded substrates with a high affinity and a very slow off rate, thus effectively capturing the transiently unfolded state. This ability of the nucleotide free high affinity form of GroEL to easily trap folding intermediates has led us to propose that this form of the GroEL chaperonin can be utilized to act as a general thermodynamic and kinetic sink. This efficient GroEL capture/partitioning reaction should enable one to probe the intrinsic dynamic equilibrium between folded and misfolded forms of a given substrate protein, thus allowing one to capture kinetically transient misfolded forms. Furthermore, since GroEL has a broad binding specificity towards a huge variety of substrate proteins, its ability to capture misfolded intermediates can be

used to screen for stabilizers for a wide variety of misfolded proteins that contribute to an array of diseases.

a Rationale.

In the late 80s, Gatenby and colleagues observed that the overexpression of GroEL suppressed mutations in several genes encoding diverse proteins (*127*). In this study, they used temperature sensitive mutants which had point mutations in the *his* operon of *E. coli*, which is essential for growth in media deficient in histadine. The mutants with normal levels of GroEL were observed to be thermosensitive at 37^{o}C. On the other hand, GroEL overexpression constructs containing *his* mutants were observed to survive heat shock. This result led the authors to suggest that GroEL directly interacts with mutant proteins allowing these mutant proteins to achieve their final fold. This temperature sensitivity is a hallmark of misfolding diseases as was observed with CFTR.

In another landmark study, Lorimer and colleagues observed that incubating the high affinity nucleotide free GroEL with the native form of dihydrofolate reductase (DHFR) resulted in a time dependent decrease in the DHFR activity and a concomitant decrease in free DHFR concentration (*128*). Once ATP is added to the chaperonin, DHFR activity returns, indicating that the missing DHFR activity and protein was bound to GroEL. Further experimentation showed that the loss of activity was slow and this activity loss was prevented when DHFR substrates such as dihydrofolic acid or nicotinamide adenine dinucleotide phosphate (NADPH) were present. The recovery of DHFR activity following ATP addition is a hallmark of GroEL binding to the partially unfolded states of DHFR, that are in equilibrium with native populations. Thus, transiently unfolded intermediates were shown to partition from their natively folded states onto GroEL, provided that this native state is in a dynamic equilibrium with the unfolded

transient states. This observation was important to this dissertation as it demonstrated that one can utilize GroEL to selectively bind to partially unfolded intermediates of proteins as they kinetically appear; a ligand stabilized native form no longer shows appreciable partitioning and binding.

The range of proteins that GroEL interacts with *in vivo* was initially thought to be not more than 5% of all *E. coli* proteins (*129*). However, Horwich and colleagues have shown that GroEL may interact with a huge array of protein substrates (*130*). They used a temperature sensitive E461K point mutant of GroEL, which is associated with the loss of allosteric communication both within and between rings. At non-permissive temperatures, long-range ATP induced binding changes are no longer transmitted within both the subunit and within each ring (loss of allosteric communication), resulting in a state that tightly binds protein substrates but can no longer release them. As a result, all of the GroEL can no longer cycle to its low affinity protein releasing state after a rapid temperature upshift. In particular, the E461K mutant fails to release the bound substrate, thus behaving as an *in vivo* polypeptide "trap". At these non-permissive temperatures, the rapid inhibition of the cellular GroEL results in massive aggregation and precipitation of wide range of *E. coli* proteins. This suggests that GroEL is directly or indirectly involved in maintaining the solubility of a wide range of proteins. The precipitated protein mass was subjected to MUDPIT proteomic analysis. The paper lists 330 different proteins. The authors note that they stopped identifying proteins because there were too many of them. It was observed that the precipitated protein masses contained a wide variety of proteins including metabolic, stress, ribosome proteins, DNA transcription proteins, as well as a large number of membrane proteins. Since GroEL can bind multiple aggregation prone proteins both *in vitro* and *in vivo*, it is apparent that GroEL can serve as a general binding platform for a

wide array of proteins and will be useful as a screening tool to catch protein transients that result from misfolding diseases.

b Hypothesis.

The above data lead to the hypothesis that **one can utilize the ability of the high affinity form of the GroEL chaperonin to act as a general thermodynamic and kinetic sink to capture the transient misfolded forms of proteins that are prone to misfolding.** It is also predicted that general hydrophobic binding properties will enable one to develop a broad platform to rapidly screen for specific stabilizers for a wide variety of protein misfolding diseases. In the subsequent chapters, the experimental support for this hypothesis and the process of development and validation of the chaperonin sink assay will be discussed.

CHAPTER 2: DEMONSTRATING PROOF-OF-PRINCIPLE FOR THE CHAPERONIN SINK ASSAY

a On the advantages of using the GroEL chaperonin.

The nucleotide free form of GroEL is known to bind proteins that transiently expose hydrophobic surfaces even in reactions where these transient intermediates are in rapid equilibrium with the native fold (*128, 131*). GroEL can be thought of as a ‘‘promiscuous antibody’’ that binds to non-native folding intermediates (defined epitope) with high affinity (sometimes approaching antibody/antigen interactions) (*132*) as hydrophobic surfaces are exposed to the aqueous environment. This makes GroEL an excellent tool to kinetically partition (capture) transient partially folded intermediates as they form folded populations. It is these transient forms that often lead to the development of protein misfolding diseases (*68*). The advantage of directly capturing transient forms as they form allows one to rapidly monitor initial unfolding reactions rather than waiting for downstream accumulation of aggregation prone intermediates. In addition, one can control this kinetic partitioning reaction, allowing one to speed up the assay so that partitioning can occur in the time span of minutes, rather than depending on slower complete unfolding reactions and downstream aggregations. The kinetics of partitioning follows pseudo first order reaction because the reaction depends on the transient concentrations of the partially unfolded species and GroEL. More specifically, with GroEL concentrations in vast excess to the concentration of the rapidly interconverting population of newly formed transient species, as the GroEL concentration increases, a limiting partitioning rate is likely to be reached. This would be the result of the rate limiting step involved in the dynamic interconversion between the folded and transiently folded forms (see (*131*) for example).

Additionally, GroEL is a stable heat shock protein so that it can be utilized at slightly elevated temperatures (~40-45ºC) to speed up the kinetics of unfolding and hence partitioning. Since GroEL binding mimics general hydrophobic driven *in vivo* chaperone interactions, pharmacological chaperones that stabilize the misfolding protein in the presence of GroEL, may also prevent partitioning onto intracellular chaperones, ultimately leading to improved protein expression during later clinical trials. All these factors make GroEL an extremely attractive option to be utilized in the development of a broad based platform to rapidly screen for stabilizers of proteins that tend to misfold.

In this chapter, experimental evidence that supports the hypothesis that the chaperonin can be used to probe the dynamic folding state of a protein and to search for protein folding stabilizers has been demonstrated. To accomplish this, the feasibility of the system was initially demonstrated with model proteins. Here, DHFR was used as a model substrate along with its intrinsic protein stabilizer, NADPH, to investigate the partitioning and refolding from the GroEL chaperonin. This was followed by demonstrating that the GroEL chaperonin sink can be used to screen for stabilizing conditions of two different disease proteins, the cystic fibrosis transmembrane conductance regulator nucleotide binding domain (CFTR-NBD1) and the iron binding protein frataxin, which is involved in Friedrich's ataxia.

b On the form of the chaperonin best suited for the assay.

In these first sets of experiments, the partitioning of partially folded proteins onto GroEL was examined by determining the time dependent loss of soluble protein in solution. To easily quantify the amount of soluble native (folded) protein at various time points and to obtain an accurate quantification of the amount of protein that has partitioned onto GroEL, it was essential to be able to rapidly separate the substrate protein from the soluble non-partitioned substrate

protein. This is based on the observation that the substrate protein dissociates very slowly from the high affinity nucleotide free GroEL chaperonin. There are different modes of rapidly separating GroEL-protein substrate complexes from soluble remaining protein substrate. In one method, the separation of the chaperonin from the native substrate protein can be carried out by using ultrafiltration to separate high molecular weight (800 kDa) GroEL (oligomer) from the substrate protein. In a second method, one can directly examine the loss of soluble substrate protein as a function of time as the dynamically fluctuating protein is incubated with immobilized GroEL Sepharose beads. In this latter case, these beads can be rapidly removed from solution by centrifugation. The remaining protein in solution can then be quantitated.

In the first instance tested, there were some drawbacks using the ultrafiltration centrifugation method. Ultrafiltration (100 kDa MW cutoff) can separate large complexes from smaller proteins. In principle, any protein that does not partition onto the GroEL flows through an ultrafiltration membrane and is captured in a filtration cup. The remaining larger complexes (GroEL and GroEL substrate complexes) are retained in the retentate cup. Unfortunately this first method encountered procedural problems beyond our control. Specifically, when the protein samples within the filtrate cup were subjected to high pressure liquid chromatography (HPLC) size exclusion chromatographic analysis to detect substrate protein flow through, in some instances, GroEL tetradecamer (802 kDa) was also detected. This indicated that the chaperonin could leak through the ultrafiltration membrane even though the MW cutoff was 100 kDa. From the accumulated data, we found that the failure rate of the ultrafiltration membrane exceeded manufacture specifications (Amicon, Pall and Millipore ultrafiltrators). Manufacturer specifications were listed at a less than 5% failure rate while we noted that this rate was much higher (~20%).

On the other hand, the immobilized GroEL beads method was found to be superior to using free GroEL. With the immobilized GroEL Sepharose bead system it was possible to assay the soluble protein faster due to the easy and more rapid separation by simply spinning down the beads, which contain GroEL and the partitioned protein. This method of separation also lends itself to be more amenable to scale-up and automation of the screening system. The screening can be performed in multiwell plates into which a fixed quantity of beads has been incubated with the partially folded protein. The beads can then be easily separated from the free protein in solution, which can be rapidly quantified. Another advantage of using GroEL beads is that they could be regenerated by treating them with a mixture of ATP and glycerol. On regeneration, the substrate is released from the chaperonin on the beads and the beads can then be reused. Hence, one of the initial decisions was to utilize GroEL beads instead of free GroEL in the chaperonin assay to monitor the time dependent loss of substrate protein during the partitioning reactions.

2.1. Part 1: Demonstrating the proof-of-principle for the partitioning assay utilizing a model substrate dihydrofolate reductase (DHFR).

2.1.1 On the use of DHFR as a model substrate protein for assay development.

Any assay development involves the optimization of assay parameters. The principal components in the chaperonin assay were GroEL and the substrate protein, and the secondary components were the pH-adjusted buffers, temperature and other physicochemical parameters. While optimizing the principal component i.e., the substrate protein, a disease protein was an ideal substrate. However, these are usually difficult to purify and in short supply. Therefore, the assay conditions were optimized using a test substrate protein that was easily available and was known to dynamically partition onto GroEL. It is also predicted that utilizing a monomeric substrate will be useful to monitor refolding without depending on complications of oligomer formation. One such monomeric substrate that dynamically partitions onto GroEL from its monomeric state is DHFR (*108, 133*). As mentioned in the chapter 1, DHFR was also the first protein whose partitioning onto GroEL was documented from an originally folded substrate (*128, 133*). It is an essential enzyme that converts 7,8-dihydrofolate (DHF) to 5,6,7,8, tetrahydrofolate (THF) in the presence of the reduced form of NADPH. The binding of the cofactor NADPH has also been shown to carry out a large increase in the thermodynamic stability of the protein causing a shift in the transition midpoint of urea induced unfolding from 1.4 M urea to 2.8 M urea. More important for our assay development is the observation that NADPH stabilized DHFR no longer partitions onto the chaperonin at physiological temperatures and conditions (*128*). It was hence predicted that DHFR could be utilized as a model protein to initially

demonstrate proof-of-principle for the chaperonin assay. DHFR could also be utilized to develop and validate assay conditions, platforms and high throughput array systems. Additionally, one can either monitor the loss in DHFR protein concentration or its activity to measure partitioning rates. The return of DHFR activity after ATP addition demonstrates that the protein did indeed partition onto GroEL.

2.1.2 Materials and methods.

a Materials.

DHFR was obtained from Sigma. The nucleotide high affinity form of GroEL was produced and purified in the lab (*134*). N-hydroxysuccinimide (NHS)-activated Sepharose fast flow beads were obtained from GE Healthcare. All other chemicals and reagents were of the highest available purity and obtained from standard sources.

b Preparation and validation of GroEL beads.

GroEL beads were generated using the nucleotide free form of the chaperonin and NHS-Sepharose fast flow beads. The beads were initially cleaned by washing with two column volumes of methanol and three column volumes of 1 mM HCl. The cleaned beads were then further treated with five column volumes of coupling buffer (0.2 M $NaHCO_3$, 0.5 M NaCl, pH 8.3) to activate the NHS ester. The activated beads were incubated with the nucleotide free GroEL in the amine free coupling buffer at a volumetric ratio of 1 (GroEL oligomers): 2 (beads wet volume) to covalently couple the chaperonin to the beads via the NHS ester. These were mixed for 3 hours at room temperature under continuous mixing via a rotating shaker. After 3 hrs., GroEL not bound on beads was recovered by collecting filtrate from beads. The beads were then sequentially washed with two column volumes of refolding buffer (50 mM TRIS, 50 mM

KCl, 10 mM $MgCl_2$. 0.5 mM EDTA) pH 8, refolding buffer pH 6 and regeneration buffer (refolding buffer with 100 mM Dithiothreitol (DTT), pH 7.5). The beads were then finally washed with three column volumes of refolding buffer pH 7.5 to obtain the GroEL loaded beads.

The GroEL concentration on the beads was determined from the labeling efficiency and wet bead volumes. The labeling efficiency was determined by measuring the difference in GroEL concentration prior to and after incubation with the beads. The wet bead volume was calculated by measuring the total void volume of the wet beads. Specifically, a fraction of the wet beads was centrifuged to dryness in a spin column (Pierce) and the buffer collected. The volume of this buffer was indicative of the void volume of the beads. This void volume in conjunction with the difference in the GroEL concentration prior to and after incubation with the activated NHS-Sepharose beads allowed us to reasonably estimate the concentration of GroEL bound to the beads. This concentration is however not an absolute value, but an estimate of the protein immobilized on the beads.

$$Approximate\ GroEL\ conc.on\ the\ beads = \frac{Initial\ GroEL\ conc. - Final\ GroEL\ conc.}{Void\ volume}$$

The beads were also tested for leaching of the bound GroEL. The beads were stored at 4^{o}C and periodically the supernatant buffer was analyzed for the presence of GroEL by both Ultraviolet (UV) spectroscopy as well as by HPLC. No leaching was observed over a period of 2 months of bead storage indicating that the covalently immobilized GroEL maintains its integrity on the beads.

c Carrying out chaperonin sink screening assay/GroEL partitioning assay with DHFR.

A diagrammatic representation of the protocol for the partitioning assay is shown in Figure 2.1. The GroEL beads generated by the method detailed in section b were incubated with DHFR in a silanized microcentrifuge tube in a 2:1 ratio. This reaction mixture containing DHFR

and the GroEL beads was incubated at either room temperature or at 37°C. To ensure adequate mixing, samples were continuously rotated slowly using a rotary mixer. The rotary mixer was chosen because this method ensures proper mixing and mass transfer. Other mixing methods involving vibrating shakers or orbital shakers were not found to be helpful in ensuring proper mixing.

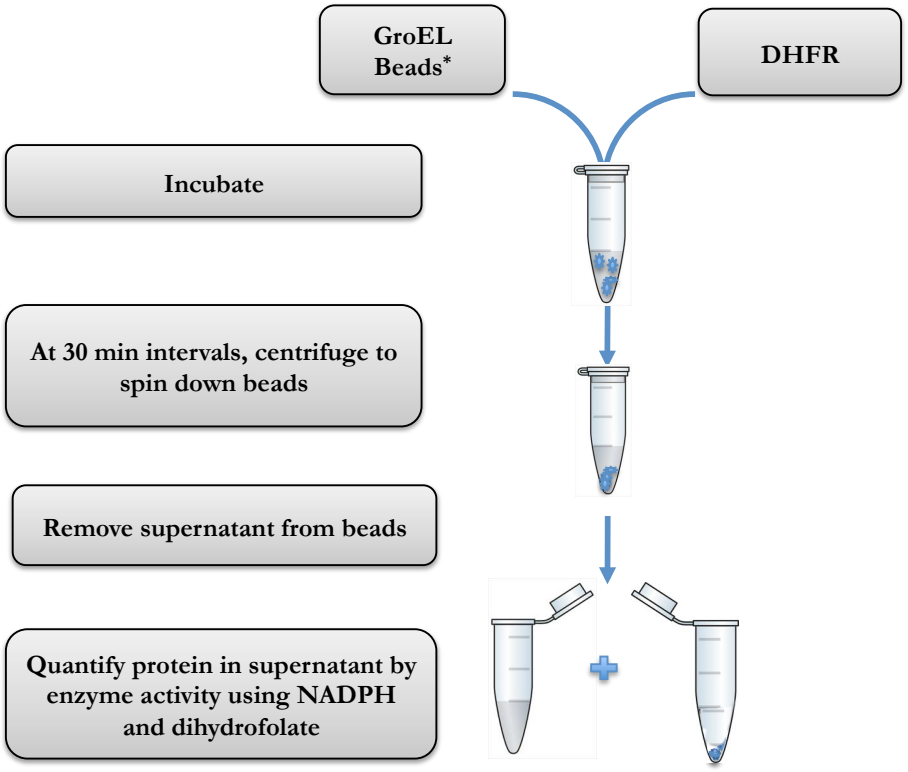

Figure 2.1: The experimental methodology to carry out partitioning experiments with chaperonin beads involves incubating the beads with the substrate protein. The loss of soluble native protein from the reaction mixture could be followed by spinning the mixture down to obtain the supernatant. This could then be assayed for protein concentration by various protein quantification techniques such as UV-visiable spectroscopy, SDS-PAGE, etc.

At periodic intervals, the GroEL bead-DHFR reaction mixture was spun down for 10 seconds at 1500xg so that the GroEL beads would sediment at the bottom of the centrifuge tube. Taking care that the bed of the beads at the bottom was not disturbed, an aliquot of the supernatant was removed and assayed for protein concentration. This quantification can be carried out using UV absorption spectroscopy (A_{280}), fluorescence spectroscopy, and/or SDS-PAGE. With DHFR, measuring the enzymatic activity is a good approach as it allows one to measure the concentration of the free native DHFR in solution. The DHFR that is unfolded or aggregated would not show any enzymatic activity. Plotting the protein concentration as a function of time gave the partitioning kinetic profile for the sample. Control experiments were run where DHFR was incubated with blank Sepharose beads.

d Measuring the enzymatic activity of DHFR.

The DHFR enzyme catalyzes the reduction of dihydrofolate to tetrahydrofolate while utilizing NADPH as a cofactor. DHFR enzymatic activity was assayed by following the decrease in the UV absorbance of NADPH at 340 nm in the presence of dihydrofolic acid (DHF) (*133*). 100 µl of substrate mixture was generated by combining DHF with NADPH to obtain final concentration of 7 µM DHF and 5 µM NADPH. 10 µl of the DHFR containing supernatant was then combined with the assay mixture to a final volume of 100 µl. The absorbance of this solution was then monitored at 340 nm for 60 seconds and the consistently linear decrease in absorbance was measured, denoting the presence of active DHFR. This decrease in NADPH absorbance was expected to be proportional to the concentration of active DHFR in the solution.

2.1.3 Results and discussion.

a On the suitability of DHFR as a model substrate protein for assay optimization.

The chaperonin platform can be utilized for virtually any protein that undergoes a dynamic folding ⇄ unfolding transition. These transitions are common to most if not all mesophilic (normal temperature) proteins, when a small amount of partially folded population is generated by physically perturbing the equilibrium under a variety of mild solution conditions. This system will work with natively folded proteins as well as specific missense disease proteins. To demonstrate this, the partitioning of the test protein DHFR with GroEL beads was carried out. The goal of these partitioning experiments was to demonstrate that we could utilize DHFR as a test substrate for further optimization studies and to demonstrate that a ligand based stabilization of DHFR could be detected utilizing the chaperonin sink assay. It had previously been reported in the literature that GroEL sequesters DHFR within its central cavity (*117*). DHFR was incubated with immobilized GroEL and a decrease in DHFR activity was observed (Figure 2.2). Blank Sepharose beads (no GroEL control) were used as the control. It was observed that the decrease in DHFR concentration was faster in the presence of the GroEL beads as compared to the blank beads. The decrease in the DHFR concentration in the blank beads might be due to thermal inactivation of DHFR or its aggregation and subsequent spin down with the beads.

As discussed previously, the transient partially unfolded form of DHFR is what partitions onto GroEL. To generate this transient form, DHFR needs to be perturbed slightly, such that the equilibrium of

$$(DHFR)_f \rightleftarrows (DHFR)_{pf}$$

is shifted towards the transient partially unfolded species. This equilibrium shift can be achieved by using mild denaturation conditions such as temperature, detergents, and/or chaotropic osmolytes. In this instance, 1M urea (at 25ºC or room temperature) was included in the reaction mixture to achieve the desired equilibrium shift

$$(DHFR)_f \rightleftarrows (DHFR)_{pf}$$

and observe if the mild destabilizing effect of the chaotropic agent affected the partitioning rate. It was predicted that this solution should increase the generation of the transient species and thus increase the overall DHFR partitioning rate onto GroEL (GroEL remains active in its tetradecameric state in the presence of 1M urea). This in turn was expected speed up the partitioning reaction cycle. It was observed that partitioning was faster in the presence of urea (Figure 2.2, filled squares). This observation supports our hypothesis that slight perturbation of the native species leads to the generation of transiently unfolded species, which can be recognized by GroEL. This observation also demonstrates that mild denaturation conditions can be used to perturb and shift the equilibrium towards non-native species. This aspect of being able to modulate the equilibrium is especially useful in exploring the partitioning conditions for stable mesophilic proteins representing the baseline prior to identify stabilizing condition for such proteins.

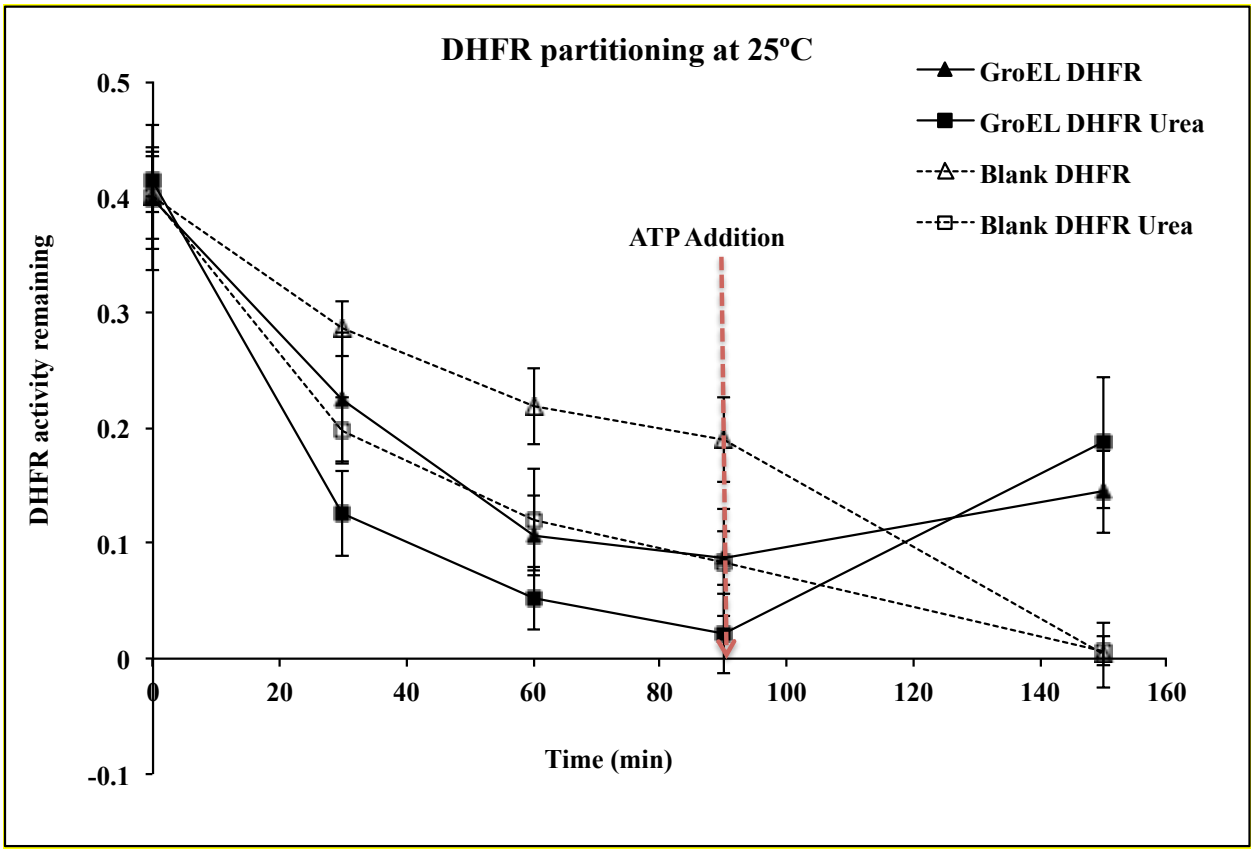

Figure 2.2: The chaperonin sink assay was utilized to follow DHFR partitioning and refolding from GroEL beads at room temperature. It can be observed that urea denatured DHFR partitions onto the chaperonin beads (filled squares) at a higher rate than DHFR alone (filled triangles). DHFR concentration was also observed to decrease at a higher rate in the presence of the chaperonin beads (filled points) than the control beads (open points). To ensure that the decrease in concentration was due to the partitioning of DHFR onto the GroEL beads, 10 mM ATP was added to the beads. The addition of ATP causes refolding only from the chaperonin beads and not from the control beads.

In both the presence and absence of urea, it is observed that at the end of 90 min., the DHFR activity is nearly zero. This indicated that DHFR in the reaction mixture had undergone

inactivation by denaturation or had partitioned onto GroEL. To determine which of these two options occurred, the beads were extracted and resuspended in a mixture containing 10 mM ATP and 4 M glycerol. It has been frequently observed that this mixture can be used to refold any protein that has partitioned onto GroEL. Usually the folding reaction for GroEL requires the presence of a co-chaperone GroES. However, in our laboratory, the presence of 4 M glycerol has been observed to abrogate the necessity of utilizing GroES. If a protein partitioned onto the GroEL immobilized on the bead support, the release and refolding of substrate protein after ATP/glycerol addition is indicative of GroEL capture. In contrast, DHFR protein that was not successfully captured by GroEL would undergo aggregation or heat denaturation and does not fold or refolds with very low efficiency. Refolding appears to occur in the presence of GroEL beads alone, validating the capture and refolding from the GroEL platform. Incidentally, this assay is used to verify and validate GroEL function each time GroEL beads are synthesized.

The rate of formation of the transiently unfolded species is accelerated with increasing temperature. As noted with 1 M urea, one prediction is that the partitioning rate of a substrate protein onto GroEL will increase as the temperature of the solution is increased. The partitioning assay carried out at the physiologically relevant temperature of 37°C (Figure 2.3) revealed that the DHFR partitioned onto GroEL beads at faster rates than the control (blank beads). It was also observed that partitioning occurred at a faster rate than what was observed at 25°C (Figure 2.2). The limited kinetic time points that were used does not allow one to distinguish any differences between partitioning in the presence and absence of 1 M urea. To determine any earlier partitioning rate differences it may be necessary to measure partitioning at timepoints earlier than ten min.

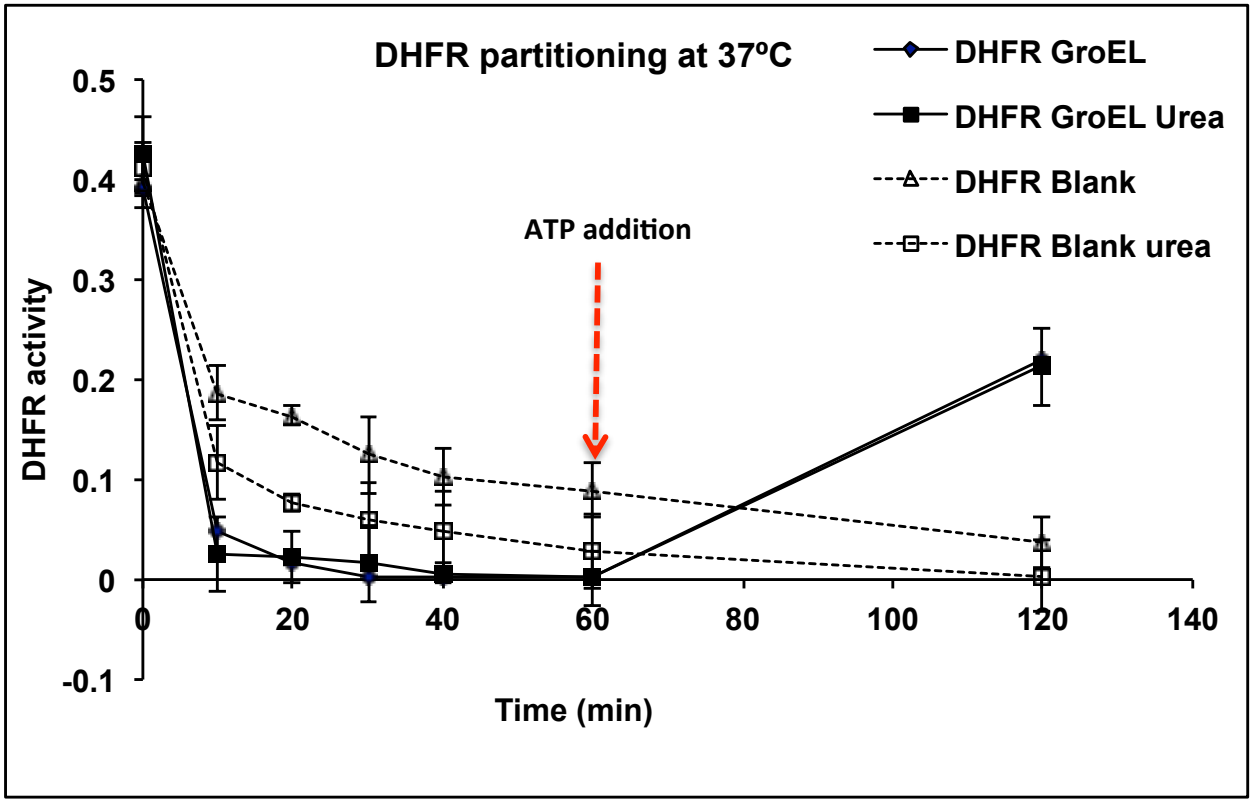

Figure 2.3: Following the partitioning of DHFR onto GroEL beads at 37ºC. Increasing the reaction temperature increased the partitioning of DHFR onto GroEL beads (filled data points) as compared to the blank control beads (open data points). DHFR was incubated with GroEL beads in the presence (filled squares) or absence or urea (filled diamonds). In both cases, DHFR activity associated with the native protein was observed to decrease rapidly. This decrease, also observed in control beads, was predicted to be due to heat inactivation. To distinguish between partitioning and heat inactivation, the beads were treated with a mixture of ATP-glycerol that helps refold any partitioned protein. The GroEL beads showed refolding of DHFR while the control beads did not show any regain in activity, confirming heat inactivation. The experiments were repeated in triplicate.

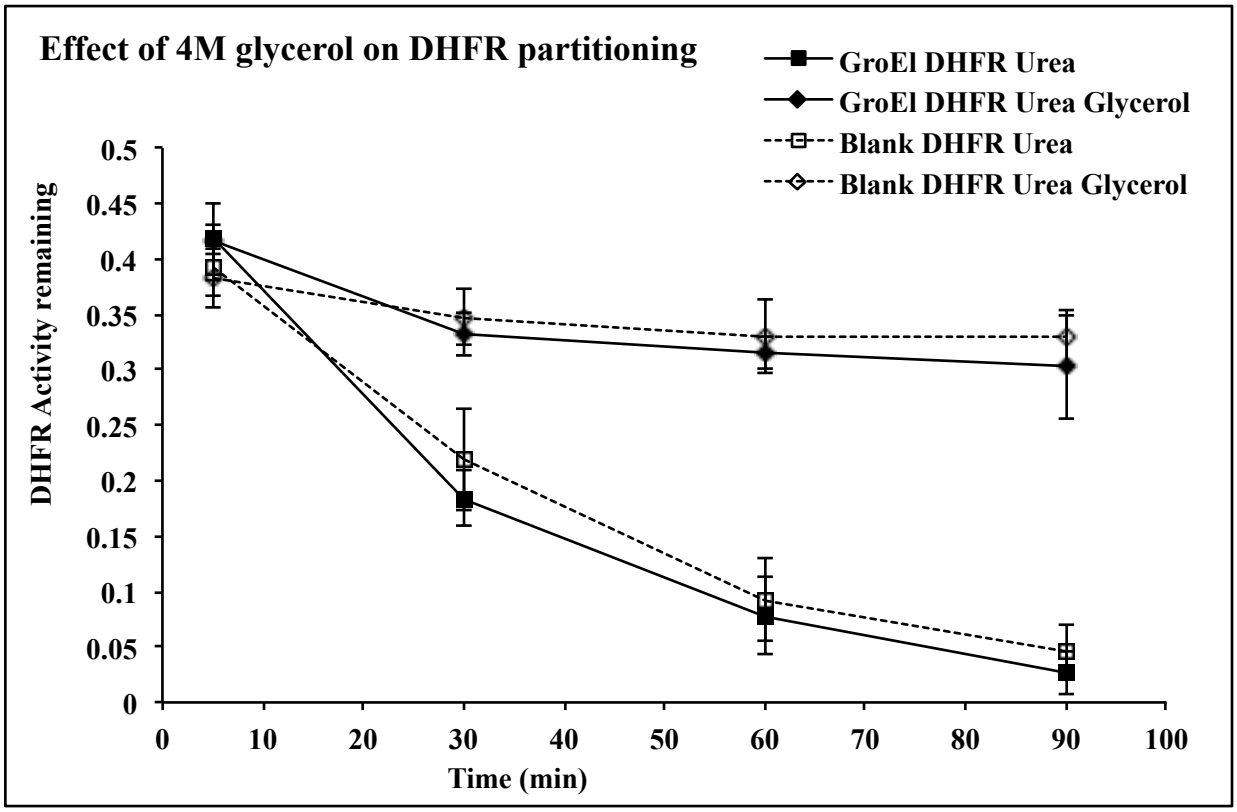

Figure 2.4: Glycerol prevents loss of DHFR activity in the presence of GroEL beads (filled diamonds) as well as the control beads (open diamonds) indicating stabilization of DHFR native state. DHFR incubated with GroEL beads in the presence of urea and 4M glycerol (filled diamonds) shows that the activity was maintained over 90 min., while without the osmolyte (filled squares), the activity rapidly decreased. The experiments were carried out in triplicate with duplicates of each time point assayed for activity.

Given the demonstration that partially unfolded species partitions onto immobilized GroEL, the next step in assay development was to demonstrate that the introduction of an authentic stabilizing ligand will prevent or diminish the partitioning rates of initially folded DHFR binding onto the immobilized chaperonin bead supports. As discussed in chapter 2, osmolytes can also be used to stabilize the native state of a protein and decrease the populations

of partial unfolding forms. The most common folding osmolyte that was tested was glycerol. At 4 M glycerol concentrations (normal cryoprotectant concentration of the wood frog) partitioning of DHFR was diminished and activity of the DHFR remained high. This indicates that glycerol stabilizes the DHFR protein in its functional state and prevents its general unfolding (Figure 2.4). This stabilization was also found to occur both in the presence of 1M urea and at elevated temperature. Since both these conditions favor the formation of non-native species, this indicated that it was possible to stabilize the native form of the protein.

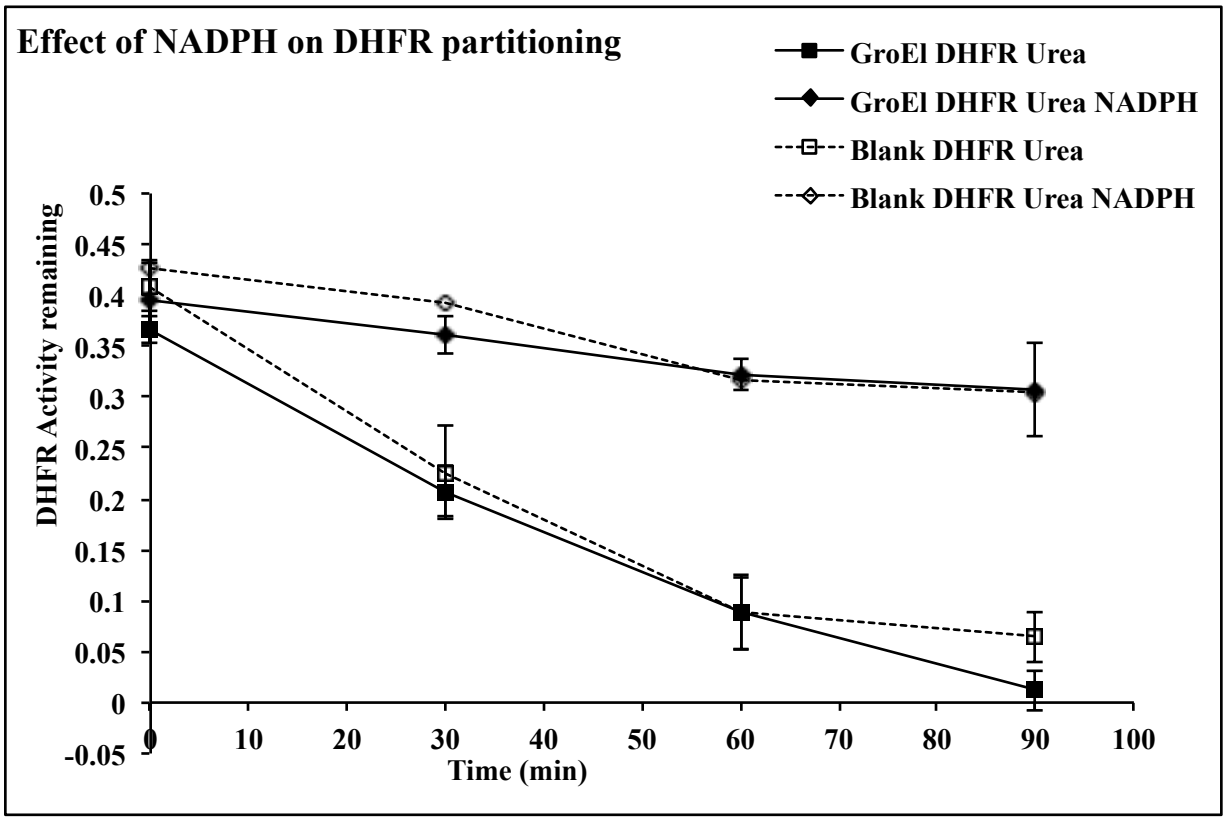

Figure 2.5: A small molecule ligand NADPH that binds to the DHFR native state stabilizes the protein as shown by a decrease in loss of DHFR activity in the presence of GroEL beads (filled diamonds) as well as the control beads (open diamonds). DHFR incubated with GroEL beads in the presence of urea and 5 mM NADPH (filled diamonds)

shows the activity was maintained over 90 min., while without the osmolyte (filled square), the activity rapidly decreased. The experiments were carried out in triplicate with duplicates of each time point assayed for activity.

It has been documented that small molecule ligands of proteins bind preferentially to the natively folded state and stabilize this state. For example, biotin increases the thermostability of streptavidin and prevents its general unfolding while maintaining structural order (*135*). DHF and NADPH are small molecule ligands that bind to DHFR. Similarly, methotrexate is another molecule that binds to native DHFR (*136*). In the case of methotrexate, this compound is a competitive inhibitor that binds to the NADPH binding site with very high affinity. Although this compound will also stabilize DHFR, the competitive inhibition of DHFR with methotrexate was expected to nullify DHFR activity assayed with NADPH. To demonstrate proof-of-principle ligand stabilization and prevention of partitioning onto GroEL, NADPH was utilized. In the presence of 5 mM NADPH, DHFR essentially shows very minimal slow partitioning onto GroEL beads (Figure 2.5). As predicted, NADPH stabilized the protein in the control sample (blank beads) as well.

2.2 Part 2: Demonstrating proof-of-principle for partitioning and stabilization of a disease protein CFTR NBD1.

2.2.1 Introduction to cystic fibrosis and CFTR.

Once proof-of-concept for the chaperonin assay was demonstrated with a model protein, the next logical step was to recapitulate the same results with a relevant misfolding disease protein. One of the more common misfolding diseases is cystic fibrosis (CF). It is one of the most common, fatal genetic diseases to affect caucasians but currently there are no curative therapeutics. The CF protein is well characterized and known to be stabilized by nucleotides. This makes it an attractive model to be used with the chaperonin to demonstrate proof-of-concept for stabilizing misfolding disease proteins.

a Cystic fibrosis.

Cystic fibrosis is an autosomal recessive genetic disease that affects about 1 in 2500 individuals, especially children and young adults. The term cystic fibrosis was coined and the disease comprehensively described by Dr. Anderson in 1938. The genetic nature of the disease was hypothesized by Lowe and coworkers in 1949 (*137*). However, identifying the gene responsible for the disease took more than 40 years. The gene was finally identified using positional cloning by several researchers independently. The CF gene product was determined to be encoded by a 230 kb gene located on chromosome 7 (region q31) (*138-140*). The researchers named the gene product cystic fibrosis transmembrane conductance regulator (CFTR). Based on hydropathy plots along with amino acid sequence homology to the transmembrane ATP binding cassette (ABC) proteins, the gene product was predicted to be a transmembrane protein containing 1480 residues (*138*). This was subsequently supported by various studies where the

coding region of CFTR was expressed in various cell types (*141*). Presently, sequence analysis of numerous genomes that are associated with CF indicates that over 1800 mutations have been found. These mutations include deletion, missense and nonsense mutations located throughout the gene that result in CF disease.

CF patients were observed to have high levels of salt in their sweat. Extensive investigations into the salt concentrations in the sweat of CF patients demonstrated chloride salt concentration greater than 60 mEq/liter (*142*) compared with normal Cl^- concentrations (10-35 mEq/liter). Understanding the pathology of the disease came from studies by Quinton in the 1980s, who based his assessment on examining abnormal Cl^- transport as the underlying mechanism for the disease (*143*).

CF is now known to be caused by protein defects in the CFTR expression system. This leads to pathological changes in CFTR expressing organs involving the lungs, pancreas, liver, intestines and reproductive organs. The chief cause of CF symptoms is due to thick dehydrated mucosal secretion and obstruction of organs and glands as a result of these abnormal secretions. In the lungs, where the CF symptoms are primarily manifested, the submucosa of the bronchial airways is obstructed due to thick viscous mucosal secretions. The submucosa, which usually expresses the CFTR channel protein (*144*), secretes the mucous, which also containing of neutrophils and cellular debris. Over time, the secretions are infected with pathogens such as *Pseudomonas aeruginosa*, *Staphylococcus aureus* and *Haemophilus influenza*. These infections are usually very difficult to eradicate and can lead to fatalities.

The increased mucosal secretions can also lead to complications in other organs. In and around pancreatic ducts it leads to fibrosis, fatty replacement and pancreatitis (*145*), while similar obstruction of bile ducts in the liver can lead to cirrhosis. The pancreatitis is observed in

about 90% of CF patients and is thought to be due to accumulation of digestive proenzymes within the secretion ducts that are then prematurely activated. Chronic liver disease due to impaired biliary secretion leads to cirrhosis and portal hypertension. Although men with CF are more susceptible to infertility due to mucosal obstruction in the vas deferens (*146*), women have normal reproductive functions. CF patients are also observed to have reduced bone marrow density, due to malabsorption of vitamins and calcium (*147*).

b Structure and function of CFTR protein.

Structure: CFTR is a novel ABC transporter protein. ABC proteins are a family of ATPase transporter proteins that transport substrates against a concentration gradient and are structurally characterized by two homologous nucleotide binding domains (NBD) (*148*). Interestingly, CFTR acts as a simple ion channel rather than an active transporter (*149*). ATP is involved in gating the ion channel. Conformational changes in the CFTR protein brought about by ATP binding to the NBD domain keeps the channel open allowing ion flow (*150*). In addition, this flow of ions is down the electrochemical gradient unlike other ABC proteins where ions are actively pumped against the gradient. As mentioned previously, there are more than 1800 CFTR mutations. These mutations can be grouped into the following six classes:

a. Class 1:CFTR synthesis problems
b. Class 2: Defective CFTR processing
c. Class 3: Defective regulation
d. Class 4: Conductance problems
e. Class 5: Partly defective production / processing
f. Class 6: Defective regulation of other associated channels (*151*).

ΔF508 mutation (class 2 defect) is the most common mutation and is present in at least 90% of known patients and results in a manifestation of all of the physiological defects mentioned above.

High-resolution details of the CFTR structure are currently unavailable because; i) it is a large membrane protein, ii) exists in low copy numbers *in vivo*, and iii) it cannot be produced in large quantities due to low expression levels in bacterial/insect/mammalian systems. Mammalian expression systems have been used to purify protein for low resolution structures by 2-dimensional crystal arrays as well as 3-D electron microscopy (*152*). The low resolution structure (20 Å) obtained by these techniques is similar to the initially hypothesized structure with respect to the overall shape (*138*). The CFTR structure is similar to other ABC transporters and consists of two NBD and two membrane spanning domains, each consisting of six transmembrane alpha helices. CFTR differs from other ABC transporters due to the presence of a regulatory R-domain between the two NBD (Figure 2.6). The R-domain is a 200-residue region that is highly unstructured (*153*) and has a conserved set of phosphorylation sites (serine and threonine) that are responsible for activating the channel (*154*). A newer study obtained a better-resolved structure (18 Å) using electron crystallography (unstained two-dimensional crystals imaged by cryoelectron microscopy and processed by software). The structure was modeled using the bacterial ABC protein Sav1866, a multidrug efflux transporter, as a template (*155*). This study suggested that the protein adopts an outward facing state when it is actively gating in the presence of ATP and was inward facing when inactive. A high-resolution structure (1.7 Å) of the smaller soluble domain (NBD1) of the protein synthesized in a bacterial system has also been determined (*156*).

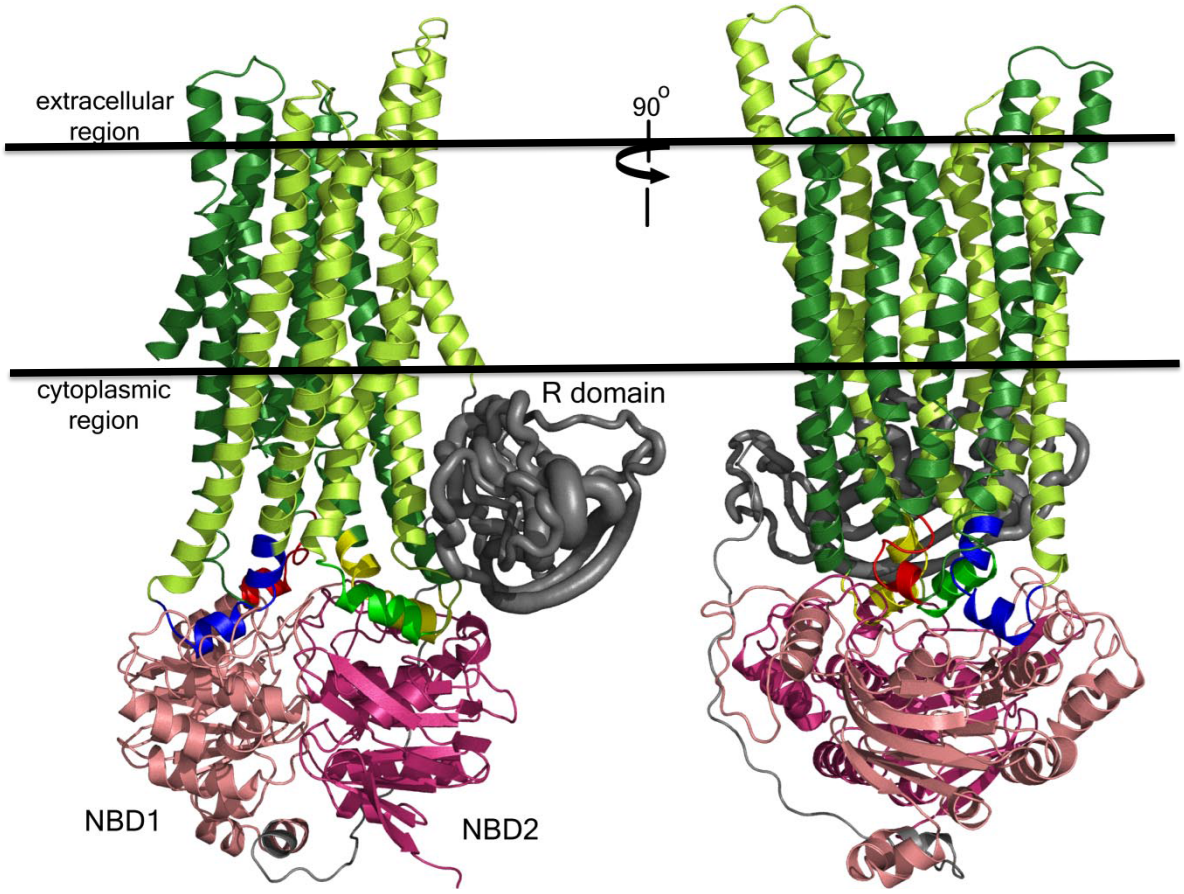

Figure 2.6: Theoretical homology model of CFTR structure constructed from the bacterial Sav1466 transporter protein, shows two transmembrane domains (green and light green), two nucleotide binding domains (pink and light pink) and a regulatory domain (grey). The black lines through the structures represent the lipid bilayer. The right panel shows the molecule rotated 90°. Figure adapted from (*157*)

Function of CFTR: Initially, CFTR was thought to function as a transporter based on its structural similarity with other ABC transporters (*158*). However, it was later found to act as an ion channel. It was demonstrated that the expression of CFTR in cells that lacked chloride channels led to the restoration of the chloride pathway (*159*). Later observations that point mutations in the CFTR gene caused alterations in ion channel selectivity, single-channel

conductance, channel gating, and other properties of CFTR, supported a direct role of the CFTR protein functioning as a chloride channel. The role of CFTR functioning as a chloride channel was finally confirmed when CFTR was reconstituted in lipid bilayers and was shown to act as an ion channel regulated by cyclic AMP (cAMP) (*160*). It is now known that CFTR transports chloride ions across the cell membrane and this transport is regulated by protein kinase A (PKA) via cAMP. CFTR is involved in down-regulating sodium transport in conjunction with the epithelial sodium channel (*161*), and in regulating calcium-activated chloride channels and potassium channels. CFTR is also involved in exocytosis and the formation of molecular complexes in the plasma membrane (*158*). Targeted deletions of the *cftr* gene influences the expression of proteins important in inflammatory responses, protein maturation, ion transport, and cell signaling, indicating that CFTR may play a role in several other cellular processes (*162*).

c Treatment strategies.

No treatment currently exists for CF. The lack of a suitable treatment strategy primarily stems from having only low resolution CFTR structures. Higher resolution structures could certainly lead to a better understanding of the molecular mechanism dictating CFTR function. Despite the lack of such information, better management of CF symptoms and complications has contributed to improved patient survival. Antibiotics (Tobramycin, Flucoxacillin, Ciprofloxacillin, etc.) are used for prophylaxis, suppression or eradication of respiratory pathogens (*147*). Anti-inflammatories such as NSAIDs, steroids lower inflammation in the airways (*163, 164*). Another strategy to manage CF is to improve hydration of the lung airways by decreasing Na^+ channel function and utilizing alternate Cl^- channels. Denufusol seems to stimulate an alternate Cl^- channel and is one such promising drug in Phase III clinical trials (*165*).

Several CFTR pharmacological agents aimed at correcting CFTR expression, folding and activity are in clinical trials. These are classified according to the nature of the defect that they target. Potentiators interact with CFTR that is properly trafficked to the cell surface and result in an increase in channel gating. Correctors are drugs that seem to increase the concentration of properly folded CFTR trafficked to the cell membrane. An example of a potentiator molecule is the recent drug developed by Vertex (Vx770). This drug increases ion transport activity and is currently being tested in Phase III clinical trials. Similarly, a CFTR corrector (Vx809) has shown encouraging results in Phase II trials (*166*). Another class includes drugs such as Ataluren that prevents premature termination and truncation of CFTR and is currently undergoing Phase III trials (*167*).

In this section, the chaperonin sink assay was utilized with nucleotide free CFTR NBD1 to establish proof-of-principle for a relevant disease protein. It was demonstrated that the assay could be used to search for stabilizers of misfolding disease proteins.

2.2.2 Methods and materials.

a Materials.

The nucleotide high affinity form of GroEL was produced and purified in the lab (*134*). CFTR NBD1 was a gift from Dr. Phil Thomas (UT Southwestern). The CFTR NBD1 antibodies were obtained as a gift from the CFTR folding consortium. All other chemicals were of the highest purity and obtained from Sigma.

b Removal of nucleotide from CFTR NBD1.

CFTR NBD1 is stabilized by ATP nucleotides and these ATP nucleotides will invariably interfere with the chaperonin assay. To avoid interference and insure chaperonin binding, ATP

was removed from the protein utilizing commercially available spin columns (Pierce) and following the manufacturer specified protocol. The column was initially spun at 1000xg for 1 minute to remove the storage buffer. The ATP stabilized CFTR NBD1 was then loaded onto the column matrix along with an equal volume of phosphate buffer, pH 7.4. The protein-loaded column was then spun for 2 minutes at 1500xg to remove the ATP. The process was then repeated by loading the filtrate onto another fresh spin column. The complete removal of ATP was confirmed by spectroscopic analysis of the filtrate.

c CFTR NBD1 partitioning experiments.

To study the partitioning of CFTR NBD1 onto the chaperonin, the monomeric nucleotide free CFTR NBD1 was incubated with oligomeric GroEL beads in a molar ratio of 5:1. The reaction mixture was then spun down to assay the supernatant. The supernatant was then assayed for CFTR NBD1 concentration using UV absorbance spectroscopy (A_{280}) to monitor the decline in absorbance. The concentration of CFTR NBD1 was determined using an extinction coefficient of 13.490 $M^{-1}cm^{-1}$. Alternatively, the amount of CFTR NBD1 can also examined using SDS-PAGE (*168*) or in our case using a dot blot assay. For carrying out the dot blot assay, the supernatant was blotted onto a PVDF membrane followed by blocking with 3% BSA solution for 1 hr. The blocked membrane was then incubated at $4^{\circ}C$ overnight with CFTR NBD1 monoclonal antibodies (1:1000 in 3% BSA in Tris buffered saline-0.5% tween 20 buffer (TBS-T)) as the primary antibody. The blot was washed thrice with TBS-T for 5 min. each. This was followed by probing with a secondary anti-mouse antibody conjugated with alkaline phosphatase for 3 hrs. The presence of CFTR was then determined by treating the blot with a combination of nitro-blue tetrazolium chloride (NBT) and 5-bromo-4-chloro-3'-indolyphosphate p-toluidine salt (BCIP).

2.2.3 Results and discussion.

A majority of the individuals affected by CF carry the delta F508 mutation. This mutation present in the NBD1 domain of the CFTR protein, results in the general misfolding/mistraffiking of CFTR. The NBD1 domain that contains the mutation, is by itself a small soluble protein that is much easier to handle than the entire membrane protein. Moreover, the structure of this domain has been solved. Some researchers (*169, 170*) use this particular expressed domain to search for stabilizers of both the native and mutated NBD1. It has been noted that this isolated domain is stabilized by ATP nucleotides (*171*).

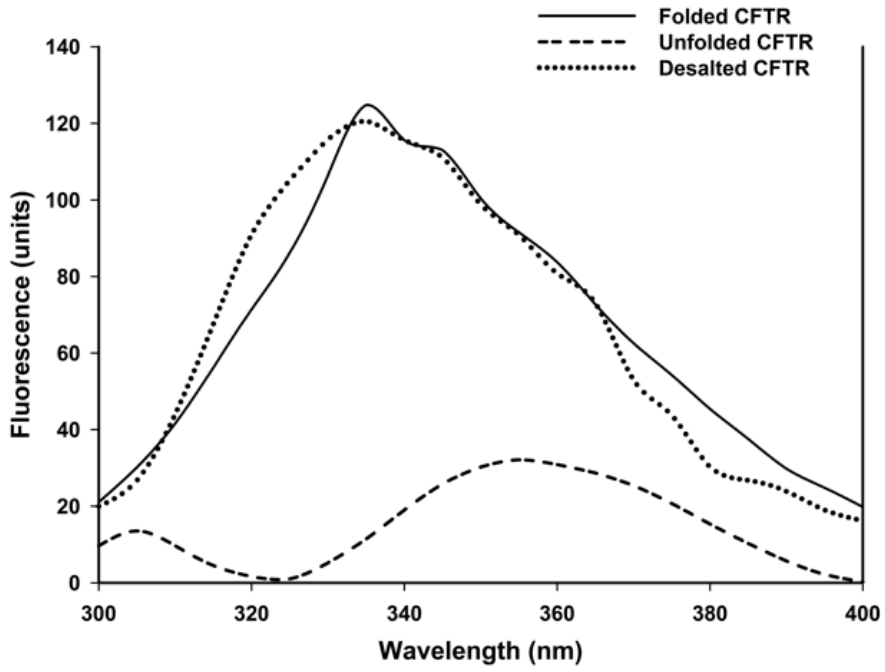

Figure 2.7: The folding state of CFTR NBD1 was analyzed utilizing its intrinsic fluorescence. The ATP free (desalted) CFTR NBD1 (dotted line) on excitation at 295 nm, shows a fluorescence profile similar to that of the ATP stabilized CFTR NBD1 (solid line), whereas unfolded CFTR NBD1 (dashed line) loses the 340nm absorbance peak

Upon removal of ATP, the folded domain begins to populate a more aggregation prone intermediate. However, the removal is essential as the nucleotide can affect the partitioning onto GroEL. The removal of the nucleotide is a simple process of desalting via spin nucleotide columns (Pierce). The protein was then analyzed by flourimetry and by gel electrophoresis to determine the effect of nucleotide removal on protein structure. Both demonstrated that the nucleotide free protein had characteristics similar to that of the ATP bound protein (Figure 2.7).

This nucleotide free CFTR NBD1 was then utilized for the partitioning assay. 1 μM of the protein was incubated with GroEL (oligomer) in a 1:5 molar ratio and the extent of CFTR NBD1 partitioning was measured as a function of the amount of free protein remaining in solution. The amount of free protein was assessed by measuring the corrected A_{280} of the supernatant. The corrected absorbance was obtained by subtracting the absorbance at 350nm from the 280nm absorbance to account for any baseline drift (due to presence of any particulates/ beads). It was observed that CFTR NBD1 readily partitions onto GroEL. It was also observed that the presence of urea did not increase the partitioning rate of CFTR NBD1 onto GroEL (Figure 2.8).

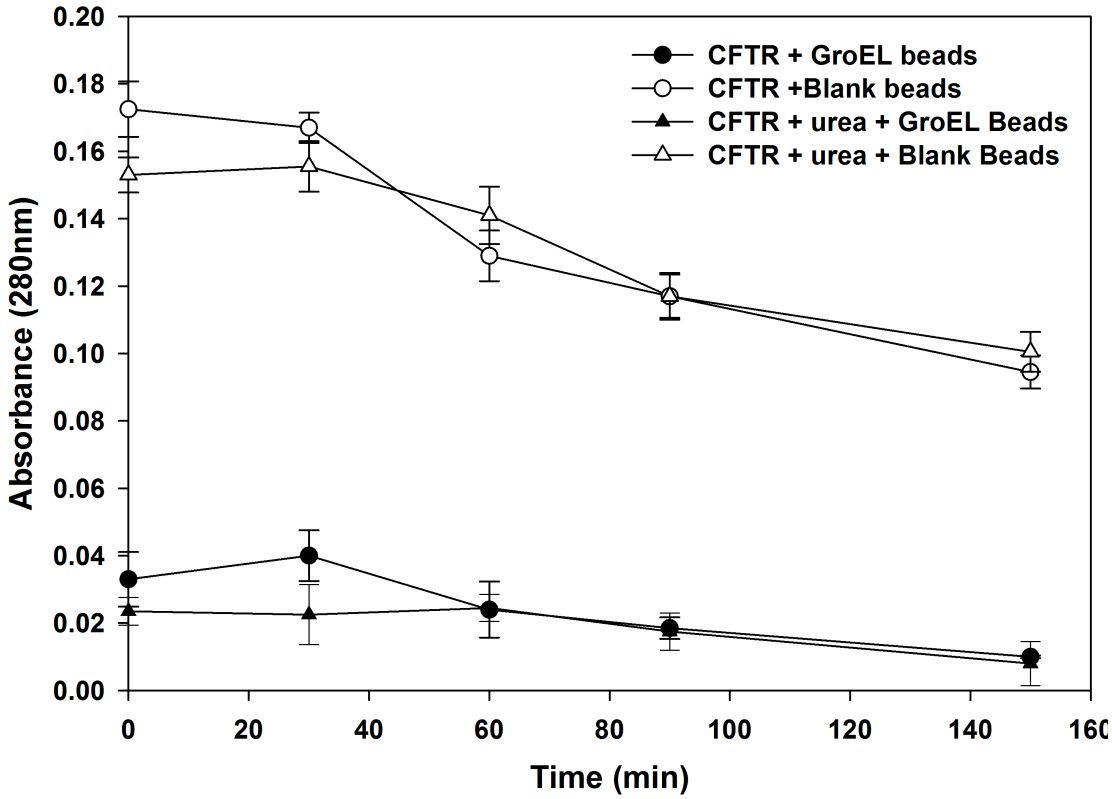

Figure 2.8: ATP free CFTR NBD1 was observed to readily partition onto the GroEL beads. CFTR NBD1 incubated with the GroEL beads in the presence (filled triangles) or absence of urea (filled circles) as a mild denaturant showed a rapid decrease in concentration indicating CFTR NBD1 partitioning. The amount of protein did not decrease as rapidly with the control blank beads both in presence (open circles) and absence (open triangles) of urea.

The partitioning rate was observed to be very rapid and occurred within a 30 sec. mixing time at 37^{o}C. As one would predict from a kinetic partitioning reaction, the CFTR NBD1 partitioning rates decrease as the amount of GroEL present decreases. The partitioning can also be followed by dot blot analysis. Thus both the assays confirmed the partitioning of CFTR onto the chaperonin and illustrate the ease of using multiple detection schemes.

Before we search for small molecule stabilizers it is essential to determine if the native state of the protein can be stabilized. A simple and facile method of achieving this is to utilize osmolytes. The full length CFTR protein has been shown to be stabilized by the addition of glycerol or by decrease in temperature (*91*). However, an osmolyte cannot be used as a drug. A small molecule stabilizer that can bind to the protein and prevent or delay unfolding may be an ideal candidate for CFTR therapy, particularly since this domain is the one that contains the most common mutation (ΔF508). If a small molecule stabilizer is present, that molecule could effectively increase downstream CFTR expression efficiency by preventing misfolding of this domain, thus preventing global mistraffiking. One could potentially facilitate proper expression and trafficking of the CFTR protein to the membrane by rescuing the folding of only a small amount of the protein. To demonstrate that one can utilize the chaperonin assay to search for such a stabilizer, it is necessary to demonstrate that the assay can be used to distinguish between a stable folded form of the protein and an unstable unfolded form, i.e. it is essential to demonstrate a proof-of-principle for a known CFTR stabilizer to decrease CFTR partitioning. It is known that the CFTR NBD1 fragment also binds Guanosine-5'-triphosphate (GTP) (*172*) and this interaction is known to stabilize this protein domain. Importantly, unlike ATP, GTP does not bind to the chaperonin GroEL and does not result in polypeptide release (*132*). Upon the addition of GTP to the CFTR NBD, partitioning onto GroEL (as assessed by immunodot blot assays) is prevented (Figure 2.9). The use of the dot blot assay to measure partitioning was necessitated by the presence of GTP. GTP is a nucleotide and demonstrates a strong absorption maximum at 260nm. This absorption overlaps and masks the protein absorption maximum at 280nm thus preventing the use of spectroscopy (both UV and fluorescence) to measure the protein quantitatively. Bradford assay or other dye based protein quantitation assays could not be used

since the protein concentration used in the assay was below the detection limits of such assays. This partitioning was also prevented even when a low concentration of denaturant such as 1 M Urea was added in addition to the GTP. These results indicate that GTP is an excellent stabilizing ligand that prevents the CFTR NBD1 from unfolding even under mild denaturing conditions.

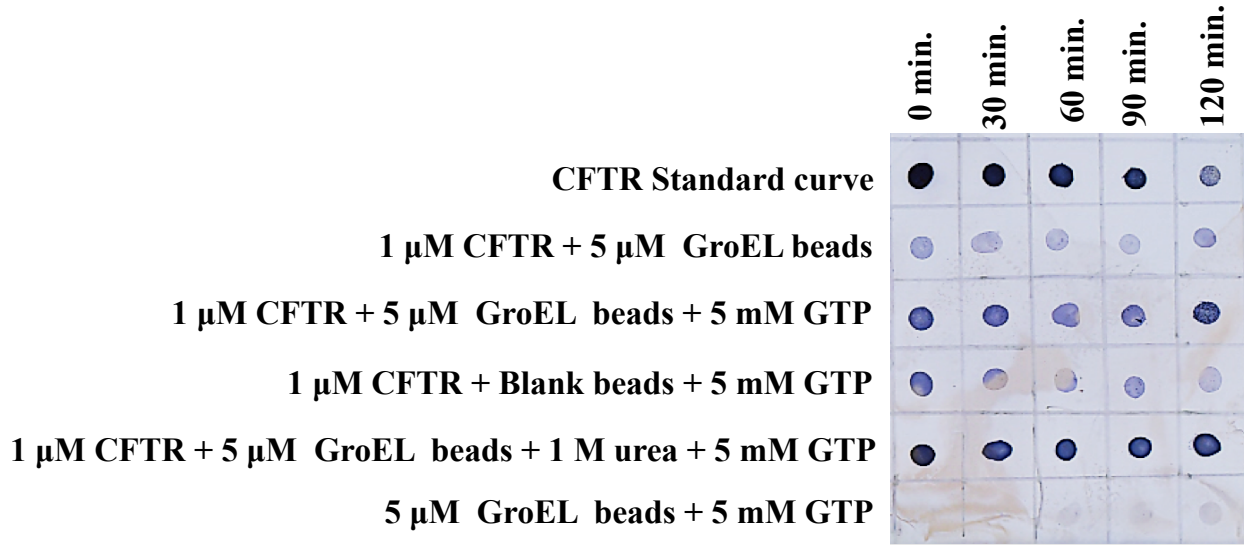

Figure 2.9: CFTR NBD1 partitioning is demonstrated by decrease in the intensity over time (row 1). On addition of the nucleotide GTP, the intensity of the dots remains constant both in the presence and absence of GroEL (Rows 2 and 3) indicating that GTP inhibits the partitioning of CFTR NBD1 onto GroEL. The intensity remains constant even in presence of a mild denaturant (row 4). Row 0 establishes a standard curve for measuring the intensity of the dots while row 5 is a control demonstrating that the monoclonal antibody has no cross-reactivity with GroEL.

As with any potential stabilizing ligand, one must rule out the possibility that the ligand (in this case GTP) inhibits CFTR NBD1 binding to GroEL because GTP binds to GroEL. This

secondary screening control is necessary to rule out this possible outcome. For a secondary screen, the ability of to GTP interfere with the partitioning and capture of another unrelated protein substrate (one that does not bind to GTP) was tested. To test this possibility, dihydrofolate reductase (DHFR) was tested in the presence of GTP. As shown in Figure 2.10, the inclusion of GTP into the partitioning reaction mixture does not interfere with capturing DHFR as it partially unfolds. With DHFR as a test substrate, the partitioning rates remain the same regardless of the presence or absence of GTP indicating that GTP does not interfere with GTP partitioning. If it did interfere, the partitioning would have occurred at a lower rate and a higher concentration of DHFR would have been in solution (or the two curves would not have been equivalent).

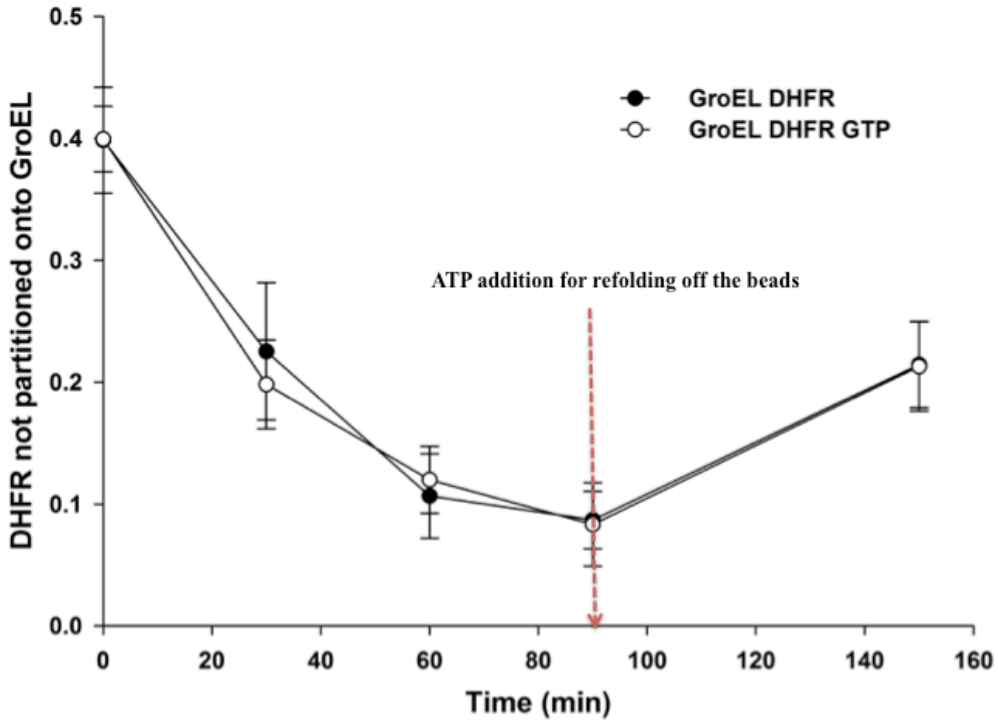

Figure 2.10: GroEL partitioning ability is not affected by GTP. DHFR was incubated with the chaperonin beads and the partitioning onto the beads measured by

following the decrease in enzyme activity. DHFR partitioning was observed to follow the same profile both in the presence (open circles) or absence of GTP (filled circle) indicating that GTP has no effect on GroEL partitioning ability. The partitioning of DHFR onto the beads was confirmed by the addition of 4 M glycerol and 10 mM ATP that causes the release of the substrate from the chaperonin. Here addition of the ATP and glycerol mixture leads to an increase in activity confirming partitioning of the protein onto the beads.

This outcome is not surprising since GTP neither binds to GroEL, nor does it facilitate release and folding of proteins from GroEL (*132*). In Figure 2.9, the blot intensity is a bit higher with GTP and urea present. The slightly lower signal with GTP alone might be due to small losses of CFTR NBD1 on the sides of the incubating vials. In summary, we have demonstrated that the chaperonin platform can be used to screen for stabilizing conditions for the CFTR NBD1, opening up the prospect that one could use the chaperonin system platform to screen for other pharmacological small molecule stabilizers of the CFTR NBD1 protein fragment.

2.3 Part 3: Demonstrating the utilization of the chaperonin sink assay to distinguish between the kinetic stabilities of different point mutants of the same disease.

2.3.1 Introduction to Friedreich's ataxia and Frataxin.

a Friedreich's ataxia.

Ataxias are a group of conditions characterized by shaky movements and unsteady gait. One of the more common ataxias is Friedreich's ataxia (FRDA) that was initially described by Nicholaus Friedrich in 1863. The disease affects 1 in every 40,000 caucasians worldwide and 1 in 120 Europeans are thought to be a carrier for the disease (*173, 174*). It is an autosomal recessive neurodegenerative disease that is highly devastating and is characterized by limb spasticity, absence of motion and speech impediments in young adults and adolescents. About 30% of patients develop optic atrophy and hearing loss. There is no treatment to treat or slow down the disease progression and afflicted patients rarely survive to adulthood. The disease progressively targets various organs though the major cause of death is usually due to cardiac myopathy (thickening of the heart muscles), which leads to arrhythmias and congestive cardiac failure (*175*). The various symptoms exhibited by FRDA patients are thought to be due to primary degeneration of dorsal root ganglia which are present in the posterior columns, spinocerebellar tracts, and corticospinal tracts, and large myelinated fibers of the peripheral nerves. The majority of patients with FRDA have a GAA trinucleotide repeat expansion in the first intron of the gene encoding frataxin. Normal alleles contain 6–34 uninterrupted GAA repeats. However many patients with FRDA have between 67 to over 1,300 GAA repeats in both alleles. This leads to impaired transcription and a decrease in the gene expression. The length of the triplet repeat region correlates with the onset and severity of the disease. The gene

responsible was cloned and sequenced in 1996. The gene product, frataxin (fxn) is found to be highly conserved mitochondrial protein from bacteria to humans.

b Frataxin and its mutants.

FRDA is due to inability of patients to produce frataxin which leads to a loss of function disease characterized by disruption of cellular iron homeostasis (*176*) and accumulation of iron within the mitochondrion (*177*). Downregulation of several other enzymes involved in systemic iron metabolism was also observed (*178*). The causative agent for FRDA, frataxin, was initially mapped to chromosome 9 in 1988 by Chamberlain and colleagues (*179*) after linkage analysis with about 25 families and was subsequently supported by a similar study the next year (*180*). In humans, it is expressed in tissues with high ATP utilization such as the heart, brain, and spinal cord, liver, skeletal muscle and pancreas (*181*). The wild type frataxin is a 210-residue protein with a mitochondrial signal sequence at the N-terminus (*182*). Frataxin imported into the mitochondria is cleaved by mitochondrial processing peptidase and the processed protein is found peripherally associated with the membranes (*183*). A small percentage of FRDA patients are also characterized by point mutations in frataxin (*184*). Although the single site missense mutant proteins have reduced thermostability and easily aggregate, the wild type frataxin is thermostable (Tm ~ 60^{o}C).

Structure: Nuclear magnetic resonance (NMR) and crystallography based structural studies on frataxin and its bacterial homolog have revealed that the protein contains a novel structural motif called a frataxin fold. As shown in Figure 2.11, frataxin is characterized by the presence of an N-terminal α-helix, a middle β-sheet region composed of seven β-strands, a second α-helix, and a C-terminal coil in a α1β1β2β3β4β5β6β7α2 topology. The two alpha chains are in one plane while five antiparallel beta strands are in another while the other two beta 6 and

7 strands intersect the two planes. The β sheet is solvent exposed on one side and is packed tightly to two helices on the other side due to hydrophobic residues on the beta sheet (*185*). The fifteen residue (196-210) C-terminal domain interacts with α1 and α2 helices. It has also been reported that deletion of this C-terminal domain leads to a decreased stability of the protein (*186*).

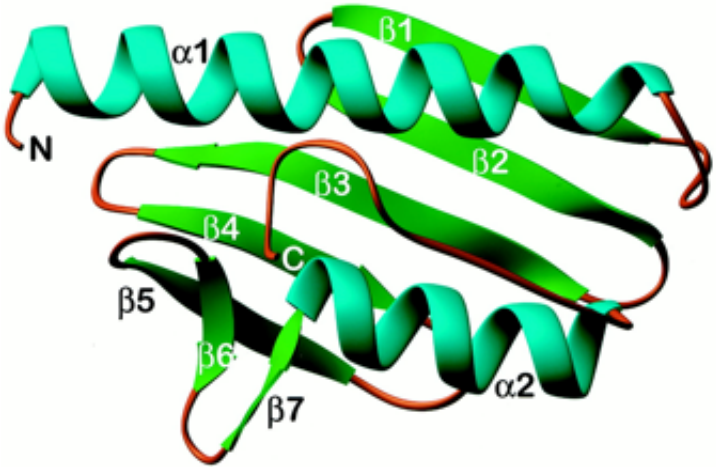

Figure 2.11: Frataxin structure (PDB 1 shows the presence of a novel structural motif with two α chains in one plane while five antiparallel β strands are in another. The other two β strands 6 and 7 intersect the two planes. The C-terminal domain interacts with the α1 and the α2 helices. Figure adapted from (*187*).

The human frataxin has about 60% sequence similarity and 30% sequence identity with the bacterial and yeast homologs. The mature protein that is formed after cleavage of the signal and transport sequences spans residues 75 to 210. The last seventeen residues on the C-terminus are unstructured. About a quarter of the protein surface is negatively charged and the carboxylate side chains in this region are proposed to help with metal binding (*187*). NMR studies indicate that ferrous ions bind to frataxin through acidic residues localized in the α1 and β1 region (*188*).

The structure does not show the presence of any specific iron binding motifs that are observed in other iron proteins such as ferritin or transferritin.

Frataxin is thought to play a role in iron homeostasis and transport. The iron binding function of frataxin was initially determined in the yeast homolog and later in the human and bacterial proteins (*189*). Frataxin binds to iron utilizing the surface carboxylates of the alpha helix-1 and beta strand-1 (Figure 2.9). Human frataxin binds to six ferric ions with a K_d of ~ 10.2 μM (*190*) and to ferrous ions with K_d of ~ 55 μM. The yeast frataxin forms oligomers on binding to ferrous ions but the human frataxin does not (even at high protein concentrations). Frataxin is also involved in formation of iron-sulfur clusters (ISC) and in heme biosynthesis. ISC are involved in the respiratory electron transfer chain. Frataxin is proposed to function as an iron transport protein by transiently binding to free iron in the mitochondria and transferring the bound iron to the protein Isu. Frataxin is also implicated in transferring iron to aconitase for ISC repair and reactivation. Frataxin also interacts with the enzyme ferrochelatase that catalyzes insertion of ferrous ions into the porphyrin ring suggesting a possible role in heme synthesis (*191, 192*).

c Existing treatment strategies for FRDA.

Several treatment strategies are currently being investigated to treat patients with FRDA (Figure 2.12). Decreased frataxin levels indicate that there is an increase in mitochondrial iron and the resulting oxidative stress environment leads to a worsening of the disease state. To overcome iron dependent oxidative damage, antioxidants and chelators have been used with varying degrees of success. It was demonstrated that more common therapeutic iron chelators such as desferoxamine actually decreased frataxin mRNA levels as well as overall protein expression, exacerbating the disease (*193*). This has led to the development of specific

mitochondrial targeted iron chelators like deferiprone that decrease free iron within intracellular compartments without affecting other cellular iron-enzymes like aconitase or affecting the transferrin-bound iron.

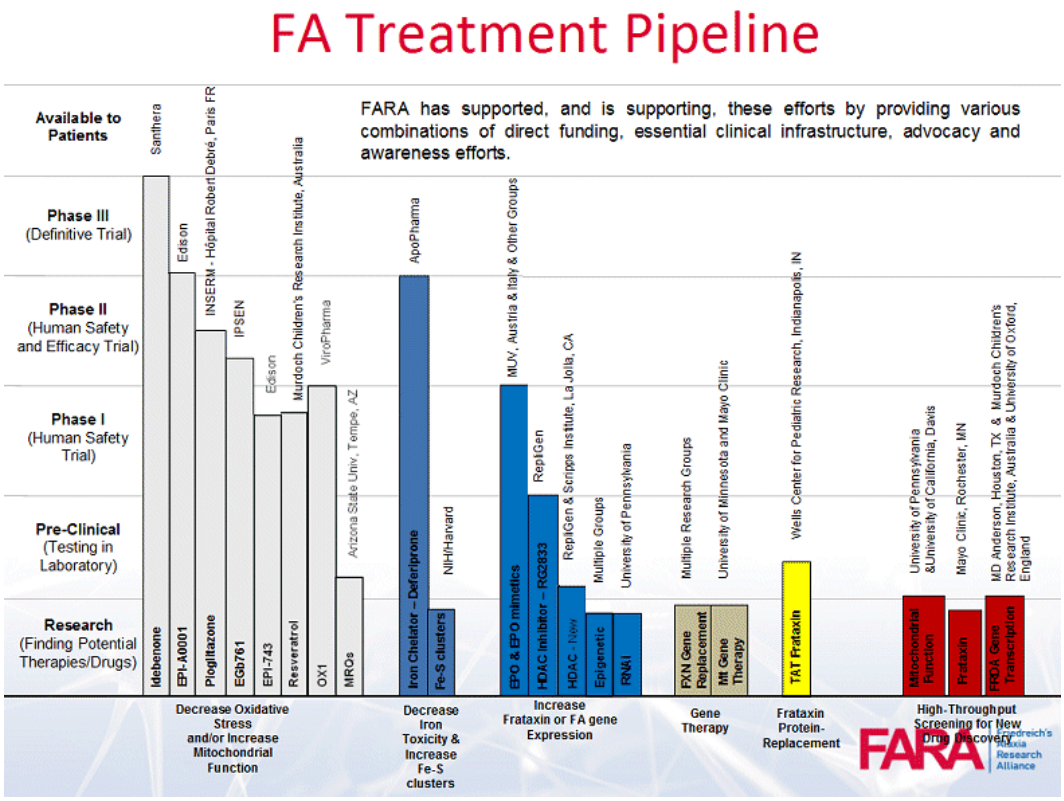

Figure 2.12: Although there are several classes of drugs that are being investigated for their therapeutic potential, most of them are still in clinical trial stages (Figure sourced from http://www.curefa.org/pipeline.html).

An alternate approach administered the antioxidant Coenzyme Q (CoQ10) along with vitamin E. This combination showed an improvement in cardiac and skeletal muscle bioenergetics and FRDA symptoms but did not have any beneficial effect in improving gait and posture, nor did it decrease incidences of cardiomyopathy (*194*). Another short-chain CoQ10 analogue called Idebenone that initially showed promising results, failed to show statistical

significance improvement in neurological function and is unlikely to be approved for treatment. Other antioxidants in trial includes MitoQ, a CoQ10 analogue, to specifically target mitochondria Fe oxidation and α-tocopherol quinone which improves mitochondrial function (*195*). Both these compounds prevent oxidative damage associated with FRDA.

Individuals afflicted with FRDA may be homozygotes or heterozygotes for the GAA repeats. About 98% of individuals are homozygous for the trinucleotide repeat sequence on both alleles. In patients that are heterozygotes having one copy of the GAA repeat and one copy of a clinical mutation, the protective effect of the native protein is eventually lost as genetic expansion progresses later in life. For folding mutants, it is unclear where the defect in folding competence occurs (i.e. poor synthesis, misfolding inside or outside the mitochondria). Within these particular individuals it would be beneficial if strategies were developed to specifically increase the stability of the missense folding mutant using small molecule chemical chaperone approaches. Here, it was predicted that the chaperonin sink screening system could be utilized to determine the stability of the frataxin mutants and search for ligands that stabilize the mutants. It was also hypothesized that one could utilize the chaperonin to distinguish between the biophysical differences between two missense FRDA mutants, D122Y and I154F, that show very similar thermal and chemical stabilities. Since folding diseases for the most part are kinetic diseases (i.e, they are based on the kinetic stabilities of proteins), we propose to first determine if the frataxin mutants kinetically partition onto the chaperonin at different rates. This would then be followed by searching for ligands or conditions (i.e. osmolyte screens) that can stabilize the mutant proteins.

2.3.2 Materials and methods.

a Materials.

Highly purified GroEL was obtained using a protocol derived at EDGE BioSystems using a modified purification scheme (*134*). NHS-derivatized Sepharose fast flow beads were purchased from GE Healthcare Inc. All other chemicals were of the highest purity available and purchased from Sigma Aldrich. GroEL beads were generated by the method described previously (2.1.3 section b).

b Frataxin protein purification.

All purified frataxin samples were gifts from Dr. Claudio Gomes (IQTB, Portugal). The constructs were expressed in *E. coli* cells (BL21 (DE3)) and frataxin was purified as previously described (*185, 196*). Plasmid-derived protein expression was induced by addition of 0.5 mM IPTG. All protein variants contained the conserved C-terminal domain (amino acids 91–210). The vectors were His tagged at the C-terminal and to simplify purification. Although the mutants were stable in solution at room temperature, both purified mutants showed visible precipitation on slow freezing (*196*). To prevent this, the frataxin wild type and mutants were flash frozen by dropping drops of the protein via a syringe into liquid nitrogen. This procedure insured that all of the frataxin variants retained both their native spectroscopic properties and exhibited reproducible cooperative melting profiles.

c GroEL partitioning assay.

Partitioning studies were carried out by incubating the wild type frataxin and the mutants D122Y and I154F with the GroEL beads at 25°C, 37°C or 45°C. 2 μM frataxin was incubated with 2 μM GroEL beads (estimated) in refolding buffer (50 mM Tris pH 7.5, 50 mM KCl, 5 mM

MgCl2, 0.5 mM EDTA) with 1 M urea and this reaction mixture was incubated while being constantly mixed on a rotary mixer at the described temperatures. GroEL remains tetradecameric and functional under all of these conditions (*197, 198*). The reaction mixture was spun down to separate the protein partitioned onto the chaperonin beads from the native soluble protein in the supernatant. Aliquots of the supernatant were withdrawn from the reaction bead mixture at the described time points to quantify the soluble frataxin that had not partitioned onto the GroEL beads. The soluble protein remaining in the supernatant was quantified by UV absorbance spectroscopy (Shimadzu UV-2401) at 280 nm or alternatively on a SDS/PAGE gel. After spectroscopic quantification, the withdrawn sample was reintroduced back into the reaction mixture in order to maintain a near constant frataxin concentration.

2.3.3 Results and discussion.

a Kinetic differences between frataxin mutants.

This study was used for determining if the frataxin mutants could partition onto the chaperonin and if the chaperonin assay could be used to search for stabilizers. Two of the more common frataxin mutants, D122Y and I154F, show very similar thermal and chemical stabilities (*196, 199*), but result in distinct disease phenotypes (*200, 201*). While D122Y is associated with a mild phenotype in GAA/D122Y heterozygotes, heterozygotic individuals containing the I154F point mutation manifest a more severe disease phenotype. These differences were also manifested while expressing these proteins. While the D122Y mutant is mostly in a soluble form in *E. coli*, most of the I154F is expressed in the form of insoluble inclusion bodies (*199*). It was hypothesized that these solubility differences as well as the differences in the disease states might be due to differences in the stabilities of these proteins. Gomes and colleagues had

observed that a thermal melting profile demonstrated that both frataxin variants begin to populate denatured forms following a thermal denaturation starting at 40ºC (red dotted arrow, Figure 2.13A) whereas the native fold remains predominantly in its native folded form up to ~ 65^{o}C (Green dotted arrow).

Unfortunately, this approach only examines the consequences of a global unfolding reaction within non-physiological denaturant conditions. Since the differences between these mutants may reside in the folding/unfolding kinetics, it is best to detect these kinetic transients at near physiological conditions unlike the high temperatures used in Figure 2.10 A. One could certainly investigate the stabilities of proteins by examining differences in unfolding kinetics in denaturant solutions. However, the amount of protein available for extensive stopped flow kinetic studies was limiting, especially for the I154F mutant. Alternatively, it was predicted that the chaperonin assay could be used to distinguish the biophysical differences between two missense FRDA mutants. To achieve this, the high affinity nucleotide free form of the chaperonin GroEL can be predicted to capture the transient dynamic states by sequestering them via kinetic/thermodynamic partitioning. To carry out such partitioning, the frataxin wild type and mutants were subjected to mild destabilizing conditions such as those imposed by mild denaturant concentrations and/or slightly increased temperature, which help to modulate frataxin equilibrium dynamics and partitioning onto the GroEL. The particular conditions chosen to follow the kinetic partitioning of frataxin missense mutants (D122Y and I154F) were derived from examining thermal denaturation scan profiles (Figure 2.13 A) (*199*). From the thermal denaturation profiles, it was predicted that the frataxin mutants should be able to kinetically partition onto GroEL at temperatures greater than 40^{o}C, while the wild type should not.

To test the first hypothesis (differences in kinetic partitioning), the partitioning of the different variants onto GroEL was carried out at increasing temperatures of 25ºC, 37ºC and 45ºC. An estimated 1:1 molar ratio of GroEL (oligomer) to frataxin monomer was incubated at the different temperatures. In these assays, the time dependent decline in the amount of soluble protein can be easily measured by following the decline in protein concentration using UV-visible spectroscopy, fluorescence spectroscopy or SDS/PAGE analysis. In the experiments presented herein, the partitioning of the frataxin was measured by the decrease in the protein concentration in the supernatant as quantified by UV spectroscopy. As predicted, even under these slight denaturing conditions (1 M urea, 25-45ºC), native frataxin shows no decline amount of total soluble protein and no partitioning onto GroEL was observed (Figure 2.13 B). Likewise, neither one of frataxin variants partitioned onto GroEL at 25ºC or 37ºC (Figure 2.13 C, D), indicating that, at these temperatures, the most prevalent variant populations remain in their predominantly in their folded soluble forms. It is only at temperatures above 40ºC (specifically 45ºC) that the increase in the transient unfolded/partially folded populations could be observed resulting in a increasing amount of protein that partitioning onto bead immobilized GroEL as a function of time (Figure 2.13 C, D).) For these variants, the time dependent decline in protein concentration indicated that the partially folded states of the D122Y and I154F variants appears to easily partition onto continuously mixing NHS-Sepharose GroEL beads as was demonstrated with other dynamically unstable proteins (CFTR and DHFR).

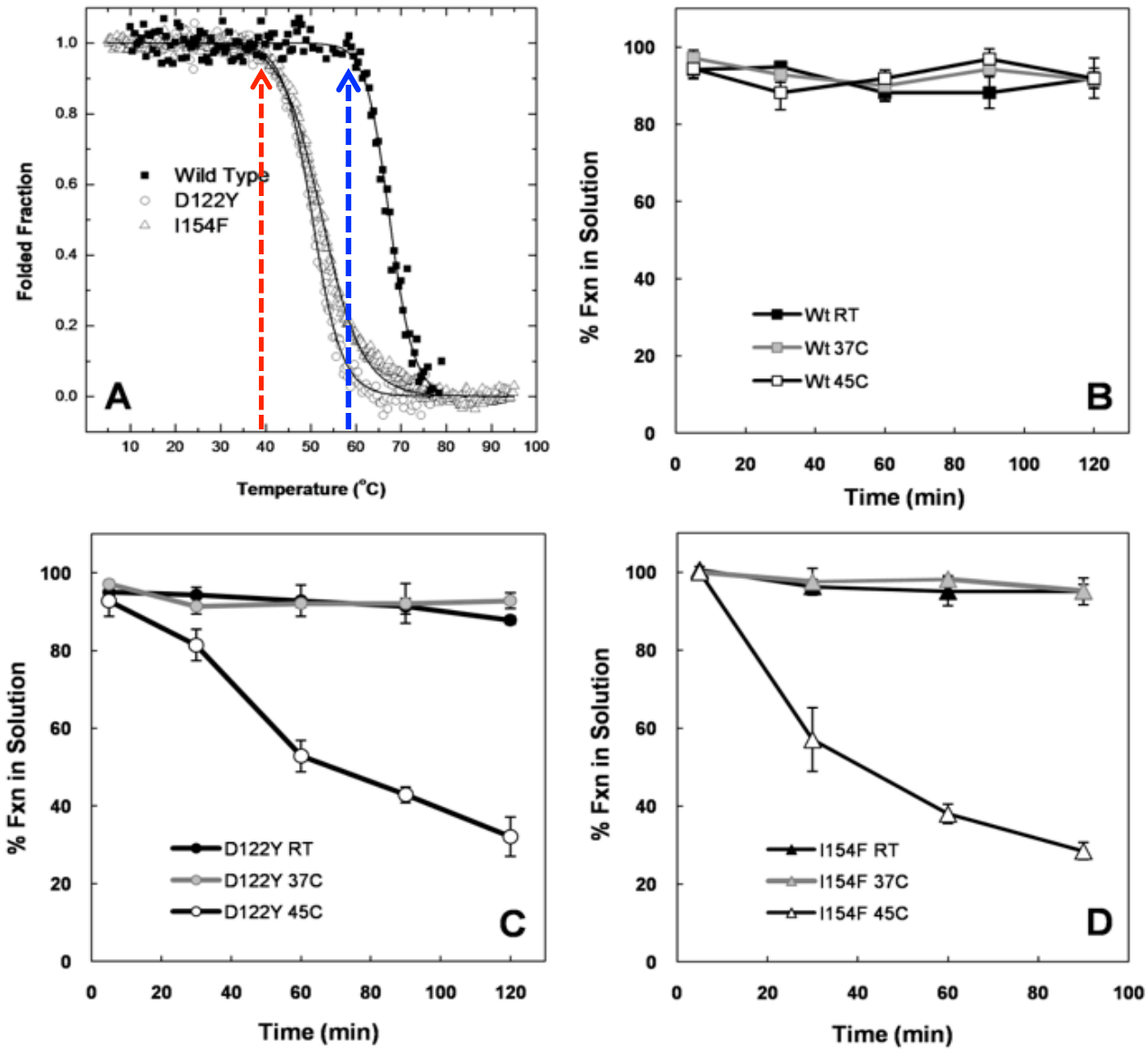

Figure 2.13: (A) Thermal melting profiles of the wild type and mutant frataxin. Partitioning of wt (B), I154F (D) and D122Y (C) onto GroEL beads at temperatures of 25ºC (black data points), 37ºC (grey data points) and 45ºC (open data points) shows that the frataxin mutants partition only at temperatures higher than 37ºC, while the mutant do not.

The maintenance of protein function relies on dynamic processes dictated by inherent protein homeostasis mechanisms and protein folding/unfolding kinetics. *In vivo*, protein stability or more correctly, optimal steady state levels of functional protein results from overall synthesis rates, folding competence, maintenance of the acquired fold (chaperone buffering) and degradation rates. Increases in partial unfolded state populations, often found with marginally stable missense mutants, can be easily generated under typical stress conditions such as elevated temperatures (e.g. fever or heat stress). This experiment thus demonstrates that such an increase in the partially folded state is possible for the frataxin mutants under slight protein folding stress conditions (temperature 45 $^{\circ}$C and 1 M urea).

$$\text{Protein}_{(\text{native})} \underset{k_{\text{folding}}}{\overset{k_{\text{unfolding}}}{\rightleftharpoons}} \text{Protein}_{(\text{non-native})} + \text{GroEL} \rightleftharpoons \text{GroEL-Protein}_{(\text{non-native})} \qquad (1)$$

If partitioning is occurring, the interaction between GroEL and the partially folded frataxin intermediates is dictated by a bi-molecular collisional process (scheme 1 above). We also assume that interaction occurs between the chaperonin and a monomeric frataxin protein. Over the short time span of the assay, the slow partitioning of the variants onto GroEL most likely indicates that the capture of the dynamic population of the transient unfolded/partially folded species is small compared with that of the native population. If this is so, as mentioned in the beginning of this chapter, the chaperonin concentration should be in vast excess compared with these transient and dynamic misfolded/unfolded populations. From a kinetic perspective, this would provide a reasonable explanation as to why the partitioning kinetics should typically fit a first order decay approximation, or more correctly, a pseudo first order decay kinetic

profiles (*99, 131*). In addition, as was previously observed for rhodanese partitioning onto soluble GroEL, it is predicted that the observed partitioning rates for both of the transient frataxin variants onto the immobilized GroEL should increase and then approach a limiting rate as the GroEL bead concentration increases. The characteristic kinetic response should follow a rise and then reach a plateau as the partitioning rates of misfolded protein populations in equilibrium with native states bind onto GroEL approaches to an increasing chaperonin concentration. This type of kinetic partitioning response for native proteins slowly partitioning onto chaperonins with increasing chaperonin concentrations has been observed in every case tested thus far independent of whether one uses soluble (free) or bead immobilized GroEL (*99, 131*). One logical explanation for the observation of a plateau in kinetic partitioning rate is that these partitioning rate approaches a limiting value that is dictated by the intrinsic unfolding/partial unfolding microscopic rates. At high GroEL concentrations, the unfolding/partial unfolding of the transient chaperonin binding conformer becomes rate limiting. As demonstrated by earlier experiments by Walter *et al* (*202*), the high affinity GroEL chaperonin does not actively unfold natively folded proteins nor does it affect the microscopic unfolding rate constants as GroEL concentrations increase. GroEL simply binds the partially folded populations as they form, and partitioning occurs by simple mass action effects. This mass action effect results in a shift of the folding-unfolding equilibrium toward a tighter binding GroEL bound partially unfolded protein substrate.

The partitioning profiles of the I154F frataxin mutant indeed shows a saturation at a higher limiting rate than does the D122Y mutant. Likewise, the frataxin I154F partitioning rates are clearly accelerated compared with than those observed with D122Y and show larger amplitudes of change as estimated GroEL concentrations increase (Figure 2.14). For instance,

after a 60 min incubation at ~ 3μM GroEL, the soluble fraction of I154F declines to ~ 25% of its original starting concentration while under the same conditions, the amount of soluble D122Y is present at 55% of its original concentration (Figure 2.14 A, B). From these data, it can be inferred that the kinetic stability of the I154F mutant appears to be lower than that of the D122Y mutant.

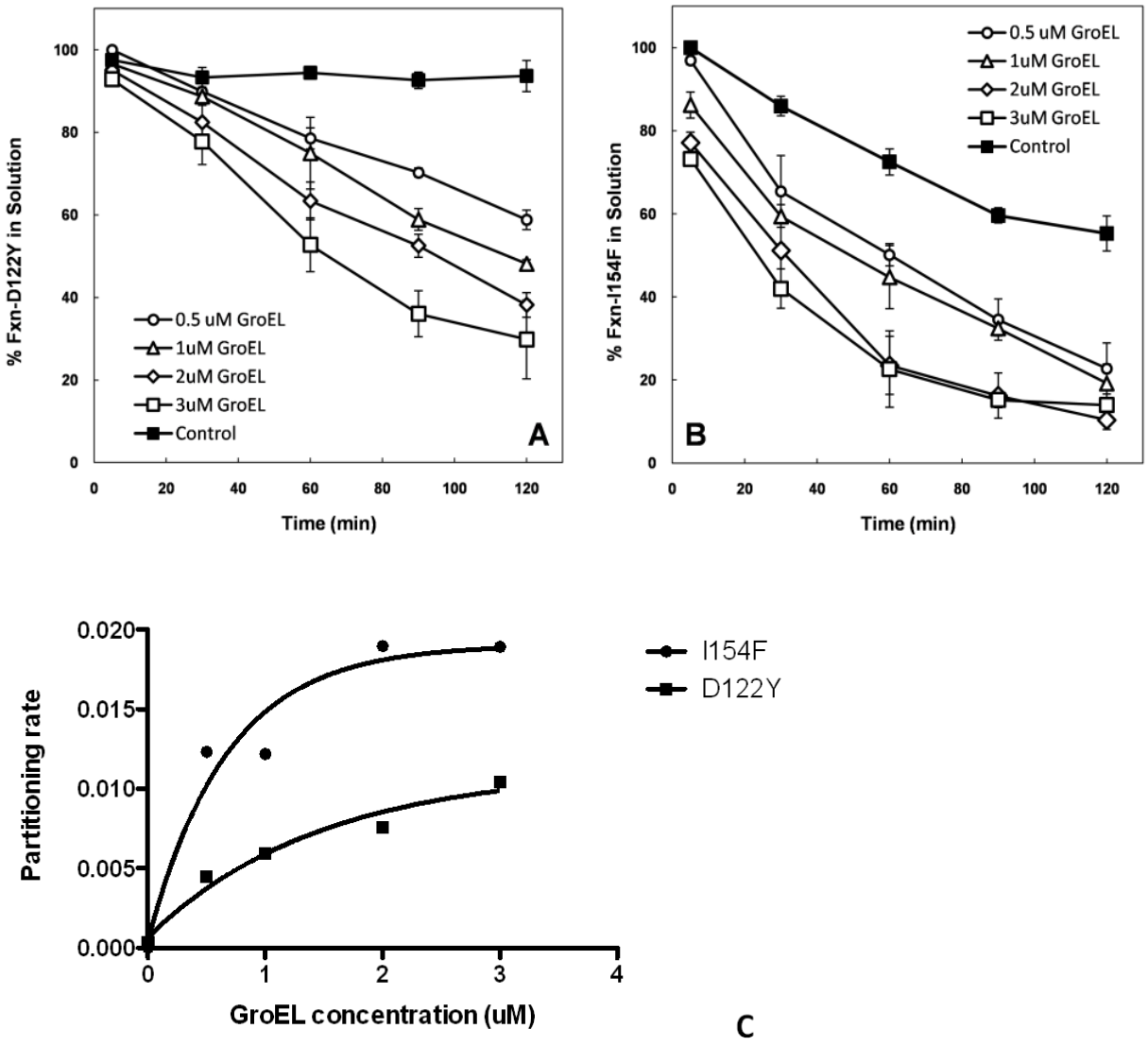

Figure 2.14: (A, B) Partitioning frataxin mutants on to various concentrations of GroEL beads. (C) Compiled partitioning rates increase with the GroEL bead concentration.

The partitioning rates were fit to a first order relationship and the plot of the partitioning rate as a function of estimated GroEL concentration shows a hyperbolic relationship.

The behavior of the two mutants in solution also shows slight differences at elevated temperatures because the amount of recoverable I154F slowly declines in concentration even in the absence of the GroEL chaperonin (control experiments). This slow decline is not detected in the D122Y control profile (Figure 2.14 A). UV Spectroscopic analysis (i.e. light scattering contributions) indicates that under the conditions of assay, the I154F variant slowly aggregates in the absence of GroEL. Light scattering at 350 nm is commonly used to monitor aggregation. This scattering is a function of the wavelength and particle size. Light scattering intensity increases with λ^{-4}. 350 nm is therefore the shortest wavelength that can be used as proteins absorb in the 200-320nm range. It is important to note however, that when immobilized GroEL beads are present, this general aggregation side reaction is suppressed since the remaining soluble I154F mutant within the supernatant shows no evidence of aggregation dependent light scattering contributions particularly at the beginning of the partitioning reaction. It is well known that the chaperonin binds to the unfolded proteins and suppresses aggregation. This decrease in aggregation leads to a corresponding decrease in light scattering and this assay was used in early studies with protein folding and GroEL as an end point to measure global aggregation suppression (*203, 204*). In the end analysis, it is clear that the I154F preferentially partitions onto GroEL at a substantially higher limiting rates than does D122Y (Figure 2.14 C).

b Osmolytes differentially stabilize frataxin D122Y and I154F mutants.

The aggregation as well as the partitioning of the substrate onto GroEL observed in the previous section can be decreased by stabilizing the substrate protein. This can be achieved by using protective osmolytes. These protective osmolytes act on the protein backbone and force

proteins to fold into their native state. Thus, they prevent protein unfolding and aggregation. We have used the chaperonin sink approach to examine if folding osmolytes can stabilize the native conformation of frataxin variants and prevent aggregation. This approach helps to determine if the protein can be stabilized and aggregation can be prevented in a broad sense before screening for specific small molecule stabilizers (pharmacological chaperones). In addition, this approach is important to determine if all mutants can be similarly stabilized by these small molecule chemical chaperones. As stated in the chapter 1, the different osmolytes actually have differential effects on backbone stabilities and solubilities (described as an osmophobic effect where some work at lower concentrations than others). Here a series of folding osmolytes where backbone burial free energies (collapse) ranges from weaker (glycerol) to strong folding osmolytes (TMAO) (*205*) was studied. The osmolytes sets that appeared to provide some stabilization of the native folds of I154F and D122Y were substantially different with respect to its folding strength (weak/strong).

A weaker folding osmolyte (4 M glycerol) appears to be effective at stabilizing the native, properly folded forms for both mutants. This results in a near complete inhibition of their observed partitioning onto GroEL (Figure 2.15) while simultaneously inhibiting general aggregation side reactions. At first glance, the stronger folding osmolyte TMAO also appears to prevent partitioning of both mutants onto GroEL. However, a closer examination of the I154F protein that remained in solution revealed that the stronger osmolytes used here actually induced aggregation for this mutant as assessed by light scattering measurements. In contrast, the strong folding osmolyte TMAO prevent both GroEL partitioning as well as any large-scale aggregation of the D122Y mutant. It is notable that osmolyte-dependent inhibition of chaperonin partitioning is not due to inhibition of the chaperonin binding reaction, since it has been repeatedly been

demonstrated in our laboratory as well by others that weak or strong folding osmolytes cannot prevent the binding of either completely denatured proteins or highly populated partially folded proteins onto GroEL (*134, 206*).

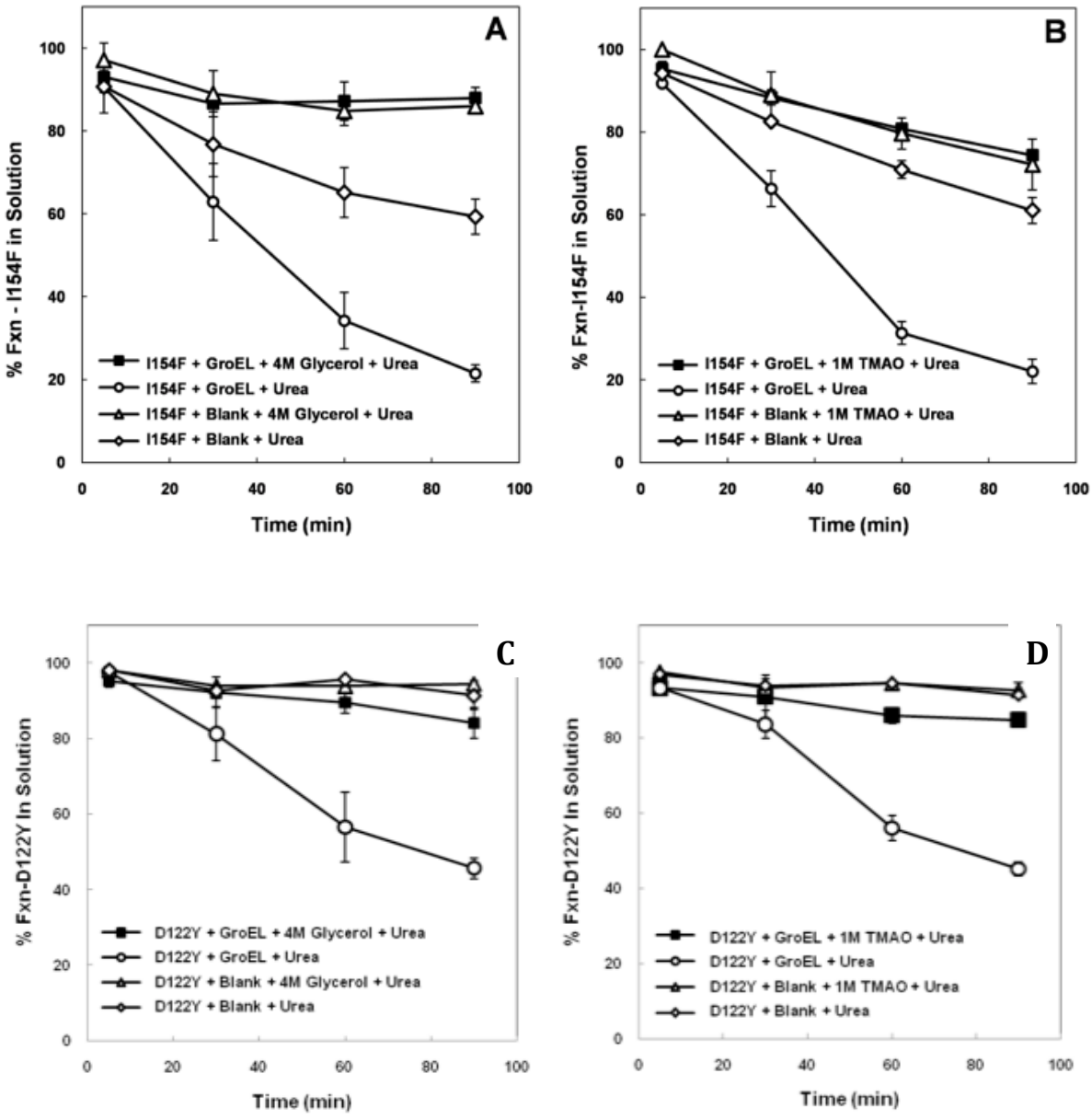

Figure 2.15: Partitioning of the two mutants (I154F and D122Y) onto GroEL beads in the presence of 4 M glycerol (A, C) and 1 M TMAO (B, D) demonstrates that the

osmolytes stabilize both mutants preventing partitioning even in the presence of a mild denaturant.

Strong and weak folding osmolytes are defined by the magnitude of free energy burial of the peptide backbone in proteins as defined by Bolen and colleagues (*207*). Thus the different effects observed for each mutant may result from the different locations of the mutations within the protein structure. I154 is fairly buried within the protein core while D122 is located on a more solvent exposed loop region.

The kinetic and aggregation differences that we observed for these two missense frataxin mutants may reflect difficulties in identifying global therapeutic stabilizing ligands. For instance, although it is highly desirable to find one ligand that will stabilize a broad range of single site mutants within one protein, the kinetic and particularly osmolyte stabilization studies presented here may indicate that the identity of stabilizing ligands may be mutant specific. Folding proteins are cooperative systems and it may be unlikely that one single ligand would bind and kinetically suppress all misfolding intermediates generated by a wide array of missense mutants.

Percentage increase in protein aggregation with time (A_{260}/A_{280}) x 100			
Solution	**Wt (units)**	**I154F (units)**	**D122Y (units)**
Buffer	0.2	100	24
1M Proline (Weak osmolyte)	0.4	6	3
4M Glycerol (Weak osmolyte)	0.5	0.1	6
1M TMAO (Strong osmolyte)	0.4	45	10
1M Trehalose (Strong osmolyte)	0.2	136	0.5

Figure 2.16: Measuring the increase in protein aggregation as a function of the change in ratio of the UV absorption spectra at 260 and 280 nm over time (lower the value, lower the aggregation observed). Weak osmolytes were observed to stabilize both mutants while strong osmolytes led to increases in observed aggregation. The green highlighted cells indicate the low aggregation observed in the presence of weak osmolytes for I154F.

In the course of our frataxin partitioning/stabilization experiments, it was observed that larger scale protein aggregation would prevent the partitioning onto the chaperonin (Figure 2.13 B), particularly if the aggregation is rapid. This rise in aggregation could most easily be assessed by observing the increase in light scattering profiles of the free protein. Consequently, these aggregation reactions will interfere with or even diminish the extent of the partitioning reaction (i.e. less substrate being partitioned onto the GroEL beads). Also, although our test solutions are continually mixed with GroEL immobilized on a Sepharose bead support, the diffusion of the target protein from the bulk solution to the microenvironment of the functional immobilized GroEL could limit the kinetics of the collisional processes that lead to tight binding. A review of

association constants between GroEL and partially folded or collapsed folding intermediates indicates that the kinetic range is anywhere from 10^8 $M^{-1}s^{-1}$ (diffusion controlled) (*208*) to 10^3 $M^{-1}s^{-1}$ (*209*). These association rates vary because they depend on the nature of the folding intermediate (degree of hydrophobicity), electrostatic nature of that intermediate (GroEL surface is negatively charged) and/or the kinetic collapse of that particular intermediate (*132*). The easiest way to circumvent this aggregation problem is to either increase the chaperonin concentration by using smaller bead constructs effectively competing out aggregation reactions or by using different immobilized platform systems. For example it was demonstrated by our laboratory and others, that a large excess of soluble chaperonin (10 GroEL to 1 target protein molar ratio) effectively prevents competing aggregation side reactions and under these conditions, all of the protein eventually partitions onto the chaperonin. Nonetheless, even with this limitation at high enough GroEL concentrations, this particular chaperonin could be possibly used as a platform to readily identify protein stabilizing conditions, even for the aggregation prone proteins like I154F frataxin or previously the aggregation prone CFTR NBD1 (*99*).

2.4 Conclusions.

In this chapter, the proof-of-principle for the chaperonin sink assay with a test substrate, dihydrofolate reductase, was established. This was followed by demonstrating the utility of the assay to identify small molecule stabilizers for disease causing proteins such as CFTR and frataxin. It was also demonstrated that differentiating the kinetic stabilities between different mutants or between different proteins could be achieved in a facile manner utilizing the chaperonin assay. As with all bead-based assays, it was necessary to ensure the separation of the beads from the supernatant and also ensure that the beads did not interfere with the signal output. This signal that is used to determine partitioning is dependent on the remaining protein in

solution. Thus, the absorption spectra, fluorescence or enzyme activity of the protein that remains in solution could be measured as a function of time. To ensure a good signal, a high concentration of soluble protein in the assay is required. These studies, although instrumental in assay development, have to eventually be scaled up to generate a higher throughput prototype. The first prototype high throughput assay system that was developed involves the bead-based system described in this chapter coupled with a rapid plate reading system to evaluate protein stability in solution. This approach is discussed in the next chapter.

CHAPTER 3: OPTIMIZING THE PARAMETERS FOR SCALING UP THE CHAPERONIN SINK SCREENING ASSAY TO A HIGH THROUGHPUT PLATE BASED SYSTEM

3.1 Introduction to high throughput screening.

HTS is the process in which large numbers of chemical compounds are tested for binding or biological activity preferentially against a biological target (frequently proteins). Moderate to HTS screens provides the means to investigate the effectiveness of large numbers of compounds against a specific biological target of interest in a comparatively short period. HTS was initially established by large pharmaceutical companies like Pfizer and Eli Lilly during the early 1990s. The development of HTS progressed rapidly during the human genome-sequencing project in the early 2000s. This interest in developing HTS dovetailed with the human genome project, which was bringing several new potential protein targets in focus. At about the same time, the trend of automating large-scale searches using large combinatorial chemistry libraries expanded the drug candidate testing platforms. This made the more traditional low throughput screening methods (such as enzyme assays) ineffective and forced the development of strategies that could carry out multiple assays simultaneously within a single plate formats (96 wells originally, now up to 1536 in ultra-high throughput systems).

The traditional biochemical and pharmacological drug discovery screening methods utilized prior to HTS had limited assay capacities. These low throughput assays were generally used to uncover structure activity relationships (relation between chemical structure and biological activity) of the small molecules to improve them further or generate new molecules using combinatorial chemistry (*210*). Such assays used about 5-10 mg of compound in a volume

of 1 ml or more. They could be carried out with a frequency of about 25-50 assays/week. In contrast, HTS carries out hundreds of individual assays at the same time and can be used to screen more than 10,000 compounds per day. It is thus an ideal method to probe large chemical libraries against a specific drug target. Advances in microplate based instrumentation, robotics and cheap computational power helped to make the leap to higher throughput facile and routine. The development of analytical techniques such as scintillation assays, fluorescence polarization, etc. to be used in conjunction with the robotic set-up further helped to improve screening rate and throughput. It also led to the miniaturization of the assay volume to fit into 384 and 1536 well plate formats. Continuing improvements in screening technologies have enabled the screening of literally millions of compounds per week. Such screenings that occur at rates of 100,000 compounds per day or higher (1,000,000 per day) are usually called ultra-high throughput screens or uHTS

HTS and uHTS assays can be either cell-based, biochemical or *in silico* screens and involves drug targets, assay methodology, compound libraries, robotic automation systems and data analysis programs. Cell-based studies report functional end points while biochemical assays usually measure the affinity, stability or enzymatic activity resulting from introduction of the test compounds for the target. *In silico* based screens are computer simulation based methods where the energy of interaction of the compound binding to the active site or another druggable site of the target is used to identify hits. Hits are the compounds that exhibit the desired end points of a HTS assay. The hits generated from the primary screen usually have to undergo a secondary screen system to confirm their effectiveness or verify the specific interaction with the target protein or system. The secondary screening assay can be a non-HTS assay. Secondary screening

approaches are also used with other applications in genomics, crystallization, drug pharmacokinetics and pharmacodynamics, materials evaluation and environmental toxicity.

Although several HTS screens have been carried out to identify small molecule stabilizers for misfolding proteins, most of these are cell-based assays (*211, 212*). The advantage of such cell-based assay systems is that they provide information about functional read-outs while providing information about cytotoxicity, which then help to predict *in vivo* behavior. However, it is difficult to miniaturize and scale-up such assays. These assays are also plagued by cell culture variability, poor reproducibility, and low signal intensity. Automating feeding, sorting and maintaining the cells increases the number of steps and the costs involved in the assay. Alternatively, *in silico* assays have been used to identify small molecule stabilizers of misfolding proteins (*213, 214*).

Another system that could potentially be used to screen for small molecule stabilizer of biochemical targets is the ThermoFluor system (See Chapter 1, section 1.1.4a). An offshoot of this system that uses intrinsic fluorescence of the protein to measure shifts in T_m has been used in several studies to carry out HTS (*215*). Many of the HTS assay systems that have been developed for protein misfolding diseases have primarily focused on a subset of diseases that results from lysosomal storage defects (*216-218*), such as Tay-Sachs and Gaucher's disease. In these instances, these assays are only specific for each folding disease state. Prior to the initiation of the current study, a broad generalized screening platform did not exist for misfolding diseases in general. The chaperonin platform looks to fulfill this broad based requirement.

A good HTS platform is low cost, precise, sensitive and robust. The robustness of an assay is an indication of its reliability. It is a measure of the capacity of an assay to remain unaffected in case of well to well, plate-to-plate or day-to-day variability, changes in users, and

instruments. A good assay should also have simple steps that can be easily automated. It is predicted that the chaperonin assay could be scaled up to a platform design that could be potentially be used with a HTS set-up. From what was described thus far, this would involve optimizing assay components including the reliability of the plate systems used, the beads used for immobilizing the chaperonin and the assay readout to obtain reliability and reproducibility. At the end of this evaluation, a prototype platform system that could then potentially be used to screen stabilizers for protein prone to misfolding could be developed.

3.2 Materials and methods.

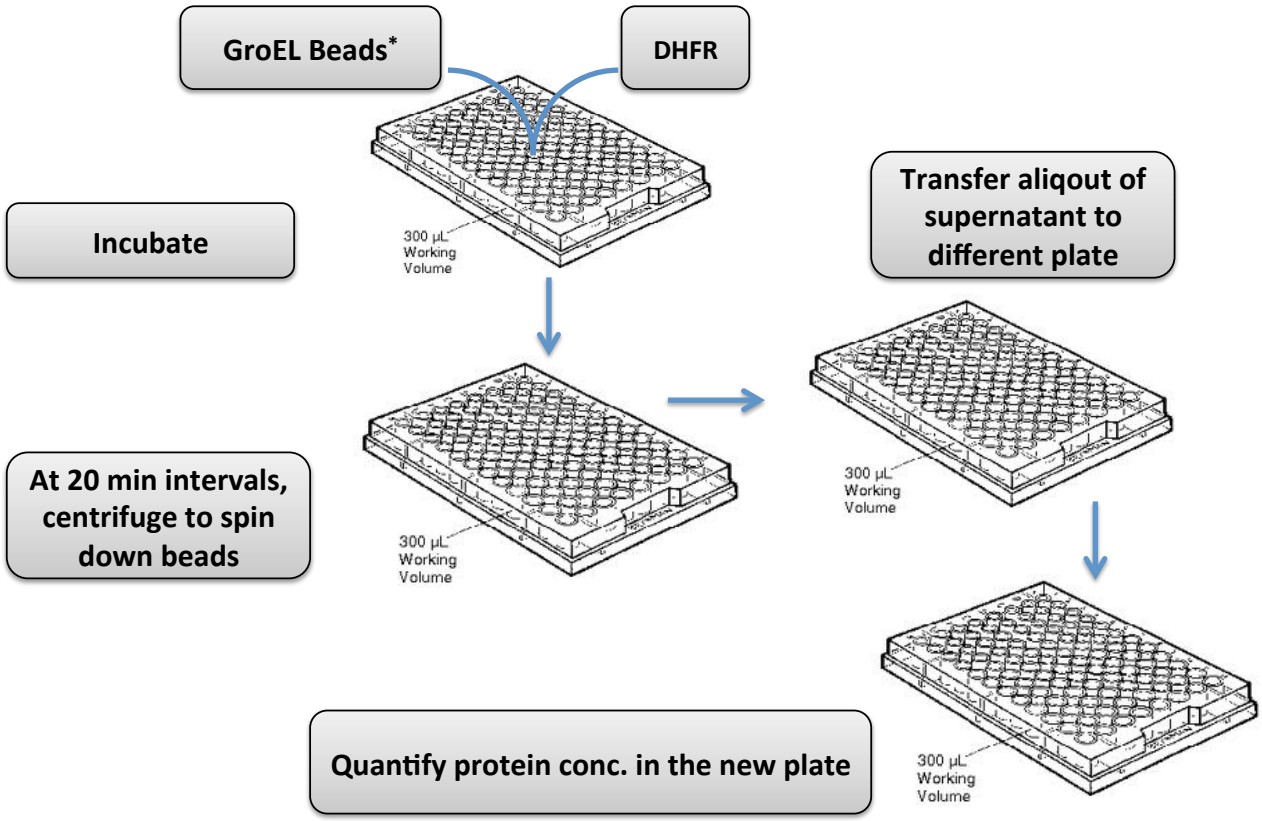

Figure 3.1: The protocol test setup for carrying out the chaperonin based partitioning assay in multiwell plates. In this instance, chaperonin beads were incubated in the wells of a multiwell plate with the substrate protein to be tested. At twenty min.

intervals, the plates were spun down and the supernatant containing the remaining protein was transferred to another plate. The amount of substrate protein remaining in the supernatant in the second plate was quantified using UV spectroscopy, fluorescence spectroscopy or by measuring the enzyme activity.

a Materials.

GroEL beads were prepared and assayed as described earlier in section 2.2.2. To test assay efficiency, the test model protein, dihydrofolate reductase and known ligands, dihydrofolic acid and NADPH were the protein/ligand pairs of choice. All of these compounds and proteins were obtained from Sigma. Microplates with 96 and 384 wells were obtained from the standard sources. Silicone mats to cover the 96 and 384 well plates were obtained from Axygen Inc. All other chemicals were of the highest purity and obtained from standard sources.

b Following DHFR partitioning onto chaperonin beads using standard microplates.

The partitioning assay in microplates was carried out following the scheme outline in Figure 3.1. The assay was modified based on whether a 96 or 384 well plate was used. For example, the total reaction volume per well was adjusted to 100 µl in a 96 well plate or to 70 µl per well in a 384 well plate. 2 µM DHFR was incubated with a roughly equimolar quantity (oligomer GroEL to monomer DHFR) of GroEL linked onto beads in clear V-bottomed plates (Whatman). The Whatman V-bottom plate was preferred to a U-bottomed or a flat-bottomed plate as it facilitated separating the supernatant from the beads during the centrifugation step (Figure 3.1). The plate was sealed with a silicone mat (Axygen) to prevent evaporation while incubating. The plate was then incubated on an orbital shaker at 25°C. The plate was centrifuged to spin down the beads every 20 min. 10 µl of supernatant was then carefully removed from the

test well taking care not to aspirate any beads. Although this step was carried out manually in these studies, it can easily be automated. The 10 µl of supernatant was added to a mixture containing dihydrofolic acid and NADPH in another plate. This mixture in the second plate was then assayed for DHFR content via the DHFR assay using a plate reader in a black 96 well plate. The slope of the decrease in the 340 nm absorbance associated with NADPH utilization of DHFR was used as the readout for DHFR activity. Alternatively, the amount of protein left in the well could be determined via spectroscopic methods.

c Following DHFR Partitioning assay using an alternative filter bottomed microplate method to separate the chaperonin beads from the test partitioning protein.

Plates with 96-well filter bottoms were obtained from Pall (Figure 3.3). These plates had a filter membrane on the bottom of each well. 2 µM DHFR was incubated with a roughly equimolar quantity (oligomer GroEL to monomer DHFR) of GroEL linked onto beads in these filter bottomed plates. The total reaction volume per well was 100 µl. The plate was sealed with a silicone mat (Axygen) to prevent evaporation while incubating. The plate was then incubated on an orbital shaker at 25^{o}C. At 20 min. intervals, the filter plates were placed on top of a receiving plate (any 96 well plate). The two plates were centrifuged together for 15 seconds at 3000xg resulting in the supernatant filtering through into the bottom plate while the GroEL beads were left behind in the retentate solution (on top of the filter membrane in the top plate.) Care was taken while spinning to avoid the beads drying out (all solution removed). 10 µl of the filtrate was then carefully removed from the well in the bottom plate (filtrate). This 10µl of supernatant was added to a mixture containing dihydrofolic acid and NADPH in another plate. This mixture in this plate was then assayed for DHFR content via the DHFR assay using a plate reader in a black 96 well plate. The slope of the decrease in the 340 nm absorbance or

fluorescence associated with NADPH utilization of DHFR was used as the readout for DHFR activity. The remaining filtrate was then added back to the beads and re-incubated. This cycle continued until the signal (enzyme activity or protein quantitation) approached a limiting value (plateau).

3.3 Results and Discussion.

3.3.1 Optimization of the components of HTS set-up for the chaperonin sink assay.

HTS is frequently used in drug discovery to identify hits for a wide variety of lead compounds that can be potential candidates for therapeutic development. However, little progress has been made in rapidly identifying protein folding disease stabilizers using HTS due to the inherent instability of the target proteins themselves. In chapter 2, a broad based screening system based on the promiscuous chaperonin GroEL that could potentially be utilized for HTS of small molecule stabilizers of transiently stable target proteins was introduced. Adapting the assay for HTS, however, requires the optimization of several factors. As mentioned in the introduction, the primary goal outlined in this chapter was to demonstrate that the assay to identify lead stabilizer compounds could be scaled up to potential HTS platform. The easiest path to demonstrate the efficacy of a viable prototype system is to utilize a model protein with a known stabilizing molecule. In this case, the goal was to demonstrate that a bead and plate set-up can recapitulate low throughput solution results of chaperonin binding to an easy to obtain substrate protein, DHFR, in the presence and absence of the stabilizing compound NADPH. Additionally, as mentioned above the assay must be robust (results easy to replicate), rapid and easy to use. One way of testing this robust nature is to demonstrate that the assay can be reproduced using a variety of different assay screening plate systems. Other HTS experimental parameters that

needed to be optimized include testing different bead platforms and demonstrating ease of reproducibility during the bead/supernatant separation phase prior to protein assay measurement.

The signal to background noise of the assay (ruling out non-specific binding, robust partitioning) should also be sufficiently high. In the case of DHFR, the first initial signal that is used relates to the changes in native DHFR enzyme activity as partitioning onto the chaperonin platform proceeds. Even though we will eventually construct a broad based assay, using the DHFR enzyme activity will create a high signal to background noise ratio. Once the assay has been validated in these plate based HTS formats, cost concerns in the form of the amount of protein used also have to be addressed.

a Optimization of type of beads used in the studies.

As with any bead-based assay, one has to be aware that the success of these experiments depends in part on the nature and chemistry of the beads themselves. Ideally the beads that are used should be cheap, stable (should not leach the bound protein), inert (they also should not act as surfaces onto which the substrate protein adsorbs non-specifically) and easy to handle. One added feature of the chaperonin system is that the partitioned protein could be released from the GroEL bead surface. This could potentially make the system reusable for a number of assays. The microtube scale experiments carried out during proof-of-concept studies (Chapter 2) utilized NHS-Sepharose beads. The plate based bead assay protocol involves separating the beads from the reaction mixture to quantify the native protein concentration (or enzyme activity) in the supernatant. In an HTS format, the plate based system separation can be carried out by spinning down the microplate using a centrifuge to sediment the beads. An aliquot of the supernatant can then be easily withdrawn from wells and transferred into another multiwell microplate. Another plate based separation method was carried out using chaperonin immobilized magnetic beads

that can be separated from the supernatant using a powerful magnet system. This latter method was explored because centrifugation steps increases the time involved the HTS set-up. Utilizing the magnetic bead-based systems may speed up the assay.

To determine the effectiveness of these magnetic beads, GroEL was initially immobilized onto the NHS-activated magnetic beads using amine coupling. The immobilization simply entailed incubating the chaperonin with magnetic beads for two hours at room temperature in an amine free buffer. The chaperonin covalently couples via free lysines to the beads through NHS ester chemistry. The free activated surface on the beads was quenched by incubating the GroEL loaded beads with 1 M ethanolamine (pH 8) for one hour at room temperature. The beads were then washed with refolding buffer to obtain GroEL loaded magnetic beads. The successful immobilization of GroEL onto these beads was confirmed by boiling the beads in SDS, disrupting the attached GroEL oligomer and carrying out gel electrophoresis on the supernatant to verify the presence of the ~60kDa band of GroEL monomers. GroEL attached magnetic beads were then utilized to carry out partitioning experiments with DHFR. A parallel set of experiments with GroEL immobilized on Sepharose beads was run as a positive control. However, partitioning of DHFR onto the magnetic beads did not yield any recoverable refolding of DHFR when a mixture of 10 mM ATP and 4 M glycerol was added to the GroEL magnetic beads. In contrast, under the same conditions, DHFR was able to partition and refold from the control Sepharose beads (Figure 3.2). Furthermore, no DHFR was observed to partition onto the magnetic beads following a similar SDS removal of GroEL. Only the band corresponding to GroEL monomer was observed indicating that DHFR had failed to partition onto the beads. Not only did DHFR fail to partition onto GroEL magnetic beads, the costs associated with procuring these beads for large-scale studies also limited the magnetic bead feasibility. At this time, it is

unknown why GroEL failed to remain in an active polypeptide capture competent state when attached to the magnetic bead supports. It was therefore decided to utilize the Sepharose based beads for the assay prototype and use centrifugation as the method for separating GroEL beads from partitioning protein.

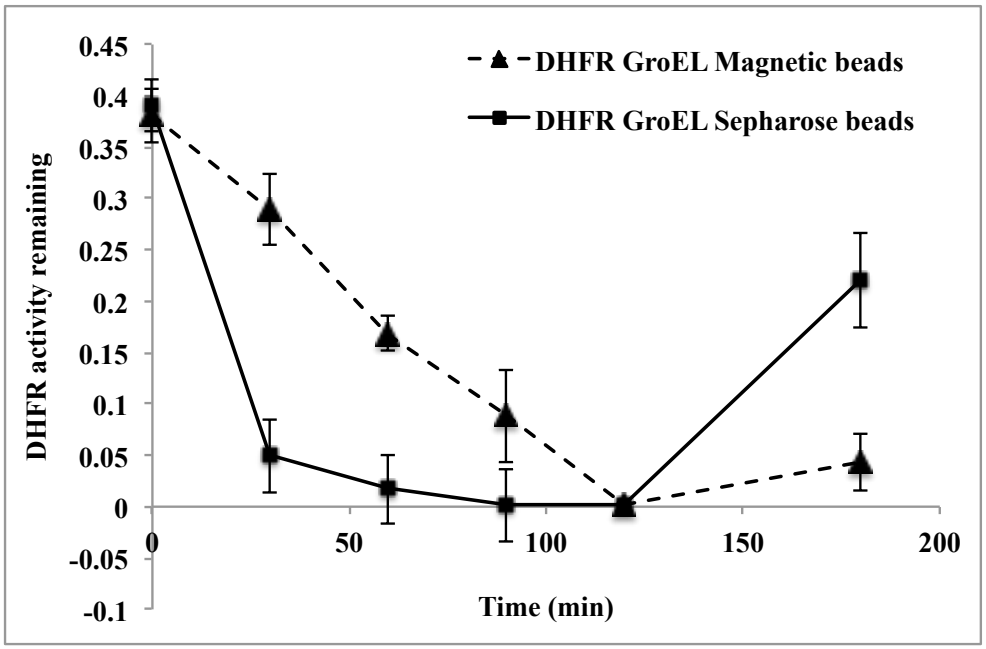

Figure 3.2: No partitioning or refolding of DHFR was observed with the magnetic beads. NHS-magnetic beads were loaded with GroEL using amine coupling and then incubated with DHFR. At 20 minute intervals, the beads were spun down and the supernatant assayed for DHFR. As compared to the control NHS-Sepharose (filled squares), no partitioning or refolding of DHFR was observed with the magnetic beads (filled triangles).

During HTS optimization, the National Institutes of Health (NIH) guidelines for assay development and optimization were followed. One of the initial requirements in the guidelines is to demonstrate the stability of the beads under storage and during the assay. An aliquot of the bead sample was stored at 4ºC for long-term studies. It was observed that the beads were stable

and active even after a year of storage at 4ºC. Additionally, during studies involving frataxin, the beads could be incubated at elevated temperatures as high as 45ºC with complete reversibility. These conditions are similar to an accelerated stress test. It was observed that even under these harsh conditions, the beads maintained GroEL activity (refolding DHFR). The only caveat during these optimization tests was that the beads were required to be maintained in a hydrated state, since spinning the fluid away from the beads inactivated the immobilized GroEL.

Another crucial test for the bead construct system and GroEL is to insure that the GroEL remains active in the solvent used in most chemical libraries. Compounds from a chemical library that are utilized in HTS are frequently water insoluble. This necessitates them being solubilized in water utilizing a dimethyl sulfoxide (DMSO) co-solvent. The concentration of DMSO used in these libraries can approach 10%. To ensure that GroEL beads are stable in the presence of DMSO, the partitioning assay was carried out in several concentrations of DMSO and it was determined that the GroEL beads and soluble GroEL remains stable and active for the duration of the assay in the presence of DMSO.

b Optimization of the separation technique for the chaperonin beads.

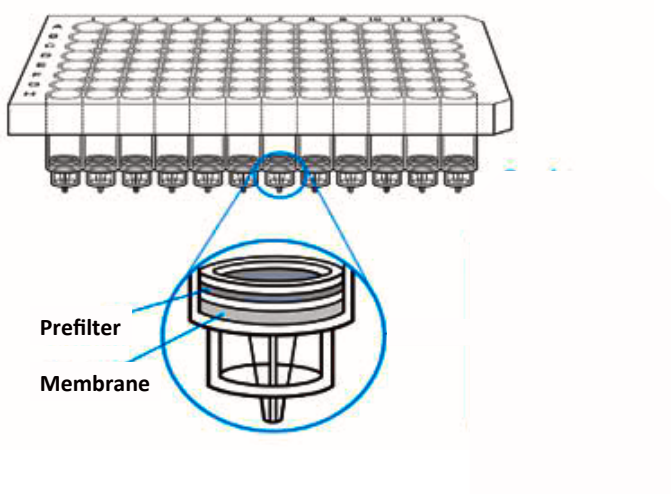

Figure 3.3: A filter bottom microplate consists of a polypropylene housing with membranes placed and sealed in the individual wells. The assay was carried out in such plates with DHFR being incubated with GroEL beads. At specific intervals, the plates were spun down to obtain the supernatant and the concentration of native active DHFR was assayed using the NADPH assay (*219*).

In addition to centrifugation, another approach that can be used to separate the GroEL beads from the test protein in the supernatant is to utilize plates with ultrafiltration pads on the bottom of each well. These plates have an isolated well design and individually sealed filter discs that eliminate potential for reagent flow from well to well and can be easily used with particle based assays in a high throughput set-up (Figure 3.3). Such plates are called filter bottom plates. Although these plates are comparatively more costly than normal plates, the reduction in steps associated with the assay and the ability to reuse the plates could be useful for higher throughput and would decrease overall assay costs.

In this experiments, the chaperonin beads were incubated with DHFR in the filter bottom plates. As a control, DHFR was also incubated with blank beads in the same plate. To measure the concentration of the native DHFR, the filter plates were fitted with a receiving plate on the bottom (any regular 96 well plate) and centrifuged. The buffer containing the native protein easily passed through the large MW cutoff filter (100 kDa cutoff) while retaining the chaperonin beads and any partitioned DHFR in the top plate (retentate volume of the filter bottom plate). The concentration of the native DHFR in the filtrate in the lower plate was measured and quantitated using the DHFR assay. It was observed that the assay could be carried out using this set-up to follow the partitioning and refolding of DHFR (Figure 3.4).

However, several operational problems were also encountered while utilizing these filters plates. It was observed that the DHFR containing buffer easily leaked through the filter membrane at the bottom of the plates into the receiving plate during the course of the assay. This undermines the assay since a portion of the DHFR concentration would be unable to partition onto the GroEL, skewing the results toward lower partitioning which in turn would lead to a false positive result. To overcome this problem, the bottom of the plates were sealed utilizing a SealMate® adhesive microplate film. This prevented the buffer leakage over the course of the experiment and could be easily removed prior to spinning down the plate. Another problem encountered with this step dealt with the drying of the chaperonin beads and subsequent inactivation of the immobilized GroEL during the supernatant separation step. Consequently, fresh beads had to be added after each run, increasing the quantity of beads that had to be used and requiring a multiple sampling procedure. Due to these difficulties and the high costs associated with these plates, it was concluded that the filter plates were not useful as a platform prototype.

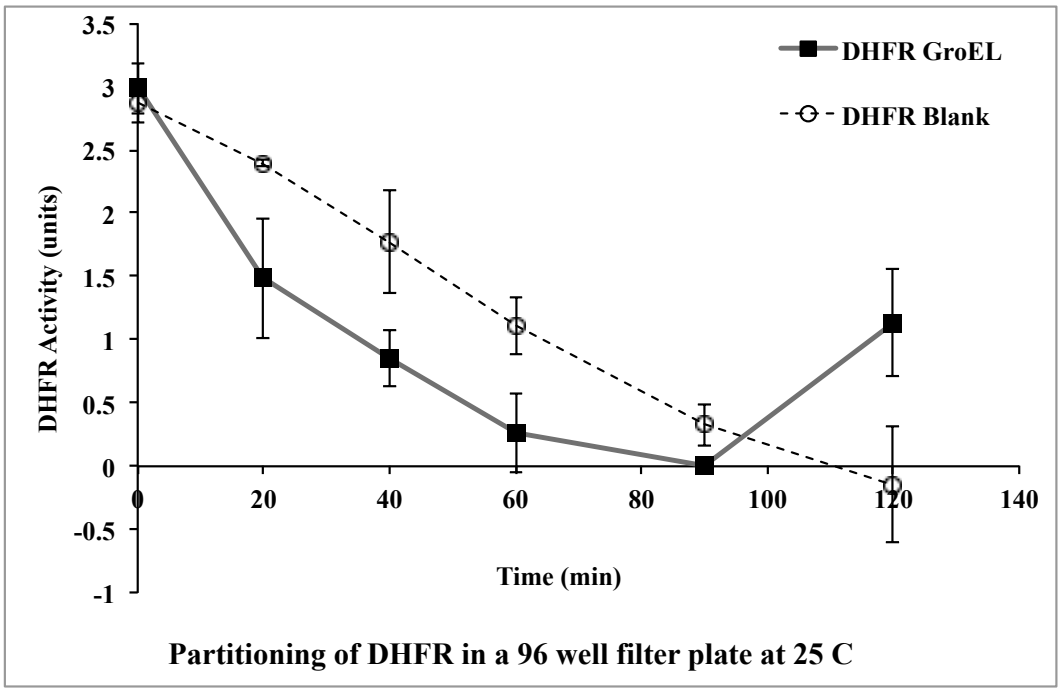

Figure 3.4: Partitioning and refolding of DHFR in the presence of GroEL beads (filled squares) could be followed using filter plates. The decrease in DHFR activity in the presence of blank beads (open circles) is due to heat deactivation and aggregation. Filter plates could be utilized to carry out the assay but each assay point required the addition of fresh GroEL beads. The experiments were repeated in triplicate.

c Optimization of microplates used for HTS studies.

Determining the robustness and reproducibility of the results is an important facet of HTS, where multiple factors relating to the type of microplates, liquid handling system, and evaporation all contribute to difficulties in the assay outcomes as well as execution. Plate based systems are still the predominant platform for typical HTS assays because these are the preferred set-ups for screening a libraries of several thousand compounds. The plate based assays must not demonstrate large intra-plate and inter-plate variations as these will lead to statistically unfavorable variations in the output signals (in this test case the enzyme activity). We

investigated these variations by carrying out the assay utilizing three different plates, Corning 96 well NBS, Whatman 96 well low binding and Griener 96 well low binding plates. Prior to carrying out the assay the background signal (enzyme activity in the case of DHFR) from the beads was investigated and found to be negligible. This establishes a high signal to background ratio as is required of a good HTS assay. The partitioning assay was carried out in quadruplets in four different corners of the plate and each assay was repeated thrice thus giving a total of twelve data points per time point. It was observed that the intra-plate and inter-plate variance was comparatively low (Figure 3.5) with all data points being within one standard deviation. However, since the cost associated with the V-bottomed Whatman 96 well low binding plates was comparatively lower than the other two, we decided to utilize these plates for further studies.

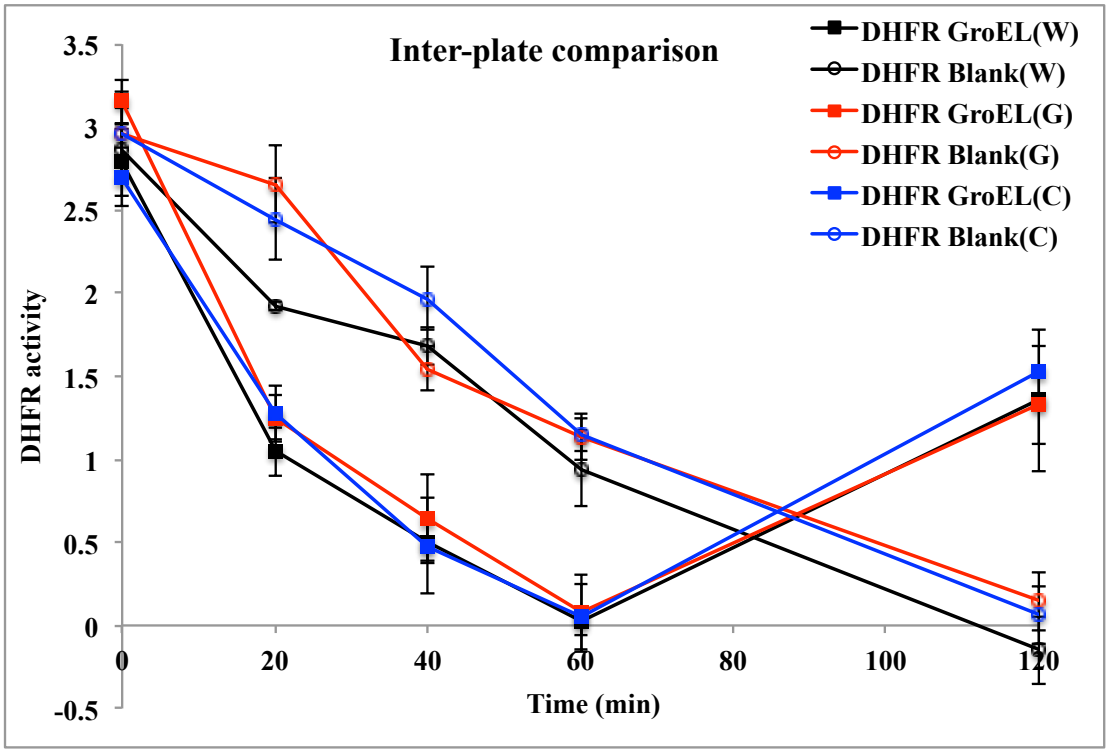

Figure 3.5: Three different plates Corning 96 well NBS (blue traces), Whatman 96 well low binding (black traces) and Griener 96 well low binding plates (red traces) were

utilized to measure inter-plate variations. The assays were carried out in quadruplets for each time point and each assay was repeated thrice thus giving a total of 12 data points for each point. It was observed that the DHFR traces overlapped with each other for both the GroEL beads (filled squares) and the control beads (open circles) demonstrating low variance.

d Optimization of the format of microplates used.

In recent years, the trend of HTS studies has shifted towards higher throughput set-ups that utilize 384 and 1536 well plates. Such set-ups ensure that higher numbers of screens are carried out in the smallest possible time. The miniaturization of the assay also decreases the volume required for the assay and thus the amount and cost of reagents required per well. The 1536 well set-up however requires specialized instrumentation that handles lower volumes. The typical set-up that is more common and that is readily available is the 384 well plate format. This provides sufficient throughput while retaining the same footprint as a 96 well plate (*220*). The assay conditions that work in a 96 well platform could also be predicted to work in 384 well format. However, the reagent volumes have been miniaturized to 384 well format. To test the efficacy of using the chaperonin with these smaller volumes, the partitioning assays were carried out concurrently utilizing a 96 well plate (Whatman) and a 384 well plate (Nunc). These experiments were carried out in triplicate. The molar concentration of both DHFR (monomer) and GroEL (oligomer) in the assay was maintained at 2 μM. The total volume in the 384 well plate was reduced to 70 μl. At 20 min. intervals during partitioning, 5 μl of aliquot was withdrawn from the 384 well plate while 10 μl was withdrawn from the 96 well plate utilizing positive displacement pipettes to control for volume efficiency in the sample. Both aliquots were assayed for DHFR concentration and the readings were normalized to 10 μl. It was observed

(Figure 3.6) that the partitioning of DHFR onto the chaperonin beads as well as its refolding were easily measured in both the 96 and 384 well plates. The partitioning and refolding traces obtained with the 384 well plate was observed to closely follow those traces obtained with the 96 well plate. This demonstrates that the assay can be easily carried out in a 384 well format with a reduced volume and potentially a higher throughput.

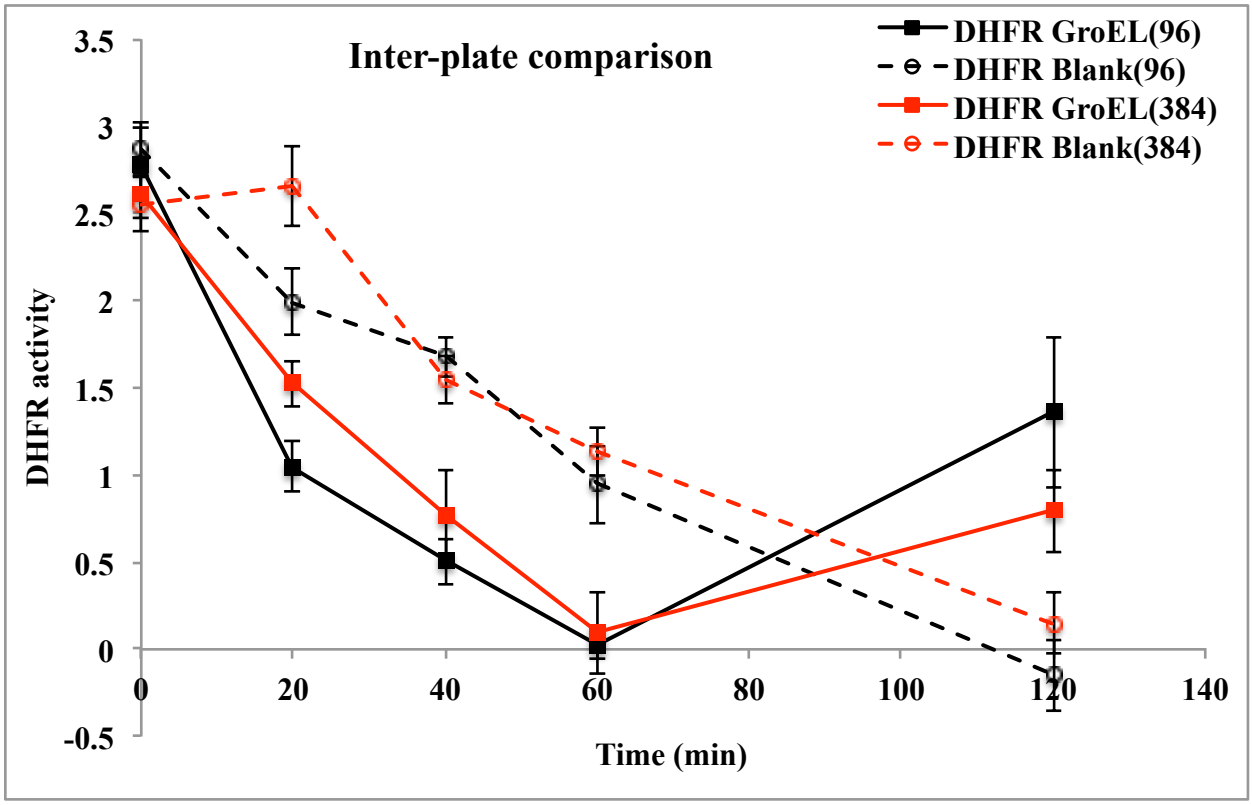

Figure 3.6: Comparison of chaperonin assays carried out in 384 well plates (red traces) and 96 well plates (black traces) showed that the partition and refolding from the chaperonin beads (filled squares) could be easily followed even at the lower volumes (70 µl) used in a 384 well plate. The assays were carried out in duplicate for each time point and each assay was repeated thrice.

e Optimization of detection read-outs.

Most HTS assays rely on very sensitive read-outs that detect the presence of the test protein of interest. The development and utility of the chaperonin prototype system with the bead supports depends on enzyme assay detection of the test substrate DHFR. However, almost all of the disease proteins that would be utilized as a screening target will not have similar enzymatic activity measurements. Thus, it is essential to examine other detection techniques to follow the partitioning of transiently folded species while measuring the remaining protein in solution. An ideal detection readout must be universal (same technique used for all substrate proteins), sensitive to low protein concentrations, rapid and reproducible. One approach involves labeling the substrate proteins with radioactive or fluorescent labels. However, utilizing such labeling reagents increases the costs associated with the assay, increases detection time and has proven to be challenging with the low volumes used in HTS assays (*221*). Another sensitive, facile and rapid method to probe the folded state of the protein is to utilize the intrinsic fluorescence of the protein. This intrinsic fluorescence is due to the fluorescence emission by phenylalanine, tyrosine and tryptophan. However, only tyrosine and tryptophan are used experimentally because of reasonable quantum yields. DHFR has six tyrosine and three tryptophan residues. Accordingly one should be able to follow partitioning utilizing the intrinsic fluorescence of DHFR. In this instance, partitioning was measured as before at 25°C using a V-bottomed Whatman microplate. At 20 min. intervals, the plate was spun at 4000xg for 30 sec. to sediment the beads. 50 µl of the supernatant aliquot was then transferred to a 96 well black microplate. The DHFR fluorescence was measured using a Spectramax M5 plate reader (Molecular Devices). The sample was excited at 295 nm and the emission measured at 340 nm.

As DHFR partitions onto GroEL beads, one would expect a concomitant decrease in the supernatant fluorescence. Initially, as DHFR partitions onto GroEL, there is a decrease in tryptophan fluorescence (Figure 3.7). However, after the initial sharp decrease, the tryptophan fluorescence shows smaller changes. The control (partitioning onto blank beads) shows that the fluorescence remains virtually the same throughout the course of the experiment (Figure 3.7). Thus, although one can utilize fluorescence to detect differences between the DHFR that partitions onto GroEL beads and the control, these results are in marked contrast to the enzyme activity based results where the DHFR activity reaches zero in the presence of the chaperonin. From these observations, one possible reason for the remaining fluorescence may be due to a portion of the DHFR that undergoes heat based inactivation and aggregation to remain in solution. As shown in chapter 2, any aggregation of the target protein can remain in solution and fail to partition onto GroEL. The aggregated DHFR still contributes to a fluorescence signal even though it may lose activity. Hence an activity based readout that shows complete loss of activity may be due to both a combination of partitioning and inactive aggregation.

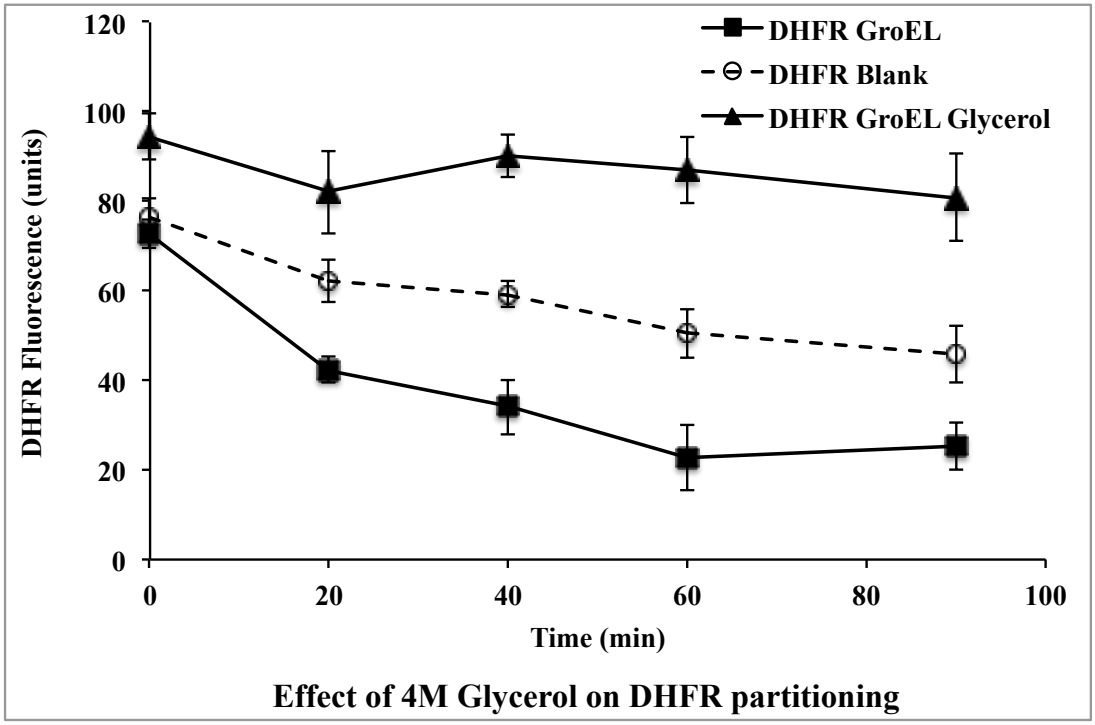

Figure 3.7: DHFR intrinsic fluorescence can be utilized to follow its partitioning where it shows an initial rapid decrease with the chaperonin (filled squares) while the control beads (open circles) do not show a similar decrease in fluorescence. The continued presence of the DHFR fluorescence over time in both the samples can be due to aggregation of the remaining DHFR protein.

Another problem with using protein fluorescence that depends on UV excitation (295 nm) is that many small molecule ligands are polyaromatic that may interfere with both excitation or may possess their own intrinsic fluorescence. For example, NADPH is a fluorescent molecule. It was concluded that intrinsic fluorescence cannot be used as a measure of partitioning transient folds onto the GroEL chaperonin.

f Utilizing the prototype to demonstrate ligand based stabilization of misfolding proteins.

The optimization studies carried out using the multiwell plates provides a useful prototype chaperonin based partitioning platform provided that an enzyme assay is available success of the plate platform is to utilize it for carrying out screening for small molecule stabilizers of misfolding proteins. However, prior to carrying out such a large-scale screening, one needs to demonstrate that such stabilization can easily be detected using this set-up. The proof-of-concept (Chapter 2/microtube based) assays shows that DHFR can be stabilized by NADPH or folding osmolytes. By default these stabilizers should also work within the plate based system. To carry out such a study, the chaperonin beads were incubated with DHFR alone, in the presence of 4 M glycerol or 10 mM NADPH. As predicted, the plate based prototype confirms the prediction of stabilization (Figure 3.8).

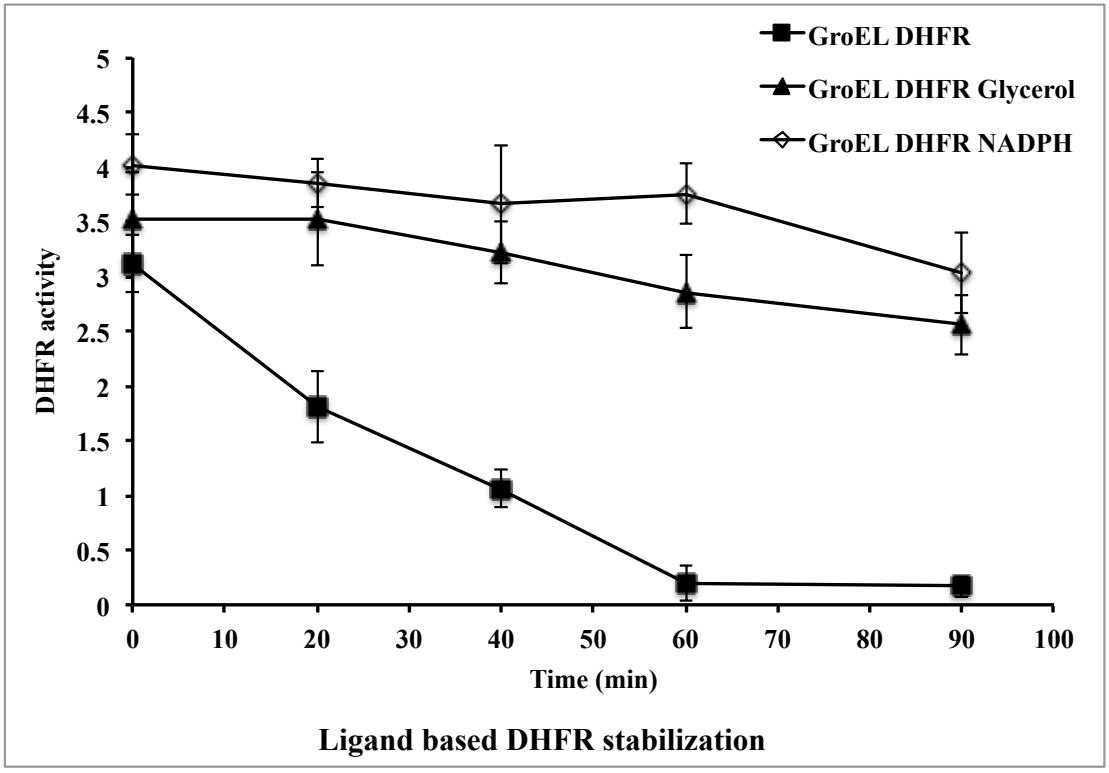

Figure 3.8: The prototype could be utilized to follow a small molecule and an osmolyte based stabilization of DHFR. DHFR without any stabilizers (filled squares) showed partitioning onto GroEL, while the rate of partitioning was much lower for DHFR stabilized with NADPH (crosses) and with 4 M glycerol (filled triangles).

3.4 Conclusions

The development of a successful prototype platform is a crucial step prior to carrying out a successful screening to obtain hits that might be useful to generate leads for protein misfolding diseases. In order to obtain the right set of hit compounds (one that could easily generate lead compounds), the assay should be precise, sensitive and robust. This chapter involved the optimization of several parameters that help in achieving this goal. These parameters involve factors such as the assay components (type of beads, type of plates), assay throughput (96 vs. 384 wells) as well as those that help in obtaining a sensitive assay with high signal to noise ratio.

A sensitive detection method and high substrate protein concentration per well is essential for the higher signal to noise ratio. However, the high per well concentration of the substrate protein subsequently increases the overall amount of protein required for a screening study. This is particularly problematic for misfolding disease proteins that are difficult to purify. Another problem associated with such disease proteins is that they tend to aggregate. As observed with DHFR, the shaking set-up required in the assay increases the mass transfer and might lead to the partially unfolded species interacting and aggregating. If the aggregation rate is higher than the partitioning rate, this might lead to the protein aggregating in solution. In such a case, as with the proof-of-concept system, the one problem that continually arises in these systems that depends on protein partitioning onto immobilized GroEL is that aggregation will lead to higher false positive hits. Thus, although the initial goals of developing a robust and reproducible prototype were partially met (one could still utilize the assay to look for differences between stabilized and non-stabilized protein), the problems associated with high protein concentrations needed, the need for using specific enzyme assays and in solution aggregation makes this particular assay cumbersome to use for a HTS. Hence, one needs to look at alternatives that prevent the aggregation and at the same time use a lower concentration of the disease protein.

CHAPTER 4: USING LABEL-FREE METHODS TO IDENTIFY PROTEIN STABILIZERS (PART 1 – SURFACE PLASMON RESONANCE).

4.1 Alternatives to the chaperonin bead platform systems.

In chapter 3, the development of a bead-based chaperonin assay to identify stabilizers for protein misfolding diseases was discussed. However, there are numerous disadvantages of using a bead-based approach to develop a reasonably high to moderate throughput protocol. One such problem centers on the large concentration of chaperonin and target protein required during the assay. It is often a challenge to purify such high concentrations of missense disease causing proteins that might be required for a HTS assay, especially in the case of proteins that tend to misfold. The higher concentrations are required to ensure that a sufficiently high signal to noise ratio is achieved for all of the spectrophotometric methods used thus far.

One method overcoming the problem associated with substrate protein aggregation is to immobilize the substrate protein on a solid support. This would potentially prevent the interaction among the substrate protein and prevent aggregation. It would be even more advantageous if such a system could get away with utilizing low concentrations of protein. Additionally, since the chaperonin protein interaction is reversible, there also exists the potential of recovering the substrate protein containing beads and reusing them over several assays.

A recent advance in examining protein-protein interactions involves the AlphaScreen (Amplified Luminescent Proximity Homogeneous Assay) system (*222*). It is a bead-based technology to study interactions in a microplate. It is a proximity assay where the binding of molecules that are captured on two different kinds of beads leads to energy transfer between the beads (Figure 4.1). There are two kinds of beads, a donor bead and an acceptor bead. Both bead

surfaces are coated with latex-based hydrogels containing reactive aldehydes that not only reduces non-specific binding but also provides a functionalized surface to which different macromolecules can be affixed (*223*). The donor bead contains pthalocyanine that on illumination at 680 nm produces reactive singlet oxygen from ambient oxygen (*224*). This singlet oxygen has a half-life of 4 μs and can diffuse about 200 nm in solution. If there is an acceptor bead in the vicinity, the singlet oxygen transfers its energy to dyes (thioxene, anthracene, and rubrene derivatives) on the acceptor bead (*225*). This transfer leads to the acceptor emitting light at 520-620 nm. The advantage of AlphaScreen is that it can be used for a wide range of interaction affinities (pM to mM) and is easily adapted for HTS and uHTS systems (384-1536 well systems).

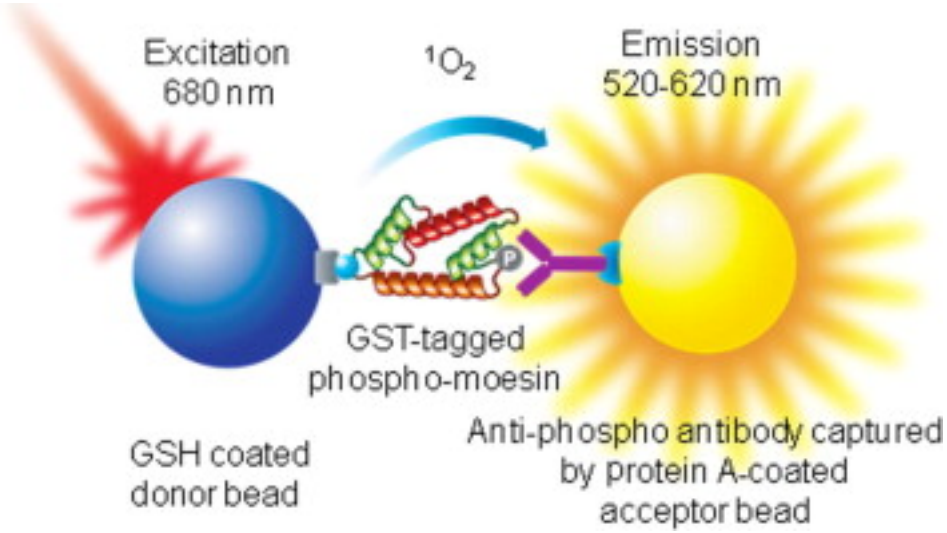

Figure 4.1: The AlphaScreen assay studies the interaction between two macromolecules bound on two different beads. Here, two antibodies to the same molecule are immobilized on a donor and an acceptor bead. When the two antibodies interact with the molecule in solution, they are in proximity to each other. On excitation of the donor bead at 680 nm, the dyes within the bead convert ambient oxygen into singlet state. This

singlet oxygen diffuses for about 200 nm before returning to the ground state. If the acceptor bead is within this range, the singlet oxygen reacts with the chemicals within acceptor bead and emits light at 615 nm. Figure adapted from (*226*)

However, AlphaScreen has its own set of disadvantages. The AlphaScreen is light and temperature sensitive. This can be a major problem since in some instances; the chaperonin partitioning assay sometimes depends on elevating the temperature of the assay to shift the equilibrium of a protein to populate larger steady state populations of the partially unfolded test substrate. Another disadvantage that is unique to the target proteins used for protein folding diseases relates to the intrinsic aggregation propensity of the disease protein even when it is attached to the bead support. This intrinsic aggregation would lead to a situation where the substrate beads self aggregate, resulting in a decrease in interaction with the chaperonin bead. This aggregation tendency also increases due to the constant stirring that is required in the AlphaScreen set-up.

4.2 Introduction to surface plasmon resonance.

A viable alternative to partitioning onto chaperonin beads from solution or using the AlphaScreen technologies is to explore the possibility to using label-free technologies. For these systems, the detection of interactions is more sensitive. The advantage of these detection systems is that one can easily immobilize one component on a biosensor surface and examine the increases or decreases of binding interactions of the other protein component in real-time. These methods probe physical properties that result from the formation of bio-molecular interactions due to changes in protein density and refractive index changes. Many such label-free techniques are typically faster than traditional assays, and changes due to interactions can be easily determined by following the binding kinetics (*227*). Optical biosensing techniques are among the

most commonly used label-free techniques. All optical biosensing label-free techniques have three basic components: the biological molecules whose interaction is to be probed, a biosensor that captures the molecule to be probed and a detector that converts the physical properties of the biological interaction into a photometric, electrochemical, electrical, or acoustical signal change. Label-free systems have been utilized for primary screening of small molecules (*228*), fragment-based screening (protein binding to peptide fragments of 100-300 Da, reviewed in (*229*)), and epitope mapping. Label-free techniques are especially useful in small molecule screening to optimize identification of lead compounds obtained by primary screening, determine affinities of interactions and identify optimal affinities.

One of the most popular and successful label-free interaction techniques used to evaluate protein-protein interactions is surface plasmon resonance (SPR). SPR (Figure 4.1) is a microfluidic optical biosensing instrument that enables one to analyze real-time binding amplitudes between a ligand and an analyte while observing their association and dissociation kinetics. Here, the term ligand refers to a molecule that is immobilized onto the biosensor surface while the analyte is the molecule that interacts with the ligand. The biosensor used in SPR is in the form of a sensor chip. A variety of sensor chips are available for SPR depending on the type of application. A common feature associated with these chips is that they have microfluidic flow channels with a total volume of 20-60 nL. The flow channels deliver liquid to the sensor surface at varying flow rates. The sensor surface is covered with a thin gold film of 50 nm thickness. A ligand is frequently immobilized on the gold surface. However, since immobilizing high concentrations of the ligand directly to the gold surface is challenging and in some cases can denature proteins, a layer of carboxymethyl dextran is applied and serves as the major immobilization matrix to serve as a base layer for ligand attachment. With this layer,

immobilization can be carried out through non-covalent interactions or by covalently linking the ligand directly to the dextran surface via a variety of chemistries such as through an amine, thiol or aldehyde group (*230*). The most common method used is amine coupling used for macromolecules containing amine groups (lysine). The immobilization of proteins is discussed in a later section in this introduction.

The ligand and the flow cell are under perpetual flow conditions to generate the initial baseline refractive index (defined as the ratio of the velocity of light in a vacuum to its velocity in a specified medium, it is a number that describes the propagation of light through a specific medium) environment (Figure 4.2 A). Below the gold film lies the flat surface of a prism. A light source shines incident red or infrared light (630-1200 nm) on the gold surface through the prism. The beam reflected back is detected by a photodetector. During the initial SPR resonance event, the incident light transfers energy and excites the electrons on the gold surface to generate a surface plasmon at the gold/glass interface. The surface plasmon is a cloud of electrons. When this resonance occurs, there is a dip in the intensity of the reflected light. This reduction in intensity or the resonance detected by the photodetector happens at a particular incident angle called as the resonance angle (see label T1 in Figure 4.2A). The resonance angle is extremely sensitive to any change in the refractive index of the medium adjacent to the gold surface (due to changes in the refractive index or protein density at the surface). If the optical properties at the surface change due to changes in analyte/ligand concentration, buffers or pH, these changes lead to a concurrent change in the solution refractive index. During an interaction, the analyte binds with the immobilized ligand, leading to a change in the solution refractive index or dielectric constant near the surface of the gold surface. Such a change in the refractive index causes a change in the surface plasmon generated at the glass/gold interface. Changes in this surface

plasmon (resonance), results in a compensating change in angle of the incident light (see label T2 in Figure 4.2 A). The prism adjusts to pinpoint the changes in the resonance angle that have to be made in order to identify the new reflectance angle generated by the new SPR resonance by changing the wavelength to find the particular wavelength that initially causes the SPR resonance. The changes in refractive index result in changes in the resonance angle (Figure 4.2 B, top panel). This change in resonance angle (T2-T1) is exhibited as a change in the signal output (*231-233*) and is measured in terms of an arbitrary unit called resonance unit (RU). The RU change as a function of time gives rise to the changes in the kinetic amplitude that results in an experimental SPR sensorgram (See Figure 4.2 B, lower panel). The signal change (RU change) is thus dependent on time dependent changes as well as the extent of changes in the solution refractive index/dielectric constant. These time dependent changes translate into a kinetic parameter and a quantitative component. If other conditions are maintained constant under experimental conditions (following buffer subtractions, etc.), the increase in signal output (RU) change is directly proportional to the mass/concentration of the macromolecule (in this case a protein) that is present at the surface. The sensorgram thus provides one with real-time quantitative information on the active concentration of molecule in a sample, its specificity of binding as well as the kinetics and affinity. In terms of protein binding, 1 RU is approximately equivalent to the attachment or binding of about 1 pg of protein immobilized on the sensor.

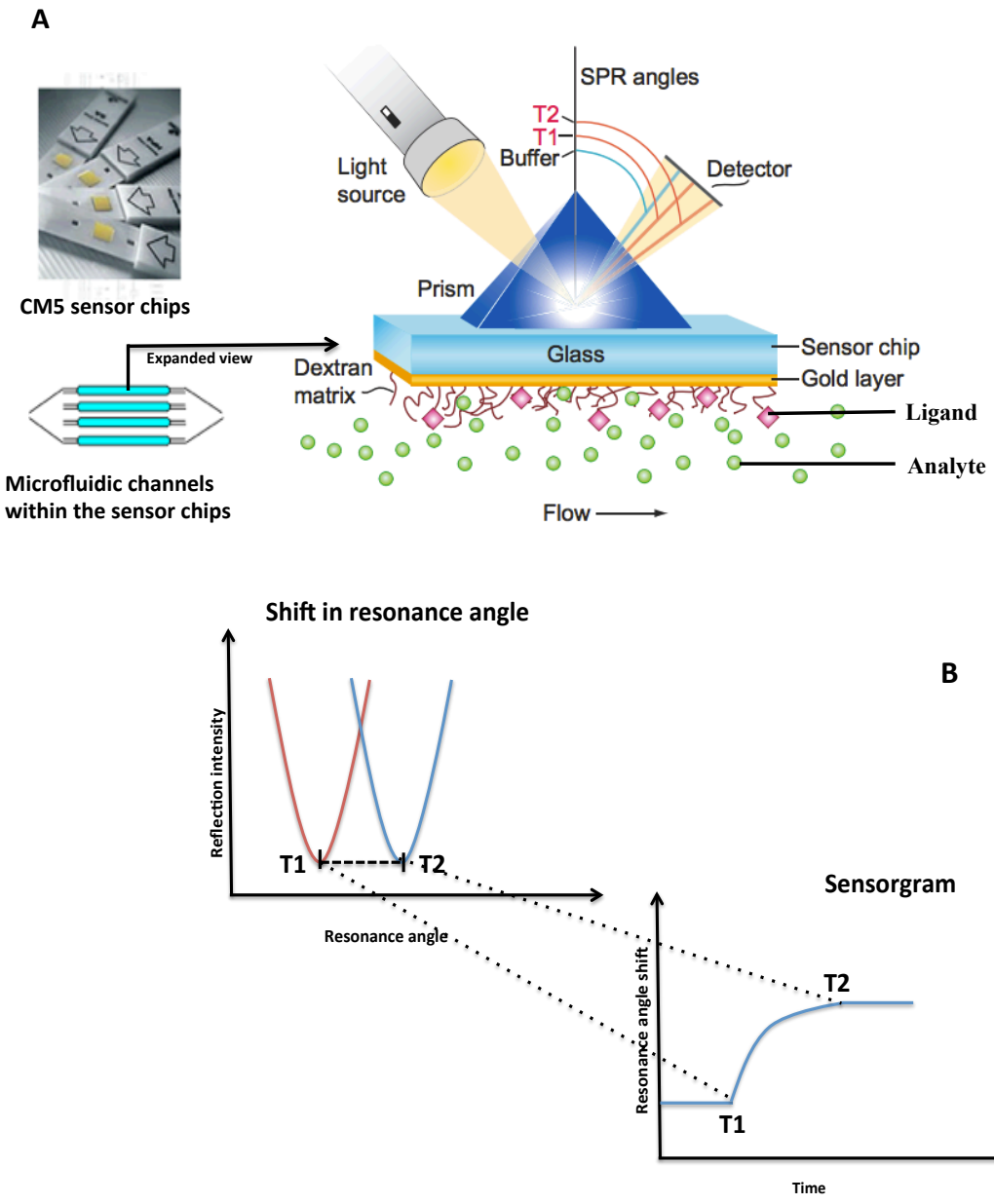

Figure 4.2: The principle behind surface plasmon resonance. (A) Each microfluidic channel consists of a glass chip on which ligand (pink squares) is immobilized. Incident light generates a surface plasmon at a resonance angle T1. As the analyte (green circles) interacts, the prism shifts the resonance angle to T2 to maintain surface. (B) This shift in resonance angle T2-T1 when plotted as a function of time gives a SPR sensorgram plasmon. Figure adapted from (*234*).

Developing an SPR assay involves preparing the sensor surface, carrying out the interactions, regenerating the surface and finally evaluating the results. Preparing the sensor surface by immobilization of the ligand is an important facet of the SPR system. The immobilization can result from direct covalent coupling, high affinity capture or hydrophobic adsorption. The type of immobilization method depends on the nature of the biomolecule as well as the specific application of the study (*235*). Covalent coupling, one of the more commonly used immobilization technique, results in a stable attachment and usually does not require the ligand to be modified in any way. The most common attachment protocol used for protein immobilization is to covalently attach the protein to activated carbonyl groups on the sensor surface. They can also be immobilized through amine, thiol or aldehyde functional groups. Thiol coupling is used for thiol containing compounds while aldehyde coupling is used in macromolecules containing cis-diols and sialic acid groups.

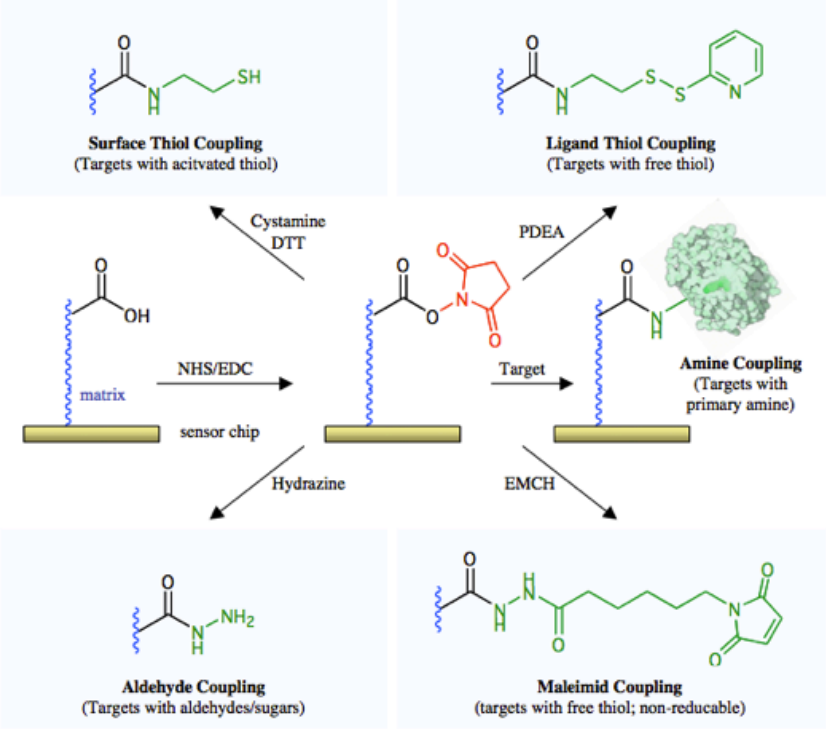

Figure 4.3: Different methods of covalently linking a protein to a CM5 biosensor involve using amine, thiol or aldehyde functional groups. The CM5 matrix consists of a 100nm thick carboxymethyl dextran matrix that provides a hydrophilic environment for biomolecular interactions. It can be easily chemically modified using a broad range of well defined chemistries including amine, aldehyde and thiol couplings .

The process of immobilizing a protein covalently usually occurs in a buffer below the isoelectric point of the proteins (which now have an overall positive charge) to take advantage the inherent electrostatic attraction that can be realized to enhance attachment because the electrostatic field of the dextran surface present on top of the gold layer carries an overall negative charge. This process called a pre-concentration step enhances the immobilization efficiency on the surface. The use of a low ionic buffer to maintain the charge state of the protein is extremely important during this step. One general problem with covalent coupling is that it is

non-specific and the proteins are coupled in heterogeneous orientations (i.e. active site or binding site not optimally place to face flow channel). For instance, in certain cases, improper attachment might obscure the binding site, reducing the analyte affinity for the ligand (*236*). Efforts to achieve a more homogenous, defined orientation will prevent this reduction in affinity and the number of titratable binding sites. An example of homogenous orientation has been discussed in detail in chapters 5 and 6. In certain instances, when covalent coupling is unsuitable, the ligand can also be coupled through tight affinity binding where the ligand is bound to a secondary molecule that can be easily coupled to the surface of the biosensor. Examples of affinity binding include using antibody-antigen interactions, proteins that are biotinylated-streptavidin and his tagged proteins interacting with Ni-NTA systems (*237*). In some cases, affinity coupling may require modification or in the case of proteins, genetic engineering of the ligand.

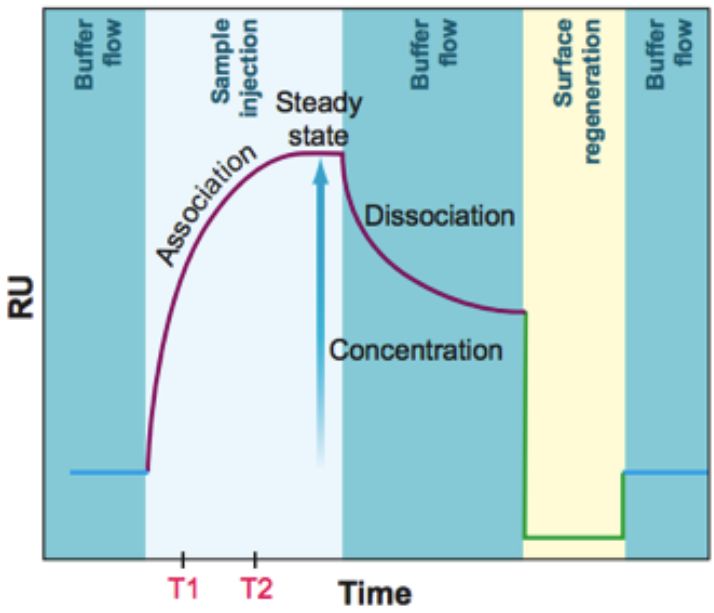

Figure 4.4: An SPR sensorgram is the plot of signal change as a function of time and provides real-time quantitative information on the analyte concentration, and specificity of binding as well as the kinetics and affinity of binding. Figure adapted from (*234*)

After immobilizing the ligand, the analyte is usually injected into the sensor flow channels. Prior to injecting the analyte, the baseline is determined by washing the sensor surface with a suitable buffer known as the running buffer. This period of the analyte being injected is termed as the association phase (Figure 4.4). During the association phase there is both binding as well as dissociation of the analyte from the sensor bound ligand. The association rate, therefore, depends on the concentration of the analyte, the concentration of the ligand and the intrinsic association rate constant (k_{on}). As the concentration of the analyte bound to the ligand increases, it approaches steady state conditions where the rate of association and dissociation of the analyte is equal. The dissociation of the analyte can be observed by reintroducing the running buffer without the analyte to the flow channel above sensor surface, as the analyte now

dissociates from it ligand bound state. This phase is termed as the dissociation phase and is independent of the analyte concentration. If the analyte does not completely dissociate from the ligand, sometimes an appropriate regeneration method can be used to regenerate the sensor surface. The changes in refractive index during the regeneration phase may cause the signal to drop below the baseline, but if regeneration is achieved and no ligand is lost, then the introduction of the starting buffer should result in the return to the original baseline. The advantage of utilizing SPR is that it is a powerful tool to monitor biological interactions that require very low amounts of non–labeled proteins to get data over a wide range of concentrations. Additionally, despite the low volume and the concentrations that are used, the system is very sensitive (picogram detection levels). This high sensitivity at low protein concentration is an advantageous parameter utilizing the chaperonin–misfolding protein substrate complex formation and achieves a necessary prerequisite for establishing a viable HTS assay using this platform. The following sections will highlight the SPR dependent interactions between GroEL and an immobilized substrate to determine the feasibility using a label-free platform system to carry out partitioning and ligand based stabilization of unfolded proteins.

4.3 Materials and methods.

a Materials.

The SPR interaction of GroEL with various substrate proteins was analyzed by Biacore 3000 (GE Healthcare) at KU Lawrence in the Protein Production Core laboratories. CM5 sensor chips, which are the most common and versatile sensor chips, were purchased from GE Healthcare. The high affinity form of extremely pure GroEL was purified in the lab using established purification protocols (*134*). Dihydrofolate reductase (DHFR) and α-lactalbumin

were purchased from Sigma. Purified ATP stabilized CFTR NBD1 (~30 kDa) was a kind gift from Dr. Phil Thomas (UT Southwestern).

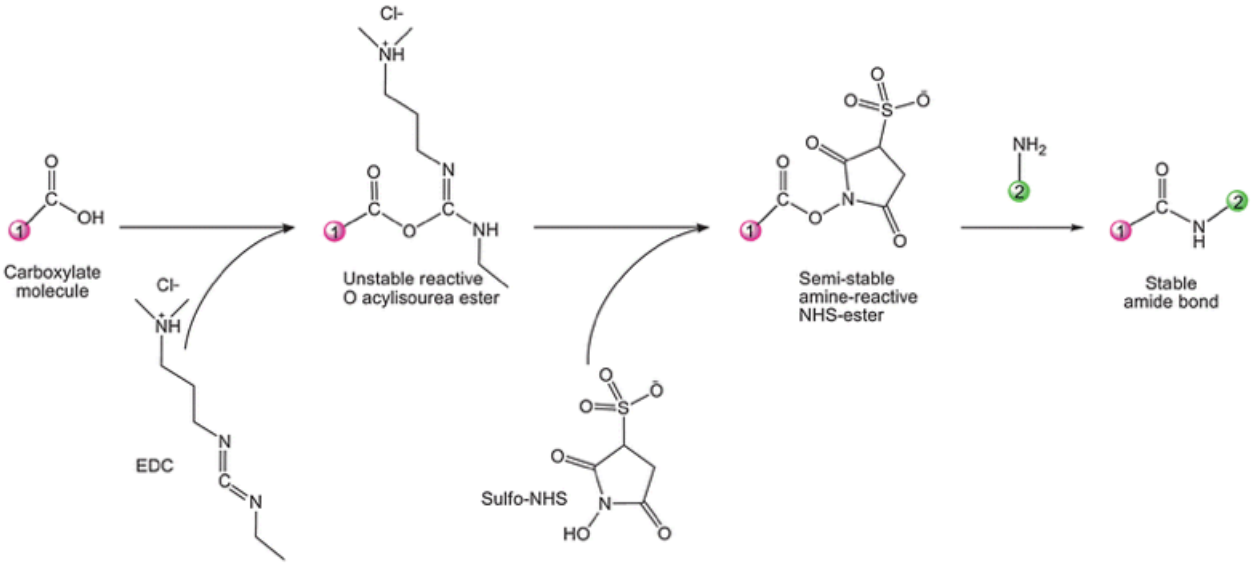

Figure 4.5: Chemistry of EDC and NHS binding for amine coupling of amine containing macromolecules to the carboxyl coating on the dextran surface of a CM5 chip

b Coupling of the protein to surface.

The SPR signal is easily disrupted by small air bubbles or any particulates that pass through the flow channel. To prevent this interference, all solutions used in the system were degassed and filtered through a 0.22 µm filter prior to use. The native form of the substrate protein was immobilized onto the dextran surface of a Biacore CM5 chip by amine coupling (Figure 4.5). While HEPES buffered saline (HBS) buffer (10 mM HEPES (pH7.4), 150 mM NaCl, 3.4 mM EDTA) was utilized for α lactalbumin, refolding buffer (50 mM TRIS (pH 7.5), 50 mM KCl, 10 mM $MgCl_2$, 0.5 mM EDTA) was used as the running buffer for the studies involving CFTR NBD1 and DHFR. The dextran matrix of the CM5 sensor chip was initially activated with a 1:1 mixture of N-ethyl-N'-(dimethylaminopropyl) carbodiimidehydrochloride (EDC) and NHS with a flow rate of 5 µl/min for 10 min. (Figure 4.3). The protein to be

immobilized was then applied to the CM5 chip at a flow rate of 5 µl/min in 10 mM sodium acetate buffer for 10 min. The pH of the acetate buffer was adjusted according to the pI of the protein that was to be immobilized. Once the protein becomes attached to the sensor chip surface (as determined by a large increase in the SPR signal), any unreacted carboxyl groups were quenched by treating the sensor surface with 1 M ethanolamine (pH 8.5) for 5 minutes at a flow rate of 5 µl/min. The amount of protein that was immobilized was measured by the difference in the RUs after the EDC/NHS activation and the final signal.

c Measuring GroEL interactions and its kinetics with the immobilized proteins.

500nM of GroEL oligomer in refolding buffer was injected at a temperature of 25^{o}C onto the substrate protein immobilized sensor surface at a rate of 30 µl/min for 5 minutes to obtain the association phase of the sensorgram (refer to Figure 4.2, curve between time 0-660s for illustration). After 5 minutes, the running buffer was flowed over the sensor chip and the resulting dissociation trace is recorded. The traces of the association and the dissociation are both analyzed to determine the binding kinetics. To measure the concentration dependent relationship of the kinetics of the interaction, different concentrations of GroEL were injected and the resulting traces analyzed using the Biacore kinetics software to obtain the binding constants and other kinetic parameters.

4.4 Results and discussion.

As stated in the previous chapter, the bead-based assay that was developed in chapter 3 was a robust assay. Robustness of an assay has been defined by the US Pharmacopoeia and the International Conference on Harmonization (ICH) as a measure of its capacity to remain unaffected by small, but deliberate variations in method parameters and provides an indication of its reliability during normal usage (*238*). In case of the bead assay, this robustness was

demonstrated by its reproducibility under test conditions at different locations, times, reagents and instruments. However, it was slightly cumbersome to utilize for HTS due to the necessity of maintaining the beads in constant suspension as well as the need to separate the beads prior to carrying out the protein assay. Another factor that hindered efficient HTS was the formation of inactive aggregates in solution prior to binding onto the immobilized chaperonin GroEL. As observed with the frataxin mutants and perhaps even with DHFR, any preformed aggregates did not easily partition onto the GroEL beads and remained in solution along with the native proteins. Since the readout of the assay is free protein concentration in solution, the formation of such aggregates will lead to false positive results, decreasing assay reliability.

One method of decreasing the protein aggregation is to immobilize the substrate protein that tends to misfold and aggregate, thus preventing self-association. In our case, this can include proteins such as CFTR and the frataxin mutants that were discussed in chapter 2. Such proteins could potentially be immobilized and the interaction of this immobilized protein with GroEL could be then probed utilizing non-labeled techniques. SPR is one such non-labeled analytical technique that utilizes immobilized molecule (ligands) and analyzes its binding to another molecule (analyte) in real-time. It was predicted that one could utilize SPR to study the interactions between GroEL and an immobilized substrate (*116, 239*). This strategy eliminates the aggregation reactions that are observed with the substrate in solution and will yield kinetic parameters of the GroEL–substrate interactions. In addition, it was also predicted that this set-up could be used to rule out false positive hits (molecules leading to direct inhibition of the chaperonin) by using a known chaperonin substrate (control) and examining if the test ligand candidate still interferes with chaperonin binding with the control chaperonin substrate. With the SPR system, once a potential small molecule ligand is identified, one can also examine small

stabilizer compound interactions directly with the immobilized substrate protein. SPR also makes it possible to measure the binding and kinetics of binding of small analytes (in this case the small molecule ligand that stabilizes any given substrate).

a Initial proof-of principle SPR studies demonstrating chaperonin interactions with α-lactalbumin.

Previous data from Murai et al., (*239*) indicates that one can follow the extent of GroEL binding that distinguishes between folded (S-S oxidized) and a molten globular state (SH reduced forms) of an immobilized small protein α-lactalbumin using SPR. In control experiments, GroEL binding and ATP dependent release from the immobilized unfolded α-lactalbumin was easily observed (Figure 4.6). Initially, α-lactalbumin was immobilized via amine coupling on the sensor chip to a RU of about 2500 by flowing native LA in a pH 4.5 acetate buffer. Its reduced unfolded form was obtained by reducing the S-S bonds present by flowing 2mM DTT in the running buffer after immobilizing the protein. As predicted, it was observed that the chaperonin readily associates with the partially unfolded reduced form of α-lactalbumin; while the folded oxidized form shows no apparent GroEL association (Figure 4.6).

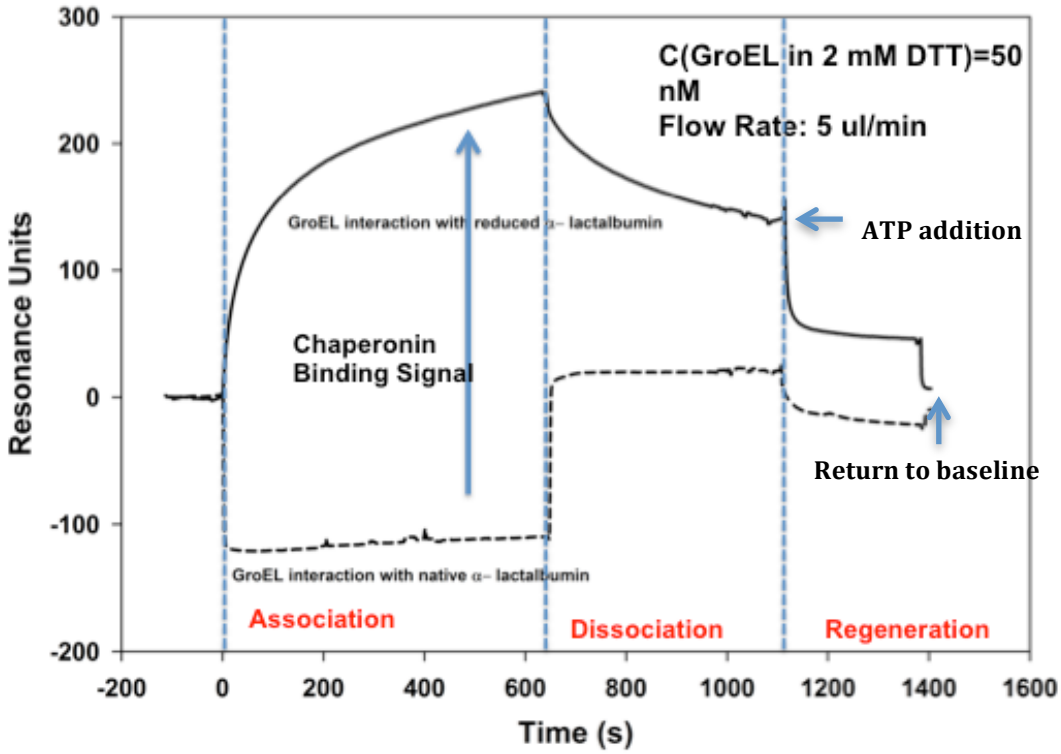

Figure 4.6: Demonstrating that SPR can be used with the chaperonin to distinguish between folded and partially folded species of a protein. The oxidized (solid traces) α-lactalbumin exists in a partially folded form and demonstrates binding to the chaperonin while the reduced (dashed traces) form is in a folded state and does not partition indicating that SPR can distinguish between a folded and an unfolded/partially states of a protein. The rapid decline in signal on addition of ATP and the signal subsequently returning to baseline thus indicating substrate release also confirms the partitioning.

b SPR studies demonstrating DHFR interaction with the chaperonin.

The validation of the previously discussed proof-of-principle experiments was followed by studying the interaction of GroEL with several GroEL binding protein substrate proteins in the absence and presence of stabilizing small molecule ligands. One such substrate was DHFR, whose interaction with the chaperonin in solution was first studied by Lorimer's group (*128*).

The present study is the first instance of SPR based verification that ligand stabilization of a protein can prevent or diminish GroEL binding. Accordingly, DHFR was immobilized onto the sensor chip via amine coupling and its interaction with GroEL in solution observed. Prior to carrying out the study, it was essential to identify the optimum buffer conditions for the efficient and maximal immobilization of DHFR. To identify these conditions, the substrate protein (1 μg/ml) was diluted in acetate buffers with pH varying by half units (4.0-5.5). These buffers were then injected over the sensor surface and the signal (RU) noted. This interaction of the protein with the dextran surface is via weak hydrophobic linkages and can be easily washed away with buffer. The pH of the acetate buffer that gives the highest signal was chosen for further covalent immobilization of the substrate. With DHFR, it was observed that a pH 4 sodium acetate buffer (10mM) gave the highest immobilization signals of DHFR attaching onto the sensor surface yielding a signal of about 150 RU.

Once the substrate protein was immobilized, the analyte (GroEL) was injected and the interactions observed as a change in the sensorgram. The signal was observed to increase to about 1100 RU indicating the binding of analyte (GroEL) to the ligand (DHFR). We injected the GroEL with a high flow rate to decrease the diffusion effects and increase the mass transfer (*240*). Thus, when running buffer was allowed to flow over the GroEL-DHFR complex during the dissociation phase, the signal showed a very slow decline. This slow dissociation trace indicates support for previously observed studies where the affinity of GroEL-DHFR interaction complex was found to be very strong ($k_{on} = 10^7\ M^{-1}\ s^{-1}$ and K_D= ~ 85nM ± 20nM). It is also possible that the chaperonin can interact non-specifically with the sensor surface. If the interactions are weak non-specific interactions, the high flow rate of the running buffer leads to a rapid dissociation of the analyte from the immobilized ligand. The observation that the chaperonin remains bound to

the ligand and shows very little dissociation indicates that the binding was likely due to specific binding of the chaperonin to the substrate and not due to non-specific interaction with the sensor surface. During the dissociation phase, there should ideally be only dissociation of the bound analyte and the dissociation rate should therefore depend only on the concentration of the analyte (chaperonin). However, a part of the dissociated analyte may rebind and lead to misleading kinetics. This can be reduced by decreasing the levels of ligand immobilized on the sensor surface, increasing the flow rate or by blocking the ligand with a competing molecule. In our case however, the slow dissociation of the analyte decreased the problems of rebinding. It can also be predicted that if rebinding were to be a problem, different dissociation kinetics that depended on the analyte concentration (in this case GroEL) would be observed. The dissociation kinetics were observed to be the same regardless of GroEL concentration supporting the hypothesis that GroEL binds very tightly and undergoes very slow dissociation.

This high affinity of the chaperonin for unfolded/partially folded proteins is specific to the nucleotide free form of GroEL. ATP binds to GroEL, and diminishes the binding interaction between partially folded proteins and the GroEL active site, resulting in a release of folded DHFR. To verify the reversibility of GroEL binding, a large concentration (25mM) ATP was added to the flow buffer. We observed that the ATP induced a very rapid dissociation of the GroEL (data not shown), thus confirming that GroEL binding was indeed specific. The ATP addition also provides one with a method for regenerating the surface. During regeneration, the analyte must be completely removed from the sensor surface while retaining the activity of the surface. An ideal regeneration thus allows one to obtain consistent responses even after repeated injections with the response curves being within 10% of the initial injection. Thus, regeneration of the sensor allows carrying out multiple rounds of binding with the same surface. Here, it was

observed that the ATP based regeneration protocol gives sensorgram curves that overlapped with each other even after repeated injections. Another factor encountered in SPR studies is an apparent increase in the signal (RU) due to changes in the dielectric constant/refractive index of the buffer by means of changes in viscosity, pH or solution components. This buffer induced perturbation in the SPR signal is referred to as the "bulk effect" and is generally subtracted form the signal output by using a reference surface (*241*). For these experiments, the bulk effects were observed to be negligible. We repeated the study utilizing the regenerated DHFR surface and found that the results were comparable with GroEL again binding to DHFR with the same amplitude (Figure 4.7).

It has been previously demonstrated by bead-based experiments (Chapter 3.3.1) that NADPH is a small molecule ligand that binds and stabilizes DHFR. It was also predicted that such NADPH based stabilization of the immobilized DHFR should be detected utilizing chaperonin based SPR measurements. Accordingly, DHFR was immobilized onto a sensor surface by the same procedure described previously. A solution of 500 nM GroEL mixed with 2 μM NADPH was injected and allowed to flow over the sensor surface. A buffer containing 500 nM GroEL without the DHFR was used as a control. It was observed that the amplitude of binding during the association phase for the NADPH containing sample was much lower than what had been observed with the control (GroEL by itself). It was inferred that this decrease in amplitude was due to the stabilization of the native state of DHFR thus leading to its decreased association with the chaperonin. The slow dissociation rate encountered even in the lower GroEL association with DHFR also indicated that the chaperonin was binding specifically to DHFR.

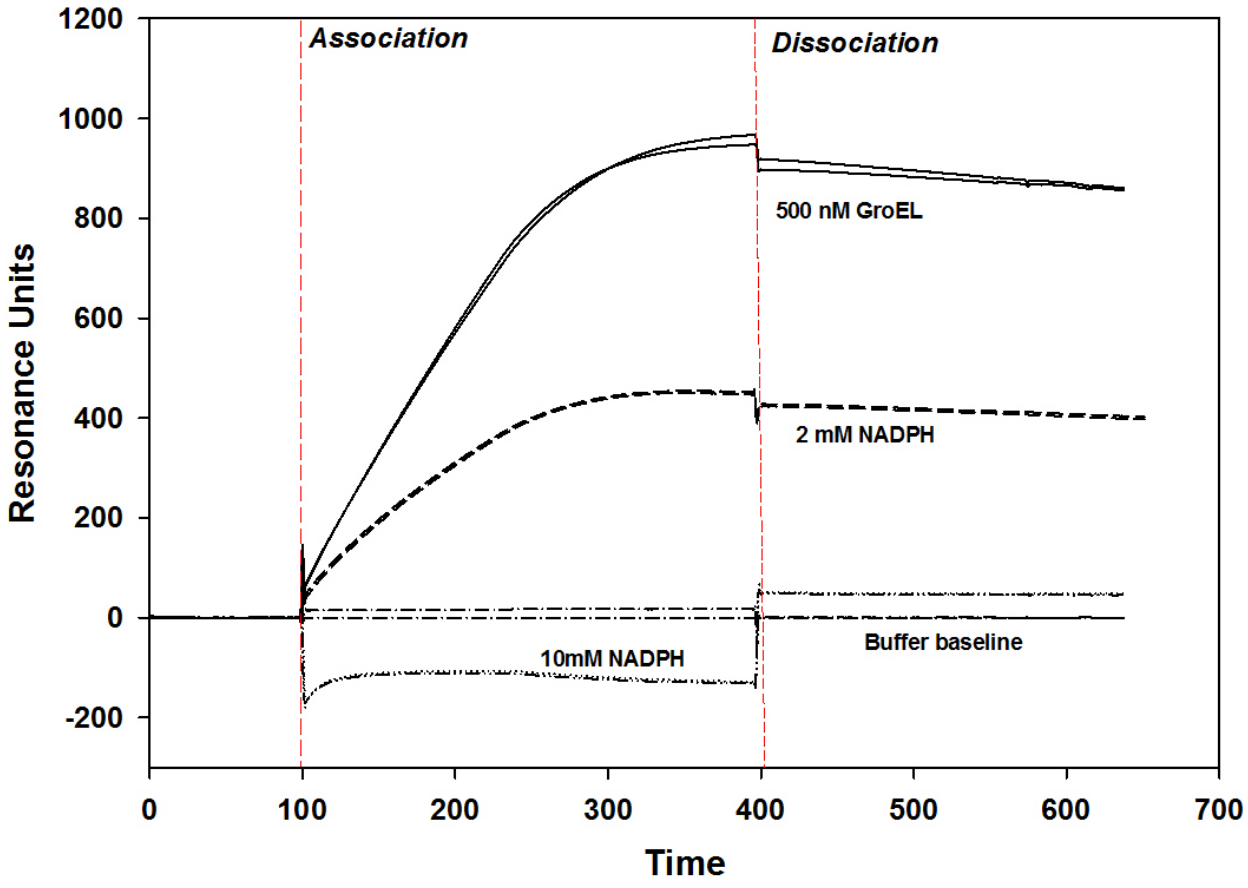

Figure 4.7: Ligand based stabilization of the model substrate DHFR could be followed utilizing SPR. DHFR was immobilized onto the sensor surface through amine coupling. 2 mM NADPH (dashed trace) stabilizes the native state of DHFR and decreases the binding of 500nM GroEL (solid trace) while 10mM NADPH (dotted trace) abolishes GroEL binding completely indicating ligand based stabilization of DHFR. The experiments were carried out in duplicates on the same sensor surface.

To demonstrate that the observed decreased amplitude was a function of DHFR stability, it was predicted that a further increase in NADPH concentration would lead to a higher stability. Since chaperonin binding is inversely proportional to stability, it was also predicted that this increased NADPH would ultimately decrease GroEL binding. To support this hypothesis, 10mM

NADPH with 500nM GroEL was injected over the DHFR surface. It was observed that at this increased concentration of the ligand the binding of GroEL with the fully saturated DHFR NADPH complex (Figure 4.7) is no longer observed. All these studies were performed in duplicates on the same sensor surface.

c SPR studies on the interaction between CFTR NBD1 and GroEL.

Once it was established that GroEL can bind to immobilized DHFR and α-lactalbumin when these proteins exist as part of an partially folded population using SPR as a detection method, the interaction between the chaperonin and a potential model disease protein CFTR NBD1 was studied. As observed in chapter 2, CFTR NBD1 rapidly partitions onto GroEL. It was also established that GTP stabilizes CFTR NBD1and decreases GroEL partitioning onto this target protein. Accordingly, it was predicted that these observations could be recapitulated utilizing the SPR platform. Here, CFTR NBD1 was immobilized on the biosensor surface by amine coupling. Again as carried out with DHFR, by varying the pH of the 10mM sodium acetate coupling buffer (a process known as pH scouting), it was observed that the best immobilization occurred at pH 4.5. Accordingly, CFTR NBD1 was immobilized on the surface to obtain a signal of approximately 2700 RU. 500nM GroEL was then injected and allowed to interact with the immobilized CFTR NBD1. GroEL bound to the immobilized CFTR NBD1 with a signal of about 1000 RU in the association phase (see Figure 4.8). Again this binding was characterized by a slow dissociation phase suggesting that the affinity of GroEL for partially folded CFTR NBD1 was high.

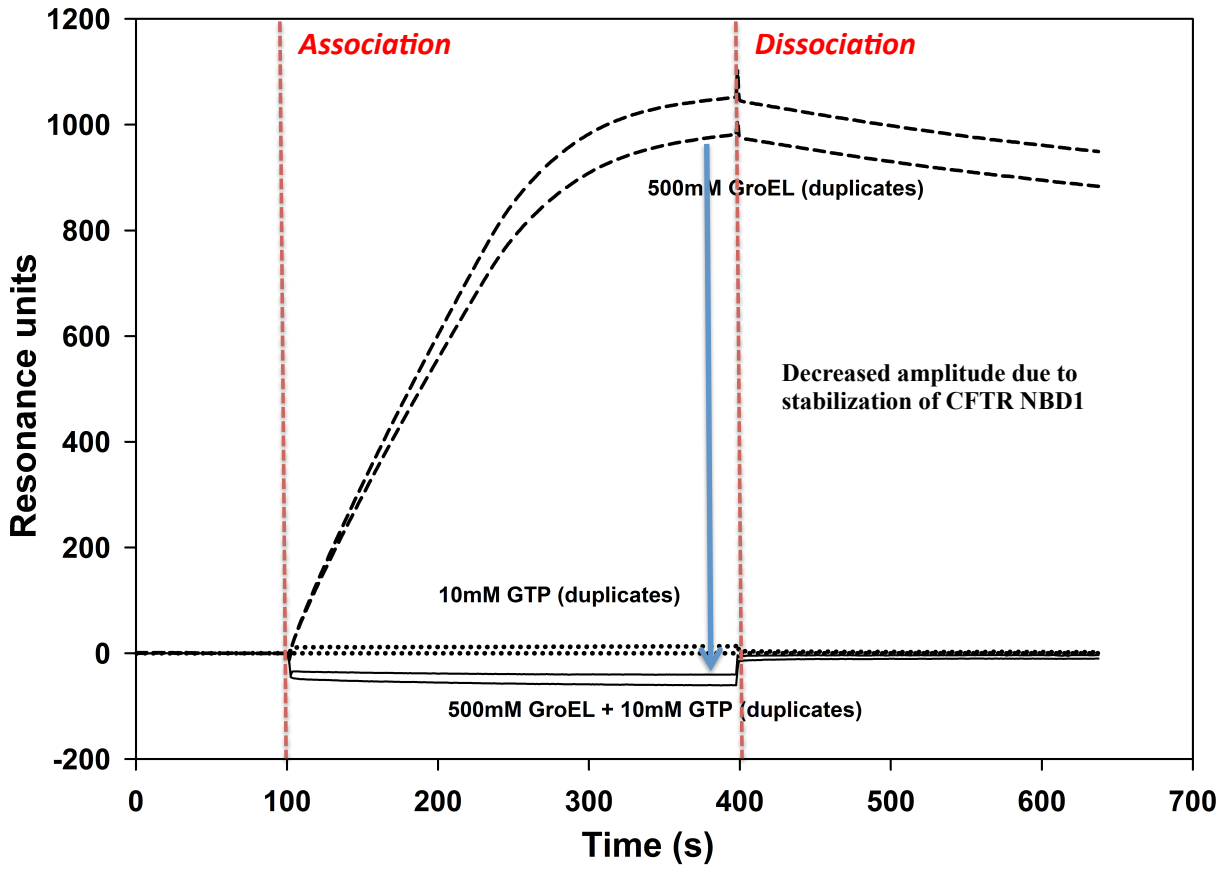

Figure 4.8: Ligand based stabilization of a disease protein CFTR NBD1 could be followed utilizing SPR. CFTR NBD1 was immobilized onto the sensor surface through amine coupling. 10 mM GTP (solid trace) was observed to completely abolish the binding of 500 nM GroEL (dashed trace) to immobilized CFTR NBD1 demonstrating ligand-based stabilization of CFTR NBD1.

As discussed in earlier sections (Chapter 2), GTP acts as a stabilizer for CFTR NBD1 without having any effect on GroEL partitioning. Here it was predicted that the experiment could be recapitulated with the immobilized CFTR NBD1 and GroEL by SPR. On addition of 10 mM GTP along with GroEL into the flow cell, the binding of GroEL to the GTP bound immobilized CFTR is abolished (Figure 4.8). Again, ATP addition was found to bring about dissociation of

GroEL leaving the sensor free to be reused for another binding study. In summary, these results indicate that SPR can be utilized to develop an assay platform that can be used to screen for potential ligand stabilizers of CFTR NBD1. This assay platform can also be used to carry out secondary screening and validate any hits obtained during the primary screen.

Unlike other physical techniques utilized previously in this dissertation that required us to measure protein quantities at specific time points, SPR reports the real-time binding of molecules. SPR is an extremely powerful and facile method of studying interaction kinetics. It was predicted that the K_d values obtained by this method should be similar to the affinity parameters (K_d) obtained in solution studies (*133*). Briefly, various GroEL concentrations ranging from 0-500 nM were injected into the biosensor to interact with the immobilized CFTR at a flow rate of 20 µl/min for 5 minutes. This was followed by introducing refolding buffer into the flow cell to follow any dissociation of GroEL from immobilized CFTR. The sensor chip regeneration was carried out by injecting three separate washes of 25 mM ATP to ensure complete removal of GroEL. This was determined by the sensorgram attaining the initial baseline recorded prior to injecting GroEL.

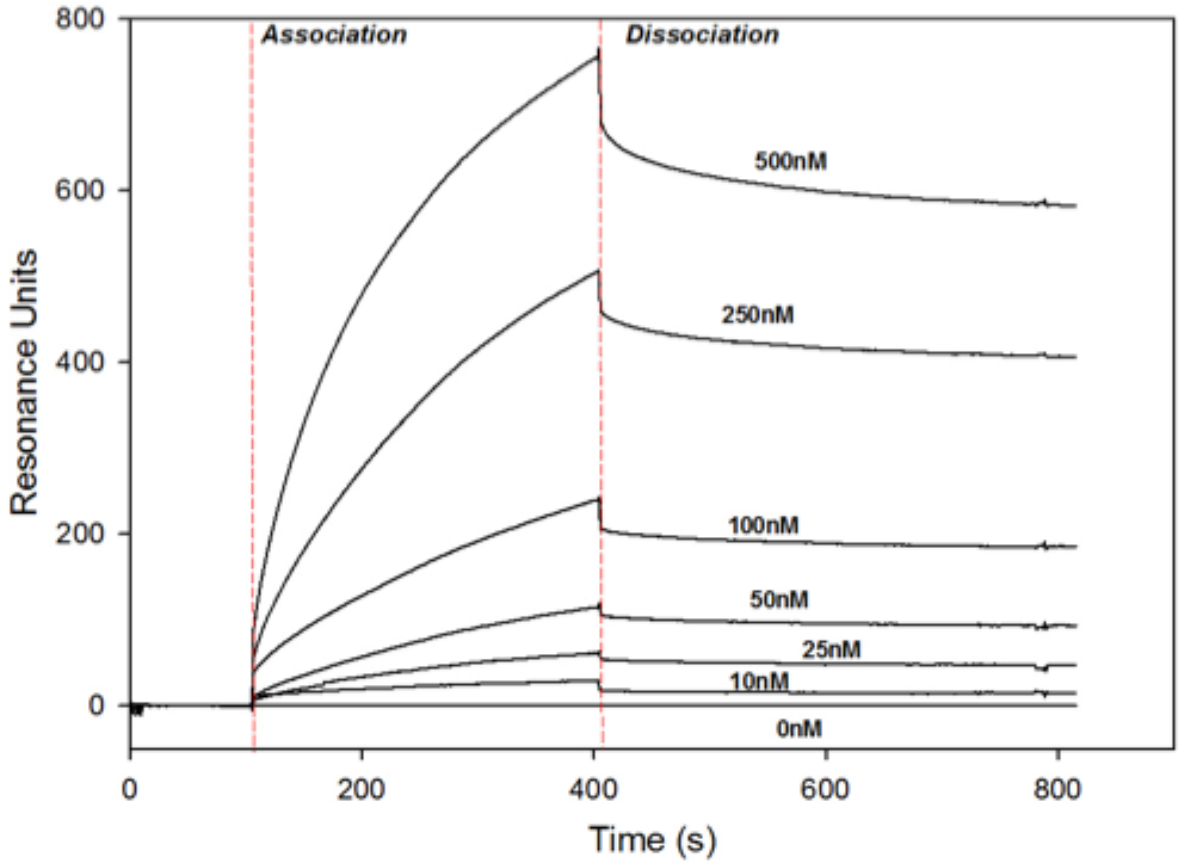

Figure 4.9: SPR could be utilized to determine the kinetics of CFTR-GroEL binding. Different concentrations of GroEL (0-500nM) were allowed to flow over the CFTR immobilized surface. The binding traces were fitted to obtain the kinetic constants.

As shown in Figure 4.9 several sensorgrams were obtained for the different concentrations of the chaperonin and they were simultaneously fitted to obtain the kinetic and equilibrium constants. The equilibrium constants could be determined either by ratios of rate constants or by fitting the steady state amplitude response as a function of the concentration of the binding molecule over a range of concentrations. Here the signal traces were analyzed by the Biacore kinetics software while applying a 1:1 Langmuir binding isotherm. This type of a binding model assumes that both the analyte and the ligand are homogeneous, and that all binding events are independent. The curves were then fitted with a non-linear fitting to obtain the

k_{on}, k_{off} and the K_d values. They were calculated to be $9.81x10^3$, $2.54\ x10^{-4}$ and 27 nM ± 10 nM respectively. This high affinity between nucleotide free GroEL and protein substrate is similar to what has been observed with antigen-antibody reactions (also approaching nanomolar to picomolar dissociation constants). These kinetic series were performed in duplicate and the values were observed to be nearly identical for both replicates.

4.5 Conclusions.

Utilizing label-free systems is an excellent method of investigating protein-protein interactions in real-time. Compared to the classical endpoint assays that are mainly based on competition or inhibition, SPR provides kinetic and binding information simultaneously. At the same time, this method uses very little protein. The protein can be easily attached to the surface and the GroEL binding can be reversed by treating the complex with ATP. This particular set-up makes SPR an ideal method for screening for protein stabilizers of potential missense disease proteins that are difficult to purify. Most importantly, the immobilization of the ligand protein = avoids protein aggregation. The aggregation of proteins that are inherently unstable was a serious drawback with the bead-based system. The experiments presented here indicate that the real-time measurements of chaperonin binding to transiently stable proteins immobilized on SPR chips provides a viable platform system to rapidly screen and identify potential protein stabilizers that exist within large chemical compound arrays. In addition, this assay is not limited to evaluating well behaved single domain proteins. The CFTR-NBD1 protein used in the above experiments readily aggregated at physiological pH values and moderate temperatures in the absence of its nucleotide stabilizer. It is also probable that this SPR attachment method will be useful in evaluating the stabilities of oligomeric proteins as well as monomeric proteins, provided that the oligomers also expose hydrophobic surfaces during transient unfolding reactions. In this latter

situation, one may need to develop more specific immobilization procedures of oligomers to create homogenous target protein populations with defined orientations.

For effective drug discovery utilizing SPR technology, the SPR assay platform must be fast, cost effective, and amenable to high throughput. The typical SPR set-up that is currently commercially available predominantly screens for four interactions at once. However, there are other systems that can achieve comparatively higher throughput. One such system is the ProteOn XPR36 system that can inject six ligands or analytes in a single injection, creating a 6 x 6 interaction array for simultaneous parallel analysis. Array based systems such as the ProtoArray (Invitrogen) and plexarray (plexera) systems can immobilize and follow the interactions of more than 1000 different macromolecules on a single chip. However, it has certain shortcomings that prevent its efficient utilization with the chaperonin assay. Since it is a microfluidics based flow system, slow flow rates might also introduce mass transfer and operational problems. The surface of the sensor chip onto which the ligand is bound also deteriorates over time necessitating ligand re-immobilization onto new sensor chips. The high cost associated with the proprietary commercial sensor chips ($120/unit) correspondingly increases the overall cost of SPR studies. The gold coating and the optical prism require a high degree of engineering sophistication resulting in the high costs. Moreover, SPR is extremely inconvenient for solutions containing DMSO, which is the common solvent used in many HTS studies.

CHAPTER 5: USING LABEL-FREE METHODS TO IDENTIFY PROTEIN STABILIZER (PART 2 – BIO-LAYER INTERFEROMETRY).

5.1 Introduction to bio-layer interferometry.

Although SPR has provided a useful tool for examining protein-protein interactions, there are limitations to its use particularly for HTS methods to identify lead compounds that target mutant folds involved in protein folding diseases. Difficulties with microfluidic flow with protein aggregates, cost of materials, low throughput and solvent interferences (e.g. screening molecules dissolved in DMSO) limit SPR with respect to its ease of use. To this end, several biosensing instruments with varying detection techniques have been introduced (*227*). Some of these achieve an increased throughput by using the standard microplate based systems that are fluidics free. One such alternative optical biosensing technique that complements SPR and addresses some of the limits listed above is bio-layer interferometry (BLI). BLI is a dip and read system used to study analyte-ligand interactions. BLI has several advantages over SPR that make it an attractive option to carry out real-time interaction studies. Primarily, it is not a microfluidics based system and does not have problems due to clogging (protein aggregates) and dissolved gases. BLI platforms are available that have a higher throughput design than one can accomplish with the standard SPR system (e.g. BiaCore 3000 described in chapter 4). It is easy to use with short set-up and run times. Most importantly, interferences from aggregation and solvent effects (DMSO) do not readily interfere with BLI signals.

a BLI principle.

BLI is a simple dip and read system that analyzes the interference pattern of white light reflected from two surfaces to study analyte-ligand interactions. It utilizes a relatively inexpensive ($2-5 per BLI biosensor vs. ~$200 per SPR microfluidic lane) disposable polished fiber optic biosensor (Figure 5.1 left panel) that is embedded into a polypropylene hub. The biosensor has proximal and distal reflecting surfaces that are separated by at least 50 nm. The proximal optical layer acts as the reference layer and is composed of a material with refractive index greater than that of the fiber optic glass. This material is usually Ta_2O_5 and has a thickness of 5-50 nm. This is followed by the distal biocompatible layer onto which different molecules can be immobilized through various chemistries or by affinity interactions. Such immobilized molecules are known as "ligand". This nomenclature is the same as with the SPR technique. The detection system depends on a light source to direct a beam of light onto the two reflecting surfaces. For the instruments presented in this chapter, polychromatic white light with wavelength range between 400-700 nm is utilized. When this light is directed through the fiber optic element, a portion (~4%) is initially reflected from the proximal surface. Some of the light that passes through is also reflected from the distal bio-layer surface containing the immobilized ligand. The two beams of reflected light (one from the proximal reference tip, the other from the distal end containing the immobilized ligand) are slightly out of phase. The out of phase light beams interfere with each other causing a characteristic interference profile with variation in the intensity across the wavelengths with different peaks and troughs. This interference pattern is captured by the CCD spectrophotometer on the opposite end of the fiber optic cable as an interference pattern (Figure 5.1 right panel grey curve). The biosensor is usually dipped into the "analyte" to measure interactions. When the analyte binds to the ligand, it leads to an increase in

the optical thickness of the whole bio-layer complex as well as small changes in the refractive index near the surface. This optical thickness depends on the size and shape of the analyte, the number of analyte molecules that bind to the biosensor as well as the refractive index of the buffer containing the analyte. It has been observed that an increase in the refractive index of the buffer does lead to an increase in the signal amplitude but is nowhere near the changes that are encountered with the SPR system. The overall increase in the optical thickness on the ligand-analyte interaction leads to a change in the interference pattern and is captured by the spectrophotometer (Figure 5.1 right panel orange curve). This change in the interference pattern is measured and given as the wavelength shift output (in nm). The changes in the wavelength shift can be followed as a function of time and gives a binding profile called a BLI sensorgram.

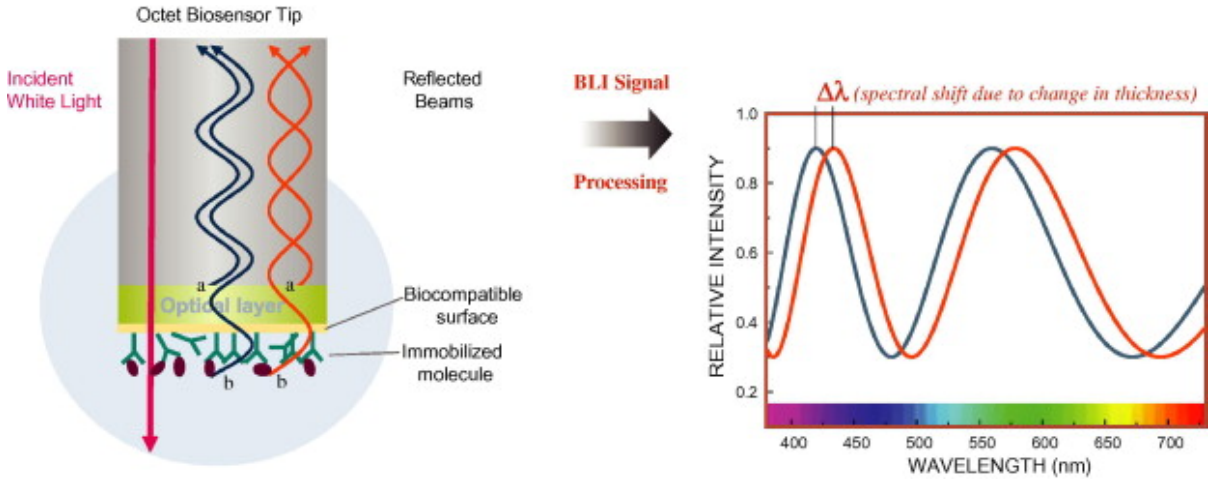

Figure 5.1: BLI utilizes a fiber optic biosensor (left panel) containing an optical reference surface and a biocompatible surface for immobilizing biomolecules. The BLI signal is generated by differences in the interference pattern generated by light reflected from two difference surfaces (right panel). Figure modified from (*242*)

b BLI instrumentation.

BLI instrumentation systems are designed to perform rapid sample analysis in 96- and 384-well format and can process up to 8 and 16 samples in parallel respectively. The Octet RED96 8-channel instrument was utilized with a collaborative effort with ForteBio Inc. (Menlo Park, CA; now owned by Pall) to perform most of the experiments detailed in this chapter. A single-channel BLI system called the BLItz was purchased later and used in the Fisher laboratory. The 96 well platform (Octet RED96) has a deck onto which a microplate can be accommodated (Figure 5.2). The deck can be heated up to 40^{o}C and also acts an orbital shaker (~1000-2000 rpm to decrease mass transport effects) adequately mixing the analyte samples. The biosensors are supplied in an 8 x 12 format tray that can be placed directly onto a stage inside the instrument. A mobile manifold can pick up to eight tips from the tray and dip them directly into the sample containing microplate. With the BLI instrumentation, the sensors are mechanically removed from one solution to the next, avoiding the problems associated with SPR microfluidic systems used to traditionally deliver samples to the stationary gold layered SPR sensor. The order in which the manifold dips into the various wells can be programmed. The manifold also consists of the light source and the spectrophotometer. For the 96 well plate format, there are eight separate light sources and eight CCD detectors (one for each biosensor).

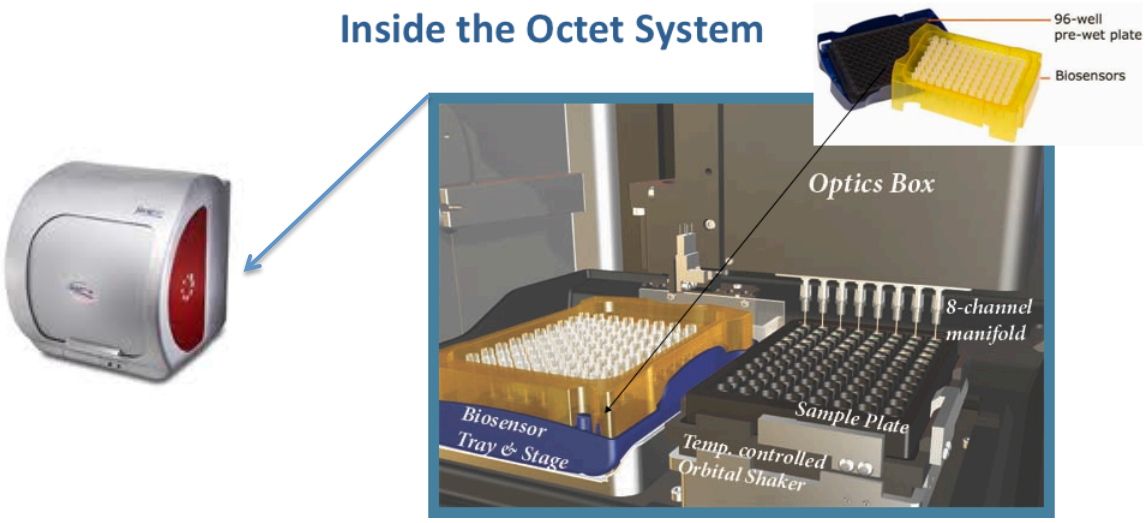

Figure 5.2: The Octet Red system consists of an automated manifold (that also doubles as the detector), which picks up the biosensors and cycles them through various steps as required.

c Experimental set-up.

The microplates used in the Octet are usually filled with 200 µl of sample or buffer per well and are agitated at 1000-2000 rpm. Sensor tips are pre-wetted in buffer immediately before use within the biosensor tray itself. The manifold can then select the biosensors required for an experiment as indicated and move them through the various rows (Figure 5.3 left panel). All these steps are programmable using an easy, well-designed and user-friendly software prior to starting the experiment. A BLI experiments consists of three different steps- 1) loading of ligand, 2) measuring analyte association with ligand and 3) monitoring dissociation from ligand (biosensor tip bound protein or small molecule). A regeneration step is optional as the biosensors are cheap and can be discarded but one can decrease costs if one regenerates the biosensor surface. Depending on the ligand and the biosensor used, the loading step can take several forms. The availability of a wide range of biosensors makes the loading of several

different types of molecules relatively easy. The protein can be immobilized through covalent linkage (Figure 4.3) or through specific affinity linking. As with the SPR system, a blocking step is also used to quench any active functional groups that still may exist after the loading step. Before carrying out the association studies, a brief equilibration step with the buffer is essential to help determine a common baseline value for the different samples. A typical association step is characterized by an increase in the sensorgram signal (Figure 5.3 right panel). The association is usually followed by a dissociation step to measure the dissociation of the analyte from the ligand.

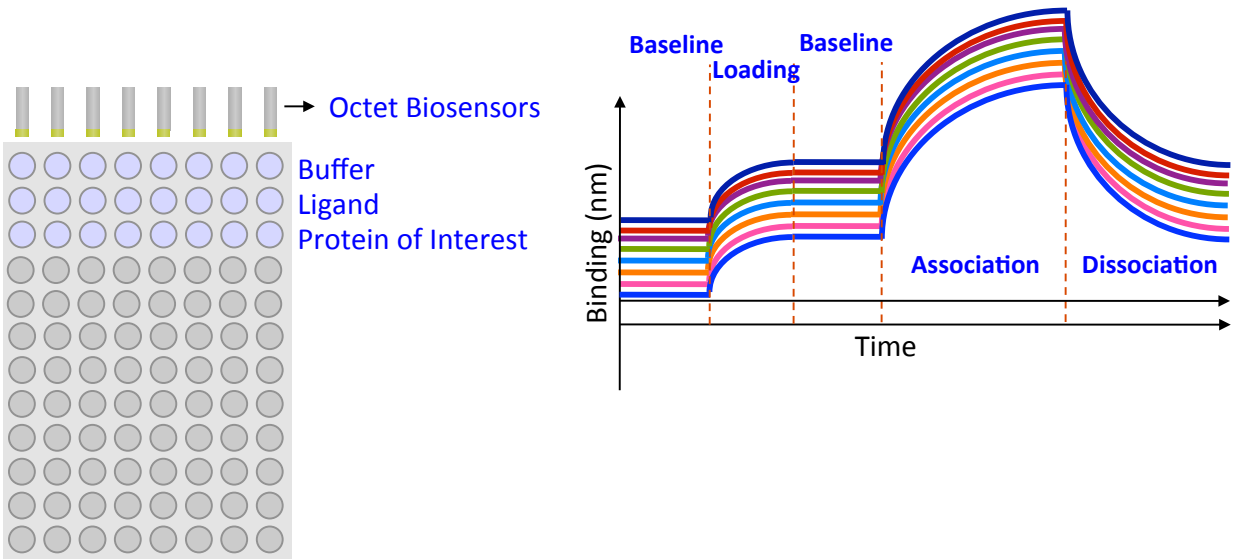

Figure 5.3: A typical experimental setup involves the reagents in specific rows in a 96 well plate (left panel) through which the manifold containing the biosensors can cycle. Right panel: The BLI sensorgram demonstrating various cycles involved in a typical binding experiment. Eight samples can be analyzed at a single time as seen in the sensorgram.

With their real-time analysis and low protein requirement, SPR and BLI are complimentary to each other. However in certain instances, BLI is superior to SPR because there is less prep time involved, lower volumes can be used and whole cell extracts or concentrated solutions (300 mg/ml protein for example) can be used with the BLI. Similar attempts to use the above mentioned solutions will invariably fail with the standard SPR systems. The problems associated with SPR microfluidics such as clogging and degassing do not arise with the BLI. Consequently, particulate molecules, refractive index changes in the surrounding medium, or flow rate changes does not severely affect the interference pattern of BLI allowing it to be an excellent resource for analyzing crude samples in various protein-protein binding, quantitation, affinity, and kinetic interactions. In addition, the biosensors can be preprepared before assay because these systems that can be loaded with the ligand molecules offline. Online loading refers to the ligand being immobilized on the biosensor as a part of the experiment and is monitored. Offline loading happens when the ligand is loaded onto the biosensor separately and then used as required for the experiment. Although offline loading cannot be directly monitored this procedure can be optimized in advance. Offline loading in turn decreases the assay time and the turnaround time as well leading to an increased throughput. Additionally, since it uses the microplate format it can be easily used with HTS robotics to carry out medium throughput assays.

5.2 Materials and methods.

a Materials.

The interaction of GroEL with various substrate proteins was analyzed utilizing an Octet RED BLI instrument (ForteBio Inc., Menlo park). The various biosensors required for this study were initially provided by ForteBio Inc. The high affinity form of extremely pure GroEL was purified in the lab using the purification method outlined by Voziyan and Fisher (*134*).

Dihydrofolate reductase (DHFR), NADPH, GTP and α-lactalbumin were purchased from Sigma. Purified CFTR NBD1 protein was kind gift from Dr. Phil Thomas (UT Southwestern) while the CFTR NBD1 antibodies and the mouse CFTR NBD1 ΔF508 were provided by the Cystic Fibrosis Folding organization (www.cffolding.org). The small molecule CFTR corrector compounds were also obtained from the Cystic Fibrosis Foundation.

b Preparing the biosensor by Immobilization of proteins.

Method 1: Both substrate protein immobilization and GroEL interactions were carried out in Octet RED instrument (ForteBio Inc.). The instrument uses an array of eight biosensors that can detect the interactions in a 96 well plate in real-time. The signal from each biosensor is analyzed by a separate dedicated spectrophotometer. This instrument uses a 96 well plate (Griener) that was incubated at 25^{o}C with continual shaking at 1000 rpm. The volume in the wells was 200 µl for all samples and reagents. The substrate proteins, CFTR NBD1, α-lactalbumin and DHFR were immobilized on the amine reactive biosensors (ForteBio Inc.) utilizing amine coupling. The biosensors are shipped as dry tips that need to be hydrated. Hence, these were initially hydrated in buffer containing 50 mM TRIS, 50 mM KCl, 10 mM $MgCl_2$, 0.5 mM EDTA (pH 7.5). This buffer is optimized for GroEL function. The hydrated biosensors were then activated by dipping them in a 1:1 mixture of sulfo-NHS and EDC for 5 min. These activated tips were further incubated with various protein solutions (CFTR NBD1, DHFR, etc.) for 10 min. The protein solution was prepared by diluting the stock protein in to 10 mM sodium acetate buffer to obtain a final concentration of ~50 µg/ml. the pH of the selected acetate buffer was adjusted to a pH lower than the pI of the protein to obtain maximum immobilization. At this pH, the positively charged protein will be electrostatically attracted to the carboxyl terminated biosensor surface, thus enhancing the efficiency of the immobilization. This process is termed

pre-concentration. To determine the optimal loading concentration to be used in the immobilization, a range of concentrations were tested. The lowest concentration that showed saturation of protein immobilization was chosen for further studies. The saturation is essential to decrease any concentration based variations and artifacts in the different biosensors used in the study. For the amine reactive surface, any portion of the activated surface on the biosensor that was not protein bound was then quenched utilizing 1 M ethanolamine (pH 8.5). These protein-coated tips were then used for investigating interactions with GroEL in solution.

Method 2: An alternative method of loading CFTR NBD1 onto the biosensors was utilized to decrease non-specific binding. This method of loading involved the use of commercially available anti-mouse Fc biosensors. These biosensors were initially hydrated and dipped in 50 μg/ml CFTR NBD1 mouse monoclonal antibody solution for 5 min. The loading of the antibody could be followed online in real-time. The antibody-loaded biosensor was then incubated with CFTR NBD1 for further five min. to obtain the CFTR biosensors. The CFTR loaded biosensors were washed for 5 min. with refolding buffer to remove any non-specifically bound protein. No dissociation of the CFTR NBD1 bound to the antibody was observed over the washing period.

Method 3: For immobilizing GroEL, the chaperonin was initially biotinylated utilizing EZ-link biotin reagent (Pierce). The biotinylated GroEL remained active as confirmed using DHFR assay that measures the partitioning and refolding of DHFR described previously (Chapter 2, section 2.1.2). The biotinylated GroEL samples can be loaded onto the biosensors utilizing the commercially available streptavidin BLI biosensors. The streptavidin biosensors were hydrated with refolding buffer. As a note of caution, the streptavidin tips are notorious for non-specific binding. One way to decrease this binding is to increase the GroEL binding onto the

tips. Hence the hydrated biosensor was then incubated with biotinylated GroEL (100 μg/ml) for 5 minutes (where the tip shows saturated binding) to load the chaperonin. The tips were finally washed with refolding buffer to remove any GroEL that was non-specifically bound. These chaperonin loaded tips could be utilized for further partitioning studies. Non-specific binding was tested with BSA. BSA does not bind to GroEL and can readily bind to free surface areas on the streptavidin tips. Optimal GroEL binding was determined to result in a phase shift $\Delta \sim 6$ nm. At this loading concentration, BSA binding was virtually nonexistent.

c Studying the interaction of GroEL with substrate proteins immobilized on the biosensor.

Figure 5.4 demonstrates the stepwise protocol to study the interaction of the chaperonin in solution with the substrate protein immobilized onto biosensors. The interaction studies between the chaperonin and the substrate proteins (CFTR, α-lactalbumin and DHFR) were carried out as soon as the substrate protein was immobilized on the biosensors (using the techniques discussed in the previous section). This was to ensure that the substrate proteins loaded on the biosensor did not have a chance to undergo any global unfolding reactions due to long-term storage. The substrate protein-loaded biosensors were initially incubated in wells containing 200 μl buffer (5 min.) to establish a baseline. The tips were then dipped and incubated (5 min) into the wells containing either 500nM GroEL or 500nM GroEL with stabilizer to observe any association with the immobilized ligand protein. This was followed by incubating the biosensors in wells containing refolding buffer (5 min.) to observe dissociation between the immobilized ligand and the analyte. In certain instances, the biosensor was regenerated by treating it with a mixture of 25mM ATP and 4M Glycerol to dissociate bound GroEL or to enable bound GroEL to release protein substrates. The regeneration step was repeated three times

to ensure complete removal of the bound analyte. All these studies were carried out at a temperature of 25^{o}C with the plate being stirred at 1000 rpm and were carried out in duplicate.

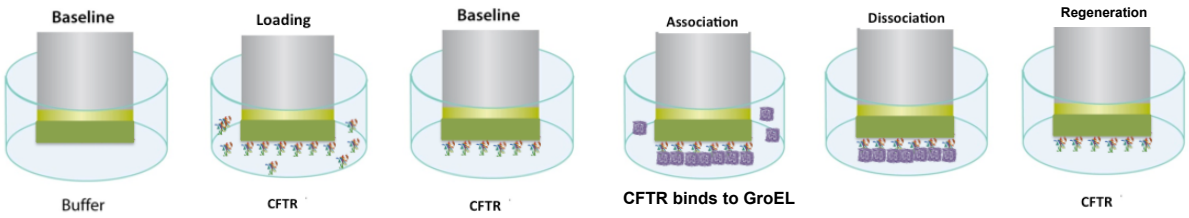

Figure 5.4: Protocol involved in generating and carrying out studies with the substrate bound biosensor. Substrate proteins were covalently immobilized onto the biosensors through amine coupling. The substrate-loaded biosensors were initially incubated with the chaperonin to observe any association followed by incubation with refolding buffer to observe dissociation. The regeneration of the tips was carried out by incubating the tip in a 4M Glycerol-10mM ATP mixture to cause dissociation of the GroEL bound to the immobilized substrate.

d Studying the interaction of GroEL immobilized on biosensors with various substrate proteins in solution.

Figure 5.5 demonstrates the stepwise protocol to study the interaction of the chaperonin immobilized onto biosensors with the substrate protein in solution. The biotinylated chaperonin was loaded onto commercially available streptavidin biosensors (ForteBio Inc.,) as discussed in section b. The GroEL biosensors were initially incubated in wells containing 200 µl buffer (5 min) to establish a baseline. The tips were then dipped and incubated (5 min) into the wells containing either the substrate proteins (CFTR, reduced (unfolded) α-lactalbumin or DHFR) or the substrate proteins and the appropriate stabilizer (GTP, oxidized (folded) α-lactalbumin or

NADPH respectively) to observe any association. This association step was followed by incubating the biosensors into wells containing refolding buffer (5 min) to observe dissociation between the immobilized ligand and the analyte. The biosensors were regenerated by treating them with a mixture of 25 mM ATP and 4 M glycerol. The regeneration step was repeated three times to ensure complete removal of the bound analyte. All the studies were carried out at a temperature of 25^{o}C with the plate shaking at 1000 rpm. All assays were carried out as duplicates (all assays show two traces) runs to compare reproducibility of the biosensors.

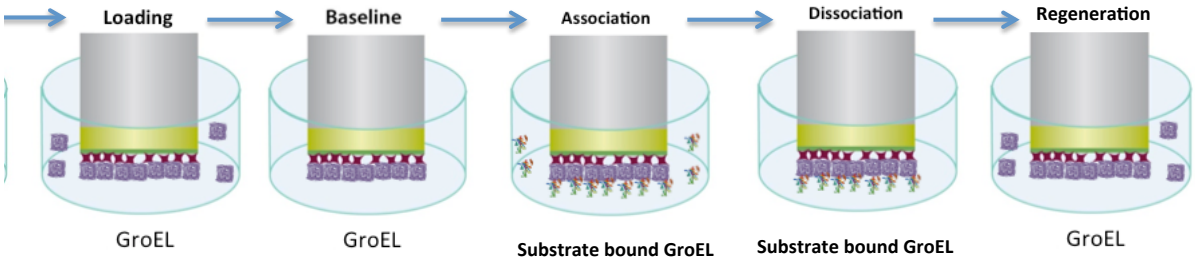

Figure 5.5: Protocol involved in generating and carrying out studies with GroEL biosensors. Biotinylated GroEL (20 µg/ml) was immobilized onto the streptavidin biosensors. The GroEL biosensors were initially incubated with the substrate proteins to observe association followed by incubating in refolding buffer to observe any dissociation. The regeneration of the tips was carried out by incubating the tips in a 4 M glycerol and 10mM ATP mixture to cause dissociation of the GroEL bound substrate.

e Screening of correctors utilizing CFTR NBD1 biosensors.

A black 96 well multiwall plate (Griener) was utilized for these studies and the volume used in the wells was maintained at 200 µl for all samples and controls. The CFTR NBD1 biosensors were generated by the method discussed in section d, method 2. Seven CFTR NBD1

biosensors were utilized for screening each batch of correctors. In addition to these, a blank biosensor was used as a control for non-specific binding of proteins to the biosensor. This biosensor was dipped in a well containing 200 µl of the chaperonin. Each batch of correctors consisted of five correctors, one negative control (GroEL) and one positive control (GroEL + GTP) into which the seven CFTR NBD1 biosensors were dipped.

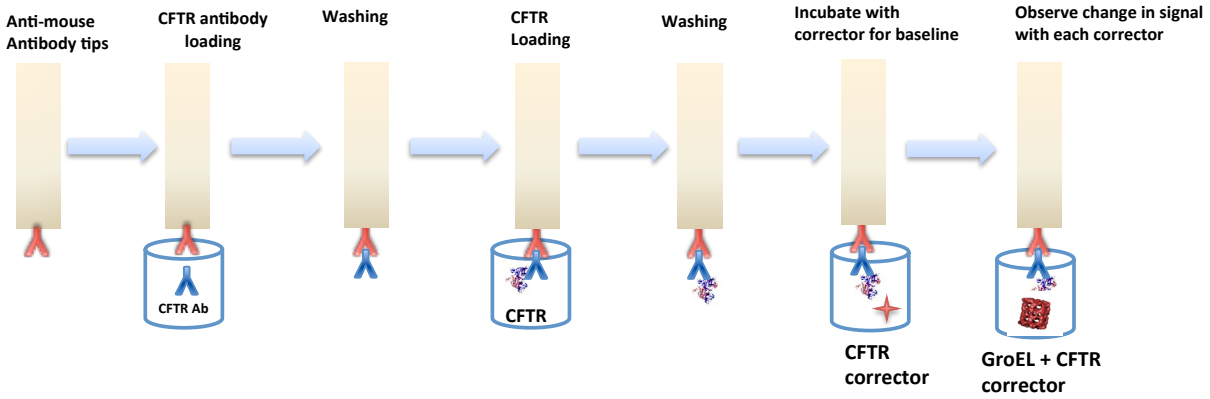

Figure 5.6: The experimental set-up involved in carrying out a CFTR screening. Steps involved in generating the biosensors involved immobilizing CFTR NBD1 on the tips using antibodies. These CFTR NBD1 tips were then utilized to study GroEL binding in the presence/absence of the correctors.

The CFTR NBD1 correctors were obtained as a stock of 4 mg/ml in DMSO. These were diluted to 200 µM in refolding buffer (standard concentrations for HTS systems). The screening process consisted of three separate stages. In the first stage, the CFTR NBD1 loaded biosensors were dipped into either the buffer itself or buffer containing 200 µM of the correctors to establish a baseline. In the second stage, the association of the CFTR NBD1 biosensors with the samples and the control was measured. Here, the tips were incubated into wells containing GroEL with the correctors or GroEL itself for 5 min. to measure the association. One well for the negative

control had buffer instead of GroEL. The association phase was followed by dissociation in the same wells utilized for the baseline step. The studies were repeated for the second set of correctors.

5.3 Results and discussion.

Before screening for CFTR NBD1 stabilizers, it was necessary to optimize the chaperonin assay to be utilized with the BLI system. BLI and SPR are competing but complimentary techniques that helps to obtain similar data using two different principles. A number of publications have indicated that the BLI data is in close agreement with the data obtained from SPR (*243, 244*). It was predicted that the data obtained from the BLI should be in agreement with the SPR data discussed in chapter 4. To support this prediction, the BLI experiments were designed to be as close as possible with the experiments previously carried out with SPR and experiments carried out in a similar manner. In SPR, DHFR was initially utilized as a substrate for the chaperonin to determine if partitioning could be detected. Hence, during BLI optimization, the initial parameters required to carry out the assay were established employing DHFR. This also makes it easier to compare the BLI results with the previous observations and determine its effectiveness in searching for small molecule stabilizers of proteins that tend to misfold. If the chaperonin assay can be utilized with BLI, as discussed before, the ease of use, higher throughput and the compatibility with DMSO will make it the screening method of choice.

Prior to carrying out these studies, it was necessary to investigate the feasibility of using the large molecular mass of the chaperonin with the BLI platform to enable one to distinguish between native and partially unfolded proteins that are attached to the tips or exist in solution. As before, it was predicted that the large mass of GroEL binding to the immobilized protein

substrates would generate a large signal when it binds to a partially folded form of α-lactalbumin whereas GroEL will not bind to the natively folded form. This prediction was based on previous studies where the reduced form of the protein that is partially folded has been shown to bind to GroEL by SPR (*239, 245*). As discussed previously, DTT was used as a reducing agent to reduce the disulfide linkages in α-lactalbumin and partially unfold the protein. Initial immobilization of folded or disulfide reduced (partially unfolded) α-lactalbumin was accomplished with amine coupling (*239*) similar to the approach used with SPR (Section 4.2.1). Once the α-lactalbumin was immobilized, the protein-loaded biosensor was incubated into a GroEL solution with and without DTT to measure the chaperonin binding. This was followed by incubating the biosensors into a refolding buffer solution to measure the dissociation of any bound GroEL. We observed that the biosensor with reduced α-lactalbumin (dipped into GroEL containing the reducing agent DTT) showed higher signal amplitude than the biosensor that contained the native protein. Here, the signal amplitude was a function of the optical thickness around the biosensor. As the signal (optical thickness) is higher with the reduced α-lactalbumin, it can be inferred that GroEL binding to the partially folded α-lactalbumin. On the other hand, ideally no binding should occur with the oxidized α-lactalbumin if all of the protein was properly folded. However, a comparatively lower signal observed with the native alpha lactalbumin indicates that GroEL might be binding to any unfolded species that exists within the native population or might be binding non-specifically to the biosensors themselves. In addition, Sigma α-lactalbumin (80% purity) may have some contaminating proteins that remain unfolded. Addition of BSA was also utilized to decrease the non-specific binding. However this approach did not work. The experiments were carried out in duplicate and the signal traces were observed to overlap (Figure 5.7).

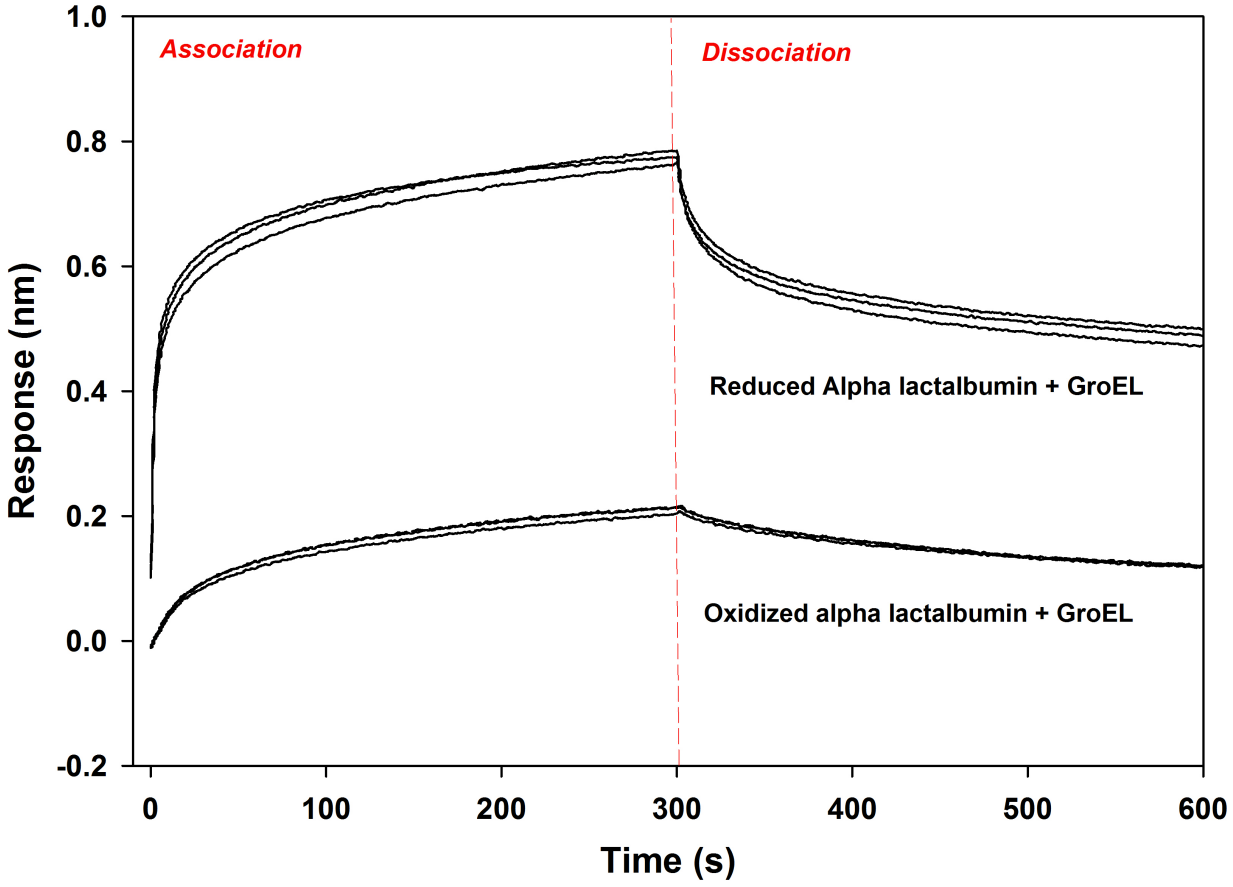

Figure 5.7: BLI can be utilized with GroEL to distinguish between folded and partially unfolded protein. The reduction of α-lactalbumin causes a partial unfolding due to reduction of a disulfide bond. Reduced (partially unfolded state) and oxidized (folded state) α-lactalbumin were covalently immobilized onto the biosensor through amine linkage and incubated with 500nM of GroEL. The chaperonin binds with higher amplitude to the disulfide reduced α-lactalbumin that contains a higher population of partially unfolded species.

It was also predicted that one could utilize the BLI to study ligand stabilization effects. As discussed in chapter 1, such ligands would bind to the native state of the protein and decrease

the free energy state of the ligand bound state thus prevent its unfolding. Similar studies to follow the binding of the chaperonin to immobilized DHFR, which exists in a dynamic equilibrium between a folded and a partially unfolded state, had been previously carried out with SPR (Chapter 4, Section 4.3.2). GroEL can be predicted to partition onto DHFR that exhibits dynamic equilibrium between its folded and unfolded states. This would result in GroEL binding with a rising GroEL dependent signal amplitude while a ligand stabilized predominantly folded DHFR would show no or low signal. Accordingly, DHFR was immobilized on the biosensor by amine coupling and the DHFR immobilized biosensor dipped into a solution of either GroEL alone or GroEL with 10 mM NADPH. As discussed earlier, NADPH is a natural ligand that binds to DHFR native state, shifting the population away from a dynamic unfolded state, thus stabilizing the native fold. It has also been previously demonstrated through microtube/plate experiments (Chapter 2 and 3) and SPR studies (Chapter 4) that this shift in the equilibrium to the NADPH stabilized DHFR native state reduces binding to the chaperonin. A jump in the signal amplitude during the association phase was observed indicating that the chaperonin is binding to DHFR. As predicted in the presence of the small molecule ligand NADPH, there is a lower GroEL binding signal (Figure 5.8), indicating stabilizing of DHFR native state by NADPH (NADPH does not interact with GroEL). These studies were carried out in duplicate and it was observed that the signals were reproducible and overlapped.

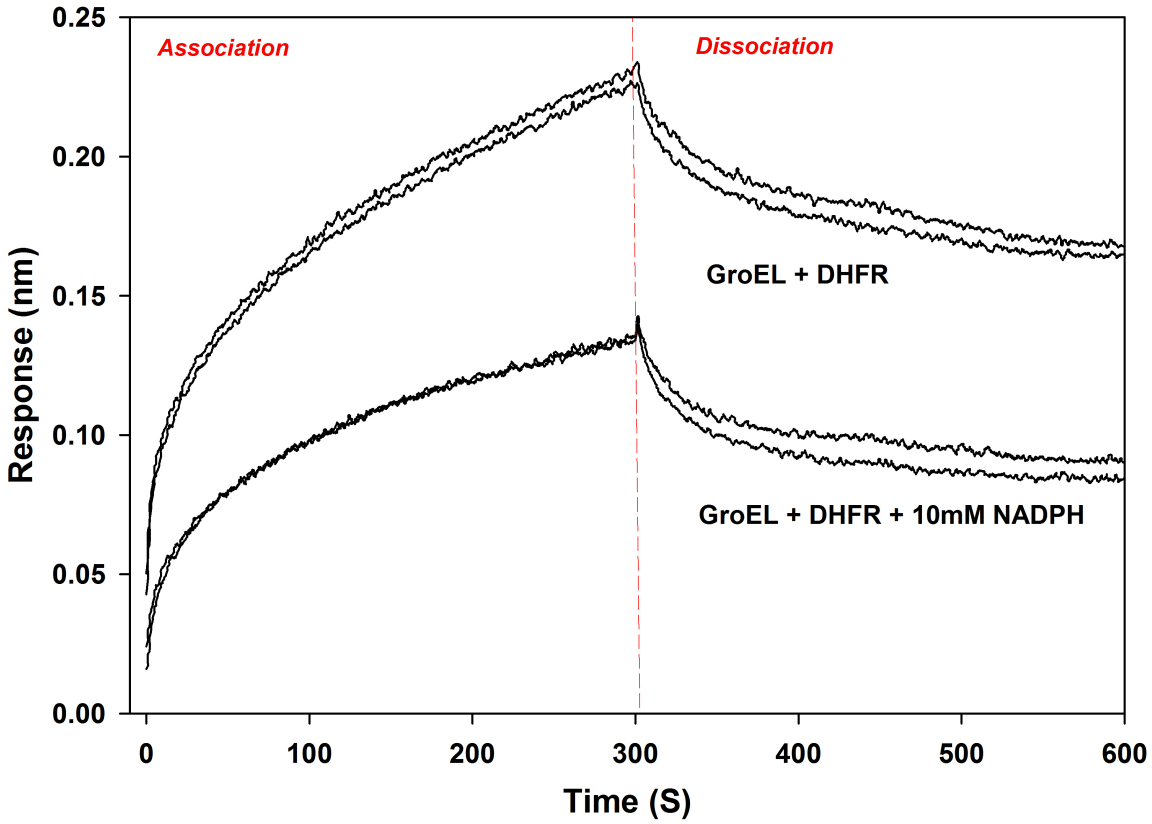

Figure 5.8: BLI can be utilized to follow the small molecule ligand based stabilization of immobilized DHFR in real time. DHFR was immobilized onto amine reactive tips through covalent coupling and incubated with GroEL alone or with 10mM NADPH. NADPH was observed to decrease the amplitude of GroEL binding due to stabilization of the DHFR native state.

Once the DHFR and α-lactalbumin proteins were examined, the stabilization of the CFTR NBD1 protein folding fragment was examined. CFTR NBD1 in the presence of its known stabilizer, 10 mM ATP was immobilized onto the amine reactive biosensors using amine coupling. The presence of the stabilizer was necessary, as the protein in the absence of ATP has been demonstrated to unfold and undergo slow aggregation. This can be counterproductive for

the chaperonin assay, as GroEL does not bind to larger aggregates as well due to burial of the extensive hydrophobic interface. Fortunately the stabilizing ligand ATP binds to NBD1 with weak affinity (μM affinity) and it is easy to wash out the bound ATP from the immobilized protein during the baseline step where the biosensor is incubated with the buffer. This procedure illustrates the utility of examining aggregation prone proteins because if they are initially immobilized, the large-scale aggregation observed in solution is avoided. Thus it was predicted that ligand free CFTR NBD1 that interacts with GroEL will most likely exist as a partially unfolded form that can now bind to the chaperonin. This prediction was supported by the observation that the BLI signal shows a jump in the association phase. Likewise, in the presence of another stabilizing molecule GTP, GroEL binding to CFTR NBD1 results in a much lower signal amplitude (Figure 5.9). These results suggest that GTP binding stabilizes CFTR NBD1 bound on the BLI surface resulting in a stable fold that results in a decreased interaction with the GroEL in solution. This stabilized form of the protein thus requires a higher energy to unfold as compared to the nucleotide free CFTR NBD1 and consequently has fewer hydrophobic residues being exposed. This in turn decreases its interaction with GroEL as has been observed. As found previously, GTP does not bind to GroEL and as predicted, GTP does not interfere with the partitioning of unliganded DHFR onto GroEL. All these observations thus indicate that the GroEL chaperonin based BLI experiments can be used to probe the folded state of protein substrates, helping us to identify potential protein stabilizers.

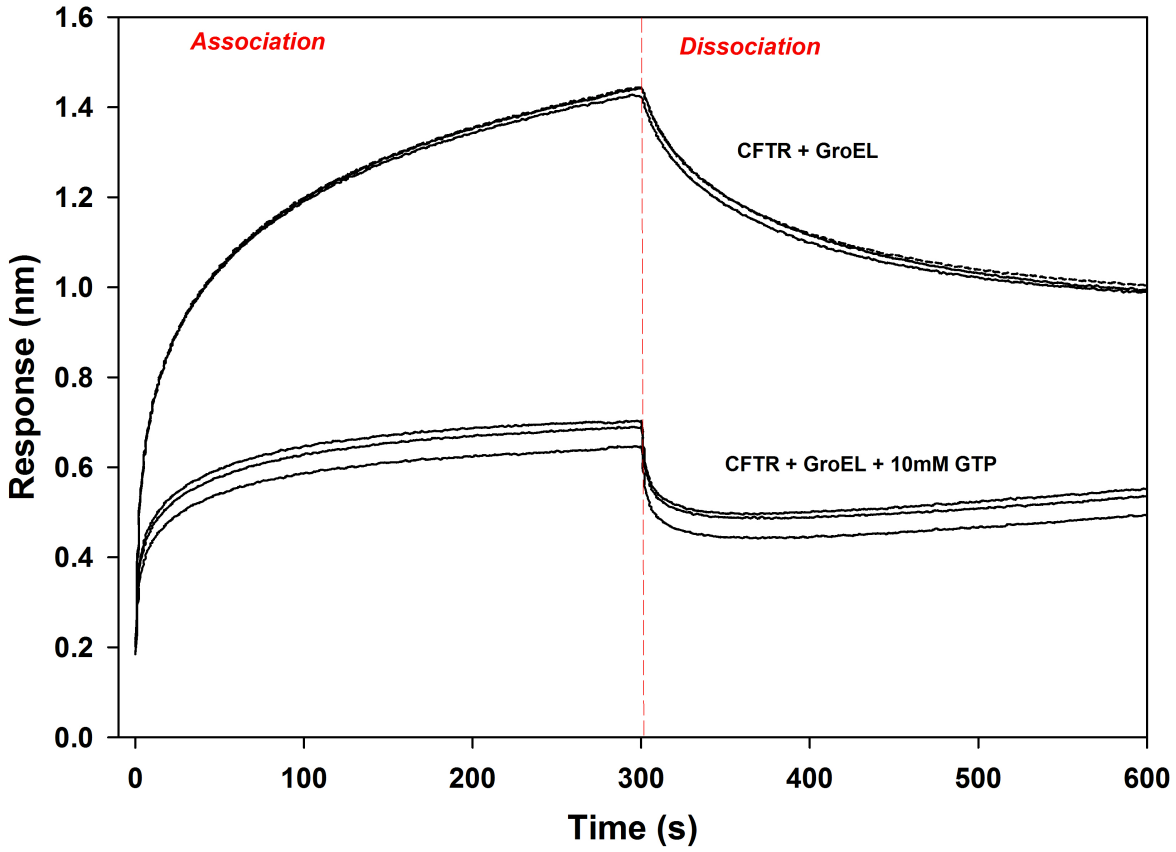

Figure 5.9: Stabilization of CFTR NBD1 as demonstrated by BLI. CFTR NBD1 was immobilized onto amine reactive tips through covalent coupling and incubated with GroEL alone or with 10 mM GTP. GTP stabilizes the immobilized CFTR NBD1 leading to a decreased GroEL binding that can be followed by BLI in real time.

An advantage of the SPR system is that it offers a facile way of evaluating the kinetic parameters that define a ligand-analyte interaction. Several studies have shown that the binding measurements obtained through BLI are comparable to those obtained by SPR (*243*). The data has also been found to be in excellent agreement with isothermal calorimetry data (*246*). Here it was predicted that BLI could be used to examine the kinetic dependence of the binding reaction between the chaperone and CFTR NBD1. To examine this dependence, different concentrations

of GroEL (0-4 μM) were pipetted into one row of a 96 well plate. Eight separate CFTR NBD1 biosensor tips were generated by amine coupling. These biosensors were incubated with the different GroEL concentrations for 5 minutes to measure the association traces, followed by incubating the GroEL bound biosensor in buffer to observe the dissociation phases. The data obtained were analyzed using the BLI analysis software. It was observed as predicted that the signal amplitude increases as a function of the concentration (Figure 5.10). The signal curves obtained were fitted globally to a 1:1 Langmuir's model. The curves were then fitted with a non-linear fitting program in the Octet RED96 system to obtain the k_{on}, k_{off} and the K_d values. The dissociation constant was estimated to be about 78 nM ± 14nM (Figure 5.10).

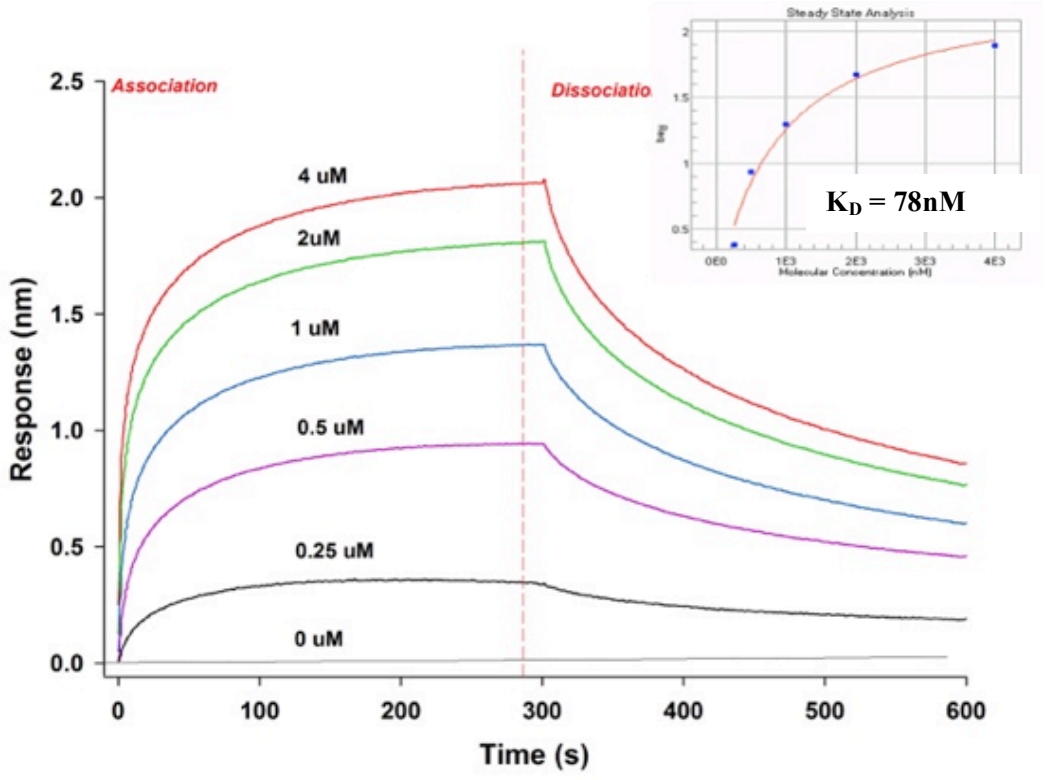

Figure 5.10: Determination of the kinetic parameters of CFTR NBD1-GroEL binding utilizing BLI. This involved immobilizing of CFTR NBD1 onto the biosensor and

incubating with increasing concentrations (0-4 μM) of GroEL. It can be observed that the binding amplitude increases with concentration. Inset: The partitioning rates for each concentration trace were calculated and plotted as a function of GroEL concentration. The K_D for the CFTR NBD1-Groel binding was estimated to be approximately 78 nM ± 14nM.

While carrying out these experiments, it was observed that in the dissociation phase, the chaperonin was undergoing dissociation from the bound ligand. However, GroEL binding to the substrate is usually a high affinity reaction with K_d values that approach nanomolar affinities (*247*). It was therefore expected that a minimal dissociation of GroEL would occur in the dissociation phase during the BLI studies. To explain this increased dissociation, one can hypothesize that it might be due to the high concentration of protein that is immobilized on the biosensor surface. This might sterically prevent the substrate from interacting with the GroEL binding sites that are present in the inner rim of the central cavity (Figure 5.11 A). Alternatively, GroEL might also be binding non-specifically to the biosensor with low affinity. This non-specific binding was confirmed by incubating the chaperonin with the unloaded biosensors where it was observed that the chaperonin binds to the biosensors non-specifically. Thus, the binding constant obtained in Figure 5.10 is not valid due to steric hindrance of the binding reaction and non-specific GroEL binding.

To avoid these interaction artifacts, it was surmised that if one were to optimize the orientation of the BLI attached protein substrate while avoiding non-specific binding, that the binding reaction under these conditions would be more realistic. To achieve this goal, a novel method of immobilizing the substrate protein was utilized. Anti-mouse Fc biosensors were utilized to immobilize a monoclonal CFTR NBD1 antibodies and then the CFTR NBD1 was bound to the immobilized monoclonal antibody (Figure 5.12). Intact antibodies can still bind to

substrates that are bound to the GroEL chaperonin (*248*). Thus, if a protein is partially unfolded and binds specifically to a monoclonal antibody, then GroEL should easily bind to this Ab-CFTR NBD1 complex. In addition, the tips used for the Fc immobilization show little background (non-specific) GroEL binding. The rationale behind this method was that the antibody would act as a protein linker and keep the protein away from the BLI surface allowing GroEL better access to the partially folded CFTR NBD1 to allow this substrate easy access to interact with the interior GroEL binding sites (Figure 5.11 B).

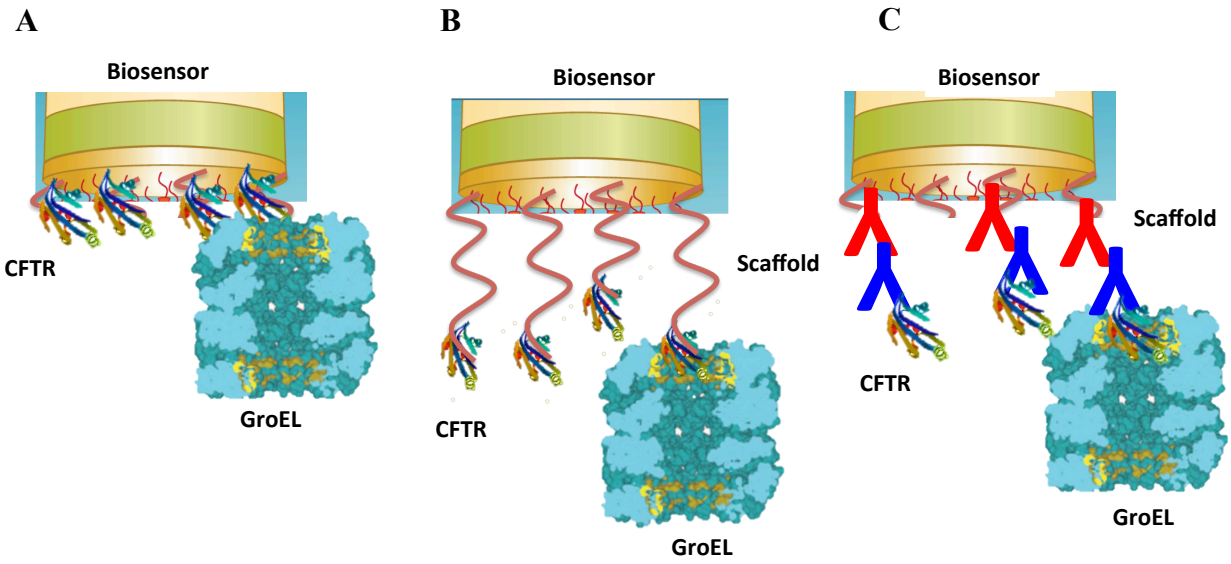

Figure 5.11: Rationale behind using a linker between the biosensor and the ligand. (A) Crowding of CFTR NBD1 on the biosensor surface prevents its interaction with GroEL binding sites (B) Introducing an extended antibody linker between CFTR NBD1 and the biosensor would increase the distance and allow better interaction with GroEL. A flexible linker might however lead to the molecules interacting with each other and aggregate on the surface. (C) A rigid scaffold like an antibody however reduces the possibility of interaction while increasing the distance between CFTR NBD1 and surface

It was observed that with this antibody extension approach, the stabilized and the partially unfolded states of CFTR NBD1 could be distinguished. The amplitude of chaperonin binding to the stabilized form (Figure 5.13 green and yellow traces) was lower than that without any stabilizing ligand. In the previous study that utilized amine coupling and amine reactive tips, GroEL was observed to show biphasic dissociation from the immobilized substrate (Figure 5.4) and GroEL could bind non-specifically to the tips. With the antibody protein substrate extension, a rapid dissociation of the chaperonin from the antibody immobilized CFTR NBD1 was not observed (Figure 5.13). The arrangement also diminishes non-specific binding of the chaperonin to the Fc antibody biosensor. Most importantly, GroEL does not bind to the CFTR NBD1 monoclonal antibody. This supports our hypothesis that increasing the distance between the biosensor surface and the immobilized protein via any suitable linker makes it easier for the chaperonin to bind to the protein. It was also predicted that the bound GroEL could be dissociated from the biosensor by the addition of ATP and glycerol. When the biosensor was incubated with a mixture of ATP and glycerol, it was observed that as predicted, the chaperonin undergoes dissociation (data not shown). The signal amplitude reaches the baseline indicating complete removal of the chaperonin and that the binding of the chaperonin was specific to the immobilized substrate on the biosensor.

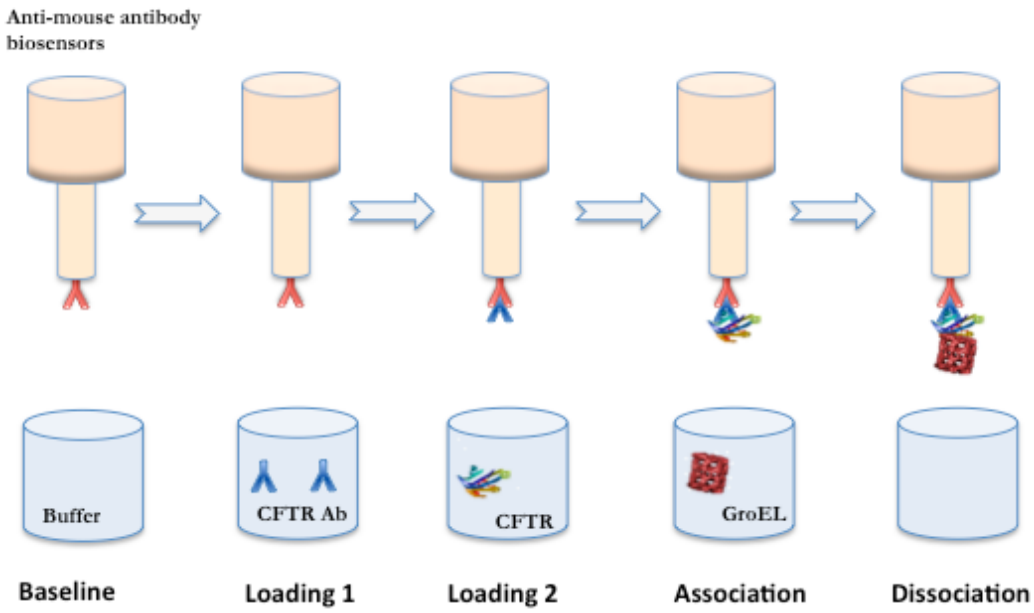

Figure 5.12: Protocol for immobilizing CFTR NBD1 through an antibody linker. A novel approach was utilized to decrease steric hindrance and non-specific binding by increasing the distance between the substrate protein and the biosensor. This was achieved through an antibody linker and an antibody binding biosensor. This configuration was observed to be stable with virtually no CFTR NBD1 dissociation and no non-specific binding to the chaperonin.

The chaperonin immobilized on the biosensor tip was also predicted to be useful to detect ligand based stabilization of substrate proteins. An advantage with this set-up is that the tips could be regenerated by an ATP wash to remove any bound substrate. The regenerated tips could then be re-utilized. In these sets of studies, GroEL was immobilized on the surface of the biosensors while the substrate protein was incubated with the stabilizer. However with GroEL, one cannot utilize amine coupling as the GroEL dodecamer falls apart at the low pH used for the amine coupling reaction. One alternative strategy for immobilizing GroEL is to utilize affinity coupling. Using a biotin–streptavidin complex is one such affinity coupling method. The

availability of commercial streptavidin biosensors makes this strategy particularly attractive and facile. Hence, the GroEL molecule was biotinylated using an EZ-Link Sulfo-NHS-LC-Biotin reagent (Pierce). This is a water soluble biotinylation reagent with an intermediate linker for labeling proteins and other molecules that have primary amines. Although this leads to the non-specific labeling of the GroEL molecule, the architecture of the chaperonin makes this problem superfluous. This is because the chaperonin has two barrels on either side with two different binding sites. Thus, regardless of the way it is immobilized there always exists one binding site that is open. The biotinylated GroEL biosensor was then incubated with either the substrate protein alone or the substrate protein in the presence of the stabilizer.

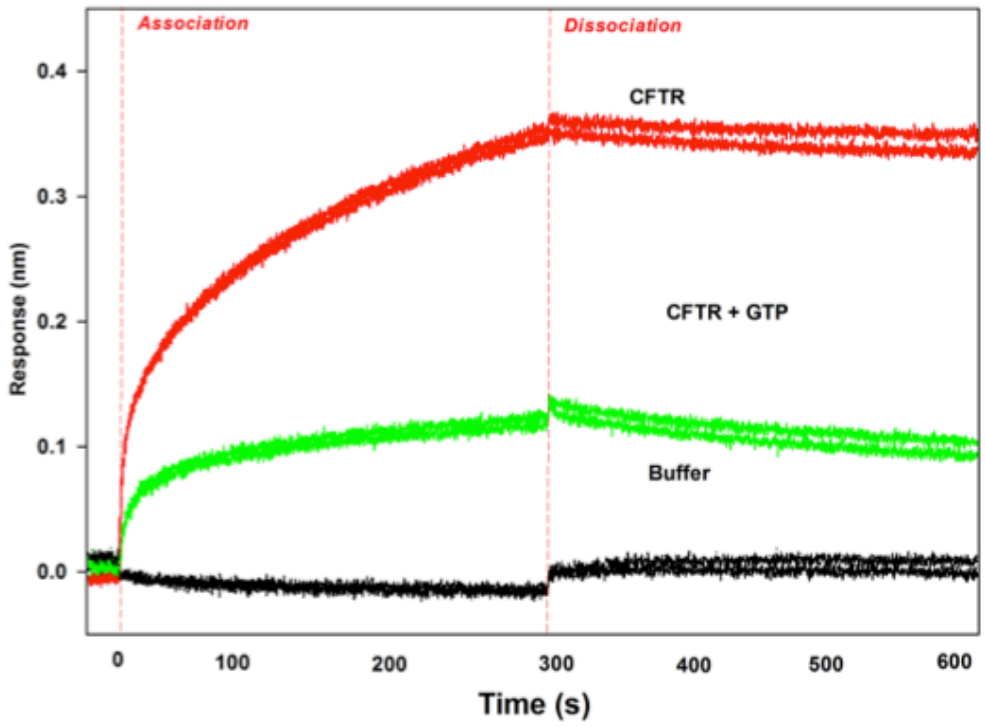

Figure 5.13: Utilizing an antibody based scaffold reduced the non-specific binding of the chaperonin to the biosensors. Here GTP based stabilization of CFTR NBD1 is demonstrated with the antibody based scaffold used to immobilize CFTR NBD1. The

antibody-based scaffold was generated by incubating CFTR NBD1 monoclonal antibodies with the commercially available anti-mouse Fc biosensors. The antibody loaded biosensors were then further incubation with the CFTR NBD1. The immobilized CFTR NBD1 biosensors were then incubated with GroEL alone (red trace) as control or in the presence of GTP (green trace). The GTP stabilized CFTR NBD1 showed decreased binding to GroEL as compared to the control (black trace, CFTR NBD1 antibody on anti-mouse Fc biosensors).

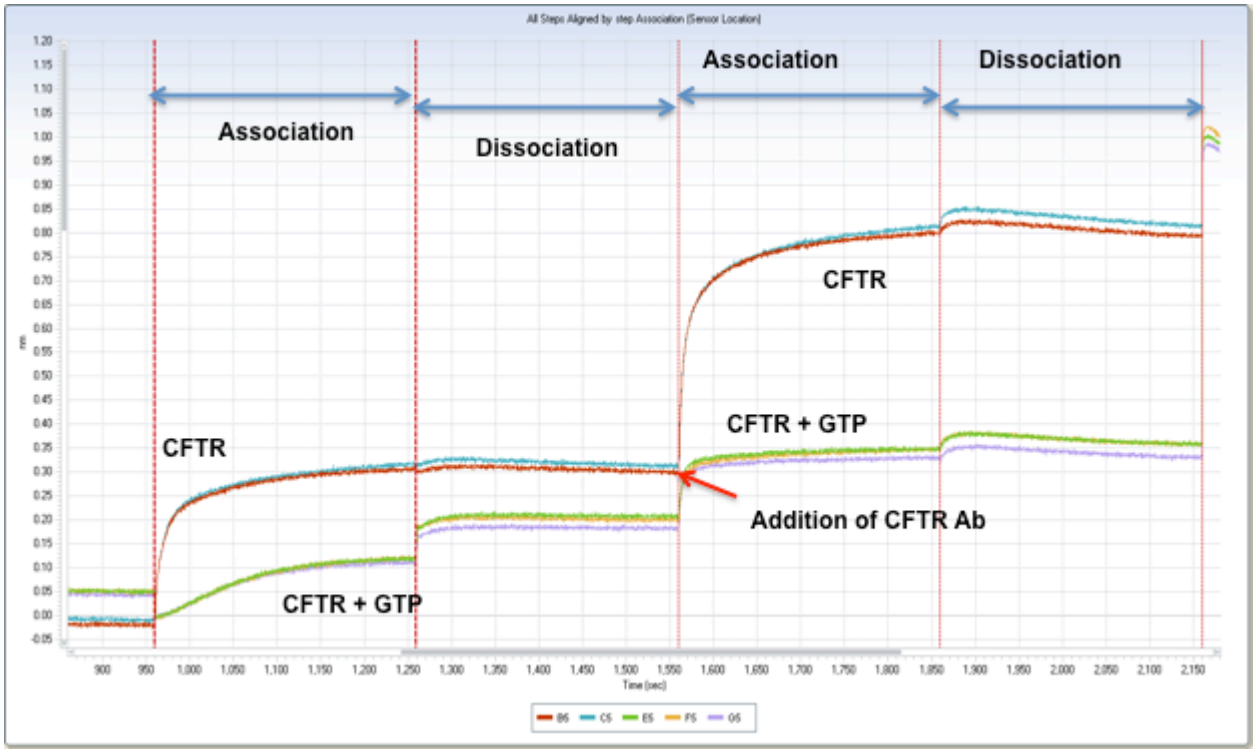

Figure 5.14: Utilizing BLI to follow ligand based stabilization of CFTR NBD1 with immobilized chaperonin biosensors. GroEL biosensors incubated with CFTR NBD1 in the presence of GTP shows lower binding amplitudes than those in the absence of GTP indicating stabilization of CFTR NBD1. The low signal obtained with the smaller CFTR

molecule was amplified using CFTR NBD1 monoclonal antibodies (having a larger mass) that bind to the CFTR NBD1–GroEL complex.

Predictably, the reverse configuration should give the same response that was previously observed with the CFTR NBD1 immobilized biosensors, but at lower amplitude. The lower amplitude is expected since CFTR NBD1 (23 kDa) is substantially smaller than GroEL (802 kDa). This is because the signal amplitude is a function of the optical thickness of the analyte, which in this case (both DHFR and CFTR NBD1) is much smaller than the dodecameric GroEL (800 kDa). Since the signal should be smaller, one can enhance the signal as follows. As stated previously, proteins that bind to GroEL are exposed to solution and antibodies are still able to bind to the protein substrate even when it is bound to GroEL. Therefore, the initial protein substrate binding signal should be enhanced if one adds a specific antibody (in the case of CFTR NBD1, a monoclonal Ab) to change the optical thickness and hence increase the phase shift of the BLI signal. As predicted, the CFTR NBD1 bound to the immobilized GroEL with substantially lower amplitude as compared to the studies where the chaperonin was in solution. It was also observed that on addition of an antibody the difference between the stabilized and non-stabilized forms was magnified. This occurs as the antibody binds as a function of concentration to the CFTR NBD1 that has partitioned onto the GroEL tips. As a higher percentage of the non-stabilized CFTR NBD1 partitions onto the GroEL tips, consequently more antibodies bound to these tips (in contrast with those tips incubated with the stabilized CFTR NBD1) (Figure 5.14).

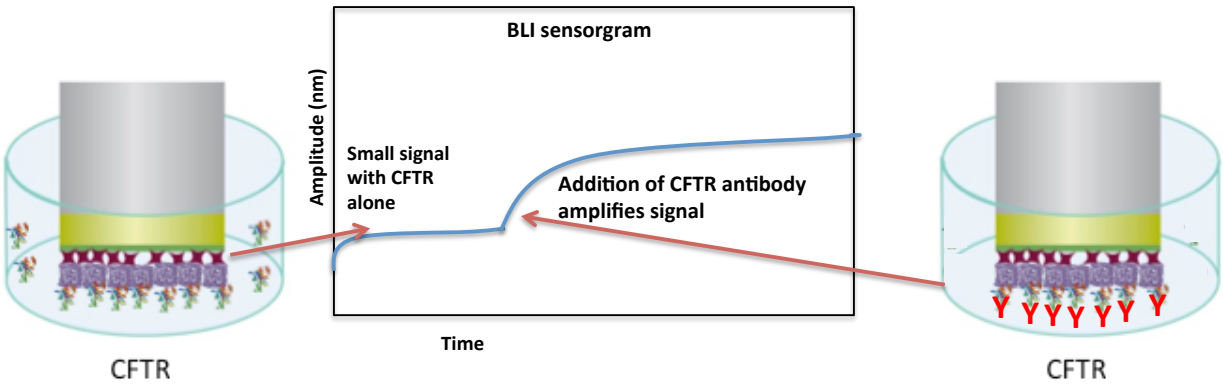

Figure 5.15: Amplification of BLI signal by addition of CFTR NBD1 antibodies. CFTR NBD1 is a small protein with a mass of 23kDa. As the BLI signal is partly dependent on the size of a protein, this signal is predicted to be very small. However, one method of increasing this signal is to utilize monoclonal antibodies against CFTR NBD1 that have a higher molecular mass and would effectively lead to amplification of the signal.

Once the assay was developed and the utility of BLI as a label-free detection method for the chaperonin sink assay was demonstrated, a limited screening to demonstrate the feasibility of the method in conducting high throughput assays was carried out. To carry out these studies 10 CFTR NBD1 "correctors" from the Cystic Fibrosis Foundation Therapeutics were obtained. Correctors are small molecule ligands that somehow restore its biosynthesis and functional expression on the cell surface (*236, 249*). These compounds are a part of a modulator compounds panel that includes human CFTR NBD1 inhibitors, potentiators and correctors. These modulator compounds have been shown to increase CFTR NBD1 expression or activity in various studies. Even amongst the compounds that were obtained, the mode of action was not clear. In these studies, the possibility that these correctors may directly bind to and stabilize the CFTR NBD1 protein needs to be determined. Thus using the BLI system, a corrector that directly interacts with the CFTR NBD1 native state should stabilize the protein and prevent or decrease its

interaction with the GroEL chaperonin. On the other hand the correctors that do not bind to CFTR NBD1 and increase CFTR NBD1 expression and export via a different indirect mechanism should not interfere with the chaperonin binding. The screening was carried out in two separate runs to make it easier to analyze the data since only five correctors at a time could be evaluated using the eight biosensor Octet RED96. Two different configurations of the GroEL and CFTR NBD1 were also utilized to validate the results. In the first configuration, CFTR NBD1 was immobilized utilizing antibodies on the biosensors as described in the methods section while in the second configuration, the chaperonin was immobilized onto the biosensors.

Configuration 1: In this configuration, immobilized CFTR NBD1 biosensors were generated by utilizing CFTR NBD1 antibodies and anti-mouse Fc biosensors as described in Figure 5.12. These biosensors were initially incubated in a buffer containing the correctors for establishing a baseline followed by incubation with the mixture of CFTR NBD1 and the correctors to measure the association. The dissociation buffer also contained the correctors to prevent dilution of the correctors that was already bound to the CFTR NBD1 during the association and thus preventing any artifacts in the output. The correctors were screened at an initial concentration of 200 μM (standard concentration for HTS). During the screening, CFTR NBD1 without any stabilizer served as a negative control while CFTR NBD1 that was stabilized with GTP served as the positive control. Since this is a qualitative assay, one needs a range to determine potential hits and eliminate those compounds that do not stabilize CFTR NBD1. The CFTR NBD1 positive control was used as a standard for determining the effectiveness of the stabilizers in binding to CFTR NBD1. Since the assay depends on the association of the chaperonin to the CFTR NBD1, only the association phase was considered during the data

analysis. Any compound with its binding amplitude lower than the positive control (GroEL binding to CFTR NBD1 alone) was considered as a hit, while compunds having higher binding amplitude than the control trace was discarded. Thus, any compund that decreases GroEL binding to CFTR NBD1 resulting in a low signal output might indicate a potential CFTR NBD1 stabilizeer

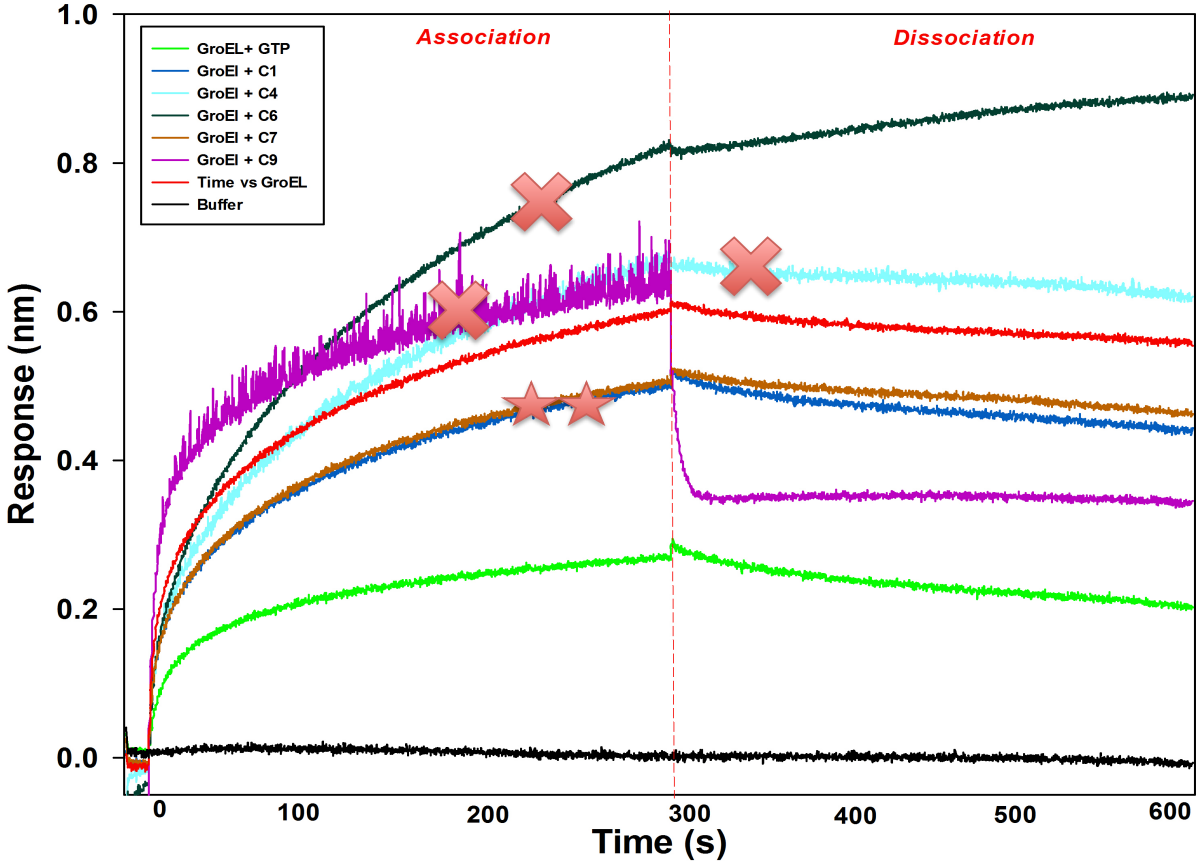

Figure 5.16: Screening CFTR NBD1 correctors utilizing BLI. CFTR NBD1 without any stabilizer (red trace) was the negative control while CFTR NBD1 stabilized with GTP was the positive control (green trace). The hits C1 (blue trace) and C7 (brown trace) that demonstrated decreased amplitude of GroEL binding are marked with a star while others C4 (light blue), C6 (dark green) and C9 (purple) that did not show a decreased amplitude were discarded and are marked with a X in the Figure. The noisy signal observed with C9

is usually associated with the aggregation of the small molecule compounds in aqueous buffers.

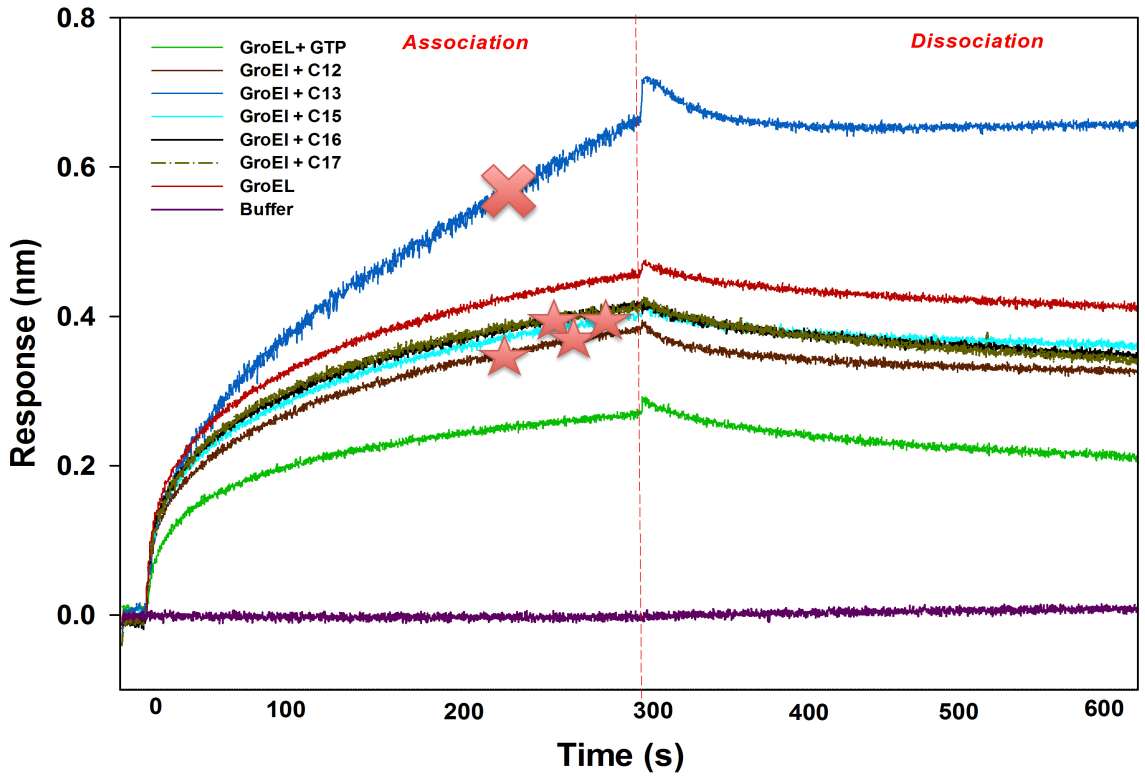

Figure 5.17: Screening a second set of CFTR NBD1 correctors utilizing BLI. CFTR NBD1 without any stabilizer (red) was the negative control while CFTR NBD1 stabilized with GTP (green) was the positive control. The binding of the chaperonin to CFTR NBD1 on the tips was lower for the hits C12 (brown), C16 (dark green), C15 (light blue) and C17 (dashed green) than the CFTR NBD1 without any stabilizer (red trace). In the Figure, the hits are marked with a star while other one that was discarded was marked with an X.

It was observed after screening both the batches that 5 of the 10 correctors (C1, C7, C12, C15 and C16) showed decreased amplitude of binding in the association phase indicating that these might be potential stabilizers of CFTR NBD1. One of the correctors demonstrated a noisy

signal, characteristic of compounds that are insoluble and lead to formation of colloids in the solution that bind to the biosensor non-specifically. To reaffirm this data set, the hits were retested. The second screen revealed that the five compounds that were considered hits all resulted in a decrease in GroEL binding to CFTR NBD1. This second screen also helped to measure the relative efficiency of the stabilizers and rank them in order of their effectiveness in stabilizing the compounds. This process of ranking the compounds is an important aspect of HTS where only the top 1% or fewer of compounds are chosen for secondary screening. Preliminary results indicate that the compounds are ranked as C7>C15> C 16> C1> C12 in their effectiveness of preventing GroEL binding to CFTR.

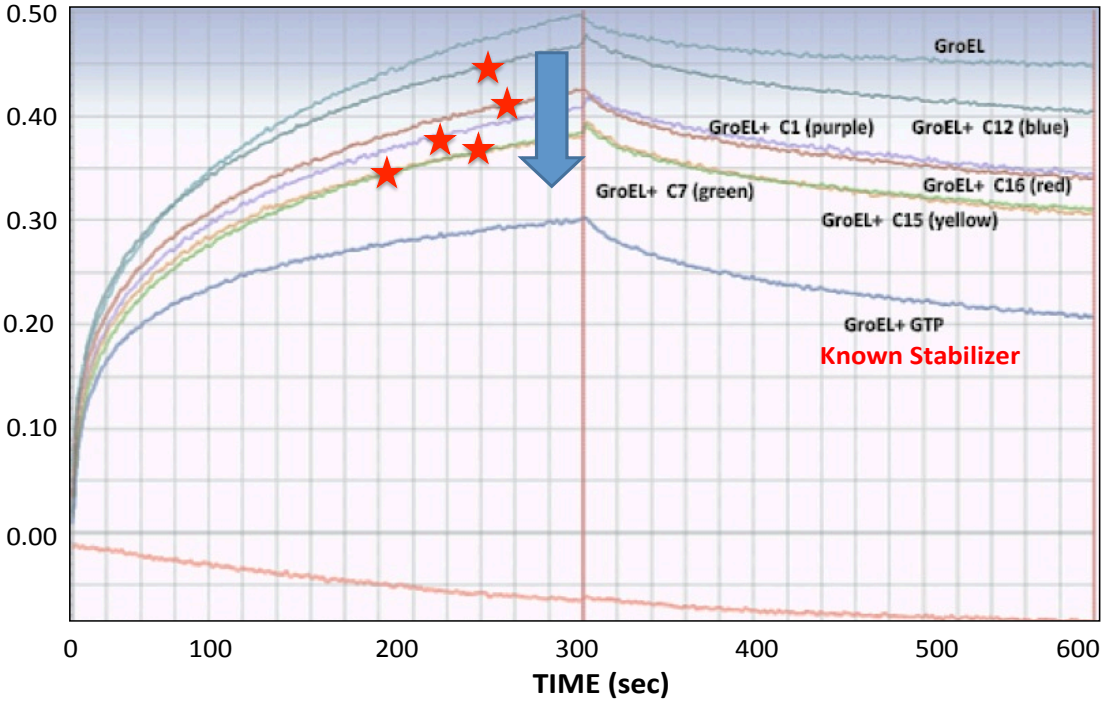

Figure 5.18: Ranking hits obtained through primary screening of CFTR NBD1 correctors utilizing BLI. The hits (stars) obtained by BLI were ranked on the basis of their effectiveness in stabilizing CFTR NBD1. CFTR NBD1 without any stabilizer (green trace) was the negative control while that stabilized with GTP (blue trace) was the positive control.

Configuration 2*:* BLI also gives another method of validating the results obtained in the primary screen. As demonstrated previously, one can utilize a reverse configuration of immobilizing GroEL on the biosensors and then probing the stability of CFTR NBD1. Accordingly, the GroEL biosensors were generated and incubated in a mixture of CFTR NBD1 alone and CFTR NBD1 with each of the five corrector compounds during association and the compounds in the buffer during dissociation. As the signals obtained during this study were very low, the signals could be amplified utilizing CFTR NBD1 monoclonal antibodies. Again, the CFTR NBD1 was used as a positive control and its amplitude used as the criterion for assigning hits, while buffer was the negative control. It was observed that even with the inverted set-up, the compounds still exhibited stabilizing of CFTR NBD1 (Figure 5.19).

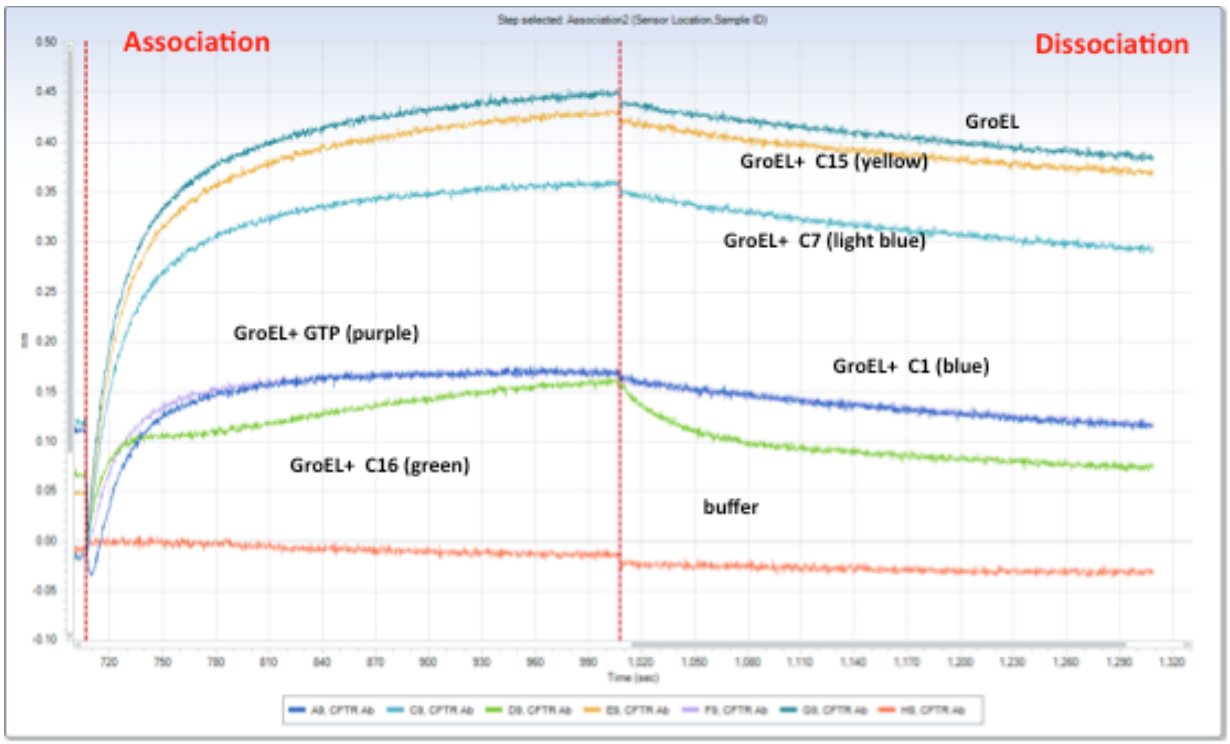

Figure 5.19: A reverse configuration with GroEL immobilized on the tips was utilized to screen for hits. Here the CFTR NBD1 was incubated with the correctors and

GroEL tips (containing biotinylated GroEL immobilized on streptavidin tips) were dipped into the CFTR NBD1 containing buffers. CFTR NBD1 without any stabilizer (GroEL, dark green trace) was the negative control while CFTR NBD1 stabilized with GTP (GroEL + GTP, purple trace) was the positive control. All the hits obtained from the previous screen were observed to demonstrate stabilization of CFTR NBD1 as shown by a decrease in binding of GroEL as compared to CFTR NBD1 without any stabilizer (dark green trace).

The small molecules utilized in screening were dissolved in DMSO. Due to its high solvent power, low chemical reactivity and relatively low toxicity, DMSO has become the solvent of choice for small molecule storage and handling. However, a possible concern is the effect of DMSO both on the proteins as well as with the instrumentation. It has been shown to change the properties of proteins in solution, leading to protein denaturation, aggregation, or degradation and can also change protein binding properties (*250*). Additionally, DMSO has a much higher RI than common buffer solutions, which can make it difficult to produce reliable readings from DMSO-containing samples using optical biosensor technologies. The combination of density changes and DMSO effects on the protein makes experimental design and interpretation of results rather complex with SPR. Small differences in concentration of DMSO lead to large changes in SPR responses (100 RU for a 0.1% change). However, unlike SPR, BLI has the advantage that it is not as sensitive to fluctuations in refractive indices and hence is more forgiving of DMSO effects. This makes it much easier to carry out screening of small molecules using BLI as compared to SPR and other optical techniques.

In these previous studies, human wild type CFTR NBD1 was utilized as a substrate protein. However, although the correctors might be effective against the wild type CFTR, they might not show similar effectiveness against mutant proteins that are the cause of CF. One of the

most common CF mutations is the ΔF508 mutant that is also the most severe and clinically relevant mutation. Since the human mutant was not available, it was decided to utilize the mouse mutant for further studies. However, since these are mouse proteins one cannot utilize the human antibody based capture method to generate mCFTR biosensors. The alternative was to generate GroEL biosensors and utilize them to carry out screening. Prior to that, it needs to confirm that the differences between the stabilized and the non-stabilized forms of the mouse protein could be distinguished. It is known that GTP also binds and stabilizes mouse CFTR NBD1. As determined previously, the mutant mouse ΔF508 mouse protein showed the same signal responses to GroEL in the absence and presence of GTP (Figure 5.20).

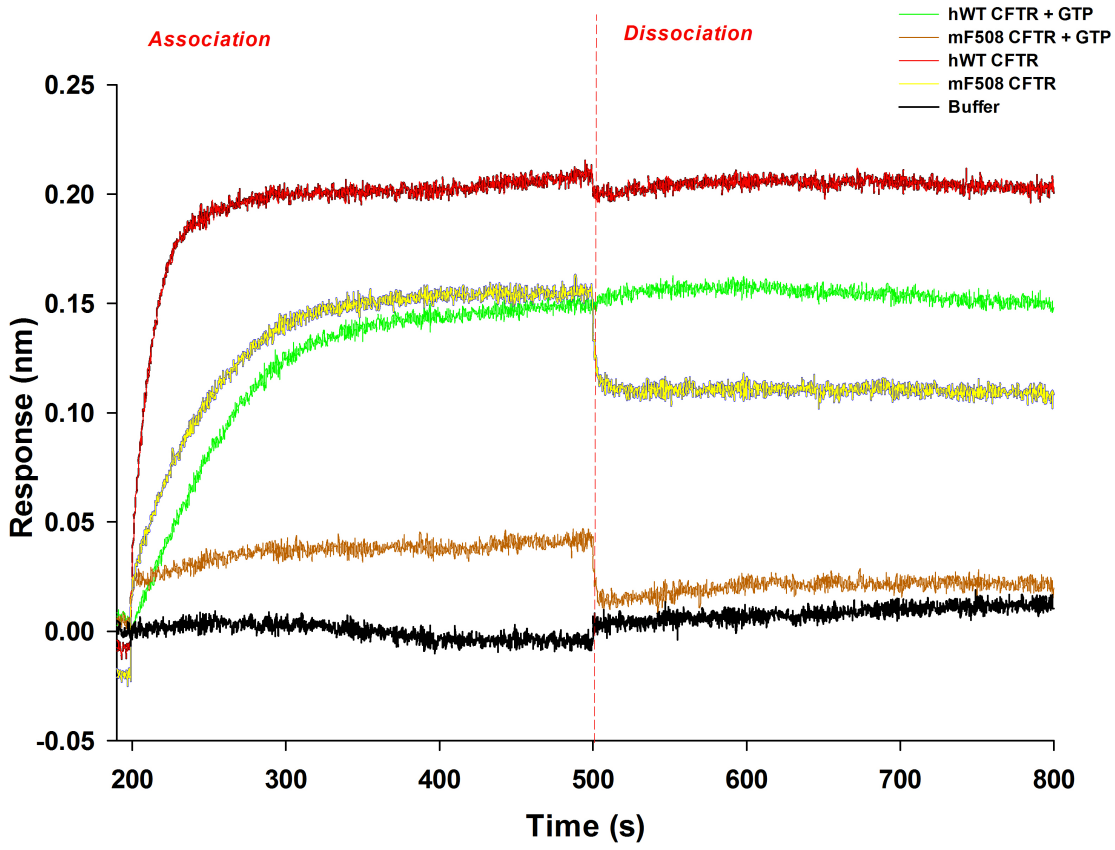

Figure 5.20: GTP stabilizes the murine ΔF508 CFTR NBD1 mutant. To observe if one could follow the stabilization of the mouse ΔF508 mutant, the protein was incubated

with biotinylated GroEL on tips in the presence (brown trace) or absence (yellow trace) of the stabilizer GTP. Human wt NBD1 was also incubated with (green trace) and without (red trace) GTP as additional controls.

For any potential CFTR corrector, one needs to determine if the candidates identified previously would also stabilize the mouse ΔF508 CFTR NBD1 mutants. The GroEL biosensors were therefore incubated with the mouse ΔF508 CFTR and the correctors. The ΔF508 mutant alone was used as the positive control against which the response of the other correctors was measured. Unfortunately, one cannot use the monoclonal anti-human CFTR NBD1 antibody to enhance the signal for GroEL bound CFTR because this antibody does not interact very strongly with the mouse Δ508 mutant CFTR-NBD1. However even with the low signal amplitudes from the mouse CFTR NBD1 binding to GroEL biosensors, one can observe (Figure 5.21) that the amplitude of the signals for all five correctors was lower than that of the positive control. This indicated that the potential positive "hit" correctors that worked with the wild type human CFTR NBD1 also diminished mouse ΔF508 CFTR NBD1 partitioning onto GroEL. In this instance, it may be valid to suggest that, at least with CFTR NBD1, that small molecule stabilizers identified for the native form of the protein may also stabilize some mutants (particularly the ΔF508 CFTR NDB1 mutant). However, this approach might not work with all misfolding proteins and as demonstrated with the frataxin mutants I154F and D122Y (Chapter 2, Section 2.3.3), each mutant might have to be screened separately.

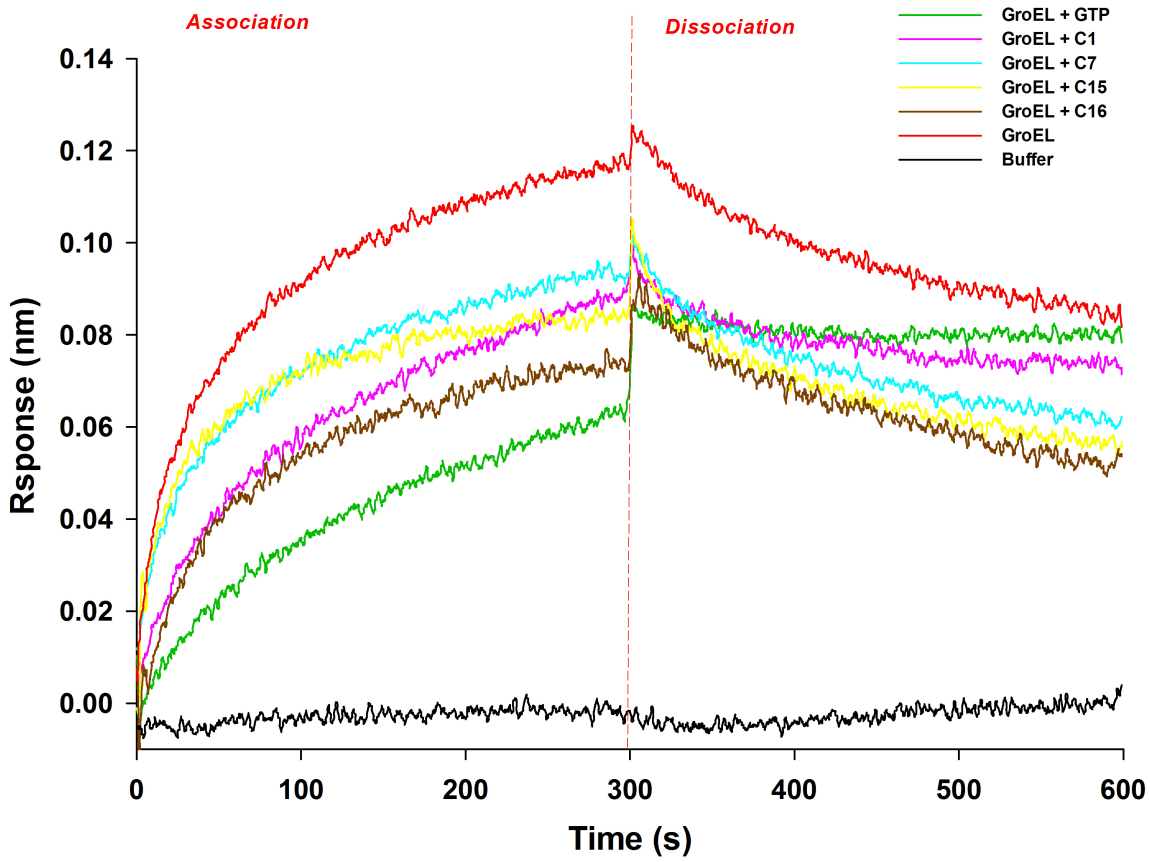

Figure 5.21: The CFTR NBD1 correctors that demonstrate "potential" stabilization of the native human CFTR NBD1 also appear to stabilize the mouse CFTR NBD1 ΔF508 mutants. The CFTR ΔF508 mouse mutant was treated with biotinylated GroEL immobilized on streptavidin biosensors. The binding amplitudes of the mutant protein in the presence of the previously identified potential "hit" correctors, C1 (pink), C7 (light blue), C15 (yellow) and C16 (brown) were observed to be lower than the CFTR NBD1 ΔF508 mutant without any corrector which is the positive control (red trace).

The objective of a HTS is to screen as many compounds as possible in the shortest possible time. The necessity to maintain a balance between the output and the robustness must also address instances where false positives may arise. It is necessary to carry out secondary assays to identify the false positives. For this particular screening set-up, a false positive result

may arise in instances where the lead compound (corrector) in question would bind and interact with the GroEL substrate binding site, thereby inhibiting the partially folded protein substrate in question from binding/partitioning onto GroEL. This event would also lead to a decreased signal. An alternative instance would be where the small molecule may adsorb onto the substrate protein to cover available GroEL binding sites. This would also give rise to false positives. However the probability of this happening would be is very rare and can be safely discarded. One way of identifying false positive results is to check if the partitioning of another substrate protein (control substrate like DHFR) onto GroEL is also affected by the potential "hit" correctors.

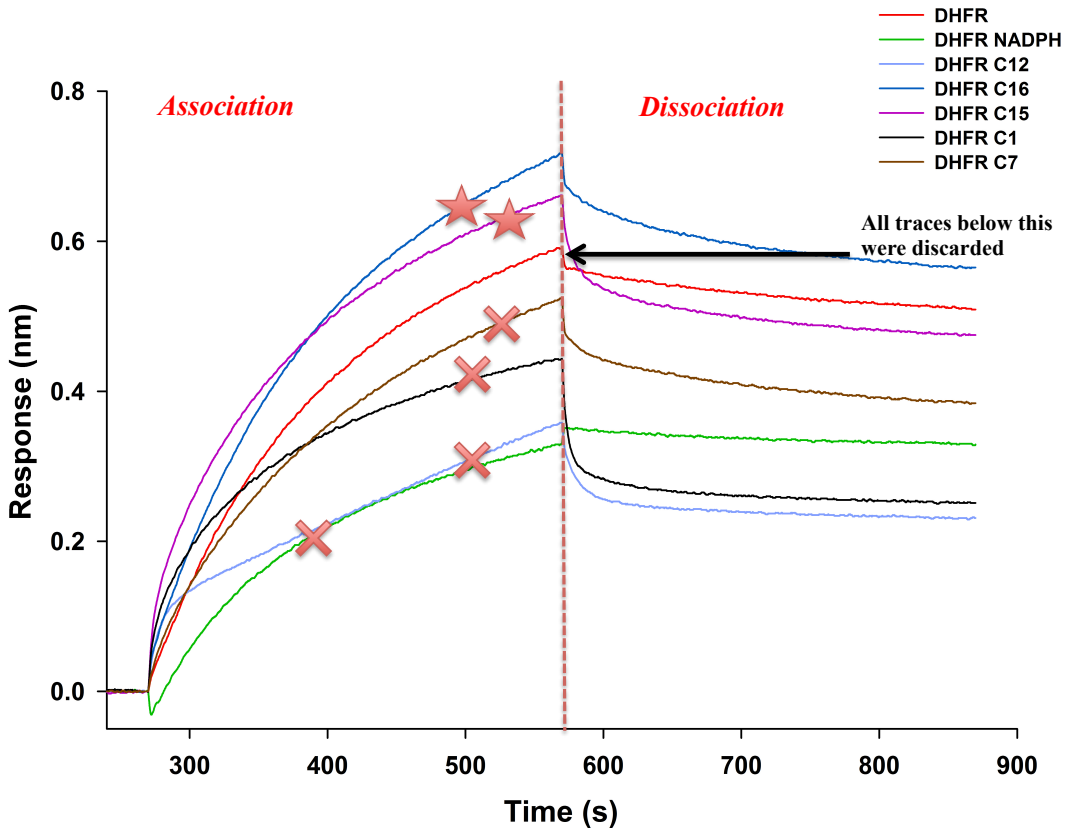

Figure 5.22: Secondary screening of the CFTR hits utilizing DHFR helped to identify any false positives and to isolate the stabilizers. The hits should not affect or

decrease DHFR binding to the chaperonin (red trace and red arrow). Any trace that shows association below the red arrow is discarded. In this assay, three of the potential "hits", C1 (black trace), C12 (light blue trace) and C7 (brown trace) were observed to decrease DHFR partitioning onto GroEL, strongly suggesting that they interfered with chaperonin binding and must be ruled as false positives. C15 (pink trace) and C16 (blue trace) (shown by stars) increases do not affect the chaperonin partitioning thus leading us to conclude that these may be valid "hits" that need to be tested further to identify direct binding.

Here one utilized DHFR as the alternative substrate protein. GroEL was immobilized onto the biosensors using streptavidin biosensors and incubated with the DHFR in solution. DHFR without any corrector (red trace Figure 5.21) was the positive control. Ideally, the correctors should not interfere with DHFR partitioning onto GroEL. The prediction was that in case of false positives, one would observe a decrease in binding of DHFR to GroEL. It was observed (Figure 5.21) that there is a decrease in the binding to DHFR in presence of the correctors C1, C7 and C12. Thus, it was inferred that these compounds might be false positives that could possibly be affecting the partitioning of the control protein substrate onto GroEL by directly interacting with GroEL (as an example). Two of the hits C15 and C16 however, did not prevent DHFR partitioning and binding, indicating that these two candidates could be potential CFTR NBD1 stabilizers that bind to the CFTR NBD1 native state and prevent its aggregation. As with all drug protein interactions, this direct interaction would need to be confirmed using other direct binding measurement techniques (spectroscopic, stability shifts).

5.4 Conclusions.

In this chapter, the feasibility of utilizing the chaperonin based BLI system to screen for small molecule stabilizers was demonstrated. This technique is similar to SPR in terms of the

data obtained but without the problems associated with the microfluidics based system of SPR. Comparison studies have established that data obtained from SPR is replicated with the BLI based platforms. Unlike SPR, BLI utilizes the shifts in interference pattern of light caused by changes in thickness of molecules bound to the sensor. The compatibility of using the BLI with existing HTS systems utilizing 96 and 384 well plates make it an excellent choice for high throughput studies. Furthermore one is able to rapidly assess the binding kinetic data parameters of the substrate protein-chaperonin partitioning amplitudes allowing researchers to identify potential "hits" that can be further characterized. BLI biosensors are available in a number of chemistries that make it easier to conjugate various types of proteins. In addition these biosensors are comparatively cheap ranging from $2-$10/unit. Furthermore, these tips can be regenerated by reversing the bound chaperonin with ATP. Thus increases in assay speed (turn around), avoidance of aggregation interferences, reproducibility, along with low cost are all factors that makes the BLI platform an excellent alternative for SPR. In this chapter, the technique was initially used to demonstrate the proof-of-principle of following in real-time the partitioning with several substrate proteins like DHFR and CFTR NBD1. The limited screening to validate potential stabilizers for both human and murine CFTR NBD1, and ruling out false positives through secondary screening allowed us carry out a screening set and validation within as little as 20 min. for ten compounds. With a 16-channel system, the assay sets can be doubled. However, as with all label-free technologies, one has to search for optimal biosensor surfaces or constructions to rule out possible non-specific binding effects with some of the biosensor platforms. Non-specific binding can be reduced by increasing the ligand concentration and immobilization density or utilizing low levels of non-ionic detergents (tween 20) or using non-specific carrier proteins like BSA to block non-specific sites. In this vein, blocking non-specific

interactions resembles common blocking reactions used for western blot analysis. Rebinding of the analyte during dissociation as well as evaporation of the analyte solution in wells over long incubation period may lead to skewed kinetics. Compared with current state of the art uHTS systems, BLI is a medium throughput instrument at best and currently cannot reach true HTS or uHTS output levels. However, in case of the chaperonin assay with transiently stable protein substrates, the benefits overweigh any associated problems and make it an instrument of choice.

CHAPTER 6: TOWARD DEVELOPING A HTS ASSAY TO INHIBIT BACTERIAL TOXIN TRANSITIONS

6.1 On the development of a high throughput assay to inhibit anthrax toxin transitions.

6.1.1 Rationale: Bacterial toxin transitioning as unfolding events and utilizing GroEL to detect these unfolding events.

Several bacterial toxins such as the pseudomonas endotoxin, anthrax toxin and the clostridium toxin undergo conformational changes during their activation. These conformational changes are often associated with the transient exposure of hydrophobic residues before undergoing an irreversible conformational rearrangement. This transient exposure of hydrophobic residues frequently leads to an increased hydrophobic character of the protein. In the absence of a membrane or a lipid component that buries the exposed hydrophobic residues, the toxins undergo aggregation in solution. This tendency of the toxins to undergo aggregation makes solution based studies of the toxins and thus drug discovery efforts difficult. The predisposition of the toxins to expose hydrophobic residues and undergo aggregation is similar to what has been observed with misfolding proteins such as CFTR. Therefore, a possibility exists that one can immobilize the bacterial toxins onto a solid surface to prevent aggregation and can be used as a platform to develop novel antimicrobial agents aimed at inhibiting toxin transitions.

One such bacterial toxin that exhibits an irreversible conformational rearrangement during its activation is the anthrax protective antigen (PA). During this conformational rearrangement, PA undergoes transitioning from a soluble form (PA prepore) to a membrane insertable pore form (PA pore). *In vitro*, the addition of detergents, 1M urea or adjusting the

solution pH towards a mild acidic nature (~ pH 5.0) at a temperature of 37°C are sufficient solution conditions that allow the initial soluble prepore protein to transition to the pore insertable state (*251*). This pore form of the PA results in the formation of a long hydrophobic beta barrel (100 Å) with a hydrophobic tip. In the absence of lipids or detergents, PA prepore fails to transition to the pore, and the resulting intermediates aggregate in solution. If the pore is allowed to somehow transition to the pore without extensive aggregation (very low concentrations), the pore itself will aggregate via the exposed hydrophobic tips. Immobilizing the PA prepore onto a solid surface would thus be predicted to prevent aggregation after transitioning. It is also possible to easily direct the immobilization to occur in a homogenous manner on the immobilized surface using the truncated (1-288 residues) lethal factor N-terminal domain (LF_N) as an affinity based binding orientation platform (*252*). This directed immobilization positions the PA pore such that the unfolding and refolding of beta barrel and the hydrophobic tip extend away from the immobilized surface (Figure 6.1). This approach also allows us to carry out proof-of-principle studies to determine whether the chaperonin assay platform could be also be used to detect these soluble to membrane insertion transitions that result from extensive refolding conformational changes. Since the chaperonin protein recognizes hydrophobic regions, it is reasonable to test if GroEL can also bind to the exposed hydrophobic tip of the pore. The binding of GroEL to PA pore can be detected using BLI or SPR. This can now be utilized as the basis for an assay to screen for small molecule inhibitor of the PA prepore to pore transitioning. Potentially novel small molecule antibacterials can be screened that prevent the transitioning which in turn would inhibit the exposure of the hydrophobic regions, detected by a decreased GroEL binding signal. Such an approach that utilizes the chaperonin for probing the transitioned state of the toxin is an extension of the chaperonin assay platform discussed

previously. Here, the anthrax pore toxin is utilized as a test substrate to carry out the initial proof-of-principle studies.

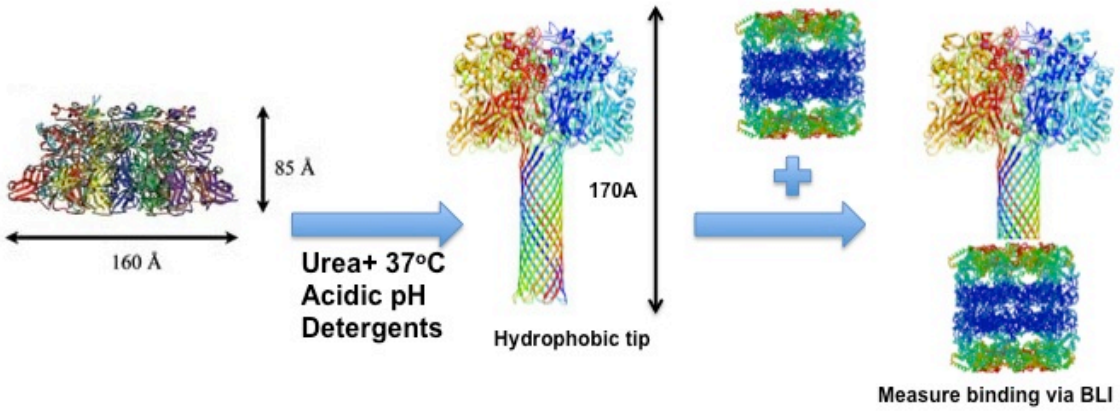

Figure 6.1: Strategy to identify inhibitors of bacterial toxin transitions using GroEL as a general detector of bacterial transitions. The PA prepore undergoes transitioning to its pore form by acidification of pH or by treatment with urea at 37°C. The binding of the prepore to a solid surface prevents the aggregation of the pore. GroEL binding to the exposed hydrophobic tip of the PA pore after transitioning could then be followed using SPR/BLI.

6.1.2 The anthrax pore toxin.

a The anthrax toxin components.

Several bacteria secrete proteinaceous toxins in order to evade the host's immune response. One such organism is the anthrax causing *Bacillus anthracis,* a gram-positive spore forming bacteria. Inhalation of the anthrax spores can lead to a fatal hemorrhagic disease (*253*). The cell injury and death associated with anthrax is due to a virulence toxin that leads to pathogenesis. The anthrax toxin is an A/B binary bacterial toxin (*254*) with two different

proteinaceous components. The A component leads to disruption of cellular processes to produce the clinical symptoms of the disease while the B component is involved in delivering the A component to the cytosol. The toxin consists of three proteins, namely protective antigen (PA), lethal factor (LF), and edema factor (EF). LF and EF are cytosolic enzymes that form the component A while the translocon PA that aids in the transport of these enzymes is component B. LF is a 90 kDa Zn^{+2} organometallic protease that inactivates MAP kinase kinases (*255*) while EF is a 89 kDa Ca^{+2} dependent adenyl cyclase (*256*). The LF and EF together in association with PA forms the lethal toxin that leads to macrophage lysis, immune-system suppression and death (*257*).

PA is an 83 kDa protein that binds to the two known anthrax receptors ANTXR1/2 (*258, 259*) in a 1:1 ratio. On binding to the receptor, PA is cleaved by a membrane protease furin into two fragments, a 20 kDa N-terminal fragment and a 63 kDa C-terminal fragment (PA_{63}) that remains bound to the receptor. As shown in Figure 6.2, the PA bound to the receptor oligomerizes into a heptamer (*260*). This complex binds with very high affinity to the EF/LF. The toxin complex then undergoes internalization to form an endosome. As the pH of the endosome decreases, the PA prepore undergoes a conformational shift leading to the formation of a beta barreled pore. This membrane insertable hydrophobic pore complex forms a new protein translocon that allows the other toxins to transverse the endosomal membrane. The enzymes EF/LF that partially unfold in the acidic endosomal environment (*261*) allowing these proteins to undergo translocation through the PA by a pH dependent mechanism. On translocation, the emerging toxin enzymes undergo refolding in the cytoplasm (*262*). A narrow phenylalanine flexible clamp that is only found within the lumen of the newly formed PA pore

channel is thought to be the crucial molecular element that controls the translocation of unfolded polypeptides (*263*).

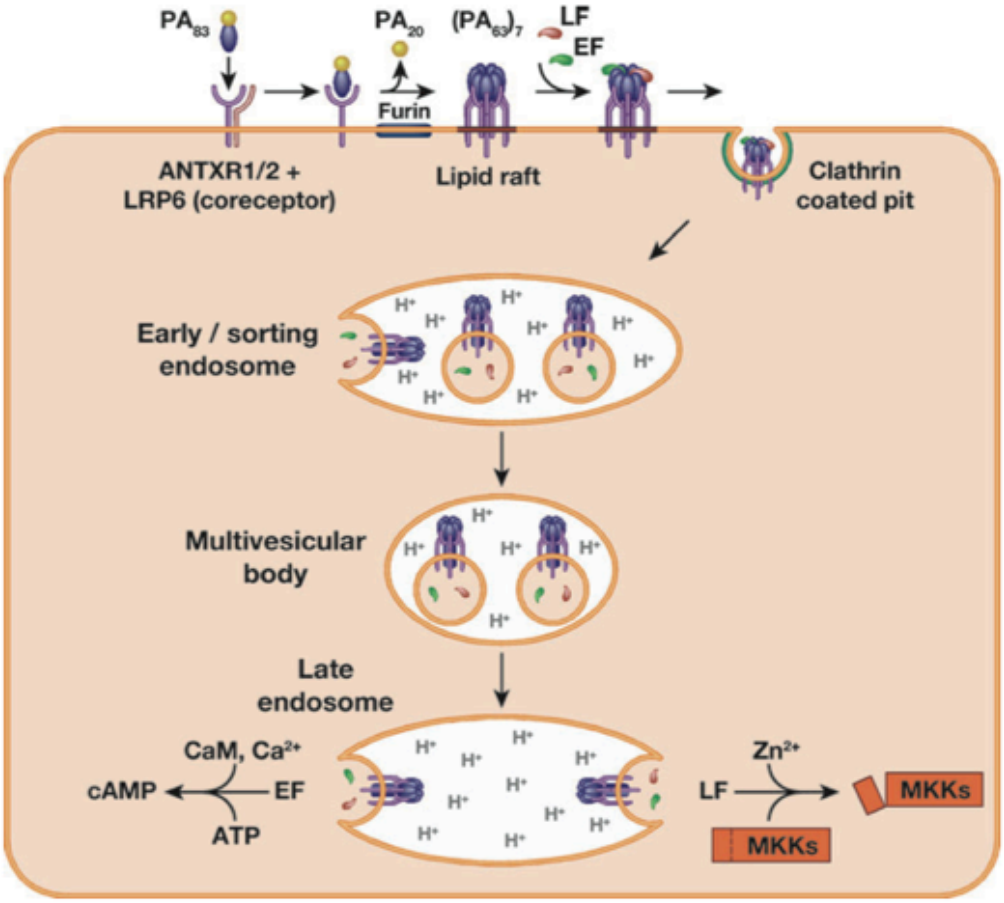

Figure 6.2: Mechanism of cell entry by the anthrax toxin. The anthrax toxin enters the host cell by binding to the anthrax receptors and undergoing endocytosis. Subsequent acidification of the endosome leads to pore formation and translocation of lethal factor. Figure sourced from (*264*)

b Structure.

Structurally, the water soluble PA prepore heptamer is a hollow ring, 160 Å in diameter and 85 Å high and each subunit consists of four domains (refer to Figure 6.3) (*265*). Most of the

domain 1 is cleaved by furin (domain highlighted in grey, Figure 6.3) after the 83 kDa PA monomer (PA_{83}) binds to specific cell receptors. This cleavage is essential as the N-terminal region of the PA_{83} sterically hinders the premature toxin oligomerization. Domains 2 (blue) and 4 (green) are not only involved in interaction with the ANTXR2 (pink) but also in the formation of the pore stem. Two β-strands (β2 and β3) from each domain of the heptamer are involved in forming the 14 strand transmembrane barrel (*266*). Four histidines (His 299, His 304, His 310, and His 336) in the loop region are protonated at endosomal pH values and are thought to be responsible for triggering pore formation (*267*). Domain 3 (purple) is involved in oligomerization while domain 4 binds to the cellular receptors (*268*).

c Anthrax therapeutics.

The Centers for Disease Control and Prevention (CDC) recommends treating anthrax infections by combining oral antibiotics such as ciprofloxacin and doxycycline with anthrax vaccine (*269*). The antibiotics are effective against the bacteria but cannot clear the protein toxins that have been already released in the body. In addition, the vaccine requires four weeks to be effective and is unlikely to be effective immediately after infection. Thus, there exists a need for rapid post-infective treatment options. Such therapeutic options that are currently under development include antibodies, toxin fragments, receptor decoys, etc. Antibodies such as Abthrax (Raxibacumab® from Human Genome Sciences Inc) (*270*) and Anthim (Elusys Therapeutics) bind to PA domain 4 with high affinity thus preventing PA interaction with the anthrax receptor. Decoys include peptides that mimic either regions of the receptor extracellular domain or fragments of PA domain 4. These act as competitive inhibitors and block toxin-receptor interactions. However, both these experimental approaches are protein therapeutics that are known in some cases to induce immune responses if these protein drugs aggregate prior to or

during administration, rendering the potential drugs ineffective. An alternative therapeutic option is to develop small molecule drugs to prevent/treat anthrax infection that can be administered orally and are easily absorbed within the blood stream. A HTS method to identify such small molecules targeting PA internalization has been reported (*271*). Another HTS assay uses Förster (Fluorescence) resonance energy transfer (FRET) to identify molecules that inhibit binding of PA to CMG2 (*272*). One target that has not been explored is to develop inhibitors that specifically target the PA prepore to pore conversion at both neutral and endosomal pH conditions.

In our case, the key issue in developing a unique anthrax toxin antimicrobial assay requires that one can detect the prepore to pore transition directly. Here the ability of GroEL to detect the prepore to pore transition of the anthrax PA shall be examined. Specifically, it shall also be determined if a GroEL binding signal to the transitioned PA pore can be used to potentially screen for inhibitors of bacterial toxin transitions. GroEL binding could thus be utilized as the basis for a HTS assay for rapidly screening novel antibacterials. This assay could also be used as a broad based platform to identify inhibitors for other bacterial toxins that demonstrate a typical soluble to membrane insertion transitions reactions (similar to the anthrax toxin prepore to pore transition). In the course of this study, it was found that although GroEL did not bind to the pore, fortuitously, the transition (from PA prepore to pore) itself could be followed using SPR and BLI label-free methods. It was also observed that the PA binding and transitioning reactions on the surface were similar to the ones occurring in the endosomal complex in real-time. One could therefore, potentially utilize this fortuitous observation to design an assay to screen for the transition inhibitors. This modified assay could also allow one to

rapidly search for novel small molecule ligands that prevent binding of the toxin to CMG2 as well as those that prevent binding of the LF to PA.

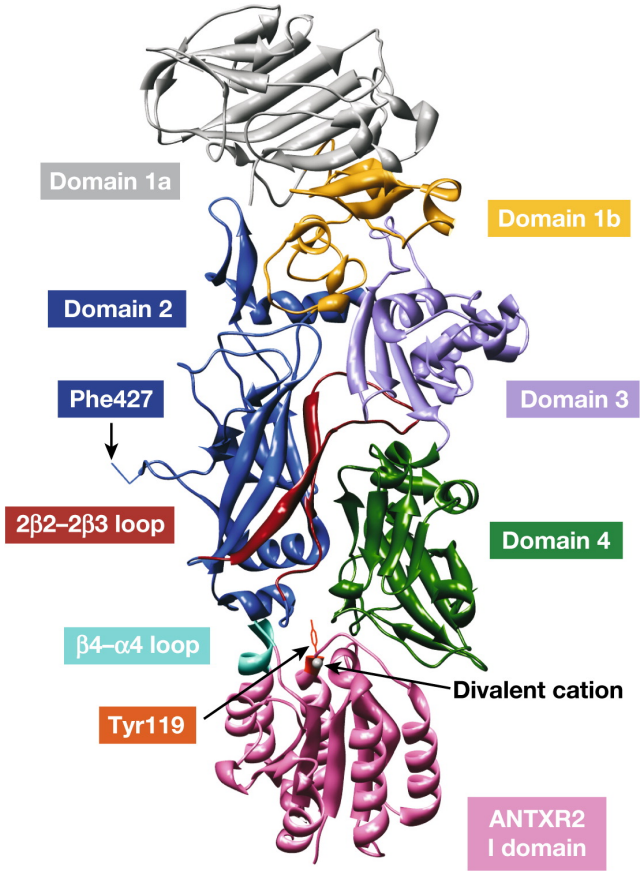

Figure 6.3: Structure of monomeric PA interacting with the anthrax receptor capillary morphogenesis gene 2 (CMG2) and showing various domains. Figure sourced from (*264*).

6.2 Materials and methods.

6.2.1 Materials.

The high affinity form of GroEL was purified in the lab using a published protocol (*134*). The SPR measurements were carried out on a commercially available CM5 chip (GE healthcare) using a Biacore 3000 (GE healthcare). CM5 is a general-purpose chip that is designed to allow

detailed quantitative interaction studies for analyzing interaction kinetics, affinity, concentration and binding between various biomolecules such as small organic molecules, proteins, lipids, carbohydrates, and nucleic acids. The BLI measurements were carried out on an Octet (multi-channel) or a BLItz (single-channel) instrument (ForteBio Inc.). PA, LF_N (A Cys mutant of N-terminal truncated lethal factor) and CMG2 were kind gifts from R. John Collier (Harvard). All other chemicals were of the highest purity and obtained from standard vendors.

6.2.2 Methods.

a Immobilization and specific orientation of the PA prepore state.

The immobilization of PA onto the biosensors for both BLI and SPR was achieved via non-covalent binding using a single cysteine containing LF_N E126C mutant that had been covalently linked to the biosensor. For both SPR and BLI, a thiol surface utilizing EDC/NHS and 2-(2-pyridinyldithio)ethaneamine hydrochloride (PDEA) (Figure 6.4) was initially generated. Briefly, EDC/NHS were mixed in a 1:1 ratio and allowed to incubate with the biosensor surface for 7 min. to activate the surface. PDEA dissolved in 0.1 M borate buffer (pH 8.3) was then allowed to interact with the activated surface for 5 min. to generate the activated thiol surface. The thiol surface was then incubated with 100 nM LF_N in 10mM acetate buffer to allow the cysteine linkage to occur. Excess reactive thiol linkages were then quenched using a solution of 50mM cysteine in a 1 M sodium chloride, 10 mM sodium acetate buffer. This protocol results in the formation of biosensors with immobilized LF_N. Increasing concentrations of PA were then incubated with the immobilized LF_N for 10 min (At this point the curve shows saturated response) to obtain the immobilized PA. The binding of PA to LF_N is high affinity binding with K_d of ~ 1 nM (*273*) and the off rate is negligible within the time-frame of the experiment, indicating that PA will most likely remain tightly bound to the sensor surface during the response

measurements. The immobilized PA biosensor was then utilized for further experiments. For obtaining a transitioned and immobilized PA pore, the previously generated biosensor was further treated with refolding buffer pH 6 for 5-10 min. to generate clean baseline controls.

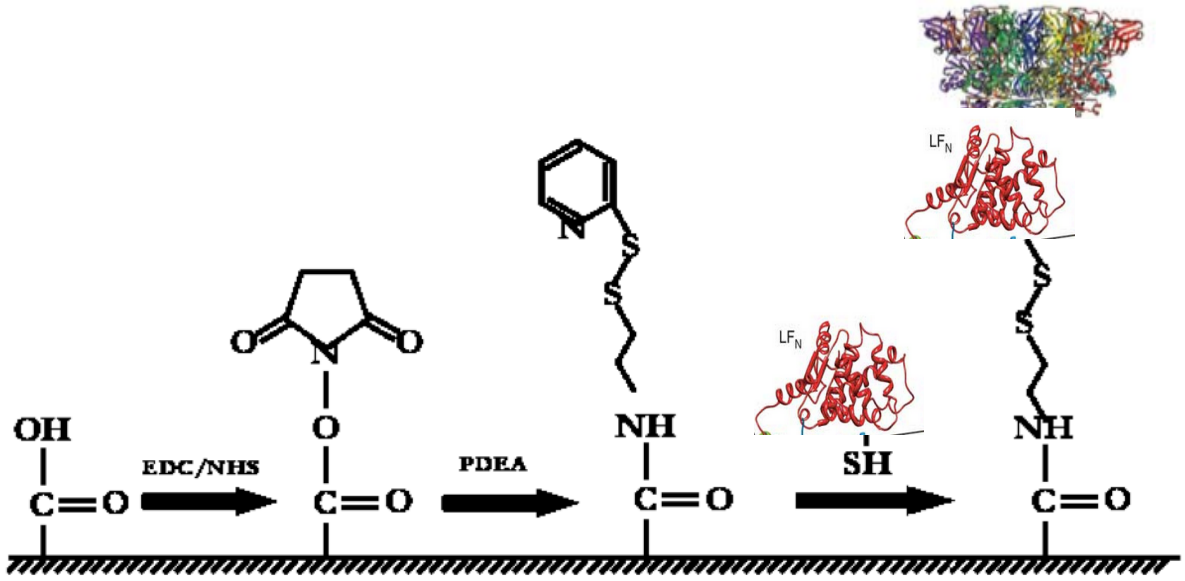

Figure 6.4: Immobilization of PA onto the sensor surface. EDC and NHS (1:1 ratio) were used to activate the sensor surface on the BLI tip or the SPR chip. This activated surface was then treated with PDEA to obtain a thiol-binding surface. A cysteine mutant of the N-terminal fragment of the Lethal factor (LF_N) could then be covalently attached to the sensor using thiol linkage. PA which binds to LF_N with nanomolar affinity was then immobilized through affinity linkage to the covalently LF_N to obtain the PA immobilized biosensors.

b Measuring the binding of GroEL to PA using BLI.

The binding of GroEL to PA pore was also investigated using BLI. PA prepore at a concentration of 20 µg/ml was immobilized onto the BLI sensor surface as described in section b above. The newly immobilized prepore was initially dipped into refolding buffer at pH 6.5 to

induce prepore to pore transitioning and obtain the pore form of the toxin. The immobilized PA pore was then incubated with 500nM GroEL in refolding buffer, pH 7.5 for 5 min. to record any possible association between GroEL and PA pore.

c Measuring the formation and the kinetics of the pore translocon using SPR.

The PA was immobilized by the method described previously in section b. All the studies were carried out at room temperature. The formation of the pore translocon was initiated by acidification of the immobilized PA. In SPR, this was carried out by flowing acidified buffers over the biosensor surface for 8 min. The experimental kinetic time course included a phase where the immobilized PA was incubated with refolding buffer of pH 6.5 or lower for 5 min. followed by increasing the pH back to 7.5 through incubation with pH 7.5 refolding buffer (50 mM TRIS, 50 mM KCl, 10 mM $MgCl_2$, 0.5 mM EDTA, pH 7.5) for 5 min. A flow rate of 5 µl/min for both the acidic buffer and refolding buffer was utilized for the SPR studies.

Since SPR signal traces are usually affected by changes in pH and buffer composition (bulk effects), the signal trace obtained during this study was due to an additive effect of the transitioning signal and the bulk effects signal. To obtain the transitioning signal alone, the solvent bulk effect signal (change in refractive index) was subtracted from the initially recorded signal. One way of recording the bulk effect contributions was to repeat the experiment with the same sensor surface and the same experimental parameters. In this case, since the PA has already undergone irreversible transitioning to the pore form, any further changes due to transitioning alone are not being observed. Any SPR signal changes would be the background signal that is solely due to the contributions of bulk effects and is predicted to be lower than the previously recorded signal trace. When such an experiment was carried out, it was observed that the change in amplitude was much lower than previously obtained with the PA prepore. In addition to this

change, no kinetic effects (slow transitions) were observed. The changes resemble step function responses. These repeated experiments with the same sensor containing the irreversible transitioned PA pore were designated as controls for the bulk effects. The control signal was subtracted from the previously obtained larger transition signal to obtain a signal trace that was solely due to PA transitioning. The studies were repeated twice for each pH. Since the transitioning was irreversible, a new immobilized PA chip had to be generated for each replicate.

d Measuring the formation and kinetics of the pore translocon using BLI.

The PA was initially immobilized on the BLI biosensor by the method described previously in section b. All studies were carried out at room temperature. The formation of the pore translocon was initiated by acidification of the immobilized PA. This was carried out by dipping the PA immobilized biosensor in an acidified refolding buffer (50 mM TRIS, 50 mM KCl, 10 mM $MgCl_2$, 0.5 mM EDTA, pH 7.0 or lower) for 5 min. This was followed by increasing the pH back to 7.5 through incubation with pH 7.5 refolding buffer (50 mM TRIS, 50 mM KCl, 10 mM $MgCl_2$, 0.5 mM EDTA, pH 7.5). The studies were repeated twice for each pH. Since the transitioning was irreversible, a new tip was generated for each replicate.

e Measuring the transitioning of the pore translocon in the presence of the receptor CMG2.

The PA was immobilized by the method described previously in section b. 500 nM of CMG2 was then injected and allowed to bind to the immobilized PA to obtain a saturated response. The formation of the pore translocon was initiated by acidification of the immobilized PA using an acidified refolding buffer (50 mM TRIS, 50 mM KCl, 10 mM MgCl2, 0.5 mM EDTA, pH 7.0 or lower) for 5 min. In BLI, this was carried out by dipping the PA immobilized biosensor in an acidic buffer, while in SPR, the acidic buffer was allowed to flow over the

biosensor surface for 8 min. This was followed by reexposing the biosensor surface (tip/chip) to a pH 7.5 refolding buffer to return to neutral pH. A flow rate of 5 µl/min for both the acidic refolding buffer and the neutral refolding buffer was utilized for the SPR studies. In SPR, care was taken to account for the bulk effect signal traces (signal change due to change in buffer composition and pH) as described in section c. All studies were carried out at room temperature and were repeated twice for both SPR and BLI.

f Electron microscopy.

The following section describes electron microscopy experiments that were performed by Dr. Narahari Akkaladevi. I provided Dr. Akkaladevi with the transitioned PA pore on the BLI biosensor tips. These BLI tips containing PDEA immobilized LF_N-PA prepore (incubated at 30 mM MES, 30 mM CHES, 30 mM phosphate buffer, pH 8.0) and pore complexes (incubated at 30 mM MES, 30 mM CHES, 30 mM phosphate buffer pH 5.0) were used as the source of the EM analysis. Briefly, the PA prepore or PA pore complexes were removed from the BLI tip by immersing the tip directly into a 2 µL solution of 50 mM DTT buffered at pH 8.0. The elution drops were spotted on a clear parafilm surface. Once the disulfide linked complexes were reduced and the pores or prepores were released from the tips, the 2 µL solution was wicked onto a carbon coated Cu 300 mesh EM grid (Electron Microscopy Science) that was glow discharged just before use.

Grids containing either untransitioned PA prepore and pH transitioned pore complexes were allowed to stand for 1 min. The grids were briefly dipped in three water droplets and subsequently negative stained using 1% methylamine tungstate in water (pH 7). Samples were viewed on a JEOL-1200 EXII Transmission Electron Microscope at 100 kV and images were recorded on film (Kodak SO163) by using a minimal-dose procedure at a defocus values

between 0.6–0.7 μm. The micrographs were digitized using a Microtek ScanMaker i900 scanner at a pixel size of 5.0 Å on the specimen.

In a second experiment, after pore formation on the BLI tip at pH 5.0, the pH was returned to pH 8.0 and followed by dipping the tip into a solution containing the micelle mixture (20 μM membrane scaffold protein, 1.3 mM POPC, 25 mM sodium cholate). Binding of the micelle to the transitioned pore was recorded and after removal from the tip, the newly formed LF_N-PA pore-micelle complexes were visualized using electron microscopy. Control experiments were done by dipping prepore containing BLI tip in to micelle mixture. It is important to note that once the prepore transitions to its pore state, this pore state does not revert to the prepore state.

6.3 Results and discussions.

6.3.1 Detecting PA transitions using GroEL binding (BLI format).

Label-free technologies had been previously utilized (Chapter 4 and 5) to decrease the aggregation of proteins prone to misfolding and measure its interaction with GroEL. Since PA exposes new hydrophobic regions that lead to aggregation, immobilizing PA on a solid surface is predicted to decrease aggregation. It was also decided to investigate the possibility of using GroEL binding as a detection signal for the prepore to pore transitions and associated conformation change. Based on a preferred immobilization of the prepore (transition perpendicular to biosensor surface) the transitioned pore form exposing hydrophobic residues was predicted to show GroEL binding while the non-transitioned form would not. To determine the feasibility of this hypothesis, the binding of GroEL to both the PA prepore as well as the pore translocon was studied utilizing BLI.

A crucial element for these experiments is to achieve a specific immobilization and orientation of the PA prepore on the sensor surfaces during these studies. This specific orientation was achieved by using a specific engineered cysteine containing N-terminal truncation domain of the lethal factor (E126C LF_N) (refer to section 6.2.2 a). LF_N was covalently attached on both SPR and BLI biosensor surfaces via a disulfide linkage to orientate the lethal factor so it can effectively bind to the prepore cap region, positioning the bound prepore on the biosensor surfaces. With this oriented set-up, the pore was predicted to interact with GroEL and show a higher binding signal as compared to the prepore. However, as observed in Figure 6.5, the transitioned PA pore did not show any binding (large positive deflection in GroEL binding signal) and there was little difference between the addition of GroEL to both the pore and the prepore. Usually GroEL binding results in a large upward positive deflection signal (anywhere from 0.5 to 4 nm phase shift).

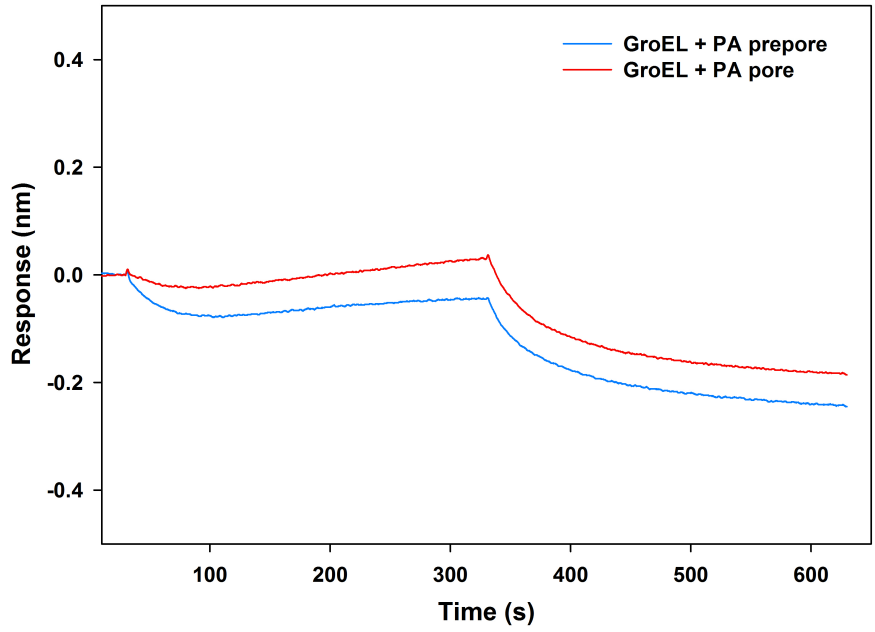

Figure 6.5: 500 nM GroEL was incubated with either the PA prepore (blue trace) or acid transitioned PA pore (red trace). It was expected that there would be a large

difference in amplitude between the two traces due to predicted GroEL binding to the PA pore. However, the kinetic traces do not demonstrate any large upward deflections that would indicate GroEL binding to either the PA pore or the prepore when PA was immobilized onto BLI biosensor tips.

Interestingly, before GroEL addition, the acidification treatments of the immobilized prepore consistently showed that there was an upward deflection in the sensorgram signal. Furthermore, these changes in the BLI and SPR signal trace remain at their elevated levels when the pH was returned to a neutral pH of 7.5 (Figure 6.6 A). These observed signal changes were not pH and buffer related as described in section 4.2.2 c. It can also be observed that this signal increase was specific in the case of PA immobilized sensor surface (Figure 6.6 A, B inset). Control experiments with the same buffer and using LF_N alone showed negligible changes in signal as compared to those observed without PA attached. Once the pore is formed, it no longer transitions back to its original prepore state. It is apparent that the acidification of the immobilized PA prepore leads to an irreversible conformational shift that results in an upward deflection in both SPR and BLI sensorgrams. It was therefore hypothesized that the increase in the SPR and BLI signals was associated with the PA prepore to pore conformational change.

There have been numerous instances where large-scale protein conformational changes have been observed using SPR (*274, 275*). SPR was previously utilized to observe large-scale conformational changes resulting from urea induced unfolding of immobilized luciferase, lysozyme and RNase proteins (*276, 277*) and DHFR (*278*). As discussed in chapter 5, the SPR signal is dependent on the refractive index in the immediate vicinity of the protein bound to the sensor surface. Large-scale protein unfolding leads to an exposure of buried hydrophobic residues. This leads to changes in the local water structure around the exposed hydrophobic sites,

thus affecting the refractive index. Here, PA prepore undergoes a large-scale conformational shift to the PA pore state leading to exposure of hydrophobic residues. This can lead to a large change in refractive index, which in turn would be reflected as a change in the SPR signal. These changes generate signals that are much lower than what is observed for the specific protein-protein interactions (e.g. LF_N-PA interactions).

BLI examines changes in thickness that consequently results in changes in the reflectance properties on the sensor surface relative to an internal reference reflectance layer. Any changes in the interference pattern results in a phase shift (Δ nm) and these changes can be followed in kinetic and quantitative modes. The PA prepore undergoes a major unfolding refolding transition (or in other words a conformational change) during acidification that results in the formation of a membrane insertable beta barreled pore. These large conformational rearrangements increase the length of the protein from 85 to 170 Å. For a PA immobilized on a BLI biosensor this would potentially result in a change in the reflective wave resulting in a phase shift in the interference pattern, leading to a signal increase. Thus, the PA transitioning leads to a change in the protein thickness and its change in hydrophobic character allows us to detect this transition using two different biophysical techniques. What makes this hypothesis more compelling is the prediction that the observed deflection in signal would not return to the original baseline position of the prepore state due to the prepore to pore transition being irreversible. Here the observed deflection was found to be irreversible in both the detection methods.

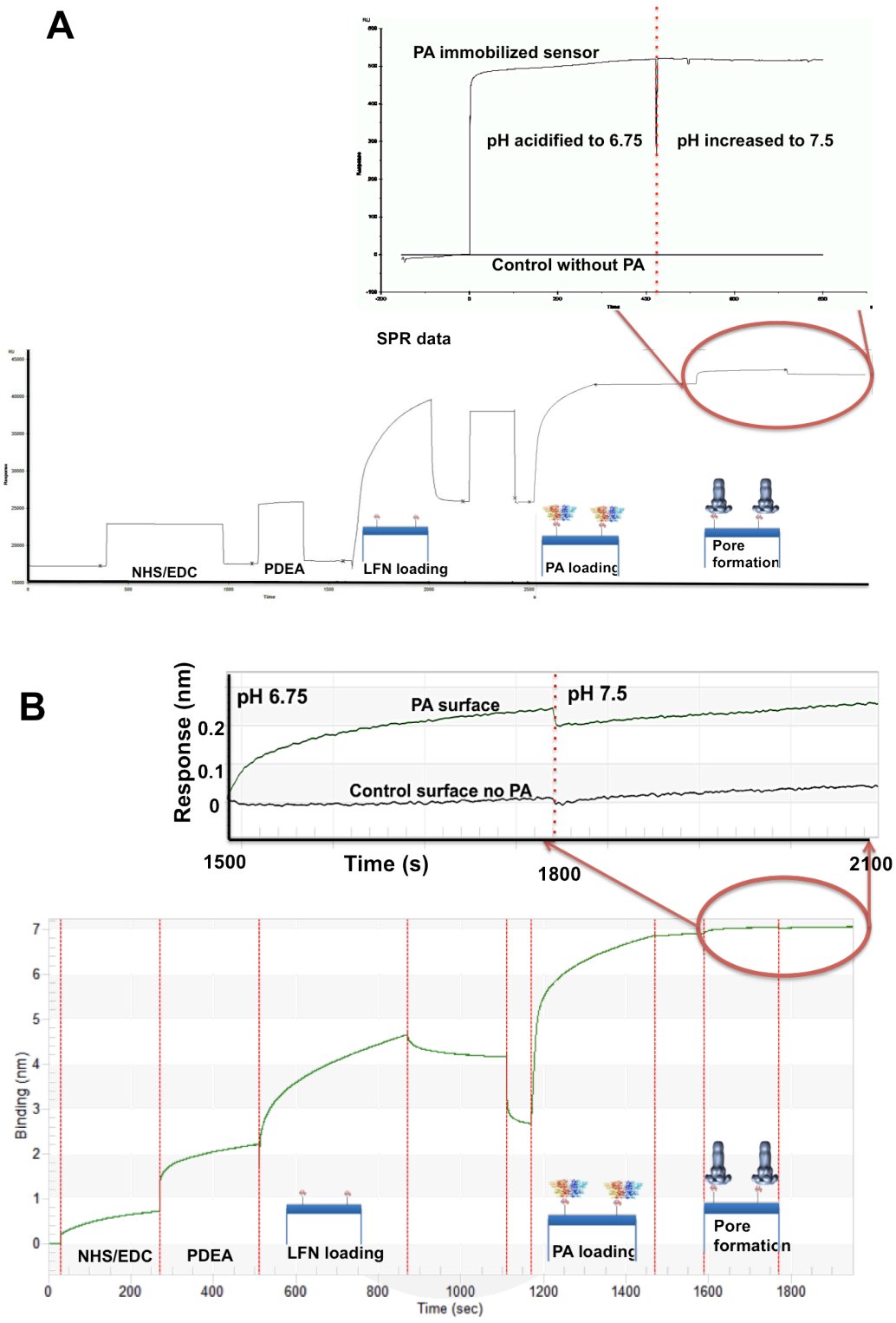

Figure 6.6: Increase in signal observed during pore formation with SPR (A) and BLI (B). To achieve a PA pore immobilized on the sensor surface the PA was immobilized through

LF_N and treated with an acidic buffer to induce transitioning. During this step, an increased signal was observed with both SPR (A) and BLI (B). It was observed that this signal was generated only with PA immobilized sensor surface. It was also observed that the signal did not go back to the baseline after the pH was increased back to 7.5 (A and B inset). This irreversible signal change coincides with an irreversible conformational change that occurs in PA during after acidification thus giving rise to the notion that PA prepore to pore conversion can be followed using BLI and SPR.

6.3.2 Monitoring PA conformational transitions using label-free methods:

The introduction of an acidic buffer (mimicking endosomal acidification) to the orientated prepore arrays on the biosensor results in a readily observable increase in signal in resonance units (SPR) and phase shifts (BLI) using both label-free instrument platforms (Figure 6.6 A, B). The specific affinity based immobilization that enables the 100Å PA pore beta barrel extension to occur in a direction pointing away from the biosensor surface (Figure 6.4) to generate an observable signal is an important aspect in these studies. Without this homogenous immobilization, the consistent small signal obtained during both the BLI and SPR studies may not have been observed.

The transitioning of PA from prepore to pore that occurs at acidic pH is apparently dependent on the protonation of histidine residues in the PA domain 2. The extent of unfolding and refolding of domain 2 could therefore be predicted to be dependent on the pH of the solution. To test this prediction, the PA prepore was immobilized on the sensor surface (both BLI and SPR) and incubated with buffer of varying acidic pH followed by incubating with a pH 7.5 buffer to increase the pH of the complex back to neutral pH. As predicted, in both SPR and BLI

label-free systems, the kinetics of the proposed pore transition was observed to depend on the pH of the final buffer. In Figure 6.7 B, pH transitions from 7.5 to 6.75 or 6.5 resulted in distinct and easily observable kinetic traces using BLI. A negative baseline drift was also observed with the control pH 7.5 buffer. As the acidic pH environments was decreased to pH 5.5 or pH 5.0, the kinetic traces corresponding to the pore transitions were more rapid. In some cases, the initial kinetics were too rapid to be followed by either label-free method. Curiously with SPR, a distinct and reproducible overshoot of the signal was observed as the pH of the flow buffer was decreased to 5.5 or 5.0. The PA prepore undergoes partial unfolding of the domain 2 loop under acidic conditions. This unfolded loop then undergoes refolding followed by folding into the beta barrel. It is not known if this initial unfolding and refolding event might be responsible for the overshoot signal.

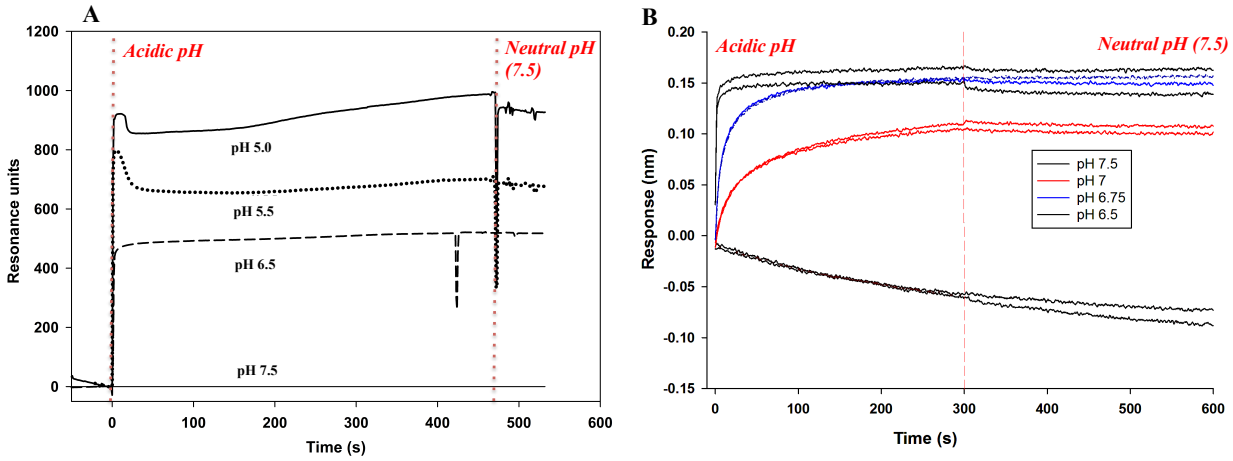

Figure 6.7: Following the PA prepore to pore transition in real time by SPR (A) and BLI (B). The PA was immobilized on the biosensors and initially treated with buffers of varying acidic pH followed by increasing the pH back to neutral. The transitioning of the prepore to pore was observed as a jump in signal. This change in signal was observed to

remain even after changing the buffer back to a neutral pH, indicating a non-reversible reaction occuring at the sensor interface. As the pH becomes more acidic, the transition occurs more rapidly thus confirming the real time observation of PA transitioning.

To further support our hypothesis that the observed increase in signal after pH change is due to the transitioning of PA from prepore to pore, the effect of PA concentration on the PA transition was examined. The SPR signal in this case is dependent on the exposed hydrophobic resdidues of the PA pore. Assuming that all the immobilized PA undergoes transitioning, it can be predicted that as the PA concentration increases the exposed hydrophobic surface will increase proportionally. This would in turn predictably lead to a SPR transitioning signal to increase proprtionally after transitioning to the immobilized PA concentration. To test this, increasing concentrations of the PA prepore (0-250 nM) were allowed to bind onto a fixed concentration of bound LF_N (100 nM). The increasing concentration of PA immobilized on the sensor surface results in an increase in the the observed sensorgram (Figure 6.8 A) (is linearly related to the pore transition signal (Figure 6.8 C) At the highest concentration used the response flattens out (Figure 6.8 B) consistant with the saturation of the PA that is affinity bound to the immobilized LF_N. Thus, as the LF_N-PA complex saturates, the transition response also shows a saturation. Thus the PA transition response was found to be a function of the concentration of the protein immobilized on the biosensor, further supporting the fact that one is observing the PA transition in real-time.

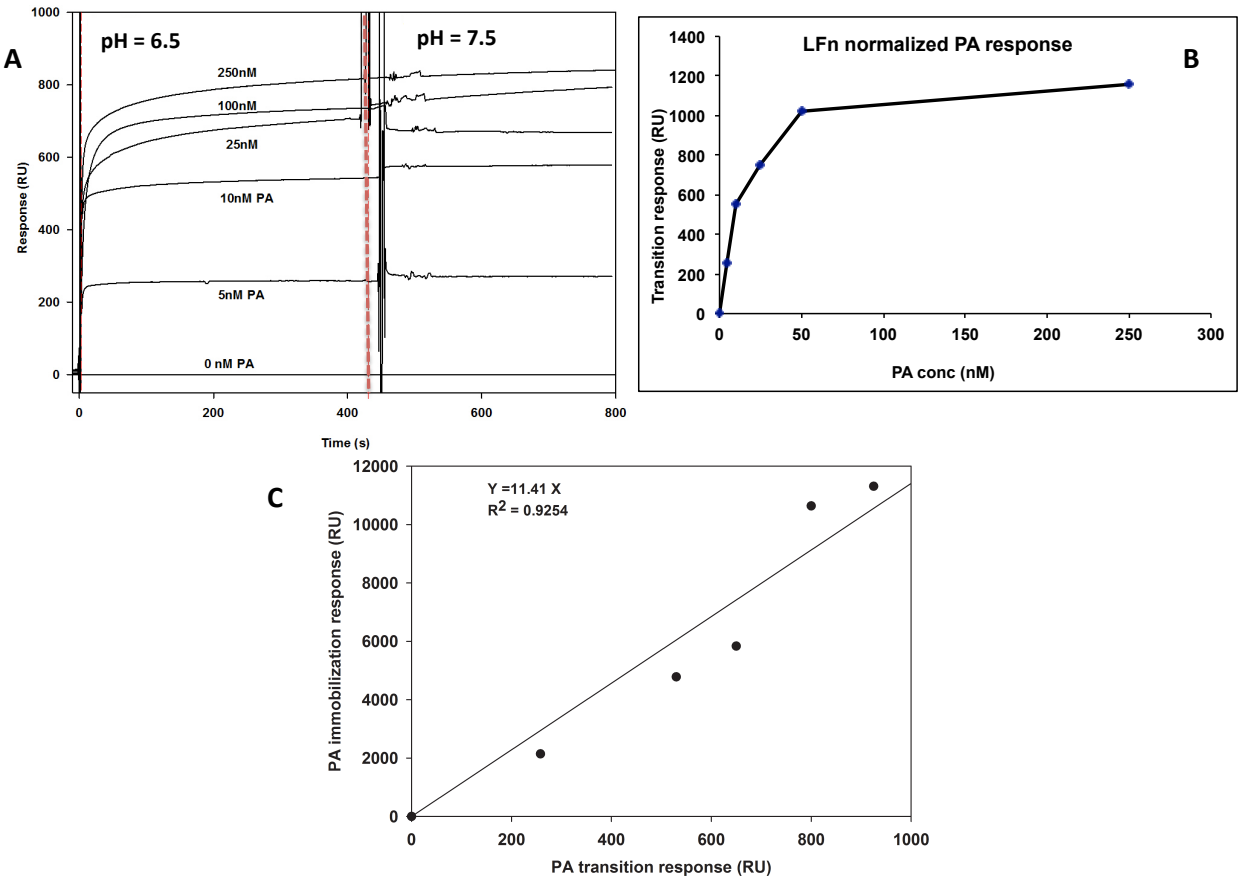

Figure 6.8: When an increasing concentration of immobilized PA prepore was treated with the acidic buffer, a linear correlation between the concentration of immobilized PA prepore on the sensor surface and the amplitude of transitioning was predicted (A, B). As predicted, the SPR derived signal amplitide of the conformational change of PA prepore to pore transition depends on the amount of the PA immobilized on the sensor surface as shown by the linear relationship between the PA loading response and PA binding amplitudes (C)

6.3.3 Visualization of the PA pore by electron microscopy

The most conclusive demonstration of observing the PA transitioning form prepore to pore is to examine these changes using electron microscopy. Previous experiments by Katayama *et al*., have demonstrated that PA pores could be easily observed using standard negative stained electron microscopy. Here the immobilized LF_N-PA prepore complex was generated on the tips as previously described. When the immobilized prepore was treated with pH 7.5 buffer, as expected, no increase in BLI signal was observed (Figure 6.9). This sample of PA was then released from the BLI biosensor tips using DTT. Since the LF_N-PA complex was immobilized on the sensor surface via a thiol linkage, one could easily break the linkage using a reducing agent such as 1 M DTT at pH 8.0. The higher pH value of the DTT was used to ensure that no PA prepore transitioned to pore during transfer onto the EM grid. The extracted samples were loaded onto an EM grid and the deposited protein was subjected to negative stain with methylamine tungsten. The stained grid was then observed with EM at 60,000X magnefication. The EM pictures show the presence of donut shaped structures that resemble the PA prepore. The PA prepore structure deposits onto EM grids in a facedown orientation and indicates that the PA prepore from the tip is indeed being observed.

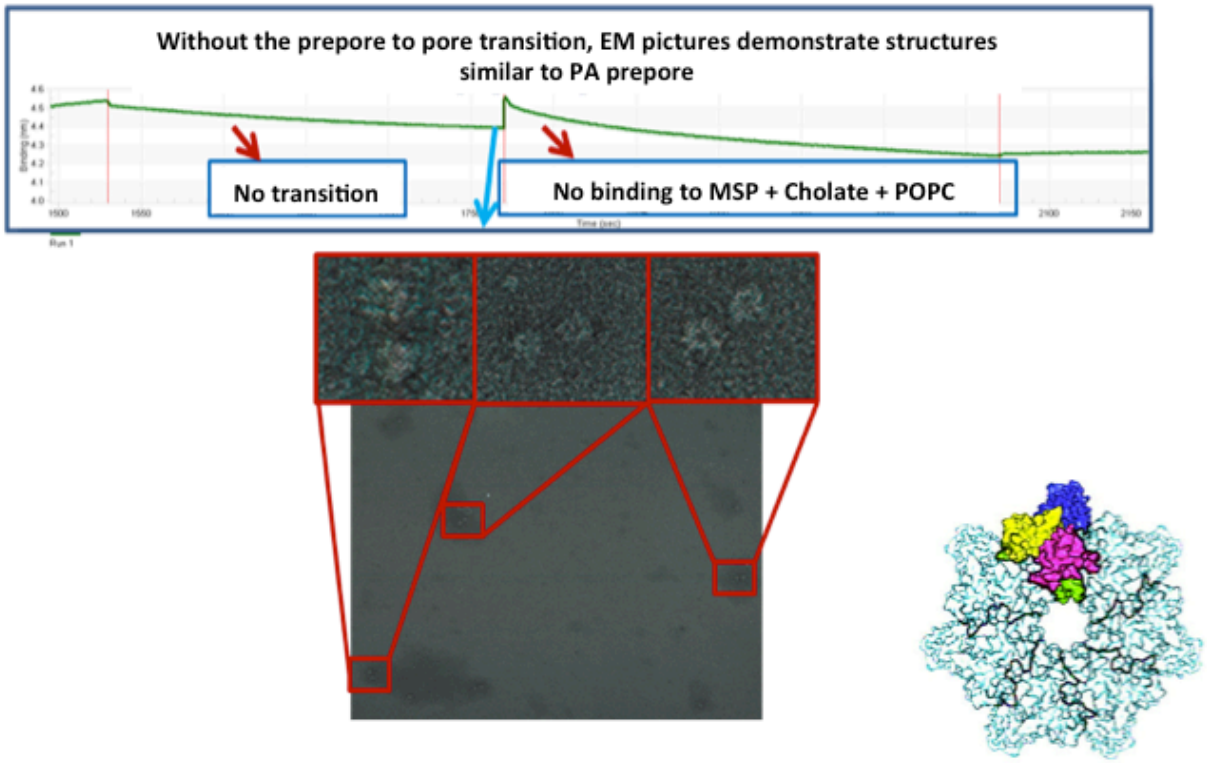

Figure 6.9: The immobilized PA prepore on the biosensors was treated with POPC micelles. The PA prepore was removed by using a reducing agent DTT, loaded onto an EM grid, negatively stained and observed at 60,000X magnification. Electromicrographs demonstrate that the immobilized PA prepore not treated with the acidic buffer does not show interactions with the micelle and under EM demonstrates a globular structure that closely resembles the prepore.

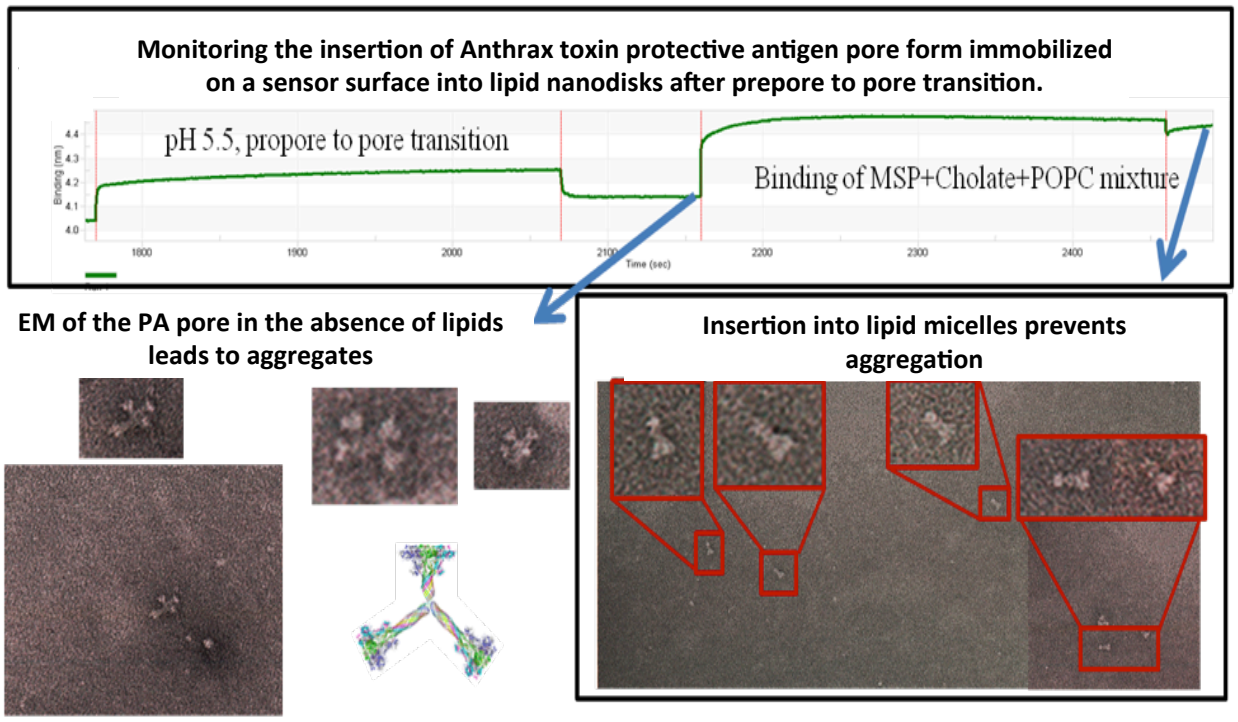

Figure 6.10: The immobilized PA pore on the biosensors was treated with POPC micelles following acidification. The PA was removed by using a reducing agent DTT, loaded onto an EM grid, negatively stained and obsevred at 60,000X magnification. On the left- hand side of the sensorgram, PA pores deposited on the EM grid showed that the pore had transitioned but these pores aggregated via their hydrophobic tips. On the right hand side, if the pore was transitioned and then POPC was added, the Electromicrographs demonstrate that the immobilized PA treated and transitioned with the acidified buffer binds to the POPC micelles and under EM shows a now solubilized conical pore structures that no longer aggregate and their structure are consistent with the transitioned micelle inserted PA pore structure

The immobilized LF_N-PA pore complex was generated on the tip by incubating the PA prepore with an acidified buffer (pH 5.5) followed by increasing the pH back to neutral (7.5). As

discussed previously, the increase in signal during acidification is presumed to occur due to the formation of the PA pore (Figure 6.10). However to confirm this observation, the acidified sample from the tip was extracted using 1 M DTT (pH 8.0) and observed under EM as described in the previous paragraph. These electron micrographs show the characteristic Y shaped features (Figure 6.10) of the PA pore lying on its side throughout the EM grid (*279*). This characteristic Y shape structural features shows both the cap and the extended beta barrel and are only observed when the anthrax toxin pore is present in its transitioned form (*251, 279*). The clumping of these Y shaped structures is due to a tendency of the PA pore to self aggregate through protein-protein interactions with the hydrophobic tip (*251*) (Figure 6.10B left EM panel). This aggregation tendency is usually reduced in the presence of a lipid environment. One method of generating such a lipid environment is through the use of lipid micelles. Here, it was predicted that one may even be able to monitor the pore insertion into the cholate-POPC-matrix scaffold protein micelles on BLI tip and this LF_N-PA pore-micelle complex could be visualized by negative stain electron microscopy (Figure 6.9). The slight decline in signal is apparently due to PA dissociating from LFn at pH 8.0. This dissociation is not observed when the buffer is maintained at pH 7.5. The PA immobilized on the BLI tip was allowed to incubate with these complex micelles before and after transitioning. Micelle binding was observed only when PA undergoes transition to its membrane insertable pore form (Figure 6.10 top panel). No binding was observed in the absence of a pore transition signal (Figure 6.9 top panel). The LF_N-PA pore-micelle complex was extracted, loaded onto an EM grid and negatively stained. The images indicate that micelle bound PA pore does not aggregate and rather than aggregating, the pore-micelle complex appears as individual soluble entities (compare left and right hand side attached EM micrographs in Figure 6.10). These EM images verified that the transitions observed on the BLI biosensor tips

are consistent with the prepore to pore transitions and provides conclusive evidence that one is indeed looking at the transitioning of PA in real-time on both BLI as well as by SPR measurements.

6.3.4 Investigating the effect of the anthrax receptor (ANTXR2/CMG2) binding on PA transitioning.

The PA transition was observed to occur as soon as the pH was slightly acidifed (Figure 6.7 B). Transitions near neutral pH have been previously observed both in lipid bilayers as well as in solution (*280, 281*), but as expected these transitions are slow and just a portion of the prepore population undergoes the transition. These slow transitions occur as histidine residues (pKa ~ 6.0) become protonated. Apparently, these histidines are not efficiently protonated at near neutral pH values. This low protonation population apparently leads to a slow transitioning to the PA pore state. However, *in vivo*, the transitioning does not occur until the endosome is acidified (*260*) to pH values around 5.5 to 5.0 that occur during late stage endosome maturation. The threshold for pore formation has also been observed to differ in kinetics depending on the type of receptor that the prepore binds to. For example, the PA prepore transitions to the pore at pH 6.2 when bound to a weaker binding ANTXR1 receptor whereas the transition occurs at a lower pH (pH 5.2) when the prepore is bound to the tighter binding ANTXR2 (CMG2) receptor. This change in the pH required for the pore formation is most likely due to the differences in the receptor prepore interaction of the domain 4 with the receptor. As the strength of the receptor binding interactions increase, this binding reaction in turn hinders the movement of the D2L2 loop (Figure 6.3), which is responsible for the unfolding and refolding into the beta barrel stem (*281*). For both the weak and strong binding receptors we predict that this binding interaction

stabilizes domain 2 against pH dependent unfolding, thereby inhibiting the PA prepore from transitioning to the pore at near neutral pH values (pH 6.5 and up).

Since the binding of CMG2 bound complex is more biologically relevent, the transitioning was studied in the presence of tighter binding soluble CMG2 (gift from J Collier). We predicted that the presence of the receptor should substantially inhibit the transitioning at near neutral pH values with either SPR and BLI platforms. Accordingly, PA was immobilized on the biosensor utilizing LF_N and then incubated with 500nM of the soluble CMG2 to form LFn-PA-CMG2 complex. The complex was observed to form easily and did not show any dissociation (Biosensogram data not shown). The lack of observable dissociation agrees with the extremely tight measured binding affinities of the CMG2/ANTXR2 interactions with the PA prepore (K_d ~ 170 pM ± 0.9 pM) (*282*). The LF_N-PA-CMG2 complex was initially generated on a BLI biosensor and then treated with buffers of various acidic pH to observe the effects on this complete complex on the PA pore transitions. As a control, a LF_N-PA complex without CMG2 was also treated with the acidified buffers and compared to the receptor PA complexes. As predicted, results indicate that the amplitude of signal associated with transitioning is almost completely inhibited that in the presence of the receptor CMG2 (Figure 6.11). This indicates that in the presence of CMG2, PA undergoes transitioning with a slower kinetics. This slow kinetics was observed with all pH values other than pH 5. At this pH, the transitioning trace shows a sharp increase followed by a rapid decrease in the signal amplitude.

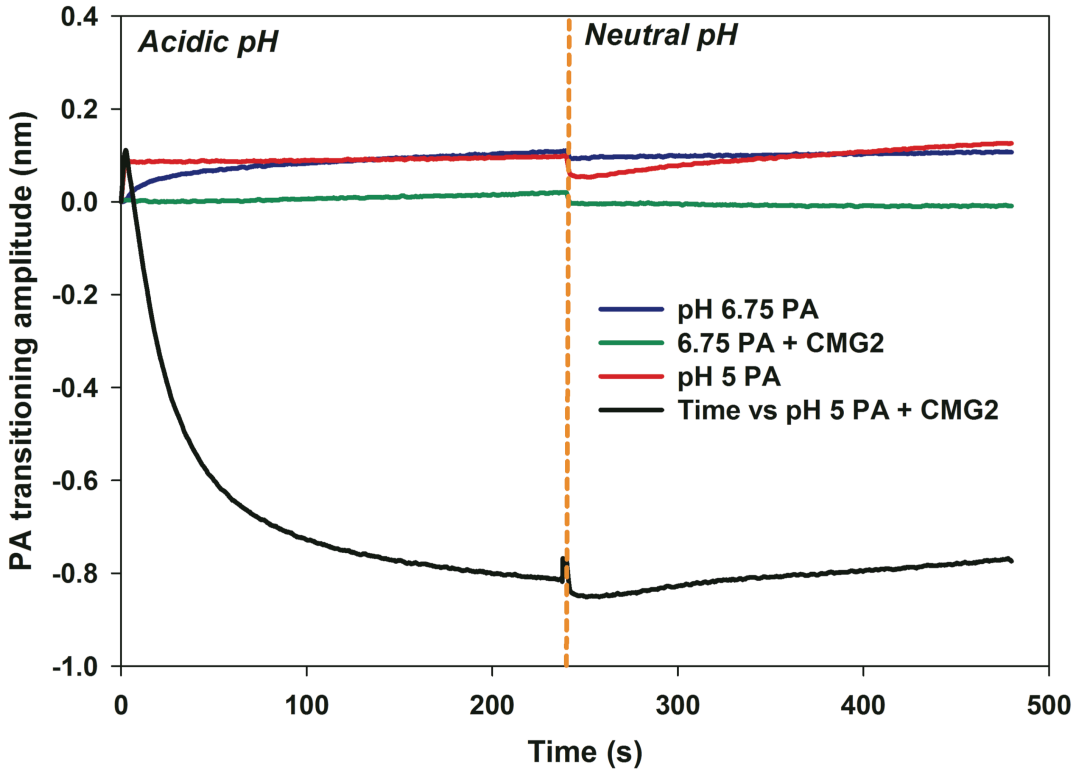

Figure 6.11: Effect of CMG2 on transition kinetics as observed with BLI. LF_N-PA-CMG2 complex was generated on the BLI biosensor and acidified to induce PA transitioning. In the presence of the receptor CMG2, the transitioning kinetics at pH 6.75 (green trace) were almost nonexistent as compared to the control without CMG2 (Bue trace). At pH 5 (endosomal pH), the transitioning shows a rapid increase indicating fast transitioning kinetics followed by a decrease in the signal (Black trace). This decreased signal in signal might be due to dissociation of CMG2 from the complex.

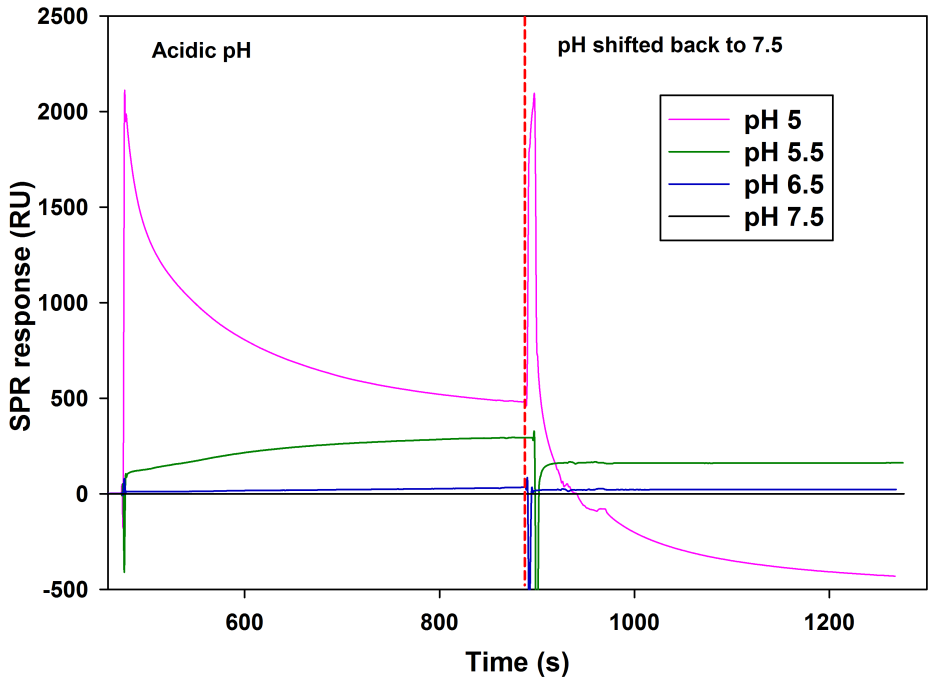

Figure 6.12: Effect of CMG2 on transition kinetics as observed with SPR. PA was immobilized onto the biosensors through affinity coupling with LF_N and susequently bound with 500 nM of the anthrax receptor CMG2. The complex was treated with buffers of varying acidic pH and followed by increasing the pH back to 7.5. The pH at which transition occurs was observed to decrease in the presence of the CMG2 receptor. At pH 6.5 (blue trace), the transitioning is negligible while at pH 5.5 (green trace), transition occurs at a slow rate. However at pH 5.0 (pink trace), the PA shows a large transitioning signal and rapid transitioning followed by a decrease in signal that is presumably due to receptor disscoiation from the PA pore.

Similar experiments were also carried out with SPR. Here it was observed that, with the LF_N-PA-CMG2 complex, the signal associated with pore transition at pH 6.5 was negligible (Figure 6.12 blue trace) as compared to previously observed signal amplitudes without the recptor (Figure 6.7 A). When the buffer was further acidified to a pH of 5.5, the amplitude of the

transition showed a slight increase with slow kinetics of transitioning. As observed with BLI, only when the pH was lowered to 5.0 does one observe a large change in the signal amplitude. The initially large upward deflection is presumably associated with extremely rapid transition kinetics. Again, as with the BLI signal at pH 5.0, the increase in the signal amplitude was followed by a decrease in signal. Since the receptor is known to dissociate from PA under endosomal acidification and the associated conformational change, the large decrease in signal appears to be consistent with the fact that the CMG2 soluble receptors undergo dissociation from the PA pore after the transition occurs at pH 5.0. This dramatic decrease in the signal is much larger than the pore transition signal amplitude. This large decrease in signal agrees with the increase in signal due to receptor binding to the PA prepore state (Figure 6.13).

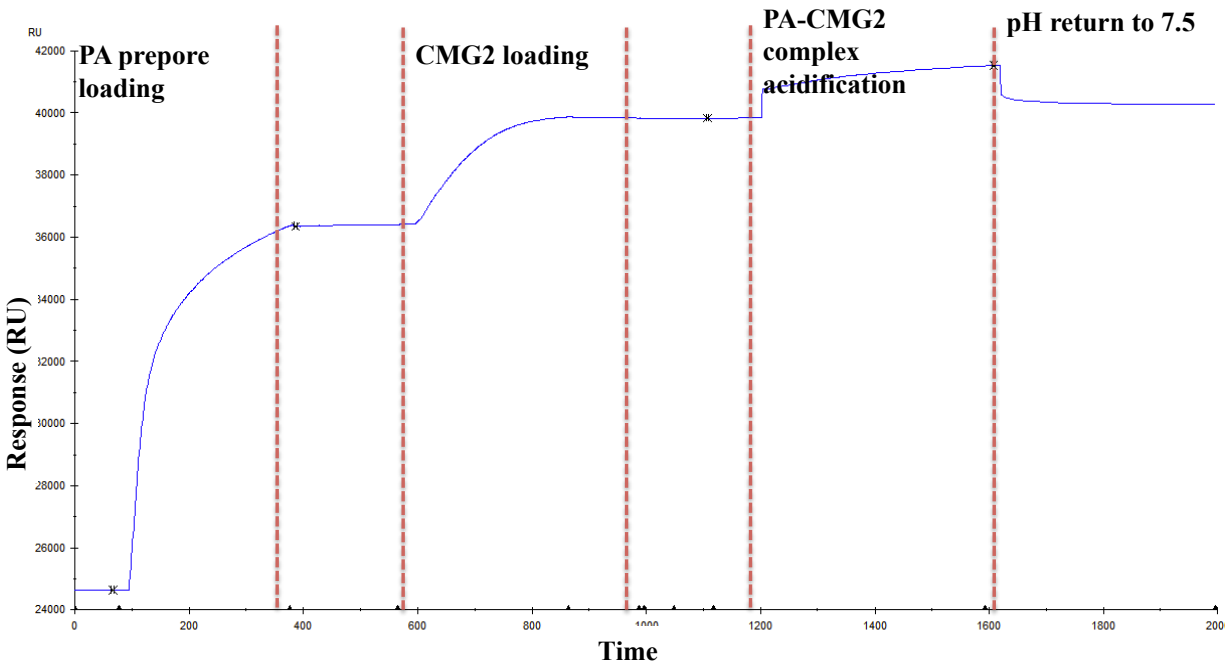

Figure 6.13: Loading curves for PA prepore and CMG2 followed by a slight to negligible transition at pH 5.9. This is confirmed by the return to the original CMG2 baseline

following the return to pH 7.5. The loading of CMG2 leads to a large increase in the SPR signal. This large increase in signal is only reversed during the dissociation of CMG2 that occurs after a pH 5.0 induced transitioning of PA prepore to pore as observed in Figure 6.12.

Ultimately, the ability to monitor the complete endosomal transition is useful if one wants to screen for global inhibitors of the pH induced endosomal transition. In addition to this transition, one may also be able to screen for small molecule inhibitor candidates that directly inhibit the binding of the receptor to the PA prepore. Thus, using these label-free BLI and SPR platforms allows one to effectively screen for inhibitors that target the PA-receptor complex itself as well as inhibitors of the pore transition in an endosomal environment (pH 5.5 to pH 5.0). This particular assay platform provides a very unique multiple targets to identify potential prophylactic agents that would bind to the PA prepore and prevent its transition to the pore in the absence and presence of the receptor. This is a truly novel screening method for potentially inhibiting anthrax pathogenesis at the molecular level under numerous conditions.

6.4 Conclusions.

As stated earlier, the purpose of these experiments was to determine if the chaperonin could be used to monitor a toxin soluble to membrane insertion transition. We suspect that we were unable to observe this transition because GroEL contains a ring of negative charge around the polypeptide binding site and preferentially interacts with the opposite face of the toxin (instead of the transitioned hydrophobic tip) (*251*). This orientation was observed in the initial EM micrographs of the GroEL-PA pore complexes. Even though this occurred in solution, we felt that this interaction between GroEL and the hydrophobic tip could be observed if the PA pore was initially immobilized. However, as was observed in solution, GroEL was unable to

interact with the exposed pore hydrophobic tip. Apparently, this accumulation of interior negative charge for the PA pore tip is vital to insuring the directional translocation of the other enzyme toxin components. However, it was found that the pH dependent conformational unfolding and refolding transition of the PA prepore to pore transition results in a large enough change in both the refractive index and change in protein thickness can be easily observed using SPR and BLI respectively. This transition nearly recapitulates what one would observe in the endosomal complex, because as in the endosome, the PA prepore is initially bound to the receptor and is orientated to form the beta barrel in a unidirectional manner to form a pore in the endosomal membrane allowing the other protein toxins to transit from the endosome to the cytoplasm. The platform that was constructed to observe this transition using the label-free methods also occurs from an immobilized and constrained orientation. The platform thus provides one with a novel and facile method to observe the transitioning of a bacterial toxin in real-time. This platform can be used to develop screens for small molecule inhibitors that prevent the both the binding of prepore to receptor complexes or prevent transitioning of bacterial toxins once the prepore is bound. Additionally, the ability to utilize at least two additional steps in the binding and transitioning cycle as potential targets, making this LF_N immobilization foundation a versatile platform for discovering novel small molecule antibacterials.

CHAPTER 7: SUMMARY AND FUTURE DIRECTIONS

Protein misfolding and aggregation caused by loss of cellular proteostasis capacity frequently leads to disease states. Such diseases are frequently termed protein misfolding diseases and are an important class of diseases that do not have a wide variety of treatment strategies. Using small molecule ligands that stabilize the native state of the protein that tends to undergo misfolding is a facile way to increase ER processing and cellular expression of that protein. We have discussed the various methods utilized to search for such pharmacological chaperones and realized that there is a need for an assay methodology to rapidly screen the huge chemical libraries that have been generated through combinatorial chemistry.

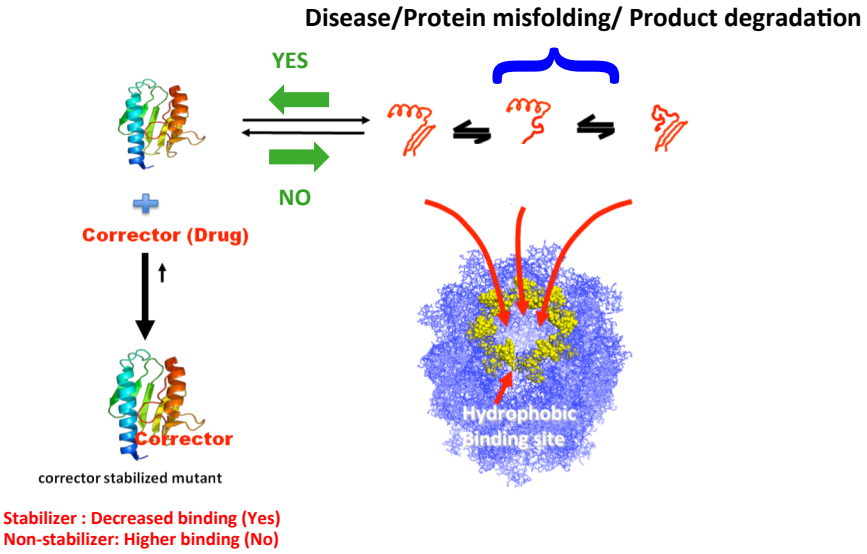

Figure 7.1: The disease proteins have a wide variety of conformational states (or in other words are moving targets) which the chaperonin can easily bind to and could be used to rapidly identify small molecule stabilizer compounds.

In this dissertation, experimental support is provided for the hypothesis that the high affinity nucleotide free form of the GroEL chaperonin can be used to detect partially folded proteins of virtually any protein that transitions to a partially folded hydrophobic form. The natural affinity of the chaperonin for partially folded proteins was utilized to rapidly sequester partially folded species (Figure 7.1). The chaperonin was thus successfully utilized to develop an assay platform to probe the folding state of a protein and also utilize the assay to screen chemical libraries for stabilizers of proteins prone to misfolding. It was also demonstrated that the kinetics of protein unfolding could be easily manipulated utilizing denaturants to increase the rate of formation of the transient unstable species. The fact that the chaperonin binds to these partially unfolded species as soon as they are formed drastically decreases the assay time thus giving an advantage over any other existing assay methodology. Instead of hours necessary for waiting for the emergence of aggregated species, one can determine the formation of preaggregates in less than an hour and for certain proteins such as CFTR in less than a minute (Figure 7.2). This decrease in time required to interrogate the folding state of a protein is an advantage as it allows one to carry out several such assays in a day. Additionally, one could also easily scale-up the assay to an HTS format that could potentially be utilized with existing HTS robotics to screen thousands of compounds per day. Initially, small scale studies were carried out using bead-based immobilized chaperonin in microtubes and utilized centrifugal separation to separate the partitioned protein from stable folded species. Through these experiments, proof-of-principle with several proteins including CFTR NBD1, DHFR, MDH, and frataxin was demonstrated. It was also demonstrated that the chaperonin has the potential to readily detect the kinetically transient partially folded states of any protein.

The bead-based nature of the assay however, made the HTS format slightly cumbersome. This is because most of the existing HTS instrumentation is not geared towards use of beads, thus leading to blockage of liquid handling and dispensing systems. Also, the bead separation required for protein assays introduced additional steps into the assay increasing the turnaround time and associated cost/assay. Another factor was the decrease in binding of partially folded proteins to the bead-based system leading to the false positive result of a decrease in partitioning onto GroEL because of increases in substrate protein self-association (blocking potential chaperonin binding sites) and larger aggregation. Aggregated proteins (dimers or higher oligomers) do not easily bind to the chaperonin. All these factors made it necessary to look for other detection platforms to take advantage of the unique binding and capture properties of the chaperonin that could be miniaturized and would be easy to use while retaining its advantages.

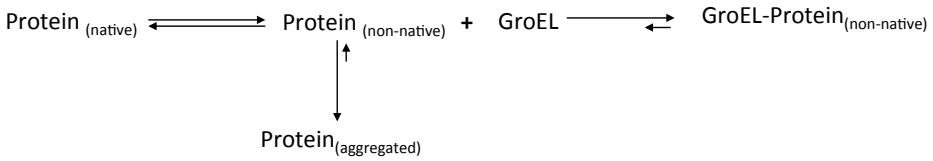

Figure 7.2: The protein exists in a dynamic equilibrium between its natively folded and the unfolded non-native form. This non-native unfolded protein might undergo aggregation. However, the chaperonin binds to partially folded species thus decreasing aggregation.

One way of preventing aggregation of substrate protein is to immobilize them to decrease intermolecular interactions. Such immobilization was the advantageous pre**requisite** for studying chaperonin protein substrate interactions via label-free interaction techniques such as SPR (*283*) and BLI. Since, chaperonin binding to protein substrates generated large signals, we were able to

successfully demonstrate that label-free methods can be utilized to observe the chaperonin interacting with partially unfolded species, and to demonstrate that ligand stabilization decreases chaperonin interactions. These methods are far superior to our bead-based plate based systems because they 1) utilize low concentrations of the substrate protein and 2) allow one the ability to observe interactions in real-time. It was observed that the assay could be carried out with a higher throughput utilizing BLI systems such as the ForteBio Inc. Octet system as compared to SPR Biacore 3000. Additionally, the BLI system decreases the total length of the assay and has a very high turnaround time. This in combination with the fact that BLI can be utilized with existing robotic HTS set-up gives one a medium throughput assay that can screen tens of thousands of compounds per week. Since the immobilization of the substrate/chaperonin onto the BLI biosensors is the step that takes the most time during the assay, one could carry out these preparations offline to generate biosensors that could then be utilized to carry out the assay in a high throughput manner.

The broad based binding affinity of a chaperonin platform system should allow us to rapidly identify potential pharmacological chaperones that display various modes of stabilization and to validate candidates generated through *in silico* computer docking programs. It is highly conceivable for example, that one does not have to be constrained with identifying potential small molecule pharmacological chaperones that only bind to protein active sites to stabilize the protein. The chaperonin detection system can potentially identify small molecule stabilizers that bind transiently at distant sites (resembling allosteric modulators) that facilitate specific folding nucleation events or stabilize dimer interfaces.

Apart from its use as a rapid assay platform to screen for pharmacological chaperones, the chaperonin assay can also be used for other applications. One such application is the

utilization to follow the transitioning of bacterial toxins *in vitro*. The proof-of-principle experiments with the anthrax pore translocon demonstrated in chapter 6 that one could utilize BLI to follow the conformational change of the anthrax prepore to the membrane insertable pore translocon (which is responsible for the disease) in real-time. This gives one a novel method to screen for inhibitors of other similar bacterial toxin transitions that are characterized by conformational changes. The immobilization of the toxin prevents their aggregation, which is a major hindrance to carry out solution based studies. Here, one can easily search for small molecules that prevent the transitioning, without worrying about the aggregation of the proteins. Additionally, this method also gives one a way to disrupt toxin-cellular receptor complexes. One can easily follow receptor – toxin interaction utilizing both SPR and BLI (as demonstrated in chapter 6). Thus, it would be possible to potentially search for inhibitors for small molecules that are potential antimicrobial compounds.

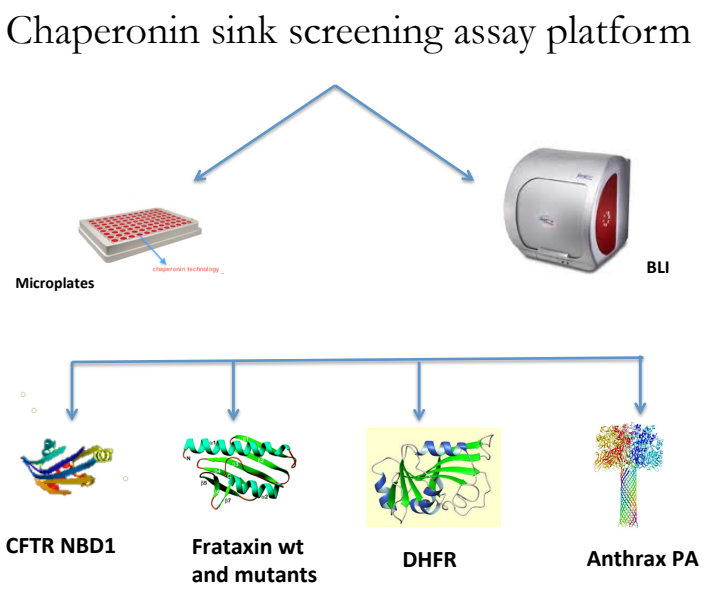

Figure 7.3: The chaperonin sink platform has been developed and validated both in bead based form and with label free techniques to search for stabilizers for a wide range of proteins.

Thus during the course of this dissertation, I have

1. Developed a novel screening system for stabilizing misfolding proteins utilizing the ability of GroEL to distinguish between folded and partially folded proteins
2. Demonstrated that GroEL can be utilized to distinguish between proteins with similar chemical/thermal stabilities but varying kinetic stabilities
3. Demonstrated that different mutants of the same proteins might need different stabilizers
4. Demonstrated that one can follow the transition kinetics of the anthrax PA prepore to pore transitions in an endosome like environment (pH drop of 7 to 5), allowing one to screen for new and novel antibacterials (*284*)

However, as shown in Figure 7.4, the applications developed so far are just the tip of the chaperonin platform iceberg. The chaperonin can be thought of as a promiscuous antibody towards all partially folded proteins, allowing for the development of a versatile system to study a wide range of protein misfolding diseases. Examples of proteins that can be examined in the near future include ß-microglobulin (that causes dialysis related amyloidosis) and α-synuclein (responsible for Parkinson's disease). Such studies should potentially provide possible lead molecules for treating these misfolding diseases. It is also probable that the assay would be useful in evaluating the stabilities of oligomeric proteins or intrinsically stable therapeutic proteins.

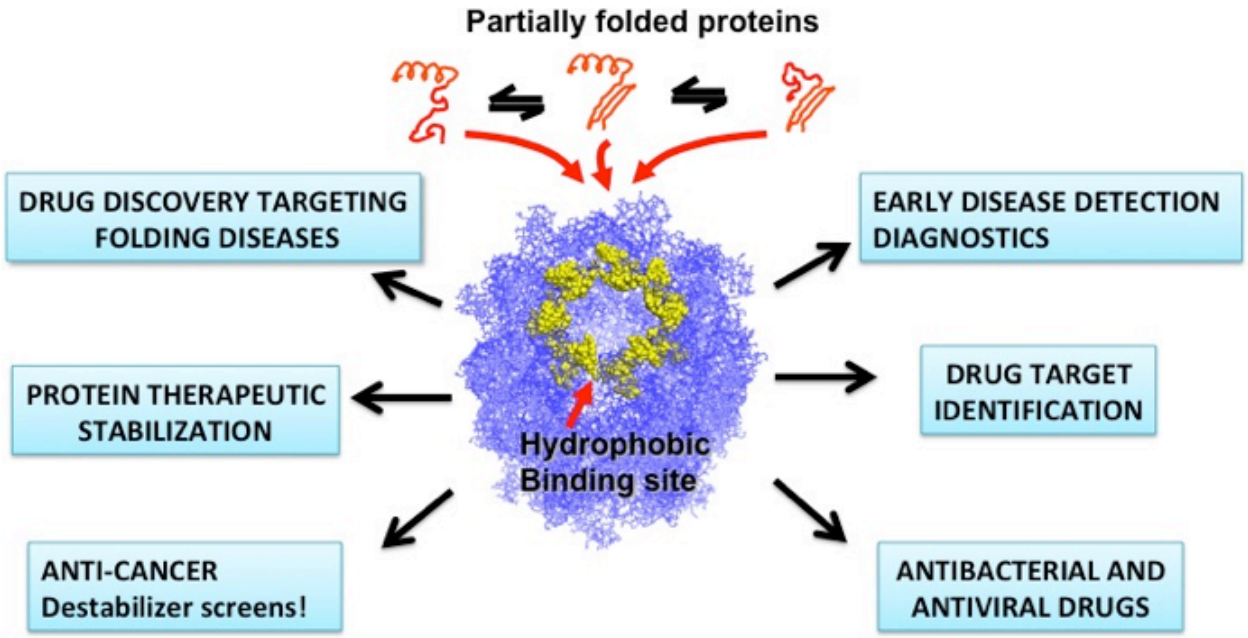

Figure 7.4: Potential unexplored uses of the chaperonin assay make it a versatile platform. Apart from being used to search for novel chemical chaperones, the assay can also b used to search for therapeutic antibody stabilizers. The platform has the potential of being developed to be used in detection of diagnostics, drug targets, novel anti-cancer agents and anti-bacterials.

The chaperonin sink assay platform can also be used to search for stabilizers for proteins that are usually stable but undergo aggregation over a long time. Such proteins include therapeutic antibodies that need to be highly pure and are administered as a concentrated bolus. The emergence of aggregates not only decreases the shelf life of protein pharmaceuticals but might also lead to immune responses. Such proteins usually do not show the emergence of dimers/multimers unless stress tested. These stress tests and formulation analysis requires lengthy HPLC studies to identify their presence. Preliminary experiments that were run at ForteBio Inc. under my direction (but not included in this thesis) indicated that it is feasible to utilize the chaperonin assay to rapidly detect (within 1-5 min) preaggregation species of IgG

proteins prior to their large-scale aggregation. Additionally, it was also shown that relatively stable proteins can be momentarily destabilized utilizing denaturants such as urea or guanidium hydrochloride in a novel application of the chaperonin assay (Denaturant dip and read BLI platform) (*284*). This assay can detect the kinetic differences of unfolding in the absence and presence of a potential stabilizer. One can also envision utilizing the assay in conjunction with other chaperone proteins such as the oligomeric Hsp100 class. This chaperone could be useful in detecting small aggregates or preaggregates of proteins. Hsp100 chaperones act on aggregated proteins as disaggregates and transfer them to the proteasome or another chaperone system such as the Hsp70/90 classes. If one has a relay system of Hsp100 with GroEL, aggregated proteins/inclusion bodies could potentially be used instead of purified folded proteins. Here the Hsp100 unfolded protein binds to GroEL in absence of a stabilizer but undergoes folding in the presence of a stabilizer.

The chaperonin assay can also potentially be utilized with Hsp90 to search for novel anti-cancer agents. Hsp90 is a target for anti-cancer agents as it stabilizes oncogenic proteins and prevents them from being degraded. It may be possible to utilize the chaperone detection assays with Hsp90 instead of GroEL to follow the Hsp90 interaction with oncoproteins / model substrates and search for Hsp90 inhibitors. The use of chaperones to detect conformation states of protein in solution can potentially yield a broad based versatile platform to probe the states of the protein fold in real-time.

REFERENCES

1. Pauling, L., Corey, R. B., and Branson, H. R. (1951) The structure of proteins; two hydrogen-bonded helical configurations of the polypeptide chain, *Proc. Natl. Acad. Sci. U. S. A. 37*, 205-211.
2. Anfinsen, C. B. (1973) Principles that govern the folding of protein chains, *Science 181*, 223-230.
3. Flory, P. J. (1969) *Statistical mechanics of chain molecules*, Interscience Publishers, New York,.
4. Tanford, C. (1968) Protein denaturation, *Adv. Protein Chem. 23*, 121-282.
5. Eaton, W. A., Munoz, V., Thompson, P. A., Chan, C. K., and Hofrichter, J. (1997) Submillisecond kinetics of protein folding, *Curr. Opin. Struct. Biol. 7*, 10-14.
6. Levinthal, C. (1968) Are there pathways for protein folding?, *Journal de Chimie Physique 65*, 44-45.
7. Zwanzig, R., Szabo, A., and Bagchi, B. (1992) Levinthal's paradox, *Proc. Natl. Acad. Sci. U. S. A. 89*, 20-22.
8. Wetlaufer, D. B. (1973) Nucleation, rapid folding, and globular intrachain regions in proteins, *Proc. Natl. Acad. Sci. U. S. A. 70*, 697-701.
9. Dill, K. A. (1985) Theory for the folding and stability of globular proteins, *Biochemistry (Mosc). 24*, 1501-1509.
10. Dill, K. A., and Chan, H. S. (1997) From Levinthal to pathways to funnels, *Nat. Struct. Biol. 4*, 10-19.

11. Frauenfelder, H., Sligar, S. G., and Wolynes, P. G. (1991) The energy landscapes and motions of proteins, *Science 254*, 1598-1603.

12. Englander, S. W. (2000) Protein folding intermediates and pathways studied by hydrogen exchange, *Annu. Rev. Biophys. Biomol. Struct. 29*, 213-238.

13. Balch, W. E., Morimoto, R. I., Dillin, A., and Kelly, J. W. (2008) Adapting proteostasis for disease intervention, *Science 319*, 916-919.

14. Gidalevitz, T., Kikis, E. A., and Morimoto, R. I. (2010) A cellular perspective on conformational disease: the role of genetic background and proteostasis networks, *Curr. Opin. Struct. Biol. 20*, 23-32.

15. Powers, E. T., Morimoto, R. I., Dillin, A., Kelly, J. W., and Balch, W. E. (2009) Biological and chemical approaches to diseases of proteostasis deficiency, *Annu. Rev. Biochem. 78*, 959-991.

16. Thirumalai, D., and Reddy, G. (2011) Protein thermodynamics: Are native proteins metastable?, *Nat Chem 3*, 910-911.

17. Bernado, P., and Blackledge, M. (2010) Structural biology: Proteins in dynamic equilibrium, *Nature 468*, 1046-1048.

18. Hutt, D. M., Powers, E. T., and Balch, W. E. (2009) The proteostasis boundary in misfolding diseases of membrane traffic, *FEBS Lett. 583*, 2639-2646.

19. Frydman, J. (2001) Folding of newly translated proteins in vivo: the role of molecular chaperones, *Annu. Rev. Biochem. 70*, 603-647.

20. Nishimura, C., Uversky, V. N., and Fink, A. L. (2001) Effect of salts on the stability and folding of staphylococcal nuclease, *Biochemistry (Mosc). 40*, 2113-2128.

21. Russo, A. T., Rosgen, J., and Bolen, D. W. (2003) Osmolyte effects on kinetics of FKBP12 C22A folding coupled with prolyl isomerization, *J. Mol. Biol. 330*, 851-866.

22. Richter, K., Haslbeck, M., and Buchner, J. (2010) The heat shock response: life on the verge of death, *Mol. Cell 40*, 253-266.

23. Lorimer, G. H. (2001) A personal account of chaperonin history, *Plant Physiol. 125*, 38-41.

24. Ellis, J. (1987) Proteins as molecular chaperones, *Nature 328*, 378-379.

25. Sauer, F. G., Knight, S. D., Waksman, Gj, and Hultgren, S. J. (2000) PapD-like chaperones and pilus biogenesis, *Semin. Cell Dev. Biol. 11*, 27-34.

26. Zahn, R., Perrett, S., and Fersht, A. R. (1996) Conformational states bound by the molecular chaperones GroEL and secB: a hidden unfolding (annealing) activity, *J. Mol. Biol. 261*, 43-61.

27. Shtilerman, M., Lorimer, G. H., and Englander, S. W. (1999) Chaperonin function: folding by forced unfolding, *Science 284*, 822-825.

28. Saibil, H. (2000) Molecular chaperones: containers and surfaces for folding, stabilising or unfolding proteins, *Curr. Opin. Struct. Biol. 10*, 251-258.

29. Fisher, M. T. (2006) Molecular roles of chaperones in assisted folding and assembly of proteins, *Genet. Eng. (N. Y). 27*, 191-229.

30. Weber-Ban, E. U., Reid, B. G., Miranker, A. D., and Horwich, A. L. (1999) Global unfolding of a substrate protein by the Hsp100 chaperone ClpA, *Nature 401*, 90-93.

31. Morimoto, R. I. (2008) Proteotoxic stress and inducible chaperone networks in neurodegenerative disease and aging, *Genes Dev. 22*, 1427-1438.

32. Akerfelt, M., Morimoto, R. I., and Sistonen, L. (2010) Heat shock factors: integrators of cell stress, development and lifespan, *Nat Rev Mol Cell Biol 11*, 545-555.

33. Sorger, P. K., and Nelson, H. C. (1989) Trimerization of a yeast transcriptional activator via a coiled-coil motif, *Cell 59*, 807-813.

34. Baler, R., Dahl, G., and Voellmy, R. (1993) Activation of human heat shock genes is accompanied by oligomerization, modification, and rapid translocation of heat shock transcription factor HSF1, *Mol. Cell. Biol. 13*, 2486-2496.

35. Abravaya, K., Phillips, B., and Morimoto, R. I. (1991) Attenuation of the heat shock response in HeLa cells is mediated by the release of bound heat shock transcription factor and is modulated by changes in growth and in heat shock temperatures, *Genes Dev. 5*, 2117-2127.

36. Gasch, A. P., Spellman, P. T., Kao, C. M., Carmel-Harel, O., Eisen, M. B., Storz, G., Botstein, D., and Brown, P. O. (2000) Genomic expression programs in the response of yeast cells to environmental changes, *Mol. Biol. Cell 11*, 4241-4257.

37. Hardy, S. J., and Randall, L. L. (1991) A kinetic partitioning model of selective binding of nonnative proteins by the bacterial chaperone SecB, *Science 251*, 439-443.

38. Hardy, S. J., and Randall, L. L. (1993) Recognition of ligands by SecB, a molecular chaperone involved in bacterial protein export, *Philos. Trans. R. Soc. Lond. B. Biol. Sci. 339*, 343-352; discussion 352-344.

39. Bhushan, S., Gartmann, M., Halic, M., Armache, J. P., Jarasch, A., Mielke, T., Berninghausen, O., Wilson, D. N., and Beckmann, R. (2010) alpha-Helical nascent polypeptide chains visualized within distinct regions of the ribosomal exit tunnel, *Nat Struct Mol Biol 17*, 313-317.

40. Rospert, S., Dubaquie, Y., and Gautschi, M. (2002) Nascent-polypeptide-associated complex, *Cell. Mol. Life Sci. 59*, 1632-1639.

41. Gautschi, M., Mun, A., Ross, S., and Rospert, S. (2002) A functional chaperone triad on the yeast ribosome, *Proc. Natl. Acad. Sci. U. S. A. 99*, 4209-4214.

42. Scholz, C., Stoller, G., Zarnt, T., Fischer, G., and Schmid, F. X. (1997) Cooperation of enzymatic and chaperone functions of trigger factor in the catalysis of protein folding, *EMBO J. 16*, 54-58.

43. Ghaemmaghami, S., Huh, W. K., Bower, K., Howson, R. W., Belle, A., Dephoure, N., O'Shea, E. K., and Weissman, J. S. (2003) Global analysis of protein expression in yeast, *Nature 425*, 737-741.

44. Blobel, G., and Dobberstein, B. (1975) Transfer of proteins across membranes. I. Presence of proteolytically processed and unprocessed nascent immunoglobulin light chains on membrane-bound ribosomes of murine myeloma, *J. Cell Biol. 67*, 835-851.

45. Walter, P., and Blobel, G. (1980) Purification of a membrane-associated protein complex required for protein translocation across the endoplasmic reticulum, *Proc. Natl. Acad. Sci. U. S. A. 77*, 7112-7116.

46. Mitra, K., Schaffitzel, C., Shaikh, T., Tama, F., Jenni, S., Brooks, C. L., 3rd, Ban, N., and Frank, J. (2005) Structure of the E. coli protein-conducting channel bound to a translating ribosome, *Nature 438*, 318-324.

47. Csermely, P., Miyata, Y., Soti, C., and Yahara, I. (1997) Binding affinity of proteins to hsp90 correlates with both hydrophobicity and positive charges. A surface plasmon resonance study, *Life Sci. 61*, 411-418.

48. Zolkiewski, M., Zhang, T., and Nagy, M. (2012) Aggregate reactivation mediated by the Hsp100 chaperones, *Arch. Biochem. Biophys. 520*, 1-6.

49. Haas, I. G., and Wabl, M. (1983) Immunoglobulin heavy chain binding protein, *Nature 306*, 387-389.

50. Flynn, G. C., Chappell, T. G., and Rothman, J. E. (1989) Peptide binding and release by proteins implicated as catalysts of protein assembly, *Science 245*, 385-390.

51. Lim, W. A., and Sauer, R. T. (1989) Alternative packing arrangements in the hydrophobic core of lambda repressor, *Nature 339*, 31-36.

52. Flynn, G. C., Pohl, J., Flocco, M. T., and Rothman, J. E. (1991) Peptide-binding specificity of the molecular chaperone BiP, *Nature 353*, 726-730.

53. Blond-Elguindi, S., Cwirla, S. E., Dower, W. J., Lipshutz, R. J., Sprang, S. R., Sambrook, J. F., and Gething, M. J. (1993) Affinity panning of a library of peptides displayed on bacteriophages reveals the binding specificity of BiP, *Cell 75*, 717-728.

54. Hamman, B. D., Hendershot, L. M., and Johnson, A. E. (1998) BiP maintains the permeability barrier of the ER membrane by sealing the lumenal end of the translocon pore before and early in translocation, *Cell 92*, 747-758.

55. Gulow, K., Bienert, D., and Haas, I. G. (2002) BiP is feed-back regulated by control of protein translation efficiency, *J. Cell Sci. 115*, 2443-2452.

56. Tian, G., Xiang, S., Noiva, R., Lennarz, W. J., and Schindelin, H. (2006) The crystal structure of yeast protein disulfide isomerase suggests cooperativity between its active sites, *Cell 124*, 61-73.

57. Ellgaard, L., Molinari, M., and Helenius, A. (1999) Setting the standards: quality control in the secretory pathway, *Science 286*, 1882-1888.

58. Meacham, G. C., Patterson, C., Zhang, W., Younger, J. M., and Cyr, D. M. (2001) The Hsc70 co-chaperone CHIP targets immature CFTR for proteasomal degradation, *Nat Cell Biol 3*, 100-105.

59. Carvalho, P., Stanley, A. M., and Rapoport, T. A. (2010) Retrotranslocation of a misfolded luminal ER protein by the ubiquitin-ligase Hrd1p, *Cell 143*, 579-591.

60. Kozutsumi, Y., Segal, M., Normington, K., Gething, M. J., and Sambrook, J. (1988) The presence of malfolded proteins in the endoplasmic reticulum signals the induction of glucose-regulated proteins, *Nature 332*, 462-464.

61. Kaufman, R. J., Scheuner, D., Schroder, M., Shen, X., Lee, K., Liu, C. Y., and Arnold, S. M. (2002) The unfolded protein response in nutrient sensing and differentiation, *Nat Rev Mol Cell Biol 3*, 411-421.

62. Shamu, C. E., and Walter, P. (1996) Oligomerization and phosphorylation of the Ire1p kinase during intracellular signaling from the endoplasmic reticulum to the nucleus, *EMBO J. 15*, 3028-3039.

63. Prostko, C. R., Brostrom, M. A., and Brostrom, C. O. (1993) Reversible phosphorylation of eukaryotic initiation factor 2 alpha in response to endoplasmic reticular signaling, *Mol. Cell. Biochem. 127-128*, 255-265.

64. Szegezdi, E., Fitzgerald, U., and Samali, A. (2003) Caspase-12 and ER-stress-mediated apoptosis: the story so far, *Ann. N. Y. Acad. Sci. 1010*, 186-194.

65. Oyadomari, S., Takeda, K., Takiguchi, M., Gotoh, T., Matsumoto, M., Wada, I., Akira, S., Araki, E., and Mori, M. (2001) Nitric oxide-induced apoptosis in pancreatic beta cells is mediated by the endoplasmic reticulum stress pathway, *Proc. Natl. Acad. Sci. U. S. A. 98*, 10845-10850.

66. Elad, N., Farr, G. W., Clare, D. K., Orlova, E. V., Horwich, A. L., and Saibil, H. R. (2007) Topologies of a substrate protein bound to the chaperonin GroEL, *Mol. Cell 26*, 415-426.

67. Pace, C. N., Shirley, B. A., McNutt, M., and Gajiwala, K. (1996) Forces contributing to the conformational stability of proteins, *FASEB J. 10*, 75-83.

68. Dobson, C. M. (2004) Principles of protein folding, misfolding and aggregation, *Semin. Cell Dev. Biol. 15*, 3-16.

69. Jahn, T. R., and Radford, S. E. (2005) The Yin and Yang of protein folding, *FEBS J 272*, 5962-5970.

70. Mu, T. W., Ong, D. S., Wang, Y. J., Balch, W. E., Yates, J. R., 3rd, Segatori, L., and Kelly, J. W. (2008) Chemical and biological approaches synergize to ameliorate protein-folding diseases, *Cell 134*, 769-781.

71. Ross, C. A., and Poirier, M. A. (2005) Opinion: What is the role of protein aggregation in neurodegeneration?, *Nat Rev Mol Cell Biol 6*, 891-898.

72. Sands, M. S., and Davidson, B. L. (2006) Gene therapy for lysosomal storage diseases, *Mol Ther 13*, 839-849.

73. Mango, R. L., Xu, L., Sands, M. S., Vogler, C., Seiler, G., Schwarz, T., Haskins, M. E., and Ponder, K. P. (2004) Neonatal retroviral vector-mediated hepatic gene therapy reduces bone, joint, and cartilage disease in mucopolysaccharidosis VII mice and dogs, *Mol. Genet. Metab. 82*, 4-19.

74. Di Domenico, C., Villani, G. R., Di Napoli, D., Reyero, E. G., Lombardo, A., Naldini, L., and Di Natale, P. (2005) Gene therapy for a mucopolysaccharidosis type I murine model with lentiviral-IDUA vector, *Hum. Gene Ther. 16*, 81-90.

75. De Palma, M., Montini, E., Santoni de Sio, F. R., Benedicenti, F., Gentile, A., Medico, E., and Naldini, L. (2005) Promoter trapping reveals significant differences in integration site selection between MLV and HIV vectors in primary hematopoietic cells, *Blood 105*, 2307-2315.

76. Mu, T. W., Fowler, D. M., and Kelly, J. W. (2008) Partial restoration of mutant enzyme homeostasis in three distinct lysosomal storage disease cell lines by altering calcium homeostasis, *PLoS Biol 6*, e26.

77. Westerheide, S. D., Bosman, J. D., Mbadugha, B. N., Kawahara, T. L., Matsumoto, G., Kim, S., Gu, W., Devlin, J. P., Silverman, R. B., and Morimoto, R. I. (2004) Celastrols as inducers of the heat shock response and cytoprotection, *J. Biol. Chem. 279*, 56053-56060.

78. Csonka, L. N. (1989) Physiological and genetic responses of bacteria to osmotic stress, *Microbiol. Rev. 53*, 121-147.

79. Zaccai, G. (2004) The effect of water on protein dynamics, *Philos. Trans. R. Soc. Lond. B. Biol. Sci. 359*, 1269-1275; discussion 1275, 1323-1268.

80. Smith, T. R., Tremblay, G. C., and Bradley, T. M. (1999) Hsp70 and a 54 kDa protein (Osp54) are induced in salmon (Salmo salar) in response to hyperosmotic stress, *J. Exp. Zool. 284*, 286-298.

81. Yancey, P. H., Clark, M. E., Hand, S. C., Bowlus, R. D., and Somero, G. N. (1982) Living with water stress: evolution of osmolyte systems, *Science 217*, 1214-1222.

82. Burg, M. B. (1995) Molecular basis of osmotic regulation, *Am. J. Physiol. 268*, F983-996.

83. Yancey, P. H., and Somero, G. N. (1979) Counteraction of urea destabilization of protein structure by methylamine osmoregulatory compounds of elasmobranch fishes, *Biochem. J. 183*, 317-323.

84. Holthauzen, L. M., and Bolen, D. W. (2007) Mixed osmolytes: the degree to which one osmolyte affects the protein stabilizing ability of another, *Protein Sci. 16*, 293-298.

85. Lee, J. C., and Timasheff, S. N. (1981) The stabilization of proteins by sucrose, *J. Biol. Chem. 256*, 7193-7201.

86. Felitsky, D. J., and Record, M. T., Jr. (2004) Application of the local-bulk partitioning and competitive binding models to interpret preferential interactions of glycine betaine and urea with protein surface, *Biochemistry (Mosc). 43*, 9276-9288.

87. Qu, Y., Bolen, C. L., and Bolen, D. W. (1998) Osmolyte-driven contraction of a random coil protein, *Proc. Natl. Acad. Sci. U. S. A. 95*, 9268-9273.

88. Liu, Y., and Bolen, D. W. (1995) The peptide backbone plays a dominant role in protein stabilization by naturally occurring osmolytes, *Biochemistry (Mosc). 34*, 12884-12891.

89. Tanaka, M., Machida, Y., Niu, S., Ikeda, T., Jana, N. R., Doi, H., Kurosawa, M., Nekooki, M., and Nukina, N. (2004) Trehalose alleviates polyglutamine-mediated pathology in a mouse model of Huntington disease, *Nat. Med. 10*, 148-154.

90. Eronina, T. B., Chebotareva, N. A., Bazhina, S. G., Makeeva, V. F., Kleymenov, S. Y., and Kurganov, B. I. (2009) Effect of proline on thermal inactivation, denaturation and aggregation of glycogen phosphorylase b from rabbit skeletal muscle, *Biophys. Chem. 141*, 66-74.

91. Brown, C. R., Hong-Brown, L. Q., Biwersi, J., Verkman, A. S., and Welch, W. J. (1996) Chemical chaperones correct the mutant phenotype of the delta F508 cystic fibrosis transmembrane conductance regulator protein, *Cell Stress Chaperones 1*, 117-125.

92. Ray, S. S., Nowak, R. J., Brown, R. H., Jr., and Lansbury, P. T., Jr. (2005) Small-molecule-mediated stabilization of familial amyotrophic lateral sclerosis-linked

superoxide dismutase mutants against unfolding and aggregation, *Proc. Natl. Acad. Sci. U. S. A. 102*, 3639-3644.

93. Loo, T. W., and Clarke, D. M. (1995) P-glycoprotein. Associations between domains and between domains and molecular chaperones, *J. Biol. Chem. 270*, 21839-21844.

94. Bulawa, C. E., Connelly, S., Devit, M., Wang, L., Weigel, C., Fleming, J. A., Packman, J., Powers, E. T., Wiseman, R. L., Foss, T. R., Wilson, I. A., Kelly, J. W., and Labaudiniere, R. (2012) Tafamidis, a potent and selective transthyretin kinetic stabilizer that inhibits the amyloid cascade, *Proc. Natl. Acad. Sci. U. S. A. 109*, 9629-9634.

95. Ong, D. S., and Kelly, J. W. (2011) Chemical and/or biological therapeutic strategies to ameliorate protein misfolding diseases, *Curr. Opin. Cell Biol. 23*, 231-238.

96. Pantoliano, M. W., Petrella, E. C., Kwasnoski, J. D., Lobanov, V. S., Myslik, J., Graf, E., Carver, T., Asel, E., Springer, B. A., Lane, P., and Salemme, F. R. (2001) High-density miniaturized thermal shift assays as a general strategy for drug discovery, *J Biomol Screen 6*, 429-440.

97. Veprintsev, D. High-precision protein stability measurement using a Rotor-Gene cycler.

98. Carver, T. E., Bordeau, B., Cummings, M. D., Petrella, E. C., Pucci, M. J., Zawadzke, L. E., Dougherty, B. A., Tredup, J. A., Bryson, J. W., Yanchunas, J., Jr., Doyle, M. L., Witmer, M. R., Nelen, M. I., DesJarlais, R. L., Jaeger, E. P., Devine, H., Asel, E. D., Springer, B. A., Bone, R., Salemme, F. R., and Todd, M. J. (2005) Decrypting the biochemical function of an essential gene from Streptococcus pneumoniae using ThermoFluor technology, *J. Biol. Chem. 280*, 11704-11712.

99. Naik, S., Haque, I., Degner, N., Kornilayev, B., Bomhoff, G., Hodges, J., Khorassani, A. A., Katayama, H., Morris, J., Kelly, J., Seed, J., and Fisher, M. T. (2010) Identifying protein stabilizing ligands using GroEL, *Biopolymers 93*, 237-251.

100. Llorca, O., Martin-Benito, J., Ritco-Vonsovici, M., Grantham, J., Hynes, G. M., Willison, K. R., Carrascosa, J. L., and Valpuesta, J. M. (2000) Eukaryotic chaperonin CCT stabilizes actin and tubulin folding intermediates in open quasi-native conformations, *EMBO J. 19*, 5971-5979.

101. Llorca, O., Martin-Benito, J., Grantham, J., Ritco-Vonsovici, M., Willison, K. R., Carrascosa, J. L., and Valpuesta, J. M. (2001) The 'sequential allosteric ring' mechanism in the eukaryotic chaperonin-assisted folding of actin and tubulin, *EMBO J. 20*, 4065-4075.

102. Friedman, D. I., Olson, E. R., Georgopoulos, C., Tilly, K., Herskowitz, I., and Banuett, F. (1984) Interactions of bacteriophage and host macromolecules in the growth of bacteriophage lambda, *Microbiol. Rev. 48*, 299-325.

103. Barraclough, R., and Ellis, R. J. (1980) Protein synthesis in chloroplasts. IX. Assembly of newly-synthesized large subunits into ribulose bisphosphate carboxylase in isolated intact pea chloroplasts, *Biochim. Biophys. Acta 608*, 19-31.

104. Goloubinoff, P., Christeller, J. T., Gatenby, A. A., and Lorimer, G. H. (1989) Reconstitution of active dimeric ribulose bisphosphate carboxylase from an unfoleded state depends on two chaperonin proteins and Mg-ATP, *Nature 342*, 884-889.

105. Goloubinoff, P., Gatenby, A. A., and Lorimer, G. H. (1989) GroE heat-shock proteins promote assembly of foreign prokaryotic ribulose bisphosphate carboxylase oligomers in Escherichia coli, *Nature 337*, 44-47.

106. Fayet, O., Ziegelhoffer, T., and Georgopoulos, C. (1989) The groES and groEL heat shock gene products of Escherichia coli are essential for bacterial growth at all temperatures, *J. Bacteriol. 171*, 1379-1385.

107. Kerner, M. J., Naylor, D. J., Ishihama, Y., Maier, T., Chang, H. C., Stines, A. P., Georgopoulos, C., Frishman, D., Hayer-Hartl, M., Mann, M., and Hartl, F. U. (2005) Proteome-wide analysis of chaperonin-dependent protein folding in Escherichia coli, *Cell 122*, 209-220.

108. Braig, K., Otwinowski, Z., Hegde, R., Boisvert, D. C., Joachimiak, A., Horwich, A. L., and Sigler, P. B. (1994) The crystal structure of the bacterial chaperonin GroEL at 2.8 A, *Nature 371*, 578-586.

109. Yifrach, O., and Horovitz, A. (1994) Two lines of allosteric communication in the oligomeric chaperonin GroEL are revealed by the single mutation Arg196-->Ala, *J. Mol. Biol. 243*, 397-401.

110. Chennubhotla, C., and Bahar, I. (2006) Markov propagation of allosteric effects in biomolecular systems: application to GroEL-GroES, *Mol Syst Biol 2*, 36.

111. Hunt, J. F., Weaver, A. J., Landry, S. J., Gierasch, L., and Deisenhofer, J. (1996) The crystal structure of the GroES co-chaperonin at 2.8 A resolution, *Nature 379*, 37-45.

112. Chandrasekhar, G. N., Tilly, K., Woolford, C., Hendrix, R., and Georgopoulos, C. (1986) Purification and properties of the groES morphogenetic protein of Escherichia coli, *J. Biol. Chem. 261*, 12414-12419.

113. Saibil, H., Dong, Z., Wood, S., and auf der Mauer, A. (1991) Binding of chaperonins, *Nature 353*, 25-26.

114. Chen, S., Roseman, A. M., Hunter, A. S., Wood, S. P., Burston, S. G., Ranson, N. A., Clarke, A. R., and Saibil, H. R. (1994) Location of a folding protein and shape changes in GroEL-GroES complexes imaged by cryo-electron microscopy, *Nature 371*, 261-264.

115. Fenton, W. A., Kashi, Y., Furtak, K., and Horwich, A. L. (1994) Residues in chaperonin GroEL required for polypeptide binding and release, *Nature 371*, 614-619.

116. Lin, Z., Schwartz, F. P., and Eisenstein, E. (1995) The hydrophobic nature of GroEL-substrate binding, *J. Biol. Chem. 270*, 1011-1014.

117. Goldberg, M. S., Zhang, J., Sondek, S., Matthews, C. R., Fox, R. O., and Horwich, A. L. (1997) Native-like structure of a protein-folding intermediate bound to the chaperonin GroEL, *Proc. Natl. Acad. Sci. U. S. A. 94*, 1080-1085.

118. Horwich, A. L. (2011) Protein folding in the cell: an inside story, *Nat. Med. 17*, 1211-1216.

119. Kad, N. M., Ranson, N. A., Cliff, M. J., and Clarke, A. R. (1998) Asymmetry, commitment and inhibition in the GroE ATPase cycle impose alternating functions on the two GroEL rings, *J. Mol. Biol. 278*, 267-278.

120. Ranson, N. A., Farr, G. W., Roseman, A. M., Gowen, B., Fenton, W. A., Horwich, A. L., and Saibil, H. R. (2001) ATP-bound states of GroEL captured by cryo-electron microscopy, *Cell 107*, 869-879.

121. Clare, D. K., Vasishtan, D., Stagg, S., Quispe, J., Farr, G. W., Topf, M., Horwich, A. L., and Saibil, H. R. (2012) ATP-triggered conformational changes delineate substrate-binding and -folding mechanics of the GroEL chaperonin, *Cell 149*, 113-123.

122. Xu, Z., and Sigler, P. B. (1998) GroEL/GroES: structure and function of a two-stroke folding machine, *J. Struct. Biol. 124*, 129-141.

123. Hartl, F. U., Bracher, A., and Hayer-Hartl, M. (2011) Molecular chaperones in protein folding and proteostasis, *Nature 475*, 324-332.

124. Saibil, H. R., Zheng, D., Roseman, A. M., Hunter, A. S., Watson, G. M., Chen, S., Auf Der Mauer, A., O'Hara, B. P., Wood, S. P., Mann, N. H., Barnett, L. K., and Ellis, R. J. (1993) ATP induces large quaternary rearrangements in a cage-like chaperonin structure, *Curr. Biol. 3*, 265-273.

125. Rye, H. S., Roseman, A. M., Chen, S., Furtak, K., Fenton, W. A., Saibil, H. R., and Horwich, A. L. (1999) GroEL-GroES cycling: ATP and nonnative polypeptide direct alternation of folding-active rings, *Cell 97*, 325-338.

126. Ranson, N. A., Clare, D. K., Farr, G. W., Houldershaw, D., Horwich, A. L., and Saibil, H. R. (2006) Allosteric signaling of ATP hydrolysis in GroEL-GroES complexes, *Nat Struct Mol Biol 13*, 147-152.

127. Van Dyk, T. K., Gatenby, A. A., and LaRossa, R. A. (1989) Demonstration by genetic suppression of interaction of GroE products with many proteins, *Nature 342*, 451-453.

128. Viitanen, P. V., Donaldson, G. K., Lorimer, G. H., Lubben, T. H., and Gatenby, A. A. (1991) Complex interactions between the chaperonin 60 molecular chaperone and dihydrofolate reductase, *Biochemistry (Mosc). 30*, 9716-9723.

129. Lorimer, G. H. (1996) A quantitative assessment of the role of the chaperonin proteins in protein folding in vivo, *FASEB J. 10*, 5-9.

130. Chapman, E., Farr, G. W., Usaite, R., Furtak, K., Fenton, W. A., Chaudhuri, T. K., Hondorp, E. R., Matthews, R. G., Wolf, S. G., Yates, J. R., Pypaert, M., and Horwich, A. L. (2006) Global aggregation of newly translated proteins in an Escherichia coli strain deficient of the chaperonin GroEL, *Proc. Natl. Acad. Sci. U. S. A. 103*, 15800-15805.

131. Smith, K. E., Voziyan, P. A., and Fisher, M. T. (1998) Partitioning of rhodanese onto GroEL. Chaperonin binds a reversibly oxidized form derived from the native protein, *J. Biol. Chem. 273*, 28677-28681.

132. Fenton, W. A., and Horwich, A. L. (1997) GroEL-mediated protein folding, *Protein Sci. 6*, 743-760.

133. Clark, A. C., Hugo, E., and Frieden, C. (1996) Determination of regions in the dihydrofolate reductase structure that interact with the molecular chaperonin GroEL, *Biochemistry (Mosc). 35*, 5893-5901.

134. Voziyan, P. A., and Fisher, M. T. (2000) Chaperonin-assisted folding of glutamine synthetase under nonpermissive conditions: off-pathway aggregation propensity does not determine the co-chaperonin requirement, *Protein Sci. 9*, 2405-2412.

135. Gonzalez, M., Bagatolli, L. A., Echabe, I., Arrondo, J. L., Argarana, C. E., Cantor, C. R., and Fidelio, G. D. (1997) Interaction of biotin with streptavidin. Thermostability and conformational changes upon binding, *J. Biol. Chem. 272*, 11288-11294.

136. Bolin, J. T., Filman, D. J., Matthews, D. A., Hamlin, R. C., and Kraut, J. (1982) Crystal structures of Escherichia coli and Lactobacillus casei dihydrofolate reductase refined at 1.7 A resolution. I. General features and binding of methotrexate, *J. Biol. Chem. 257*, 13650-13662.

137. Lowe, C. U., May, C. D., and Reed, S. C. (1949) Fibrosis of the pancreas in infants and children; a statistical study of clinical and hereditary features, *Am. J. Dis. Child. 78*, 349-374.

138. Riordan, J. R., Rommens, J. M., Kerem, B., Alon, N., Rozmahel, R., Grzelczak, Z., Zielenski, J., Lok, S., Plavsic, N., Chou, J. L., and et al. (1989) Identification of the cystic

fibrosis gene: cloning and characterization of complementary DNA, *Science 245*, 1066-1073.

139. Rommens, J. M., Iannuzzi, M. C., Kerem, B., Drumm, M. L., Melmer, G., Dean, M., Rozmahel, R., Cole, J. L., Kennedy, D., Hidaka, N., and et al. (1989) Identification of the cystic fibrosis gene: chromosome walking and jumping, *Science 245*, 1059-1065.

140. Kerem, B., Rommens, J. M., Buchanan, J. A., Markiewicz, D., Cox, T. K., Chakravarti, A., Buchwald, M., and Tsui, L. C. (1989) Identification of the cystic fibrosis gene: genetic analysis, *Science 245*, 1073-1080.

141. Collins, F. S. (1992) Cystic fibrosis: molecular biology and therapeutic implications, *Science 256*, 774-779.

142. Quinton, P. M. (2007) Cystic fibrosis: lessons from the sweat gland, *Physiology (Bethesda) 22*, 212-225.

143. Quinton, P. M. (1983) Chloride impermeability in cystic fibrosis, *Nature 301*, 421-422.

144. Engelhardt, J. F., Yankaskas, J. R., Ernst, S. A., Yang, Y., Marino, C. R., Boucher, R. C., Cohn, J. A., and Wilson, J. M. (1992) Submucosal glands are the predominant site of CFTR expression in the human bronchus, *Nat. Genet. 2*, 240-248.

145. Sharer, N., Schwarz, M., Malone, G., Howarth, A., Painter, J., Super, M., and Braganza, J. (1998) Mutations of the cystic fibrosis gene in patients with chronic pancreatitis, *N. Engl. J. Med. 339*, 645-652.

146. Chillon, M., Casals, T., Mercier, B., Bassas, L., Lissens, W., Silber, S., Romey, M. C., Ruiz-Romero, J., Verlingue, C., Claustres, M., and et al. (1995) Mutations in the cystic fibrosis gene in patients with congenital absence of the vas deferens, *N. Engl. J. Med. 332*, 1475-1480.

147. Frerichs, C., and Smyth, A. (2009) Treatment strategies for cystic fibrosis: what's in the pipeline?, *Expert Opin Pharmacother 10*, 1191-1202.

148. Higgins, C. F. (1992) ABC transporters: from microorganisms to man, *Annu. Rev. Cell Biol. 8*, 67-113.

149. Sheppard, D. N., and Welsh, M. J. (1999) Structure and function of the CFTR chloride channel, *Physiol. Rev. 79*, S23-45.

150. Vergani, P., Lockless, S. W., Nairn, A. C., and Gadsby, D. C. (2005) CFTR channel opening by ATP-driven tight dimerization of its nucleotide-binding domains, *Nature 433*, 876-880.

151. Vankeerberghen, A., Cuppens, H., and Cassiman, J. J. (2002) The cystic fibrosis transmembrane conductance regulator: an intriguing protein with pleiotropic functions, *J Cyst Fibros 1*, 13-29.

152. Rosenberg, M. F., Kamis, A. B., Aleksandrov, L. A., Ford, R. C., and Riordan, J. R. (2004) Purification and crystallization of the cystic fibrosis transmembrane conductance regulator (CFTR), *J. Biol. Chem. 279*, 39051-39057.

153. Baker, J. M., Hudson, R. P., Kanelis, V., Choy, W. Y., Thibodeau, P. H., Thomas, P. J., and Forman-Kay, J. D. (2007) CFTR regulatory region interacts with NBD1 predominantly via multiple transient helices, *Nat Struct Mol Biol 14*, 738-745.

154. Hegedűs, T., and Riordan, J. R. (2006) Search for proteins with similarity to the CFTR R domain using an optimized RDBMS solution, mBioSQL, *Central European Journal of Biology 1*, 29-42.

155. Rosenberg, M. F., O'Ryan, L. P., Hughes, G., Zhao, Z., Aleksandrov, L. A., Riordan, J. R., and Ford, R. C. (2011) The cystic fibrosis transmembrane conductance regulator

(CFTR): three-dimensional structure and localization of a channel gate, *J. Biol. Chem. 286*, 42647-42654.

156. Lewis, H. A., Buchanan, S. G., Burley, S. K., Conners, K., Dickey, M., Dorwart, M., Fowler, R., Gao, X., Guggino, W. B., Hendrickson, W. A., Hunt, J. F., Kearins, M. C., Lorimer, D., Maloney, P. C., Post, K. W., Rajashankar, K. R., Rutter, M. E., Sauder, J. M., Shriver, S., Thibodeau, P. H., Thomas, P. J., Zhang, M., Zhao, X., and Emtage, S. (2004) Structure of nucleotide-binding domain 1 of the cystic fibrosis transmembrane conductance regulator, *EMBO J. 23*, 282-293.

157. Serohijos, A. W., Hegedus, T., Aleksandrov, A. A., He, L., Cui, L., Dokholyan, N. V., and Riordan, J. R. (2008) Phenylalanine-508 mediates a cytoplasmic-membrane domain contact in the CFTR 3D structure crucial to assembly and channel function, *Proc. Natl. Acad. Sci. U. S. A. 105*, 3256-3261.

158. Rowe, S. M., Miller, S., and Sorscher, E. J. (2005) Cystic fibrosis, *N. Engl. J. Med. 352*, 1992-2001.

159. Rich, D. P., Anderson, M. P., Gregory, R. J., Cheng, S. H., Paul, S., Jefferson, D. M., McCann, J. D., Klinger, K. W., Smith, A. E., and Welsh, M. J. (1990) Expression of cystic fibrosis transmembrane conductance regulator corrects defective chloride channel regulation in cystic fibrosis airway epithelial cells, *Nature 347*, 358-363.

160. Bear, C. E., Li, C. H., Kartner, N., Bridges, R. J., Jensen, T. J., Ramjeesingh, M., and Riordan, J. R. (1992) Purification and functional reconstitution of the cystic fibrosis transmembrane conductance regulator (CFTR), *Cell 68*, 809-818.

161. Kunzelmann, K., Schreiber, R., Nitschke, R., and Mall, M. (2000) Control of epithelial Na+ conductance by the cystic fibrosis transmembrane conductance regulator, *Pflugers Arch. 440*, 193-201.

162. Xu, Y., Clark, J. C., Aronow, B. J., Dey, C. R., Liu, C., Wooldridge, J. L., and Whitsett, J. A. (2003) Transcriptional adaptation to cystic fibrosis transmembrane conductance regulator deficiency, *J. Biol. Chem. 278*, 7674-7682.

163. Lands, L. C., and Stanojevic, S. (2007) Oral non-steroidal anti-inflammatory drug therapy for cystic fibrosis, *Cochrane Database Syst Rev*, CD001505.

164. Balfour-Lynn, I. M., Lees, B., Hall, P., Phillips, G., Khan, M., Flather, M., and Elborn, J. S. (2006) Multicenter randomized controlled trial of withdrawal of inhaled corticosteroids in cystic fibrosis, *Am. J. Respir. Crit. Care Med. 173*, 1356-1362.

165. Kellerman, D., Rossi Mospan, A., Engels, J., Schaberg, A., Gorden, J., and Smiley, L. (2008) Denufosol: a review of studies with inhaled P2Y(2) agonists that led to Phase 3, *Pulm. Pharmacol. Ther. 21*, 600-607.

166. Clancy, J. P., Rowe, S. M., Accurso, F. J., Aitken, M. L., Amin, R. S., Ashlock, M. A., Ballmann, M., Boyle, M. P., Bronsveld, I., Campbell, P. W., De Boeck, K., Donaldson, S. H., Dorkin, H. L., Dunitz, J. M., Durie, P. R., Jain, M., Leonard, A., McCoy, K. S., Moss, R. B., Pilewski, J. M., Rosenbluth, D. B., Rubenstein, R. C., Schechter, M. S., Botfield, M., Ordonez, C. L., Spencer-Green, G. T., Vernillet, L., Wisseh, S., Yen, K., and Konstan, M. W. (2012) Results of a phase IIa study of VX-809, an investigational CFTR corrector compound, in subjects with cystic fibrosis homozygous for the F508del-CFTR mutation, *Thorax 67*, 12-18.

167. Welch, E. M., Barton, E. R., Zhuo, J., Tomizawa, Y., Friesen, W. J., Trifillis, P., Paushkin, S., Patel, M., Trotta, C. R., Hwang, S., Wilde, R. G., Karp, G., Takasugi, J., Chen, G., Jones, S., Ren, H., Moon, Y. C., Corson, D., Turpoff, A. A., Campbell, J. A., Conn, M. M., Khan, A., Almstead, N. G., Hedrick, J., Mollin, A., Risher, N., Weetall, M., Yeh, S., Branstrom, A. A., Colacino, J. M., Babiak, J., Ju, W. D., Hirawat, S., Northcutt, V. J., Miller, L. L., Spatrick, P., He, F., Kawana, M., Feng, H., Jacobson, A., Peltz, S. W., and Sweeney, H. L. (2007) PTC124 targets genetic disorders caused by nonsense mutations, *Nature 447*, 87-91.

168. Qu, B. H., and Thomas, P. J. (1996) Alteration of the cystic fibrosis transmembrane conductance regulator folding pathway, *J. Biol. Chem. 271*, 7261-7264.

169. Loo, T. W., Bartlett, M. C., and Clarke, D. M. (2005) Rescue of folding defects in ABC transporters using pharmacological chaperones, *J. Bioenerg. Biomembr. 37*, 501-507.

170. Zhang, X. M., Wang, X. T., Yue, H., Leung, S. W., Thibodeau, P. H., Thomas, P. J., and Guggino, S. E. (2003) Organic solutes rescue the functional defect in delta F508 cystic fibrosis transmembrane conductance regulator, *J. Biol. Chem. 278*, 51232-51242.

171. Lewis, H. A., Zhao, X., Wang, C., Sauder, J. M., Rooney, I., Noland, B. W., Lorimer, D., Kearins, M. C., Conners, K., Condon, B., Maloney, P. C., Guggino, W. B., Hunt, J. F., and Emtage, S. (2005) Impact of the deltaF508 mutation in first nucleotide-binding domain of human cystic fibrosis transmembrane conductance regulator on domain folding and structure, *J. Biol. Chem. 280*, 1346-1353.

172. Travis, S. M., Carson, M. R., Ries, D. R., and Welsh, M. J. (1993) Interaction of nucleotides with membrane-associated cystic fibrosis transmembrane conductance regulator, *J. Biol. Chem. 268*, 15336-15339.

173. Harding, A. E., and Zilkha, K. J. (1981) 'Pseudo-dominant' inheritance in Friedreich's ataxia, *J. Med. Genet. 18*, 285-287.

174. Filla, A., De Michele, G., Barbieri, F., and Campanella, G. (1992) Early onset hereditary ataxias of unknown etiology. Review of a personal series, *Acta Neurol. (Napoli). 14*, 420-430.

175. Geoffroy, G., Barbeau, A., Breton, G., Lemieux, B., Aube, M., Leger, C., and Bouchard, J. P. (1976) Clinical description and roentgenologic evaluation of patients with Friedreich's ataxia, *Can. J. Neurol. Sci. 3*, 279-286.

176. Delatycki, M. B., Williamson, R., and Forrest, S. M. (2000) Friedreich ataxia: an overview, *J. Med. Genet. 37*, 1-8.

177. Babcock, M., de Silva, D., Oaks, R., Davis-Kaplan, S., Jiralerspong, S., Montermini, L., Pandolfo, M., and Kaplan, J. (1997) Regulation of mitochondrial iron accumulation by Yfh1p, a putative homolog of frataxin, *Science 276*, 1709-1712.

178. Huang, M. L., Becker, E. M., Whitnall, M., Suryo Rahmanto, Y., Ponka, P., and Richardson, D. R. (2009) Elucidation of the mechanism of mitochondrial iron loading in Friedreich's ataxia by analysis of a mouse mutant, *Proc. Natl. Acad. Sci. U. S. A. 106*, 16381-16386.

179. Chamberlain, S., Shaw, J., Rowland, A., Wallis, J., South, S., Nakamura, Y., von Gabain, A., Farrall, M., and Williamson, R. (1988) Mapping of mutation causing Friedreich's ataxia to human chromosome 9, *Nature 334*, 248-250.

180. Fujita, R., Agid, Y., Trouillas, P., Seck, A., Tommasi-Davenas, C., Driesel, A. J., Olek, K., Grzeschik, K. H., Nakamura, Y., Mandel, J. L., and Hanauer, A. (1989) Confirmation

of linkage of Friedreich ataxia to chromosome 9 and identification of a new closely linked marker, *Genomics 4*, 110-111.

181. Jiralerspong, S., Liu, Y., Montermini, L., Stifani, S., and Pandolfo, M. (1997) Frataxin shows developmentally regulated tissue-specific expression in the mouse embryo, *Neurobiol. Dis. 4*, 103-113.

182. Koutnikova, H., Campuzano, V., Foury, F., Dolle, P., Cazzalini, O., and Koenig, M. (1997) Studies of human, mouse and yeast homologues indicate a mitochondrial function for frataxin, *Nat. Genet. 16*, 345-351.

183. Campuzano, V., Montermini, L., Lutz, Y., Cova, L., Hindelang, C., Jiralerspong, S., Trottier, Y., Kish, S. J., Faucheux, B., Trouillas, P., Authier, F. J., Durr, A., Mandel, J. L., Vescovi, A., Pandolfo, M., and Koenig, M. (1997) Frataxin is reduced in Friedreich ataxia patients and is associated with mitochondrial membranes, *Hum. Mol. Genet. 6*, 1771-1780.

184. Campuzano, V., Montermini, L., Molto, M. D., Pianese, L., Cossee, M., Cavalcanti, F., Monros, E., Rodius, F., Duclos, F., Monticelli, A., Zara, F., Canizares, J., Koutnikova, H., Bidichandani, S. I., Gellera, C., Brice, A., Trouillas, P., De Michele, G., Filla, A., De Frutos, R., Palau, F., Patel, P. I., Di Donato, S., Mandel, J. L., Cocozza, S., Koenig, M., and Pandolfo, M. (1996) Friedreich's ataxia: autosomal recessive disease caused by an intronic GAA triplet repeat expansion, *Science 271*, 1423-1427.

185. Musco, G., Stier, G., Kolmerer, B., Adinolfi, S., Martin, S., Frenkiel, T., Gibson, T., and Pastore, A. (2000) Towards a structural understanding of Friedreich's ataxia: the solution structure of frataxin, *Structure 8*, 695-707.

186. Roman, E. A., Faraj, S. E., Gallo, M., Salvay, A. G., Ferreiro, D. U., and Santos, J. (2012) Protein stability and dynamics modulation: the case of human frataxin, *PLoS One 7*, e45743.

187. Dhe-Paganon, S., Shigeta, R., Chi, Y. I., Ristow, M., and Shoelson, S. E. (2000) Crystal structure of human frataxin, *J. Biol. Chem. 275*, 30753-30756.

188. Nair, M., Adinolfi, S., Pastore, C., Kelly, G., Temussi, P., and Pastore, A. (2004) Solution structure of the bacterial frataxin ortholog, CyaY: mapping the iron binding sites, *Structure 12*, 2037-2048.

189. Adamec, J., Rusnak, F., Owen, W. G., Naylor, S., Benson, L. M., Gacy, A. M., and Isaya, G. (2000) Iron-dependent self-assembly of recombinant yeast frataxin: implications for Friedreich ataxia, *Am J Hum Genet 67*, 549-562.

190. Yoon, T., and Cowan, J. A. (2003) Iron-sulfur cluster biosynthesis. Characterization of frataxin as an iron donor for assembly of [2Fe-2S] clusters in ISU-type proteins, *J. Am. Chem. Soc. 125*, 6078-6084.

191. Maliandi, M. V., Busi, M. V., Turowski, V. R., Leaden, L., Araya, A., and Gomez-Casati, D. F. (2011) The mitochondrial protein frataxin is essential for heme biosynthesis in plants, *FEBS J 278*, 470-481.

192. Yoon, T., and Cowan, J. A. (2004) Frataxin-mediated iron delivery to ferrochelatase in the final step of heme biosynthesis, *J. Biol. Chem. 279*, 25943-25946.

193. Li, K., Besse, E. K., Ha, D., Kovtunovych, G., and Rouault, T. A. (2008) Iron-dependent regulation of frataxin expression: implications for treatment of Friedreich ataxia, *Hum. Mol. Genet. 17*, 2265-2273.

194. Hart, P. E., Lodi, R., Rajagopalan, B., Bradley, J. L., Crilley, J. G., Turner, C., Blamire, A. M., Manners, D., Styles, P., Schapira, A. H., and Cooper, J. M. (2005) Antioxidant treatment of patients with Friedreich ataxia: four-year follow-up, *Arch. Neurol. 62*, 621-626.

195. Santos, R., Lefevre, S., Sliwa, D., Seguin, A., Camadro, J. M., and Lesuisse, E. (2010) Friedreich ataxia: molecular mechanisms, redox considerations, and therapeutic opportunities, *Antioxid Redox Signal 13*, 651-690.

196. Correia, A. R., Adinolfi, S., Pastore, A., and Gomes, C. M. (2006) Conformational stability of human frataxin and effect of Friedreich's ataxia-related mutations on protein folding, *Biochem. J. 398*, 605-611.

197. Falke, S., Fisher, M. T., and Gogol, E. P. (2001) Structural changes in GroEL effected by binding a denatured protein substrate, *J. Mol. Biol. 308*, 569-577.

198. Falke, S., Tama, F., Brooks, C. L., 3rd, Gogol, E. P., and Fisher, M. T. (2005) The 13 angstroms structure of a chaperonin GroEL-protein substrate complex by cryo-electron microscopy, *J. Mol. Biol. 348*, 219-230.

199. Correia, A. R., Pastore, C., Adinolfi, S., Pastore, A., and Gomes, C. M. (2008) Dynamics, stability and iron-binding activity of frataxin clinical mutants, *FEBS J 275*, 3680-3690.

200. Cossee, M., Durr, A., Schmitt, M., Dahl, N., Trouillas, P., Allinson, P., Kostrzewa, M., Nivelon-Chevallier, A., Gustavson, K. H., Kohlschutter, A., Muller, U., Mandel, J. L., Brice, A., Koenig, M., Cavalcanti, F., Tammaro, A., De Michele, G., Filla, A., Cocozza, S., Labuda, M., Montermini, L., Poirier, J., and Pandolfo, M. (1999) Friedreich's ataxia: point mutations and clinical presentation of compound heterozygotes, *Ann. Neurol. 45*, 200-206.

201. Beauchamp, M., Labelle, H., Duhaime, M., and Joncas, J. (1995) Natural history of muscle weakness in Friedreich's Ataxia and its relation to loss of ambulation, *Clin Orthop Relat Res*, 270-275.

202. Walter, S., Lorimer, G. H., and Schmid, F. X. (1996) A thermodynamic coupling mechanism for GroEL-mediated unfolding, *Proc. Natl. Acad. Sci. U. S. A. 93*, 9425-9430.

203. Buchner, J., Schmidt, M., Fuchs, M., Jaenicke, R., Rudolph, R., Schmid, F. X., and Kiefhaber, T. (1991) GroE facilitates refolding of citrate synthase by suppressing aggregation, *Biochemistry (Mosc). 30*, 1586-1591.

204. Horowitz, P. M. (1995) Chaperonin-assisted protein folding of the enzyme rhodanese by GroEL/GroES, *Methods Mol. Biol. 40*, 361-368.

205. Bolen, D. W. (2001) Protein stabilization by naturally occurring osmolytes, *Methods Mol. Biol. 168*, 17-36.

206. Tieman, B. C., Johnston, M. F., and Fisher, M. T. (2001) A comparison of the GroE chaperonin requirements for sequentially and structurally homologous malate dehydrogenases: the importance of folding kinetics and solution environment, *J. Biol. Chem. 276*, 44541-44550.

207. Sigler, P. B., Xu, Z., Rye, H. S., Burston, S. G., Fenton, W. A., and Horwich, A. L. (1998) Structure and function in GroEL-mediated protein folding, *Annu. Rev. Biochem. 67*, 581-608.

208. Gray, T. E., and Fersht, A. R. (1991) Cooperativity in ATP hydrolysis by GroEL is increased by GroES, *FEBS Lett. 292*, 254-258.

209. Lin, Z., and Eisenstein, E. (1996) Nucleotide binding-promoted conformational changes release a nonnative polypeptide from the Escherichia coli chaperonin GroEL, *Proc. Natl. Acad. Sci. U. S. A. 93*, 1977-1981.

210. Pereira, D. A., and Williams, J. A. (2007) Origin and evolution of high throughput screening, *Br. J. Pharmacol. 152*, 53-61.

211. Janovick, J. A., Park, B. S., and Conn, P. M. (2011) Therapeutic rescue of misfolded mutants: validation of primary high throughput screens for identification of pharmacoperone drugs, *PLoS One 6*, e22784.

212. Pedemonte, N., Lukacs, G. L., Du, K., Caci, E., Zegarra-Moran, O., Galietta, L. J., and Verkman, A. S. (2005) Small-molecule correctors of defective DeltaF508-CFTR cellular processing identified by high-throughput screening, *J. Clin. Invest. 115*, 2564-2571.

213. Connelly, S., Choi, S., Johnson, S. M., Kelly, J. W., and Wilson, I. A. (2010) Structure-based design of kinetic stabilizers that ameliorate the transthyretin amyloidoses, *Curr. Opin. Struct. Biol. 20*, 54-62.

214. Noorwez, S. M., Ostrov, D. A., McDowell, J. H., Krebs, M. P., and Kaushal, S. (2008) A high-throughput screening method for small-molecule pharmacologic chaperones of misfolded rhodopsin, *Invest. Ophthalmol. Vis. Sci. 49*, 3224-3230.

215. Pey, A. L., Ying, M., Cremades, N., Velazquez-Campoy, A., Scherer, T., Thony, B., Sancho, J., and Martinez, A. (2008) Identification of pharmacological chaperones as potential therapeutic agents to treat phenylketonuria, *J. Clin. Invest. 118*, 2858-2867.

216. Geng, H., Whiteley, G., Ribbens, J., Zheng, W., Southall, N., Hu, X., Marugan, J. J., Ferrer, M., and Maegawa, G. H. (2011) Novel patient cell-based HTS assay for identification of small molecules for a lysosomal storage disease, *PLoS One 6*, e29504.

217. Tropak, M. B., Blanchard, J. E., Withers, S. G., Brown, E. D., and Mahuran, D. (2007) High-throughput screening for human lysosomal beta-N-Acetyl hexosaminidase inhibitors acting as pharmacological chaperones, *Chem. Biol. 14*, 153-164.

218. Urban, D. J., Zheng, W., Goker-Alpan, O., Jadhav, A., Lamarca, M. E., Inglese, J., Sidransky, E., and Austin, C. P. (2008) Optimization and validation of two miniaturized glucocerebrosidase enzyme assays for high throughput screening, *Comb Chem High Throughput Screen 11*, 817-824.

219. Mathews, C. K., and Huennekens, F. M. (1963) Further Studies on Dihydrofolic Reductase, *J. Biol. Chem. 238*, 3436-3442.

220. Mayr, L. M., and Bojanic, D. (2009) Novel trends in high-throughput screening, *Curr Opin Pharmacol 9*, 580-588.

221. Gribbon, P., and Sewing, A. (2003) Fluorescence readouts in HTS: no gain without pain?, *Drug Discov Today 8*, 1035-1043.

222. Bielefeld-Sevigny, M. (2009) AlphaLISA immunoassay platform- the "no-wash" high-throughput alternative to ELISA, *Assay Drug Dev Technol 7*, 90-92.

223. Eglen, R. M., Reisine, T., Roby, P., Rouleau, N., Illy, C., Bosse, R., and Bielefeld, M. (2008) The use of AlphaScreen technology in HTS: current status, *Curr Chem Genomics 1*, 2-10.

224. Ullman, E. F., Kirakossian, H., Switchenko, A. C., Ishkanian, J., Ericson, M., Wartchow, C. A., Pirio, M., Pease, J., Irvin, B. R., Singh, S., Singh, R., Patel, R., Dafforn, A., Davalian, D., Skold, C., Kurn, N., and Wagner, D. B. (1996) Luminescent oxygen channeling assay (LOCI): sensitive, broadly applicable homogeneous immunoassay method, *Clin. Chem. 42*, 1518-1526.

225. Szekeres, P. G., Leong, K., Day, T. A., Kingston, A. E., and Karran, E. H. (2008) Development of homogeneous 384-well high-throughput screening assays for Abeta1-40 and Abeta1-42 using AlphaScreen technology, *J Biomol Screen 13*, 101-111.

226. Pedro, L., Padros, J., Beaudet, L., Schubert, H. D., Gillardon, F., and Dahan, S. (2010) Development of a high-throughput AlphaScreen assay measuring full-length LRRK2(G2019S) kinase activity using moesin protein substrate, *Anal. Biochem. 404*, 45-51.

227. Rich, R. L., and Myszka, D. G. (2007) Higher-throughput, label-free, real-time molecular interaction analysis, *Anal. Biochem. 361*, 1-6.

228. Shiau, A. K., Massari, M. E., and Ozbal, C. C. (2008) Back to basics: label-free technologies for small molecule screening, *Comb Chem High Throughput Screen 11*, 231-237.

229. Neumann, T., Junker, H. D., Schmidt, K., and Sekul, R. (2007) SPR-based fragment screening: advantages and applications, *Curr Top Med Chem 7*, 1630-1642.

230. Lrofas, S., Johnsson, B., Edström, Å., Hansson, A., Lindquist, G., Hillgren, R.-M. M., and Stigh, L. (1995) Methods for site controlled coupling to carboxymethyldextran surfaces in surface plasmon resonance sensors, *Biosens. Bioelectron. 10*, 813-822.

231. Boozer, C., Kim, G., Cong, S., Guan, H., and Londergan, T. (2006) Looking towards label-free biomolecular interaction analysis in a high-throughput format: a review of new surface plasmon resonance technologies, *Curr. Opin. Biotechnol. 17*, 400-405.

232. Steiner, G. (2004) Surface plasmon resonance imaging, *Anal Bioanal Chem 379*, 328-331.

233. Pattnaik, P. (2005) Surface plasmon resonance: applications in understanding receptor-ligand interaction, *Appl. Biochem. Biotechnol. 126*, 79-92.

234. Wilson, W. D. (2002) Tech.Sight. Analyzing biomolecular interactions, *Science 295*, 2103-2105.

235. Löfås, S., and McWhirter, A. (2006) The Art of Immobilization for SPR Sensors

, In *Surface Plasmon Resonance Based Sensors* (Homola, J., Ed.), pp 117-151, Springer Berlin Heidelberg.

236. Loo, T. W., Bartlett, M. C., and Clarke, D. M. (2009) Correctors enhance maturation of DeltaF508 CFTR by promoting interactions between the two halves of the molecule, *Biochemistry (Mosc). 48*, 9882-9890.

237. Nieba, L., Nieba-Axmann, S. E., Persson, A., Hamalainen, M., Edebratt, F., Hansson, A., Lidholm, J., Magnusson, K., Karlsson, A. F., and Pluckthun, A. (1997) BIACORE analysis of histidine-tagged proteins using a chelating NTA sensor chip, *Anal. Biochem. 252*, 217-228.

238. Harmonization, I. C. o. (1996) ICH, Harmonised Tripartie Guide Prepared within the Third International Conference on Harmonisation of Technical Requirements for the Registration of Pharmaceuticals for Human Use (ICH), In *Validation of analytical Procedures: Methodology*, pp 1-8.

239. Murai, N., Taguchi, H., and Yoshida, M. (1995) Kinetic analysis of interactions between GroEL and reduced alpha-lactalbumin. Effect of GroES and nucleotides, *J. Biol. Chem. 270*, 19957-19963.

240. Lang, B., Delmar, M., and Coombs, W. (2005) Surface Plasmon Resonance as a Method to Study the Kinetics and Amplitude of Protein- Protein Binding, In *Practical Methods in Cardiovascular Research* (Dhein, S., Mohr, F., and Delmar, M., Eds.), pp 936-947, Springer Berlin Heidelberg.

241. O'Brien Ii, M. J., Brueck, S. R. J., Perez-Luna, V. H., Tender, L. M., and Lopez, G. P. (1999) SPR biosensors: simultaneously removing thermal and bulk-composition effects, *Biosens. Bioelectron. 14*, 145-154.

242. Do, T., Ho, F., Heidecker, B., Witte, K., Chang, L., and Lerner, L. (2008) A rapid method for determining dynamic binding capacity of resins for the purification of proteins, *Protein Expr. Purif. 60*, 147-150.

243. Abdiche, Y., Malashock, D., Pinkerton, A., and Pons, J. (2008) Determining kinetics and affinities of protein interactions using a parallel real-time label-free biosensor, the Octet, *Anal. Biochem. 377*, 209-217.

244. Wartchow, C. A., Podlaski, F., Li, S., Rowan, K., Zhang, X., Mark, D., and Huang, K. S. (2011) Biosensor-based small molecule fragment screening with biolayer interferometry, *J. Comput. Aided Mol. Des. 25*, 669-676.

245. Shimizu, A., Tanba, T., Ogata, I., Ikeguchi, M., and Sugai, S. (1998) The region of alpha-lactalbumin recognized by GroEL, *J Biochem 124*, 319-325.

246. Prischi, F., Konarev, P. V., Iannuzzi, C., Pastore, C., Adinolfi, S., Martin, S. R., Svergun, D. I., and Pastore, A. (2010) Structural bases for the interaction of frataxin with the central components of iron-sulphur cluster assembly, *Nat Commun 1*, 95.

247. Farr, G. W., Furtak, K., Rowland, M. B., Ranson, N. A., Saibil, H. R., Kirchhausen, T., and Horwich, A. L. (2000) Multivalent binding of nonnative substrate proteins by the chaperonin GroEL, *Cell 100*, 561-573.

248. Fisher, M. T. (1994) The effect of groES on the groEL-dependent assembly of dodecameric glutamine synthetase in the presence of ATP and ADP, *J. Biol. Chem. 269*, 13629-13636.

249. Yu, W., Kim Chiaw, P., and Bear, C. E. (2011) Probing conformational rescue induced by a chemical corrector of F508del-cystic fibrosis transmembrane conductance regulator (CFTR) mutant, *J. Biol. Chem. 286*, 24714-24725.

250. Tjernberg, A., Markova, N., Griffiths, W. J., and Hallen, D. (2006) DMSO-related effects in protein characterization, *J Biomol Screen 11*, 131-137.

251. Katayama, H., Janowiak, B. E., Brzozowski, M., Juryck, J., Falke, S., Gogol, E. P., Collier, R. J., and Fisher, M. T. (2008) GroEL as a molecular scaffold for structural analysis of the anthrax toxin pore, *Nat Struct Mol Biol 15*, 754-760.

252. Elliott, J. L., Mogridge, J., and Collier, R. J. (2000) A quantitative study of the interactions of Bacillus anthracis edema factor and lethal factor with activated protective antigen, *Biochemistry (Mosc). 39*, 6706-6713.

253. Collier, R. J., and Young, J. A. (2003) Anthrax toxin, *Annu. Rev. Cell Dev. Biol. 19*, 45-70.

254. Barth, H., Aktories, K., Popoff, M. R., and Stiles, B. G. (2004) Binary bacterial toxins: biochemistry, biology, and applications of common Clostridium and Bacillus proteins, *Microbiol. Mol. Biol. Rev. 68*, 373-402, table of contents.

255. Duesbery, N. S., Webb, C. P., Leppla, S. H., Gordon, V. M., Klimpel, K. R., Copeland, T. D., Ahn, N. G., Oskarsson, M. K., Fukasawa, K., Paull, K. D., and Vande Woude, G. F. (1998) Proteolytic inactivation of MAP-kinase-kinase by anthrax lethal factor, *Science 280*, 734-737.

256. Leppla, S. H. (1982) Anthrax toxin edema factor: a bacterial adenylate cyclase that increases cyclic AMP concentrations of eukaryotic cells, *Proc. Natl. Acad. Sci. U. S. A. 79*, 3162-3166.

257. Feld, G. K., Thoren, K. L., Kintzer, A. F., Sterling, H. J., Tang, II, Greenberg, S. G., Williams, E. R., and Krantz, B. A. (2010) Structural basis for the unfolding of anthrax lethal factor by protective antigen oligomers, *Nat Struct Mol Biol 17*, 1383-1390.

258. Bradley, K. A., Mogridge, J., Mourez, M., Collier, R. J., and Young, J. A. (2001) Identification of the cellular receptor for anthrax toxin, *Nature 414*, 225-229.

259. Scobie, H. M., Rainey, G. J., Bradley, K. A., and Young, J. A. (2003) Human capillary morphogenesis protein 2 functions as an anthrax toxin receptor, *Proc. Natl. Acad. Sci. U. S. A. 100*, 5170-5174.

260. Milne, J. C., Furlong, D., Hanna, P. C., Wall, J. S., and Collier, R. J. (1994) Anthrax protective antigen forms oligomers during intoxication of mammalian cells, *J. Biol. Chem. 269*, 20607-20612.

261. Thoren, K. L., Worden, E. J., Yassif, J. M., and Krantz, B. A. (2009) Lethal factor unfolding is the most force-dependent step of anthrax toxin translocation, *Proc. Natl. Acad. Sci. U. S. A. 106*, 21555-21560.

262. Krantz, B. A., Finkelstein, A., and Collier, R. J. (2006) Protein translocation through the anthrax toxin transmembrane pore is driven by a proton gradient, *J. Mol. Biol. 355*, 968-979.

263. Krantz, B. A., Melnyk, R. A., Zhang, S., Juris, S. J., Lacy, D. B., Wu, Z., Finkelstein, A., and Collier, R. J. (2005) A phenylalanine clamp catalyzes protein translocation through the anthrax toxin pore, *Science 309*, 777-781.

264. Young, J. A., and Collier, R. J. (2007) Anthrax toxin: receptor binding, internalization, pore formation, and translocation, *Annu. Rev. Biochem. 76*, 243-265.

265. Lacy, D. B., Wigelsworth, D. J., Melnyk, R. A., Harrison, S. C., and Collier, R. J. (2004) Structure of heptameric protective antigen bound to an anthrax toxin receptor: a role for receptor in pH-dependent pore formation, *Proc. Natl. Acad. Sci. U. S. A. 101*, 13147-13151.

266. Mogridge, J., Mourez, M., and Collier, R. J. (2001) Involvement of domain 3 in oligomerization by the protective antigen moiety of anthrax toxin, *J. Bacteriol. 183*, 2111-2116.

267. Wimalasena, D. S., Janowiak, B. E., Lovell, S., Miyagi, M., Sun, J., Zhou, H., Hajduch, J., Pooput, C., Kirk, K. L., Battaile, K. P., and Bann, J. G. (2010) Evidence that histidine protonation of receptor-bound anthrax protective antigen is a trigger for pore formation, *Biochemistry (Mosc). 49*, 6973-6983.

268. Rosovitz, M. J., Schuck, P., Varughese, M., Chopra, A. P., Mehra, V., Singh, Y., McGinnis, L. M., and Leppla, S. H. (2003) Alanine-scanning mutations in domain 4 of anthrax toxin protective antigen reveal residues important for binding to the cellular receptor and to a neutralizing monoclonal antibody, *J. Biol. Chem. 278*, 30936-30944.

269. Inglesby, T. V., O'Toole, T., Henderson, D. A., Bartlett, J. G., Ascher, M. S., Eitzen, E., Friedlander, A. M., Gerberding, J., Hauer, J., Hughes, J., McDade, J., Osterholm, M. T., Parker, G., Perl, T. M., Russell, P. K., and Tonat, K. (2002) Anthrax as a biological weapon, 2002: updated recommendations for management, *JAMA 287*, 2236-2252.

270. Subramanian, G. M., Cronin, P. W., Poley, G., Weinstein, A., Stoughton, S. M., Zhong, J., Ou, Y., Zmuda, J. F., Osborn, B. L., and Freimuth, W. W. (2005) A phase 1 study of PAmAb, a fully human monoclonal antibody against Bacillus anthracis protective antigen, in healthy volunteers, *Clin. Infect. Dis. 41*, 12-20.

271. Zhu, P. J., Hobson, J. P., Southall, N., Qiu, C., Thomas, C. J., Lu, J., Inglese, J., Zheng, W., Leppla, S. H., Bugge, T. H., Austin, C. P., and Liu, S. (2009) Quantitative high-throughput screening identifies inhibitors of anthrax-induced cell death, *Bioorg. Med. Chem. 17*, 5139-5145.

272. Rogers, M. S., Cryan, L. M., Habeshian, K. A., Bazinet, L., Caldwell, T. P., Ackroyd, P. C., and Christensen, K. A. (2012) A FRET-based high throughput screening assay to identify inhibitors of anthrax protective antigen binding to capillary morphogenesis gene 2 protein, *PLoS One 7*, e39911.

273. Mogridge, J., Cunningham, K., and Collier, R. J. (2002) Stoichiometry of anthrax toxin complexes, *Biochemistry (Mosc). 41*, 1079-1082.

274. Winzor, D. J. (2003) Surface plasmon resonance as a probe of protein isomerization, *Anal. Biochem. 318*, 1-12.

275. Chah, S., Kumar, C. V., Hammond, M. R., and Zare, R. N. (2004) Denaturation and renaturation of self-assembled yeast iso-1-cytochrome c on Au, *Anal. Chem. 76*, 2112-2117.

276. Zako, T., Harada, K., Mannen, T., Yamaguchi, S., Kitayama, A., Ueda, H., and Nagamune, T. (2001) Monitoring of the refolding process for immobilized firefly luciferase with a biosensor based on surface plasmon resonance, *J. Biochem. (Tokyo). 129*, 1-4.

277. Chen, L. Y. (2009) Monitoring conformational changes of immobilized RNase A and lysozyme in reductive unfolding by surface plasmon resonance, *Anal. Chim. Acta 631*, 96-101.

278. Sota, H., Hasegawa, Y., and Iwakura, M. (1998) Detection of conformational changes in an immobilized protein using surface plasmon resonance, *Anal. Chem. 70*, 2019-2024.

279. Katayama, H., Wang, J., Tama, F., Chollet, L., Gogol, E. P., Collier, R. J., and Fisher, M. T. (2010) Three-dimensional structure of the anthrax toxin pore inserted into lipid nanodiscs and lipid vesicles, *Proc. Natl. Acad. Sci. U. S. A. 107*, 3453-3457.

280. Blaustein, R. O., Koehler, T. M., Collier, R. J., and Finkelstein, A. (1989) Anthrax toxin: channel-forming activity of protective antigen in planar phospholipid bilayers, *Proc. Natl. Acad. Sci. U. S. A. 86*, 2209-2213.

281. Miller, C. J., Elliott, J. L., and Collier, R. J. (1999) Anthrax protective antigen: prepore-to-pore conversion, *Biochemistry (Mosc). 38*, 10432-10441.

282. Wigelsworth, D. J., Krantz, B. A., Christensen, K. A., Lacy, D. B., Juris, S. J., and Collier, R. J. (2004) Binding stoichiometry and kinetics of the interaction of a human anthrax toxin receptor, CMG2, with protective antigen, *J. Biol. Chem. 279*, 23349-23356.

283. Naik, S., Zhang, N., Gao, P., and Fisher, M. T. (2013) On the Design of Broad Based Screening Assays to Identify Potential Pharmacological Chaperones of Protein Misfolding Diseases, *Curr Top Med Chem Protein Misfolding in Conformational Disorders*

284. Naik, S., and Fisher, M. T. (2012) Systems and methods for identifying protein stabilizers.